A comparison of skin cancer and normal (healthy) cells: *in vitro* studies on the molecular mechanism of gossypol

Inaugural-Dissertation

zur Erlangung des Doktorgrades

der Mathematisch-Naturwissenschaftlichen Fakultät

der Heinrich-Heine-Universität Düsseldorf

vorgelegt von

Lisa Haasler

(geb. Scharf)

aus Castrop-Rauxel

Düsseldorf, Juni 2021

aus dem Institut für Biochemie und Molekularbiologie I

der Heinrich-Heine-Universität Düsseldorf

Gedruckt mit der Genehmigung der

Mathematisch-Naturwissenschaftlichen Fakultät der

Heinrich-Heine-Universität Düsseldorf

Berichterstatter:

1. Prof. Dr. Peter Brenneisen

2. Prof. Dr. Matthias Kassack

Tag der mündlichen Prüfung: 15. Dezember 2021

Eidesstattliche Erklärung zur Dissertation

Ich versichere an Eides Statt, dass die Dissertation von mir selbstständig und ohne unzulässige fremde Hilfe unter Beachtung der „Grundsätze zur Sicherung guter wissenschaftlicher Praxis an der Heinrich-Heine-Universität Düsseldorf" erstellt worden ist.

Diese Dissertation wurde in der vorgelegten oder in einer ähnlichen Form noch bei keiner anderen Fakultät eingereicht und es wurden keine vorherigen Promotionsversuche unternommen.

_____
Datum, Ort

_____
Unterschrift

List of figures

List of tables

Abbreviations

%	Percentage
(v/v)	Percent by volume
(w/v)	Percent by weight
µM	µmol/l
A375	Human malignant melanoma cell line
AcN	Acetonitrile
Apaf-1	Apoptotic protease activating factor-1
APS	Ammonium persulfate
ATG	Autophagy
ATP	Adenosine triphosphate
Baf	Bafilomycin A_1
BH	Bcl-2 homology
BSA	Bovine serum albumin
CCCP	Carbonyl cyanide 3-chlorophenylhydrazone
cIAP	Cellular inhibitor of apoptosis protein
CQ	Chloroquine
DAPI	4′,6-diamidino-2-phenylindole
DISC	Death inducing signalling complex
DMEM	Dulbecco's Modified Eagle Medium
DMSO	Dimethyl sulfoxide
Drp1	Dynamin-related protein 1
EDTA	Ethylenediaminetetraacetic acid
EGFP	Enhanced Green Fluorescence Protein
ERK	Extracellular signal-regulated kinase
FADD	Fas-associating death domain-containing protein
FBS	Fetal bovine serum
Fig	Figure
GP	Gossypol
h	Hour
H_2-DCF-DA	2',7'-dichlorodihydrofluorescein diacetate
H_2O_2	Hydrogen peroxide
HBSS	Hanks' Balanced Salt Solution
HCl	Hydrochloric acid
HPLC	High Pressure Liquid Chromatography
HRP	Horseradish peroxidase

IC	Inhibitory concentration
KBM	Keratinocyte Basal Medium
LB	Lysogeny broth
MAPK	Mitogen-activated protein kinase
MBM	Melanocyte Basal Medium
MEK	MAPK ERK kinase
min	Minute
MTT	3-(4,5-dimethylthiazol-2-yl)-2,5-diphenyltetrazolium bromide
NADH	Nicotinamide adenine dinucleotide
Nec1	Necrostatin-1
NGS	Normal goat serum
NHDF	Normal Human Dermal Fibroblasts
NHEK	Normal Human Epidermal Keratinocytes
NHEM	Normal Human Epidermal Melanocytes
OCR	Oxygen consumption rate
OD	Optical density
Oligo	Oligomycin
PARP	Poly (ADP-ribose) polymerase
PBS	Phosphate Buffered Saline
PVDF	Polyvinylidene difluoride
Raf	Rapidly accelerated fibrosarcoma
Ras	Rat sarcoma
RFU	Relative Fluorescence Units
RIP	Receptor-interacting serine/threonine-protein kinase
ROS	Reactive Oxygen Species
Rot/AA	Rotenone and antimycin A
rpm	Repeats per minute
RT	Room temperature
SCL-1	Cutaneous squamous cell carcinoma cell line
SDS	Sodium dodecyl sulfate
SDS-PAGE	Sodium dodecyl sulfate polyacrylamide gel electrophoresis
Sec	Second
SEM	Standard Error of the Mean
siRNA	Small interfering RNA
Smac/Diablo	Second mitochondria derived activator of caspases/direct IAP binding protein with low PI
SRB	Sulforhodamine B

SRC	Spare respiratory capacity
Sts	Staurosporine
Tab	Table
TBS	Tris Buffered Saline
TBS-T	Tris Buffered Saline with Tween
TCA	Trichloroacetic acid
TEMED	N, N, N', N tetramethylethylenediamine
TFA	Trifluoroacetic acid
TMRM	Tetramethylrhodamine methyl ester
TNF	Tumor necrosis factor
TNFR1	Tumor necrosis factor receptor 1
TOM20	Translocase of Outer Mitochondrial Membrane 20
TRADD	TNFR1-associated death domain protein
Tris	(Hydroxylmethyl) aminomethane
ULK	Unc-51 like autophagy activating kinase
VPS	Vacuolar protein sorting (yeast)

1 Introduction

1.1 Structure of the skin

The skin is the largest organ in the human body, with a size of two square metres, representing the primary interface between the body and environmental impacts. In addition to its protection against mechanical stress, UV radiation and the entry of microorganisms, the functions of the skin also include regulation of temperature and water balance (Fritsch 2009). Structurally, the skin can be divided into three layers: *epidermis*, *dermis* and *subcutis*. The outer layer is the epidermis serving as a barrier against external influences. It consists of four layers which differ in morphology and function. These include, from inside to outside, *stratum (str.) basale*, *str. spinosum*, *str. granulosum* and *str. corneum* resulting in a so-called stratified epithelium (Fritsch 2009, Muroyama and Lechler 2012). Keratinocytes represent the majority of cells in the epidermis with about 90%. The cells are formed by mitotic division of epidermal stem cells in the basal layer, followed by increasing differentiation through the epidermis finally leading to horny cells (corneocytes). Due to the balance between proliferation and cell death caused by terminal differentiation, the epidermis renews itself every 28 days (Fritsch 2009, Goebeler and Hamm 2017). In addition to keratinocytes, the epidermis also contains other cells such as Langerhans cells, Merkel cells and melanocytes. The latter are dendritic cells located in the *str. basale* and are responsible for melanin synthesis which plays a crucial role in the protection of the skin against UV radiation. This endogenous pigment responsible for skin and hair colour is transferred to neighbouring keratinocytes via the dendrites of the melanocytes in special cytoplasmic organelles, so-called melanosomes (Fritsch 2009, Wu and Hammer 2014, Goebeler and Hamm 2017). Two major pigment types are distinguished due to colour and synthesis pathway involving the brown-black eumelanin and the red-yellow pheomelanin, which define the type of skin classified into group I to VI by Fitzpatrick (Fitzpatrick 1988, Cichorek et al. 2013).

The epidermis is connected to the dermis via the basal membrane enabling the exchange of molecules between these layers. The dermis consists of fibroelastic the connective tissue and comprises the *str. papillare* and *str. reticulare*. The *str. papillare* contains vessels and nerves and supplies the dermis, whereas the latter is responsible for the architectural core structure. Tensile strength and elasticity of the skin are mediated by collagen and elastic fibres (Fritsch 2009, Goebeler and Hamm 2017). The ground substance of the dermis, consisting mainly of collagens and proteoglycans, is involved in cell-cell communication, cell migration, water storage and wound healing, among others (Fritsch 2009). Collectively, fibres and ground substance are termed extracellular matrix. In addition to the above mentioned vessels, the dermis also contains a lymphatic system for the removal of fluids and substances requiring

lymphatic drainage. Below the dermis lies the subcutis consisting of fatty tissues that serves as thermal insulation, energy storage and protector against mechanical impacts (Fritsch 2009, Goebeler and Hamm 2017).

1.2 Skin cancer

The direct exposure of the skin to environmental impacts, such as UV radiation, results in a high incidence and variety of neoplasms of the organ that increased dramatically in the last decades (D'Orazio et al. 2013, ZfKD 2019, ZfKD 2021). Most changes are benign, but some neoplasms of the skin are considered as very aggressive and metastatic (Fritsch 2009). Skin cancer is divided in non-melanoma skin cancer (NMSC), including basal cell carcinoma and squamous cell carcinoma, and melanocytic tumours, such as the highly aggressive malignant melanoma (Yan et al. 2011, Kornek and Augustin 2013). In the following, squamous cell carcinoma and malignant melanoma are described in more detail.

1.2.1 Cutaneous squamous cell carcinoma (CSCC)

Squamous cell carcinoma has its origin in diverse anatomic tissues covered with squamous epithelium. Mostly affected are areas of the skin, head and neck, oesophagus and lung (Yan et al. 2011). Cutaneous squamous cell carcinoma (CSCC) is the second most common form of skin cancer with increasing incidence over the last decades (Que et al. 2018, Stang et al. 2019, Stratigos et al. 2020). The benign form shows a good chance of cure. However, metastasis may occur in some cases which dramatically lowers the survival outcome and is associated with a poor prognosis (Varra et al. 2018). CSCC derives from proliferating epidermal keratinocytes caused by several risk factors resulting in a malignant cell type (Kwa et al. 1992, Nagarajan et al. 2019, Corchado-Cobos et al. 2020). The greatest risk of developing CSCC is due to chronic UV radiation, combined with a fair skin type (Brash et al. 1991, Armstrong and Kricker 2001, Que et al. 2018). Furthermore, human papilloma viruses (HPV) may facilitate the formation of CSCC, while personal behaviour like habits of smoking may even double the risk of cancer development (Akgul et al. 2006, Morita 2007, Yan et al. 2011). In addition, immunosuppression caused by viral infections or organ transplantation and certain drug applications promote the development of metastatic CSCC as well (Webb et al. 1997, Euvrard et al. 2003, Stratigos et al. 2020).

CSCC is grouped into an *in situ* and an invasive form. The invasive type is further classified into primary and advanced CSCC (Stratigos et al. 2020). The CSCC *in situ* is a non-metastatic form of this cancer that can be easily treated by local therapy, such as curettage and electrodesiccation, superficial therapies, like topical 5-fluorouracil (5-FU) and cryotherapy, or radiation (Bichakjian et al. 2018). In contrast, the previously mentioned therapies are often

ineffective for treatment of the advanced CSCC, which includes locally advanced and metastatic types, and there is no common standard therapy to treat these cancer cells effectively (Pickering et al. 2014, Migden et al. 2018). Tumour stages of CSCC are classified according to TNM classification as defined by the American Joint Committee of Cancer (AJCC) and the Union for International Cancer Control (UICC). TNM stands for **t**umour, **n**odes and **m**etastasis indicating the primary tumour site (T1-4 category), the number and location of involved lymph nodes (N0-N3 category) as well as the presence or absence of distant metastases (M0-M1 category) (Stratigos et al. 2020). Although this classification is an internationally accepted standard, it does not provide an estimation of the risk of CSCC patients developing metastasis (Breuninger et al. 2012).

Therapeutic options of advanced CSCC imply surgery and chemotherapy, alone or in combination with radiation, although response rates tend to be low. Despite the lack of an established standard therapy in these cases, the National Comprehensive Cancer Network guideline recommends using cisplatin alone or in combination with 5-fluorouracil (5-FU) (Burton et al. 2016, Ribero et al. 2017, Bichakjian et al. 2018). The combination of drugs increases the efficacy but is associated with increasing adverse side effects (Ribero et al. 2017). Therefore, the development of so-called targeted therapies is even more important. Epidermal growth factor receptor (EGFR) expressed in metastatic CSCC offers a potential approach (Corchado-Cobos et al. 2020). Some EGFR inhibitors tested in clinical trials, such as cetuximab and gefitinib, show an enhanced response rate, also in combination with 5-FU and radiotherapy. The use of these compounds is well tolerated, but the fast development of resistance, particularly to cetuximab, limits their use (Wheeler et al. 2008, Ribero et al. 2017). Another option is the use of programmed death (PD) 1 antibodies, such as cemiplimab, showing an efficacy of approximately 50% in locally advanced or metastatic CSCC. However, these studies only include immunocompetent patients (Migden et al. 2018).

1.2.2 Malignant melanoma

Malignant melanoma originating from melanocytes is the most aggressive type of skin cancer. The high potential to metastasise correlates with poor prognosis (Miller and Mihm 2006, Zbytek et al. 2008, Janostiak et al. 2019, Bertrand et al. 2020). The incidence is steadily increasing in the recent decades, particularly in the Caucasian population (Krensel et al. 2019, Bertrand et al. 2020, The Global Cancer Observatory 2020). High UV radiation exposure, the number of severe sunburns, especially in childhood, Clark's nevi and immunodeficiency significantly contribute to the development of melanoma. In addition to that, dispositional factors such as ethnicity, skin type I and II, albinism and impaired DNA repair play an important role in melanoma formation (Gandini et al. 2005, Fritsch 2009, D'Orazio et al. 2013). The macroscopic

differentiation of benign melanocytic nevi from malignant melanoma is based on the ABCDE guideline (**A**symmetry, **B**order irregularity, **C**olour variegation, **D**iameter >6 mm, **E**volution) (Friedman et al. 1985, Abbasi et al. 2004, Marghoob et al. 2019). Melanoma is classified into different subtypes including superficial spreading, nodular, lentigo maligna, acral lentiginous and desmoplastic melanoma which differ with regard to affected areas and their growth pattern. The classification into different tumour stages is carried out according to the TNM (**T**umour, **N**odes, **M**etastasis) classification similar to the squamous cell carcinoma, taking into account the presence or absence of ulceration, the tumour thickness as defined by Breslow and the invasion level as described by Clark (Clark et al. 1969, Breslow 1970, Balch et al. 2001).

The gold standard in diagnosis and treatment of melanoma is the surgical excision of the primary tumour with an appropriate safety margin, partially in combination with radiation therapy (Garbe et al. 2008). On the occurrence of metastasis, the use of chemotherapeutic agents is the common procedure for the treatment. The discovery of B-Raf as an oncogene and the identification of V600E being the most relevant somatic missense mutation of B-Raf in melanoma are the basis for new targeted therapies (Davies et al. 2002, Wellbrock et al. 2004). The application of specific B-Raf inhibitors, for example vemurafenib and dabrafenib, which targets the protooncogene B-Raf (Davies et al. 2002, Luke et al. 2017, Peng et al. 2017), shows improved efficacy in comparison to conventional chemotherapeutic agents, but response rates of around 50% and onset of resistances are observed within months (Nazarian et al. 2010, Chapman et al. 2011, Flaherty et al. 2012). Furthermore, immunotherapy was applied to treat melanoma. However, this is limited due to variable response rates (Larkin et al. 2015, Luke et al. 2017).

1.3 Multistep carcinogenesis

The maintenance between cell proliferation and cell death plays an important role in the body and is subject to tight regulations. An imbalance can result in cell death, but can also facilitate uncontrolled growth. Carcinogenesis is postulated as a multistage process consisting of initiation, promotion and progression (Weinberg 1994, Hiddemann and Bartram 2010, Müller-Esterl 2018). Initiation requires the emergence of a single mutated cell. Mutations occur spontaneously and constantly throughout the genome (Hiddemann and Bartram 2010). The most crucial mutations are found in genes whose products regulate the balance between cell proliferation and cell death, including protooncogenes/oncogenes and tumour suppressor genes (Morris and Chan 2015, Chandrashekar et al. 2020). Initiation is followed by promotion comprising the clonal expansion. This underlying selection mechanism is reversible and depends on the exposure to so-called tumour promoters. Thereafter, progression is the final step of tumour development (Hiddemann and Bartram 2010). Whereas a selective growth of a

(mutated) preneoplastic clone leads to the formation of a benign tumour, further mutations enhancing genetic instability facilitate the formation of a malignant tumour. These tumours differ in their boundaries and growth pattern. While the benign cancer type occurs locally and has a clear boundary, the malignant form is characterised by invasive and metastatic growth (Müller-Esterl 2018, Patel 2020). The interaction of several exogenous and endogenous factors causes tumour development. These include genetic predisposition, spontaneous somatic mutations as well as noxious agents, such as carcinogens, radiation and cancer-causing viruses (Hiddemann and Bartram 2010, Morris and Chan 2015, Schneider et al. 2017). As mentioned above, protooncogenes and tumour suppressor genes play a crucial role in this context. Mutations in the former resulting in an oncogene are dominant gain-of-function mutations leading to constitutive activation of signalling pathways (Chandrashekar et al. 2020). One well-studied oncogene is the Ras protein. These small GTPases are involved in several signalling cascades including proliferation, differentiation and apoptosis. Three isoforms are identified including H-Ras, K-Ras and N-Ras, of which the first often plays a role particularly in melanoma. The effector protein rapidly accelerated fibrosarcoma (Raf) being a kinase is activated by Ras, thus, triggering a downstream signal cascade of several kinases. For example, Raf phosphorylates mitogen-activated protein kinase (MAPK) extracellular signal-regulated kinase (ERK) kinase (MEK) which further phosphorylates ERK, resulting in the induction of cell cycle progression. The constitutive activation of this pathway can be induced by mutation in each of the individual steps (Zhang and Liu 2002, Chang et al. 2010, Manna and Stocco 2011, Han et al. 2017, Müller-Esterl 2018). In contrast, tumour suppressor genes are recessive, thus, both alleles must be mutated that is often accompanied by loss-of-function. Tumour suppressors can be grouped into gatekeeper genes regulating cell cycle processes and caretaker genes maintaining the integrity of the genome (Kinzler and Vogelstein 1997, Morris and Chan 2015, Mantovani et al. 2019, Chandrashekar et al. 2020). A prominent example is the tumour suppressor gene TP53 encoding the p53 protein which is altered in numerous different human tumours (Kandoth et al. 2013, Mantovani et al. 2019). The protein functions as a negative regulator in cell proliferation, cell cycle arrest during DNA repair and apoptosis conducting the term "guardian of the genome" (Lane 1992, Kruiswijk et al. 2015). Depending on the appearance on somatic mutation, they can be grouped into general-cancer and specific-cancer genes. For example, p53 is mutated in numerous tumour cells referred to the first group, whereas the breast cancer gene 1 (BRCA1), which is exclusively mutated in breast tissue, belongs to the specific-cancer genes. Thus, the tissue and context of each tumour has to be considered to understand the tumour biology and to identify potential points of attack for targeted therapies (Visvader 2011, Schaefer and Serrano 2016, Schneider et al. 2017, Chandrashekar et al. 2020). For better understanding of the complexity of carcinogenesis, Hanahan and Weinberg summarized the relevant biological properties of

tumours cells and named it hallmarks of cancer (Hanahan and Weinberg 2011). These include, amongst others, activating invasion and metastasis, inducing angiogenesis, resisting cell death, genome instability and deregulating cellular energetics. By identifying tumour-specific parameters, it is possible to develop new therapeutic approaches that specifically target individual characteristics. Exemplary representatives of potential anti-cancer drugs regarding the hallmarks of cancer are presented in Fig. 1.1 (Hanahan and Weinberg 2011). Since this thesis deals in particular with the evasion of cell death, this topic will be described in more detail in the following.
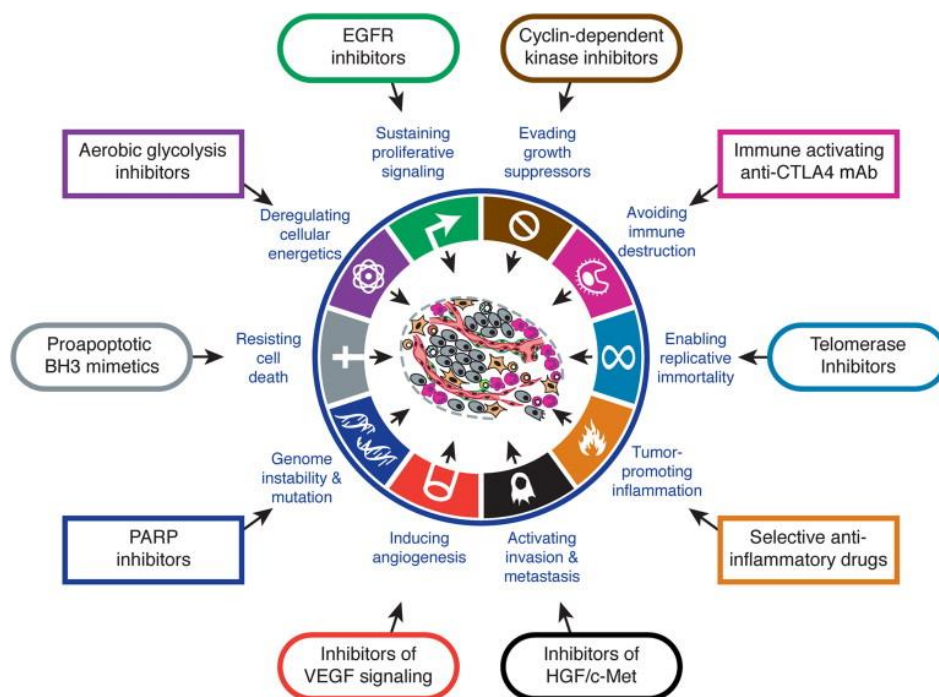
Fig. 1.1 Hallmarks of cancers summarised by Hanahan and Weinberg. Representatives of potential anti-cancer drugs with regard to the individual hallmarks are shown. Reprinted from Cell, 144/5, Hanahan and Weinberg, Hallmarks of Cancer: The Next Generation, 646-674, Copyright (2011), with permission from Elsevier; (Hanahan and Weinberg 2011).

1.4 Cell death pathways

Maintenance of cellular homeostasis requires a balance between proliferation and cell death. In this context, programmed cell death plays an important role not only for cell homeostasis but also in developmental processes relating to the nervous and immune system (Renehan et al. 2001, Czabotar et al. 2014). Dysfunction in these pathways leads to the formation of diseases such as cancer, autoimmune and neurodegenerative diseases (Renehan et al. 2001, Elmore 2007). In regard to cancer development, malfunctioning cell cycle regulation resulting in enhanced proliferation or decreased cell death facilitate carcinogenesis (King and Cidlowski

1998). Apoptosis and necroptosis, two processes belonging to the programmed cell death, are described below in more detail.

1.4.1 Apoptosis

Programmed cell death was first characterised by Kerr et al. in the early 70s. It was termed apoptosis and was defined to have two morphological features, including the formation of apoptotic bodies and phagocytosis (Kerr et al. 1972). Mechanistically, apoptosis compromises intrinsic and extrinsic pathways as well as the perforin/granzyme pathway (Fig. 1.2) (Elmore 2007). The main enzymes involved in these pathways are caspases acting as cysteine-aspartic proteases. These are synthesised in cells as inactive zymogens (procaspases) and are activated in response to apoptotic stimuli. So far, ten major caspases have been identified and due to their functions classified in initiator (2, 8, 9, 10), effector (3, 6, 7) and inflammatory (1, 4, 5) caspases. Upon activation, a proteolytic cascade is initiated for degradation of intracellular content (Cohen 1997, Rai et al. 2005, Elmore 2007).

Initiation of the extrinsic pathway occurs through the interaction of respective ligands with transmembrane receptors, so-called death receptors, resulting in recruitment of cytoplasmic adaptor proteins (Elmore 2007). The best characterised ligand/death receptor couples are Fas ligand (FasL)/Fas receptor (FasR) and tumour necrosis factor (TNF) α/TNF receptor (TNFR) 1 recruiting the adaptor proteins Fas-associating death domain-containing protein (FADD) and TNFR1-associated death domain protein (TRADD), respectively. To the latter, FADD and receptor-interacting serine/threonine-protein kinase (RIP) are binding upon activation. FADD contains a C-terminal death domain (DD), responsible for binding to death receptors, and a N-terminal death effector domain (DED), whereof procaspase 8 is binding resulting in the formation of a death inducing signalling complex (DISC) (Kischkel et al. 1995, Cohen 1997, Elmore 2007, Fu et al. 2016). This complex leads to autocatalytic activation of procaspase 8, followed by the activation of effector caspases that perform their proteolytic work (Chang and Yang 2000, Elmore 2007). In addition, effector caspases activate endonucleases and further proteases leading to the degradation of nuclear material as well as proteins. Chromatin condensation can be mediated by caspase 3 dependent activation of caspase-activated DNase (CAD) (Sakahira et al. 1998, Chang and Yang 2000). Intracellular material including RNA, DNA and proteins is enclosed in apoptotic bodies (Xu et al. 2019). The translocation of phosphatidylserine to the outer surface of the cell membrane functions as a recognition site for phagocytes to ensure a noninflammatory death (Fadok et al. 1992, Nagata 2018). A further mechanism to induce the execution phase of apoptosis is the perforin/granzyme pathway, particularly induced by cytotoxic T lymphocytes. Perforin, a glycoprotein from T cells, forms a transmembrane pore on the target cell causing a release of intracellular granules containing

granzyme A and B. Granzyme B can activate both initiator and effector caspases resulting in apoptosis. In contrast, granzyme A induces DNA degradation in a caspase independent manner (Adrain et al. 2005, Elmore 2007, Voskoboinik et al. 2015). The major type of apoptosis is the intrinsic pathway, also referred to as the mitochondrial pathway. Distinct stimuli induce alterations in the inner mitochondrial membrane resulting in pore formation and loss of mitochondrial membrane potential. These changes cause the release of pro-apoptotic proteins into the cytosol, such as cytochrome c and Smac/Diablo (Du et al. 2000, Verhagen et al. 2000, Wei et al. 2001, Gogvadze et al. 2006, Elmore 2007). In the presence of ATP, the apoptosome is formed consisting of cytochrome c, apoptotic protease activating factor-1 (Apaf-1) and procaspase 9 resulting in the activation of this caspase (Zou et al. 1999). Similar to caspase 8, the activation of caspase 9 induces the execution phase of apoptosis (Chang and Yang 2000, Elmore 2007).
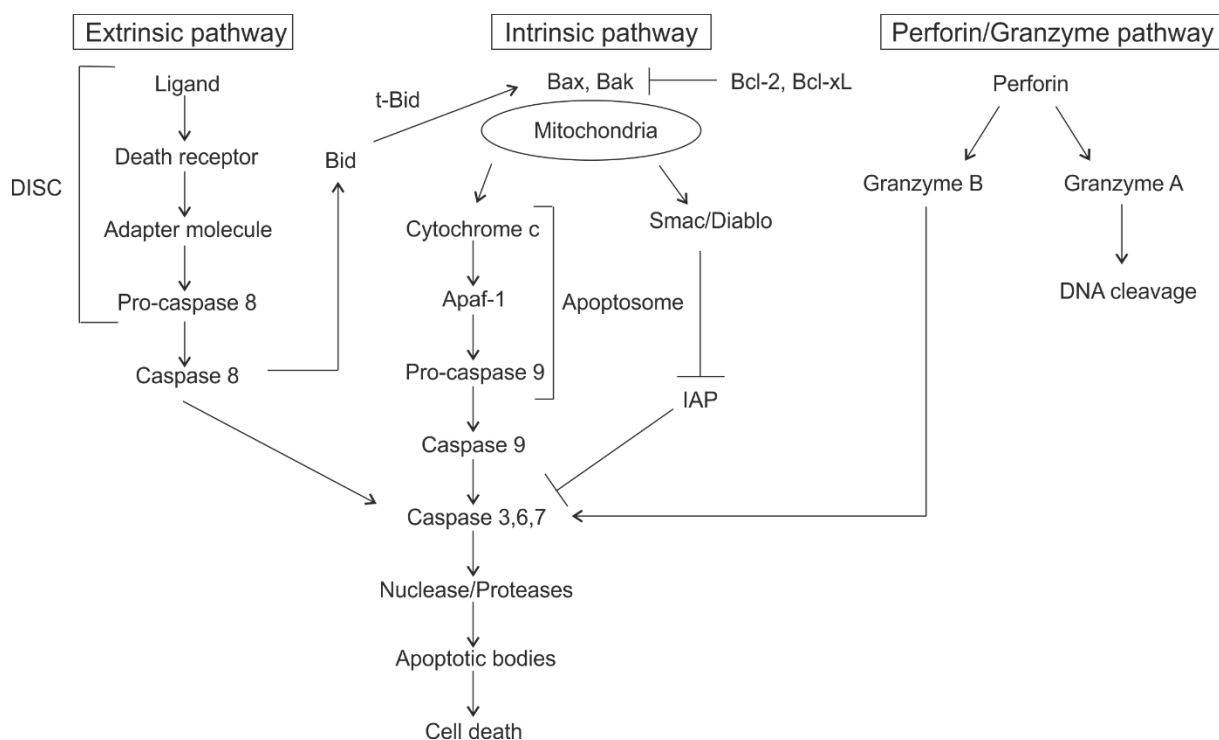
Fig. 1.2 Overview of apoptotic pathways.

The process of apoptosis is tightly regulated. With regard to the intrinsic (mitochondrial) pathway, members of the Bcl-2 family are the key regulator of this process (Singh et al. 2019). The *BCL-2* gene was first identified in lymphoma as an oncogene in B-cell malignancies (McDonnell et al. 1992). Members of the Bcl-2 protein family are grouped into three groups due to the appearance of Bcl-2 homology (BH) domains and functions (Fig. 1.3). The anti-apoptotic group including Bcl-2, Bcl-xL, MCL-1, Bcl-w, Bfl-1 contains all four BH domains. The pro-apoptotic proteins are subdivided into effector and BH3-only proteins. Bax, Bak and Bok belong to the first group and contain three to four BH domains. As the name indicates, BH3-

only proteins possess only the BH3 domain (Cory and Adams 2002, Vogler 2014, Opydo-Chanek et al. 2017, Montero and Letai 2018). In the presence of certain stressors, pro-apoptotic effector proteins oligomerize and translocate to the outer mitochondrial membrane resulting in mitochondrial outer membrane permeabilization (MOMP). The oligomerisation of Bak and Bax can be enhanced by activator BH3-only proteins, such as Bim and Bid (Letai et al. 2002, Montero and Letai 2018). Under normal conditions, anti-apoptotic proteins bind the monomeric form of effector proteins, thus, preventing MOMP. The interaction occurs through the hydrophobic pocket formed by BH domain 1, 2 and 3 of anti-apoptotic proteins and the BH3 domain of pro-apoptotic proteins (Sattler et al. 1997, Opydo-Chanek et al. 2017). Other members of BH3-only proteins so-called sensitizers facilitate apoptosis induction through competition for binding the hydrophobic groove of anti-apoptotic proteins (Letai et al. 2002, Montero and Letai 2018). A crosstalk between the extrinsic and intrinsic apoptotic pathway have been described via the BH3-only protein Bid. Upon activation of the extrinsic pathway, activated caspase 8 can cleave Bid resulting in a truncated form (t-Bid) which can translocate to the mitochondria and activate pro-apoptotic proteins like Bak (Korsmeyer et al. 2000, Zhao et al. 2010).
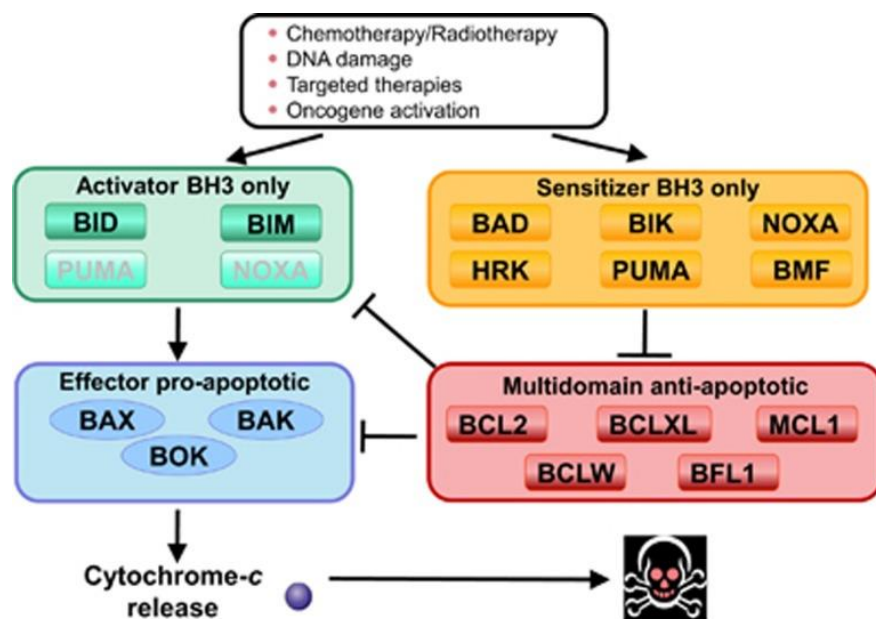
Fig. 1.3 Classification of Bcl-2 family protein members due to their function and appearance of BH domains. Taken from Montero and Letai, licensed under CC BY 4.0 (Montero and Letai 2018).

The balance between pro- and anti-apoptotic Bcl-2 family members is described by Korsmeyer's rheostat model. A shift to pro-apoptotic proteins results in apoptosis, whereas a shift towards anti-apoptotic proteins promotes cell survival which is accompanied by pathological alterations including cancer (Korsmeyer et al. 1993, Mohammad et al. 2015). The evasion of cell death is one of the hallmarks of cancer (Hanahan and Weinberg 2011). Concomitant by overexpression of anti-apoptotic proteins of the Bcl-2 family is often observed

in several cancers including lung, ovary, breast and gastric cancer as well as melanoma (Zhang et al. 2002, Yip and Reed 2008, Vogler 2014, Lee et al. 2019). For this reason, targeting these proteins offers new anti-cancer treatments. The use of antisense RNA was rejected by the Food Drug Administration (FDA) due to the lack of efficacy, but molecules mimicking the BH3 domain, so-called BH3 mimetics, entered preclinical and clinical trials demonstrating promising results (Vogler 2014, Merino et al. 2018, Han et al. 2019).

1.4.2 Necroptosis

For a long time, cell death was only divided into a programmed (regulated) cell death (apoptosis) and an uncontrolled (accidental) form called necrosis. But these two types only represent the two extremes of a cell death. Meanwhile, many other forms have been discovered that are also tightly regulated (D'Arcy 2019, Tang et al. 2019). One example is the programmed necrosis termed necroptosis (Degterev et al. 2005). Necroptosis exhibits similarities with both apoptosis with regard to mechanistic aspects and necrosis with respect to morphological characteristics (He et al. 2009, Christofferson and Yuan 2010, Gong et al. 2019). Mechanistically, a lot is known about the TNFR 1 induced necroptotic pathway being the prototype of necroptosis (Fig. 1.4), although other death receptors can initiate this pathway as well (Fulda 2013). After binding of TNF to TNFR1, a conformationally change in the receptor resulting in the recruitment of further factors, including TRADD, RIP1, TNF receptor associated factor (TRAF) and cellular inhibitor of apoptosis protein (cIAP), forms a so-called complex I (Micheau and Tschopp 2003, Vandenabeele et al. 2010, Gong et al. 2019). This complex induces NF-κB and MAPK signalling pathways to maintain cell survival (Fulda 2013). In this process, however, the ubiquitination status of RIP1 plays a crucial role (Ea et al. 2006, Liu et al. 2019). While RIP1 is normally polyubiquitinated (by cIAPs) in complex I finally promoting cell survival pathways (Bertrand et al. 2008), the deubiquitination of RIP1 through the deubiquitinase cylindromatosis (CYLD) forces the cell towards cell death (Moquin et al. 2013) as another complex will be formed. This cell death mediating complex II consists of TRADD, FADD, RIP1 and caspase 8 but lacking TNFR1 (Micheau and Tschopp 2003). Dependent on the activation status of caspase 8 either apoptosis or necroptosis is induced (Fritsch et al. 2019). In the first case, active caspase 8 initiates the activation of downstream caspase cascades resulting in an apoptotic cell death and the inactivation of RIP1 through cleavage preventing the induction of necroptosis at the same time (Lin et al. 1999). In case of non-functional caspase 8 due to genetic or pharmacological inhibition, RIP1 is phosphorylated through autophosphorylation leading to its activation (Degterev et al. 2008). The step is required for downstream (necroptotic) processes which was demonstrated by the use of the RIP1 inhibitor necrostatin-1 (Nec1) (Degterev et al. 2008, Cho et al. 2009). Subsequently, RIP3 is recruited and interacts with RIP1 through their RIP homotypic interaction motif (RHIM)

forming an amyloid structure named necrosome complex (Sun et al. 2002, Li et al. 2012, Liu et al. 2019). Hereinafter, downstream substrate such as mixed lineage kinase domain like pseudokinase (MLKL) are phosphorylated by RIP3 and gathered to the necrosome (Sun et al. 2012). In the execution phase of necroptosis, phosphorylated MLKL oligomerizes and translocates to the plasma membrane causing its permeabilization (Wang et al. 2014, Samson et al. 2020). As a consequence, endogenous molecules including damage-associated molecular patterns (DAMP) can be released, which trigger an immune response as well as inflammation and cell death (Martin 2016, Kearney and Martin 2017).
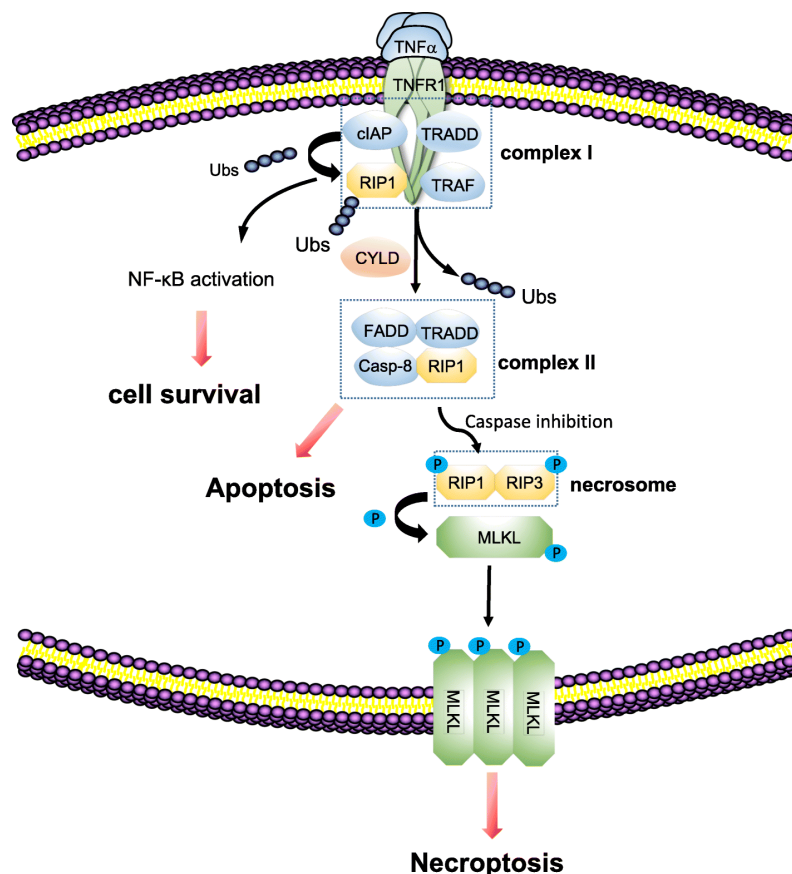
Fig. 1.4 Overview of the necroptotic cell death induced by TNFα. Taken from Gong et al., licensed under CC BY 4.0 (Gong et al. 2019).

While the physiological role of apoptosis in terms of development and cell homeostasis is well described, the role of necroptosis is not fully understood. Naturally occurring necroptosis has been shown mainly in the context of defence against viral and bacterial pathogens as well as in the induction of excitotoxicity linked with pathologies of neurodegeneration diseases (Christofferson and Yuan 2010, Chen et al. 2016, Bedoui et al. 2020) . With respect to efficient killing of pathogens, necroptosis may act as a back-up mechanism due to overcome resistance to apoptosis (Pearson and Murphy 2017). Furthermore, viral infections are associated with tumorigenesis. A possible beneficial role of necroptosis to prevent cancer development requires more studies (Chen et al. 2016). The relevance of necroptosis in cancer is discussed

controversially due to its dual role and further studies are necessary to fully understand its function. On the one hand, the release of inflammatory molecules resulting in a tumour microenvironment which may favour the tumour progression and metastasis. On the other hand, necroptosis can serve as protective mechanism against tumour development, especially via increasing the anti-tumour immunity as well as when apoptosis does not work properly (Su et al. 2016, Najafov et al. 2017, Gong et al. 2019, Liu and Jiao 2019). Combating cancer cells effectively is a major obstacle, particularly with regard to the rapid development of resistance to conventional anti-cancer drugs targeting the apoptotic pathway. In this context, necroptosis offers a new promising target for the development of new drugs to successfully treat cancer cells (Gong et al. 2019). Thus, necroptosis activates the immune system to combat the cancer cells as well as acts as back-up mechanism in apoptotic resistant tumour cells. However, targeting the necroptotic pathway is not suitable in all cancer cells due to different levels of RIP proteins (Su et al. 2016, Wu et al. 2020).

1.5 Autophagy

Autophagy describes the cellular degradation of endogenous components including proteins and organelles. The term meaning *"self-eating"* was created by Christian De Duve (Klionsky 2008). Three classes of autophagy have been identified: macroautophagy, microautophagy and chaperone-mediated autophagy. The mechanisms of the three pathways differ, but in principle they all serve the same purpose, namely the inclusion of cytoplasmic material with subsequent lysosomal degradation (Mizushima and Komatsu 2011). During microautophagy, small cytosolic components are engulfed by the lysosome through the invagination via the lysosomal membrane (Sahu et al. 2011). The chaperone-mediated autophagy based on the recognition of substrates having a KFERQ motif by chaperone proteins such as heat shock cognate (Hsc) 70. Binding is followed by translocation to the lysosome, where the import of the substrates is mediated through the transmembrane protein LAMP2A (Orenstein and Cuervo 2010). Macroautophagy is the major type of autophagy which hereinafter will be referred to as "autophagy". This process consists of several steps: induction, nucleation, maturation, fusion and degradation (Fig. 1.5). Numerous factors are involved in the respective steps demonstrating the complexity of autophagy (Chang 2020). The discovery of autophagy genes in yeast in the 1990s provided insight into the molecular mechanism of autophagy. The genes encoding these proteins as well as the proteins themselves are termed as ATG (**A**u**T**opha**G**y) (Klionsky et al. 2003). The regulation of autophagy in mammals requires several protein complexes acting in a hierarchical manner. Formation of autophagosomes starts with a double membrane structure (phagophore) near the endoplasmic reticulum (ER). The exact origin of the membrane has not been fully elucidated. In addition to the assumption that the ER membrane can be used directly, several studies indicate that membranes derived from the

Golgi, mitochondria and the plasma membrane are also involved (Hayashi-Nishino et al. 2009, Hailey et al. 2010, Ravikumar et al. 2010, Tooze and Yoshimori 2010, Mizushima and Komatsu 2011). The induction of autophagy in mammals is mediated by the ULK1 complex consisting of ULK1/2, ATG13, FIP200 and ATG101. In this context, FIP200 acts as scaffold protein for the assembly of ATG proteins. Subsequently, the class III phosphatidylinositol 3-kinase (PI3K) complex is gathered which is composed of VPS34, VPS15, Beclin 1 and ATG14L. VPS34 is required to phosphorylate phosphatidylinositol (PI) to phosphatidylinositol 3-phosphate (PI(3)P) through its kinase activity. This step is essential for the formation of the initial autophagosome structure (omegasome) (Axe et al. 2008, Chang 2020, Li et al. 2020). The subsequent elongation involves two ubiquitin like conjugation steps. ATG12-ATG5 conjugate mediated by ATG7 and ATG10 forms a complex with ATG16L1 acting as E3-like ligase. After proteolytic cleavage of microtubule-associated protein 1 light chain 3 beta (MAP1LC3B; LC3B) via ATG4, phosphatidyl-ethanolamine (PE) is conjugated to LC3B by the multiprotein complex. Lipidated LC3B, also named LC3 II, is integrated into the phagophore during elongation (Chang 2020, Li et al. 2020). The maturation step comprises the formation of a circular closed autophagosome enclosing cytoplasmic material. Subsequently, mature autophagosomes are trafficking to the perinuclear region, where primary lysosomes are predominantly located, and fuse with these resulting in the formation of an autolysosome. This process is mediated by members of the Rab family of small GTPases (Kimura et al. 2008, Wijdeven et al. 2016, Li et al. 2020). Finally, degradation takes place via lysosomal acidic hydrolases and separate the resulting degraded components can be reused again (Mizushima 2007).
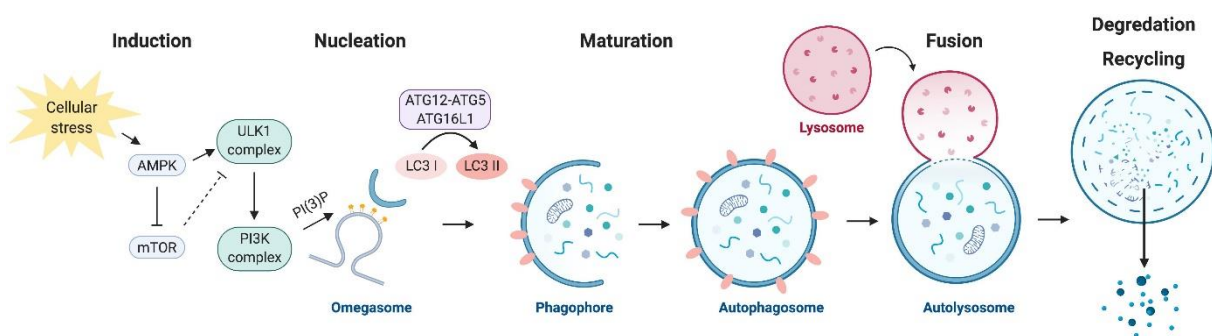
Fig. 1.5 Mechanism of macroautophagy in mammals . Taken from Chang et al., licensed under CC BY (Chang 2020).

Autophagy, as an evolutionarily conserved mechanism, is a fundamental cellular process to sustain homeostasis and immunity as well as to prevent diseases. In addition to the quality control in order to remove damaged proteins and organelles, autophagy serves to maintain energy levels during low-energy conditions, for example mediated by starvation. The pathway is induced by several stressors including oxidative stress, DNA damage, hypoxia and infection (Mizushima 2007, Mizushima and Yoshimori 2007, Mizushima and Komatsu 2011, Li et al. 2020). Defects in this tightly regulated process are associated with cancer, neurodegenerative

diseases and aging (Mizushima 2007, Mizushima and Komatsu 2011, Tran and Reddy 2020). The first link between autophagy and cancer was discovered through the identification of Beclin-1 as tumour suppressor protein (Yue et al. 2003). The role of autophagy in tumorigenesis is controversially discussed. On the one hand, prevention of tissue damage and maintenance of genome stability deals with tumour suppression properties, whereas autophagy supports tumour progression at late stages of carcinogenesis by promoting survival and resistance of cancer cells (Levine 2007, Li et al. 2020). The effect of autophagy with regard to tumour development or inhibition of tumour growth depends on the tumour microenvironment, the cancer type and stage as well as the genetic background (White 2012, Li et al. 2020).

1.6 BH3 mimetics

To overcome resistance of tumour cells acquired by upregulation of anti-apoptotic Bcl-2 proteins, small molecules have been developed to treat these cancer cells. The underlying mechanism of so-called BH3 mimetics is the antagonising of anti-apoptotic proteins by the release of pro-apoptotic proteins from their binding to anti-apoptotic proteins resulting in the induction of the intrinsic pathway of apoptosis (Zhang et al. 2007, Vogler 2014, Mohammad et al. 2015). BH3 mimetics include both peptides and non-peptide synthetic small molecules. The latter group comprises different putative Bcl-2 inhibitors already tested as single agents or in combination with other drugs in preclinical and clinical trials (Opydo-Chanek et al. 2017). ABT-737 is a synthetic acrylsulfonamide-based BH3 mimetic compound antagonising Bcl-2, Bcl-xL and Bcl-w (Oltersdorf et al. 2005, Konopleva et al. 2006). In addition to the potent single-agent activity in leukaemia and lymphoma cell lines, synergistic effects in combination with other drugs, such as the topoisomerase inhibitor topotecan and the spindle inhibitors vincristine or docetaxel, are observed in leukaemia and solid tumours (Oltersdorf et al. 2005, Konopleva et al. 2006, High et al. 2010, Oakes et al. 2012). Due to its poor bioavailability and low aqueous solubility, the use of ABT-737 is limited (Opydo-Chanek et al. 2017). Thus, new derivates have been developed like the analogue ABT-263 (navitoclax) which exerts similar activities and is available orally at the same time (Park et al. 2008, Tse et al. 2008, Lin et al. 2017). However, navitoclax tested as single drug or in combination induces thrombocytopenia (Opydo-Chanek et al. 2017). Based on this compounds, ABT-199 (venetoclax) was designed. It was the first BH3 mimetic approved by the Food and Drug Administration (FDA) for the treatment of patients with chronic lymphocytic leukaemia carrying a p17 deletion (FDA 2016, Opydo-Chanek et al. 2017). Meanwhile, venetoclax has been approved for further tumour treatments including acute myeloid leukaemia (FDA 2019). Obatoclax, a synthetic indolyldipyrromethene, represents another BH3 mimetic. This pan-Bcl-2 inhibitor shows promising results in tumour growth inhibition in xenograft mouse models of various cancer types (Li et al. 2008, Champa

et al. 2014). In contrast to synthetically produced BH3 mimetics, gossypol (GP) is a naturally occurring polyphenolic aldehyde from cotton seed plants (Adams et al. 1960). Even though it was originally tested as a male contraceptive, it is now being tested as an anti-cancer drug in preclinical and clinical phases (Wu 1989, Opydo-Chanek et al. 2017, Zeng et al. 2019). GP is described to be a pan-Bcl-2 inhibitor through interaction with Bcl-2, Bcl-xL, Bcl-2 and MCL1 (Kitada et al. 2003, Oliver et al. 2005, Lessene et al. 2008, Kang and Reynolds 2009). The natural GP is a ratio metric mixture consisting of (+) and (-) enantiomers. The bioavailable GP derivative AT101 contains only the GP (-) enantiomer and shows promising efficacy, particularly in combination with other drugs, in numerous tumour cell lines including melanoma, gastric cancer and non-small cell lung cancer (Ren et al. 2015, Wei et al. 2016, Opydo-Chanek et al. 2017). For example, B-Raf kinase inhibitor (vemurafenib) and anaplastic lymphoma kinase inhibitor (ceritinib) resistant A375 melanoma cells are sensitive to AT101 treatment (Janostiak et al. 2019).

In general, all BH3 mimetic molecules aim to activate the mitochondrial apoptosis pathway. However, also several off-target effects of these compounds are described in a tissue and context dependent manner. These include autophagy, ER-stress, necrotic cell death as well as cell cycle arrest (Zhong et al. 2012, Koehler et al. 2014, Opydo-Chanek et al. 2017, Sulkshane and Teni 2017). Relating to autophagy, anti-apoptotic Bcl-2 proteins interact not only with pro-apoptotic Bcl-2 proteins but also with Beclin-1 containing a BH3 domain required for the induction of autophagy (Liang et al. 1998, Oberstein et al. 2007). When Beclin-1 is bound to Bcl-2, this protein cannot contribute to the induction of autophagy through the PI3K complexes. Once Bcl-2 is scavenged by BH3 mimetic substances, released Beclin-1 may initiate autophagic processes (Pattingre et al. 2005). The development of BH3 mimetics offers a new approach in the fight against cancer used as single drug or in a combination treatment (Han et al. 2019). However, it has to be considered that the underlying mechanism possibly depends on the (cancer) cell type resulting in different efficacies and cell death pathways (Opydo-Chanek et al. 2017).

1.7 Aim of this thesis

Increased incidences of skin cancers including melanoma and non-melanoma skin cancer accompanied with growing resistance of tumour cells against conventional therapeutic drugs requires the development of new approaches to kill cancer cells effectively (Flaherty et al. 2012, Gracia-Cazaña et al. 2016, Luke et al. 2017). Not only the efficacy of an anti-cancer drug is pivotal but also its tolerability by the patients with regard to undesired adverse side effects (Oun et al. 2018, Songbo et al. 2019). The hallmarks of cancer summarize key features acquired for tumorigenesis and indicate potential attacking points of targeted therapies

(Hanahan and Weinberg 2011). Among them is the evasion of apoptosis by upregulating of anti-apoptotic proteins preventing the intrinsic pathway of apoptosis. BH3 mimetics have been developed to bind these proteins forcing tumour cells towards cell death. Thus, these compounds offer new therapeutic opportunities in the treatment of cancer (Kang and Reynolds 2009, Adams and Cory 2018). For that reason, different BH3 mimetics were tested in order to find an effective drug combining both a detrimental effect on tumour cells and a "beneficial" effect on normal (healthy) cells. The FDA-approved ABT-199 and the naturally occurring compound (±) gossypol (GP) were chosen to investigate their effect on both skin cancer cells A375 melanoma and SCL-1 carcinoma cells, and normal (healthy) cells such as normal human epidermal melanocytes (NHEM), normal human epidermal keratinocytes (NHEK) and normal human dermal fibroblasts (NHDF). The focus herein lies on working out concentration of the drug(s) being toxic for skin cancer cells. In this thesis, GP showed a selective toxic effect on those tumour cells and being non-toxic for normal (healthy) cells. Thereafter, the underlying molecular mechanism of GP should be studied with regard to the involved cell death pathways. Additionally, the effect of GP on mitochondria being involved in cell death should be addressed, as BH3 mimetics are described to interact with Bcl-2 proteins which are important in regulating mitochondria dependent signalling. In summary, the aim of the thesis is to study the effect of GP on tumour cells in comparison to normal (healthy) cells and to work out a possible selective mode of action.

2   Materials and Methods

2.1   Materials

All materials used in this study are listed below.

2.1.1   Substances

In this thesis, two different compounds belonging to the class of Bcl-2 inhibitors were tested: the pan-Bcl2 inhibitor gossypol (GP) and the specific Bcl2 inhibitor ABT-199.

2.1.1.1   Gossypol

(±) Gossypol (GP, CAS 303-45-7) was purchased from Abcam (Cambridge, UK). Its purity was >98% according to the manufacturer's specifications. GP was dissolved in DMSO (25 mM), aliquoted and stored at -80°C for up to one month. For treatment of the cells, 1:500 to 1:1000 working stocks were prepared in DMSO and the compound was directly added to the cells, unless otherwise stated.

2.1.1.2   ABT-199

ABT-199 (CAS 1257044-40-8) was obtained from Abcam (Cambridge, UK). According the manufacturer, the purity was >98%. ABT-199 was dissolved in DMSO (50 mM), aliquoted and stored at -20°C. Working stocks (1:500) in DMSO were used for treatment of the cells.

2.1.2   Cell lines

A375 – human malignant melanoma cell line

The A375 cell line (ATCC ® CRL-1619) originated from human, amelanotic cells of malignant melanoma, which was taken from a 54-year-old woman. The cells were obtained from the American Type Culture Collection (ATCC, Virginia, USA)

SCL-1 – human cutaneous squamous cell carcinoma cell line

The squamous cell carcinoma cell line consists of poorly differentiated human skin cells derived from the carcinoma of a 74-year-old woman (Boukamp et al. 1982). The cells were kindly obtained from Prof. Dr. Norbert Fusenig from the German Cancer Research Center (DKFZ, Heidelberg, Germany).

NHEM – normal human epidermal melanocytes

NHEM (C-12400) are normal human epidermal skin melanocytes derived from the foreskin of a juvenile donor. The cells were purchased from Promocell (Heidelberg, Germany).

NHEK – normal human epidermal keratinocytes

Primary normal human epidermal keratinocytes (NHEK, C-12001) derived from the epidermis of juvenile foreskin were from Promocell (Heidelberg, Germany).

NHDF – normal human dermal fibroblasts

NHDF (C-12300) are normal human dermal fibroblasts isolated from the dermis of juvenile foreskin which was also obtained from Promocell (Heidelberg, Germany).

2.1.3   Chemicals

2-Mercaptoethanol	Sigma, Taufkirchen
ABT-199	Abcam, Cambridge, UK
Acetic acid (100%)	Merck, Darmstadt
Acetone	VWR, Darmstadt
Acetonitrile (AcN)	VWR, Darmstadt
Agar	Sigma, Taufkirchen
Ammonium persulfate (APS)	Sigma, Taufkirchen
Bad Stabil ® Water Bath Stabilizer	neoLab, Heidelberg
Bafilomycin A_1	Sigma, Taufkirchen
Bovine serum albumin (BSA)	Sigma, Taufkirchen
Bromophenol blue	Merck, Darmstadt
Carbonyl cyanide 3-chlorophenylhydrazone (CCCP)	Sigma, Taufkirchen
Chloroquine diphosphate	Sigma, Taufkirchen
Clarity™ Western ECL substrate	BioRad, Munich
Coomassie © Brilliant Blue R250	Merck, Darmstadt
Dimethyl sulfoxide (DMSO)	Roth, Karlsruhe
Dimethyl sulfoxide (DMSO), BioUltra ≥99.5 (GC)	Sigma, Taufkirchen
D-mannitol	Roth, Karlsruhe
DMEM (low and high glucose)	Sigma, Taufkirchen
D-sucrose	Merck, Darmstadt

EDTA	Merck, Darmstadt
Ethanol, absolute	VWR, Darmstadt
Ethanol, denatured	Merck, Darmstadt
Fetal bovine serum (FBS)	PAA Laboratories GmbH, Pasching
Freezing Medium Cryo-SFM	PromoCell, Heidelberg
GeneJuice® Transfection Reagent	Merck, Darmstadt
GlutaMAX™	Gibco, Darmstadt
Glycerol	Roth, Karlsruhe
Glycine	Roth, Karlsruhe
Gossypol (GP, ab141050, CAS 303-45-7)	Abcam, Cambridge, UK
H_2DCFDA	Sigma, Taufkirchen
H_2O_2	Sigma, Taufkirchen
HBSS	Invitrogen, Karlsruhe
HCl	Merck, Darmstadt
HEPES	Sigma, Taufkirchen
Hoechst 33342 solution	Thermo Fisher Scientific, MA, USA
Kanamycin sulphate	Roth, Karlsruhe
Keratinocyte Medium *(Growth and Basal)*	PromoCell, Heidelberg
Keratinocyte Supplement Mix	PromoCell, Heidelberg
Lipofectamine RNAiMAX	Thermo Fisher Scientific, MA, USA
Melanocyte Medium *(Growth and Basal)*	PromoCell, Heidelberg
Melanocyte Supplement Mix	PromoCell, Heidelberg
Methanol	VWR, Darmstadt
Milk powder	Roth, Karlsruhe
Molecular Probes MitoTracker Green [FM]	Thermo Fisher Scientific, MA, USA
MTT 98%	Sigma, Taufkirchen
NaCl	Roth, Karlsruhe
NaOH	Roth, Karlsruhe

Necrostatin-1 (Nec1)	Cayman Chemicals, Michigan, USA
Normal Goat Serum (NGS)	Sigma, Taufkirchen
Opti-MEM™ I Reduced Serum Medium	Thermo Fisher Scientific, MA, USA
PageRuler™ Prestained Protein Ladder	Thermo Fisher Scientific, MA, USA
Paraformaldehyde (PFA)	Sigma, Taufkirchen
PBS	Sigma, Taufkirchen
Penicillin/Streptomycin	Biochrom, Darmstadt
ProLong™ Gold Antifade Mountant with DAPI	Thermo Fisher Scientific, MA, USA
Protease Inhibitor Cocktail	Sigma, Taufkirchen
Protein Assay reagents (A, B, S)	BioRad, Munich
ROTIPHORESE® Gel 40 (37:5:1)	Roth, Karlsruhe
SDS pellets	Roth, Karlsruhe
SDS ultra-pure	Roth, Karlsruhe
Seahorse XF DMEM medium, pH 7.4	Agilent Technologies, California, USA
Sodium Pyruvate	Sigma, Taufkirchen
Staurosporine	Sigma, Taufkirchen
Sulforhodamine B	Sigma, Taufkirchen
Super Signal™ West Femto Maximum Sensitivity Substrate	Thermo Fisher Scientific, MA, USA
TEMED	Roth, Karlsruhe
Tetramethylrhodamine methyl ester (TMRM)	Thermo Fisher Scientific, MA, USA
Trichloroacetic acid (TCA)	Sigma, Taufkirchen
Trifluoroaetic acid (TFA)	Merck, Darmstadt
Tris Pufferan	Roth, Karlsruhe
Triton-X-100	Sigma, Taufkirchen
Trypan blue stain (0.4%)	Gibco, Darmstadt
Trypsin-EDTA solution	Sigma, Taufkirchen
Tryptone enzymatic digest from casein	MP Biomedicals GmbH, Eschwege

Tween 20	Merck, Darmstadt
Western Blot Stripping Buffer	Thermo Fisher Scientific, MA, USA
Yeast Extract	Sigma, Taufkirchen
zVAD-(OMe-)-FMK	Santa Cruz Biotechnology, Heidelberg

2.1.4 Solutions and buffers

1x TBS-T	10% 10x TBS
	0.1% Tween
	add 1l dH$_2$O
10x TBS	0.5 M Tris
	1.5 M NaCl
	add 1l dH$_2$O
	pH 7.5
10x SDS running buffer	10 g SDS
	30.3 g Tris
	144.1 g glycine
	add 1 l dH$_2$O
12% running SDS gel	4.3 ml dH$_2$O
	3 ml ROTIPHORESE® Gel 40
	2.5 ml Tris (1.5 M, pH 8.8)
	100 µl 10% SDS
	100 µl 10% APS
	4 µl TEMED
15% running SDS gel	3.55 ml dH$_2$O
	3.75 ml ROTIPHORESE® Gel 40
	2.5 ml Tris (1.5 M, pH 8.8)
	100 µl 10% SDS
	100 µl 10% APS
	4 µl TEMED

4x SDS-PAGE sample buffer (Laemmli buffer)	40% glycerol 20% 2-mercaptoethanol 12% SDS 0.4% bromophenol blue add dH$_2$O
5% Stacking gel	3.53 ml dH$_2$O 720 µl ROTIPHORESE® Gel 40 650 µl Tris (1.5 M, pH 6.8) 50 µl 10% SDS 50 µl 10% APS 5 µl TEMED
Anode buffer 1	0.3 M Tris 10% (v/v) MeOH add 1 l dH$_2$O pH 10.4
Anode buffer 2	25 mM Tris 10% (v/v) MeOH add 1 l dH$_2$O pH 10.4
Blocking buffer (Western Blot)	5% milk powder or BSA in 1x TBS-T
Cathode buffer	25 mM Tris 10% (v/v) MeOH 40 mM glycine add 1 l dH$_2$O pH 9.4
Coomassie destaining solution	50% (v/v) MeOH 1% (v/v) acetic acid add dH$_2$O

Coomassie staining solution	0.05% (w/v) Coomassie Brilliant Blue
	20% (v/v) MeOH
	7.5% (v/v) acetic acid
	add dH$_2$O
LB agar	5 g tryptone
	5 g NaCl
	2.5 g yeast extract
	7.5 g agar
	add 500 ml dH$_2$O
	50 µg/ml kanamycin sulphate
LB medium	5 g tryptone
	5 g NaCl
	2.5 g yeast extract
	add 500 ml dH$_2$O
	pH 7.0
Mobile phase (HPLC)	90% (v/v) AcN
	10% (v/v) dH$_2$O
	1% (v/v) TFA
MTT incubation solution	10% MTT stock solution in incubation medium (DMEM without FBS, MBM, KBM)
MTT stock solution	5 mg/ml MTT in PBS
SDS lysis buffer	1% SDS
	0.1% Protease inhibitor cocktail
Seahorse Medium	supplemented with
	1 g glucose/l
	2 mM GlutaMAX™
	1% pyruvate
	pH 7.4

2.1.5 Consumables

Aluminum foil	VWR, Darmstadt
Autoclave tapes	VWR, Darmstadt
Beakers (different sizes)	VWR, Darmstadt
Bemis™ Curwood Parafilm™	Thermo Fisher Scientific, MA, USA
Cell culture plates (6-, 24-, 96-well)	Greiner Bio-One, Frickenhausen
Cell scraper	Greiner Bio-One, Frickenhausen
CELLSTAR® Tissue Culture Dishes *(3, 6, 10 cm)*	Greiner Bio-One, Frickenhausen
CELLSTAR® Tissue Culture Flask *(T-75, T-175)*	Greiner Bio-One, Frickenhausen
Centrifuge tubes	Greiner Bio-One, Frickenhausen
Coverslips (High Precision), 18 mm Ø, DHR3	Hartenstein, Würzbürg
Cryo tube 2 ml	Greiner Bio-One, Frickenhausen
Cuvettes	Sarstedt, Nümbrecht
Dispenser tips (1.25, 2.5, 5, 10, 12.5 ml)	VWR, Darmstadt
Disposable pipettes *(5, 10, 25 ml)*	Greiner Bio-One, Frickenhausen
Disposal bags	Sarstedt, Nümbrecht
Eppendorf Reagent Reservoir	Eppendorf, Hamburg
Falcon tubes (15 ml, 50 ml)	Greiner Bio-One, Frickenhausen
Filter paper	Bio-Rad, California, USA
Filter tips (10, 100, 300, 1250 µl)	Greiner Bio-One, Frickenhausen
Gas cartridges CV360	Roth, Karlsruhe
Gloves, nitrile	Ansell, Brussels, Belgium
Inoculating Loop	VWR, Darmstadt
Kleenex®	Satino Wepa, Arnsberg-Müschede
Mat Tek Glass bottom dishes	MatTek Corporation, Ashland, MA, USA
Measuring cylinder *(different sizes)*	VWR, Darmstadt
Microscope slide, 76 x 26 mm	Engelbreft, Edermünde
Microscope slides folder	VWR, Darmstadt

Novex Empty Gel Cassettes Mini 1.5 mm	Thermo Fisher Scientific, MA, USA
Pasteur pipette	Brand, Wertheim
PCR soft tubes 0.2 ml	Biozym, Oldendorf
Polyvinylidene difluoride (PVDF) membranes	GE Healthcare, Solingen
Seahorse XFe Flux Paks	Agilent Technologies, Santa Clara, California, USA

- Cell culture microplates
- Sensor cartridges
- Seahorse calibrant

Sterican®cannula (0.90x40 mm)	B. Braun, Melsungen
Sterile filter 0.2 µm	Sarstedt, Nümbrecht
Stirrers	VWR, Darmstadt
Tweezers	neoLab, Heidelberg
Vials (HPLC)	CS Chromatography Service, Langerwehe
Whatman paper	Bio-Rad, California, USA

2.1.6 Kits

Cell Meter™ Caspase 3/7 Activity Apoptosis Assay Kit *Blue Fluorescence*	AAT Bioquest, Sunnyvale, California, USA
Cell Meter™ Caspase 8 Activity Apoptosis Assay Kit *Blue Fluorescence*	AAT Bioquest, Sunnyvale, California, USA
Cell Meter™ Caspase 9 Activity Apoptosis Assay Kit *Blue Fluorescence*	AAT Bioquest, Sunnyvale, California, USA
DC™ protein assay kit	Bio-Rad, Feldkirchen
Human Lactate Dehydrogenase ELISA Kit	Abcam, Cambridge, UK
QIAprep Spin Miniprep Kit	Qiagen, Hilden
Seahorse XF Cell Mito Stress Test Kit	Agilent Technologies, California, USA

2.1.7 siRNA oligos

Control siRNA (4404021), Ambion	Thermo Fisher Scientific, MA, USA
Drp1 siRNA (ID19561, AM51331), Ambion	Thermo Fisher Scientific, MA, USA

2.1.8 Antibodies

The antibodies used in this work are listed below. For Western Blot, the primary antibodies were diluted 1:1,000 and the secondary antibodies 1:15,000 in blocking buffer. For immunostaining experiments, the primary antibodies were used at a dilution of 1:100 and the secondary 1:1,000 in 1% NGS.

2.1.8.1 Primary antibodies for Western Blot

anti-Bax (5023)	Cell Signaling Technology, MA, USA
anti-Bcl-2 (ab32124)	Abcam, Cambridge, UK
anti-Bcl-xL (54H6)	Cell Signaling Technology, MA, USA
anti-Beta actin (D6A8)	Cell Signaling Technology, MA, USA
anti-Beta tubulin (9F3)	Cell Signaling Technology, MA, USA
anti-Caspase 3 (ab32351)	Abcam, Cambridge, UK
anti-Drp1 (14647)	Cell Signaling Technology, MA, USA
anti-GAPDH (G8795)	Sigma, Taufkirchen
anti-GFP (11814460001)	Sigma, Taufkirchen
anti-Hexokinase II (C64G5)	Cell Signaling Technology, MA, USA
anti-LC3B (ab51520)	Abcam, Cambridge, UK
anti-MIC60 (ab110329)	Abcam, Cambridge, UK
anti-NDUFB4 (ab110243)	Abcam, Cambridge, UK
anti-PARP (9542)	Cell Signaling Technology, MA, USA
anti-Smac/DIABLO (15108)	Cell Signaling Technology, MA, USA
anti-SQSTM1/p62	Cell Signaling Technology, MA, USA
anti-TOM20 (11802-1-AP)	Proteintech, St. Leon-Rot

2.1.8.2 Secondary antibodies for Western Blot

HRP-conjugated rabbit anti-mouse IgG	Dako, Glostrup, Denmark
HRP-conjugated goat anti-rabbit IgG (111035144)	Dianova, Hamburg

2.1.8.3 Primary antibodies for Immunostaining

anti-phospho-RIP3 (Ser227) (D6W2T)	Cell Signaling Technology, MA, USA
anti-RIP3 (B-2) (sc-374639)	Santa Cruz Biotechnology, Heidelberg

2.1.8.4 Secondary antibodies for Immunostaining

Abberior STAR 635P goat anti-rabbit (far-red)	Abberior, Göttingen
Alexa Fluor 568 goat anti-mouse IgG (red)	Life Technologies, California, USA

2.1.9 Devices

µCuvette G 1.0	Eppendorf, Hamburg
8er Multichannel digital pipet	Eppendorf, Hamburg
Allegra® X-15R centrifuge	Beckman Coulter, Krefeld
Analytical balance TE1245	Sartorius, Göttingen
Autoclave Systec VX-95	Systec GmbH, Linden
BioSpectrometer	Eppendorf, Hamburg
Blotting apparatus (semi-dry)	Bio-Rad, Munich
Branson Sonifier 250	Emerson, Ferguson, USA
Centrifuge 5417C/5424R	Eppendorf, Hamburg
Fireboys	Integra Biosciences, Biebertal
FL Detector L7485	Merck Hitachi, Darmstadt
Freezer (-20°C)	Liebherr, Ochsenhausen
Freezer (-80°C)	Thermo Fisher Scientific, MA, USA
Fridges (+4°C)	Liebherr, Ochsenhausen
Fusion SL Advance gel documentation device	Peqlab, Erlangen

Gel champers XCell Sure Lock™, Novex Mini Cell	Invitrogen, Karlsruhe
Heating block	Peqlab, Erlangen
Heraeus Megafuge 16R Centrifuge	Thermo Fisher Scientific, MA, USA
Heraeus Sepatech Labofuge Ae	Thermo Fisher Scientific, MA, USA
HERAtherm Incubator	Thermo Fisher Scientific, MA, USA
HPLC Auto-Sampler L2200	Merck Hitachi, Darmstadt
HPLC Degasser 2004	VWR, Darmstadt
HPLC L4250 UV-VIS Detector	Merck Hitachi, Darmstadt
HPLC pump L6200A	Merck Hitachi, Darmstadt
Incubator	Thermo Fisher Scientific, MA, USA
Infors HT Multitron Pro Incubator	Infors, Einsbach
Laboratory balance	Sartorius, Göttingen
Leica SP8 confocal microscope	Leica Mikrosysteme Vertrieb GmbH, Wetzlar
Magnetic stirrer	J&K IKAMAG®RCT, Staufen
Microscope Nikon Eclipse Ts2	Nikon, Tokio, Japan
Microtiter Plate Reader FLUOstar OPTIMA	BMG Labtech, Ortenberg
Microtiter Plate Reader Tecan infinity M200 pro	Männedorf, Switzerland
Milli-Q® Integral water treatment	Millipore, Schwalbach
Neubauer counting chamber	Brand, Göttingen
PerkinElmer Spinning Disk	PerkinElmer Corporation, Waltham, MA, USA
pH meter	Hanna Instruments, Kehl
Photometer Ultrospec 1000/3000	Pharmacia Biotech, Freiburg
Pipetboys	Integra Biosciences, Biebertal
Pipettes	Eppendorf, Hamburg
Powersupplier Consort EV265	Sigma, Taufkirchen
SDS-PAGE pocket spacer (1.5 mm), Novex	Thermo Fisher Scientific, MA, USA

Seahorse XFe96 analyser	Agilent Technologies, California, USA
Shaker DOS-10L	neoLab, Heidelberg
Shaker Polymax 1040/Rotamax 120	Heidolph Instruments, Schwabach
Shaker Vibrax VXR basic	VWR, Darmstadt
Shaking water bath GFL 1083	GFL, Burgwedel
SpeedVac	Thermo Fisher Scientific, MA, USA
Stepper	Eppendorf, Hamburg
Sterile bench Clean Air	Thermo Fisher Scientific, MA, USA
Supelco pKb 100 (250 x 4.6 mm) column (HPLC)	Supelco, Sigma, Taufkirchen
Water bath Aqualine AL 250	Lauda, Königshofen

2.1.10 Software

Agilent Seahorse Wave Desktop software

ChemDraw Professional 16.0

Corel Draw 2017

FusionCapt Advance software

Graph Pad Prism 5

FIJI/Image J

Microsoft Office 2019

2.2 Methods

All methods used in this work are described below.

2.2.1 Cell culture

The cells were cultured in growth medium in a humified atmosphere (37 °C in 5% CO_2). The composition of the growth medium depended on the cell type and is listed in Tab. 2.1. For cultivation, cells were seeded in 75 or 175 cm² flasks. The growth of the cells was monitored using a microscope. After reaching subconfluence (70-80% confluence), cells were passaged for further experiments. For that, cells were washed once with PBS and incubated with 3 ml trypsin-EDTA-solution for 5 to 10 min at 37°C in 5% CO_2. For trypsination of normal human

epidermal melanocytes (NHEM) and normal human epidermal keratinocytes (NHEK), trypsin solution was diluted in PBS (1:1 ratio). After complete detachment of the cells, 7 ml growth medium was added to stop the reaction and the cell suspension was transferred to a 15 ml tube. For reduction of trypsin concentration, NHEM and NHEK were centrifuged at 500 x g for 5 min and resuspend in fresh growth medium. The cell number was determined using a Neubauer counting chamber. Subsequently, the cells were seeded for experiments with appropriate cell numbers in plates and dishes, respectively, or further cultivated in flasks. Subconfluent cells (70-80% confluence) were used for all experiments, unless otherwise stated. For treatment of the cells, cells were washed once with PBS and incubation medium was added (Tab. 2.1). The substances were directly added to the cells.

Tab. 2.1 Cell culture condition of all cell lines used in this thesis. Growth medium was used for cultivation and incubation medium for treatment, unless otherwise stated. *DMEM* (Dubecco's Minimun Eagle Medium), *LG* (low glucose), *HG* (high glucose), *MGM* (Melanocyte Growth Medium), *MBM* (Melanocyte Basal Medium), *KGM* (Keratinocyte Growth Medium), *KBM* (Keratinocyte Basal Medium)

Cell line	Growth medium	Supplements	Incubation medium	Supplements
A375 **SCL-1**	LG DMEM	10% FBS Streptomycin (100 µg/ml) Penicillin (100 U/ml) GlutaMAX™ (2 mM)	HG DMEM	Streptomycin (100 µg/ml) Penicillin (100 U/ml) GlutaMAX™ (2 mM)
NHEM	MGM	Supplement Mix Streptomycin (100 µg/ml) Penicillin (100 U/ml)	MBM	Streptomycin (100 µg/ml) Penicillin (100 U/ml)
NHEK	KGM	Supplement Mix $CaCl_2$-Solution (0.5 M) Streptomycin (100 µg/ml) Penicillin (100 U/ml)	KBM	Streptomycin (100 µg/ml) Penicillin (100 U/ml)
NHDF	LG DMEM	10% FBS Streptomycin (100 µg/ml) Penicillin (100 U/ml) GlutaMAX™ (2 mM)	LG DMEM	Streptomycin (100 µg/ml) Penicillin (100 U/ml) GlutaMAX™ (2 mM)

2.2.1.1 Cryopreservation and revitalisation

For long term storage, cells were frozen in cryopreservation medium and stored at -80°C or liquid nitrogen. Subconfluent cells growing in 175 cm² flasks were detached using a trypsin-EDTA solution as described in 2.2.1. After that, the cell suspension was centrifuged at 1000 x g for 5 min at 4°C. The pellet was resuspended in freezing medium with a density of $1x10^6$ cells/ml and transferred in cryotubes. The freezing medium for A375, SCL-1 and NHDF consisted of low glucose DMEM supplemented with 20% FBS and 5% DMSO. For NHEM and NHEK, Cryo-SFM medium was used.

For revitalisation, frozen cells were thawed for 2 min at 37°C in a water bath and diluted with 1 ml fresh growth medium. The suspension was transferred into a 75 cm² flasks containing 15 ml medium and incubated in a humidified atmosphere (37°C, 5% CO_2). Depending on the time required for the cells to adhere, the medium is changed after 6 to 24 h in order to remove residues of DMSO. Before the freshly thawed cells were used for experiments, they were passaged at least once.

2.2.1.2 Mycoplasma test

To guarantee robust and reliable data, it is important to perform all experiments under sterile conditions. In order to regularly monitor the cell cultures for contamination, the mycoplasma test was performed at frequent intervals. Mycoplasma are bacteria lacking a cell wall and cause biochemical alteration in host organisms. It has been reported that contaminated cell cultures can lead to experimental artifacts and false results (Stanbridge 1971, Pisal et al. 2016).

To ensure a contamination free cell culture, cells were seeded onto coverslips in a 3 cm dish and grown to subconfluence. After that, cells were fixed with ice cold MeOH for 1 h at 4°C and washed twice with PBS. To fix the coverslips on the microscopic slides, one drop of ProLong™ Gold Antifade Mountant with DAPI was used. DAPI is a fluorescent dye which labels DNA (Coleman and Coleman 1980). In presence of mycoplasma, smaller nuclei would be detected in addition to the nucleus of the cells used in the experiments. The cells were monitored using fluorescence microscopy. No contamination with mycoplasma was detected at any time during this thesis.

2.2.2 Cell viability assays

To investigate whether the substances used in this thesis show an effect on cell viability in different cells, two different methods were chosen as toxicity screening of the compounds. On the one hand, the MTT assay based on an enzymatic reaction and on the other hand, the SRB assay based on the staining of total protein amount were used.

2.2.2.1 MTT assay

The MTT assay is a quantitative and colorimetric assay to determine the cell viability based on the metabolic activity of living cells. The activity of mitochondrial dehydrogenase which catalyses the conversion from yellow MTT to an insoluble purple formazan dye can be measured by absorbance (Mosmann 1983). The reaction scheme is shown in Fig. 2.1.
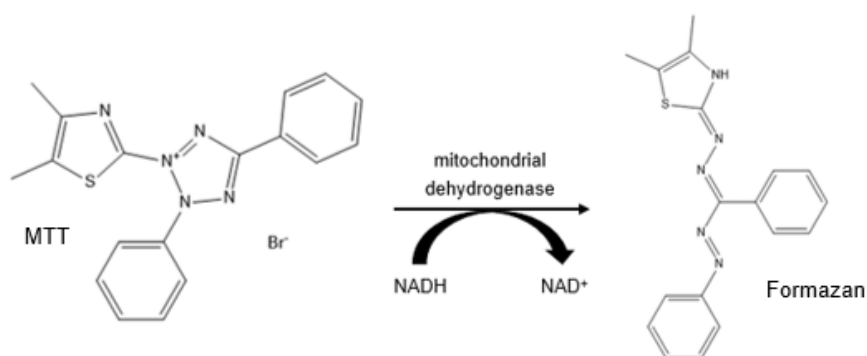
Fig. 2.1 MTT assay. Reaction scheme of the reduction of a yellow tetrazolium salt (MTT) to insoluble purple formazan by mitochondrial dehydrogenase activity.

Here, subconfluent cells were treated with a variety of substances at different concentration for different time points in 24-well plates. A solvent control served as negative controls, 2 mM H_2O_2 as positive control. Technical triplicates were used for each experiment. After incubation, cells were washed once with PBS and MTT solution (0.5 mg/ml) was directly added to the cells which were incubated for different time points depending on the cell line at 37 °C in 5% CO_2. The incubation medium as well as the incubation time of each cell line are listed in Tab. 2.2. Following, MTT was removed and the cells were washed one time with PBS. DMSO (0.5 ml/well) was added for formazan extraction and the absorbance was measured at 570 nm with a plate reader. For the evaluation, the background was subtracted and the mock-treated control of each experiment was set at 100%.

Tab. 2.2 Incubation medium and time for the MTT assay. *DMEM* (Dubecco's Minimun Eagle Medium), *LG* (low glucose), *HG* (high glucose), *MBM* (Melanocyte Basal Medium), *KBM* (Keratinocyte Basal Medium).

Cell line	Incubation medium	Incubation time of MTT (h)
A375	HG DMEM without FBS	0.5
SCL-1	HG DMEM without FBS	0.75
NHEM	MBM	2
NHEK	KBM	1
NHDF	LG DMEM without FBS	2

2.2.2.2 SRB assay

The sulforhodamine B (SRB) assay is also a quantitative and colorimetric assay for an indirect determination of cell viability. It was performed in this work to validate the results of the MTT assay. The principle is based on pH dependent staining of total protein with the dye SRB containing two sulfonic acid groups (Fig. 2.2) which can bind to basic amino acids residues under mildly acidic conditions and dissociate under basic conditions (Skehan et al. 1990, Maydt et al. 2013).
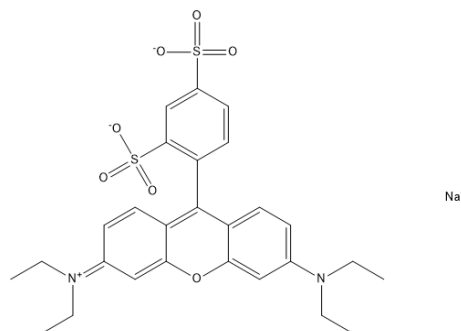
Fig. 2.2 Structure of sulforhodamine B.

Like the MTT assay, the SRB assay was carried out in 24-well plates and incubation with the test compounds was performed analogously. After washing with PBS and fixation with 0.5 ml 10% (w/v) cold trichloroacetic acid solution for 1 h at 4 °C, cells were washed five times with dH_2O and dried at RT. For the staining, cells were incubated with 0.3 ml 0.4% SRB dissolved in 1% acetic acid for 15 min at RT, washed five times with 1% acetic acid quickly and dried at RT. The dye was extracted with 0.4 ml unbuffered Tris-Base per well (10 mmol/l, pH 10.5) by gently rotation for 5 min. The absorbance was measured at 492 and 620 nm using a plate reader. For the analysis, the background values at 620 nm were subtracted from the values at 492 nm. Cell viability of control was set at 100%.

2.2.2.3 Determination of IC$_{50}$ values

The inhibitory concentration (IC) 50 value represents the concentration at which a compound exerts half of its maximal effect. The smaller the value, the stronger the effect of the compound on the cells. To compare the effect of GP between skin cancer cells and normal (healthy) cells regarding cell viability, the IC_{50} values were determined. IC_{50} values of GP treated cells were calculated by non-linear curve fit analysis using Graph Pad Prism software with $R^2 > 0.8$ and P (run tests) as parameter of goodness-of-fit.

2.2.3 Extra- and intracellular measurement of GP (HPLC)

High Performance Liquid Chromatography (HPLC) is an analytical method which is able to detect and quantify substances under certain settings including stationary and mobile phase as well as detection wavelength. In this study, two questions were addressed. On the one hand, the stability of GP in cell culture medium was investigated and on the other hand, the intracellular uptake of GP was determined.

2.2.3.1 Stability of GP in cell culture medium

To measure the stability of GP in medium used for the treatment of the cells, GP dissolved in DMSO was diluted in water and different medium including DMEM and MGM. After incubation of GP in a cell-free system for different time points, 50 µl was immediately injected. Acetonitrile (AcN) served as control. The experiments were performed using a Supelco pKb 100 (250 x 4.6 mm) column isocratically with a mobile phase consisting of AcN/water/trifluoroacetic acid (90/10/0.1, v/v/v) pumped at a flow rate of 1.0 ml/min. The detection was made at 254 and 367 nm, respectively, with a retention time of GP around 5 min (Fig. 2.3). GP concentrations were quantified using a standard curve. The concentration of GP diluted in AcN was set at 5 µM (100%) at the first measurement point.
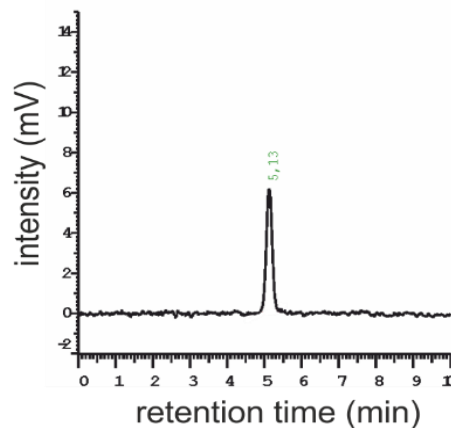
Fig. 2.3 Representative chromatogram of HPLC analysis.

2.2.3.2 Intracellular GP content

For measurement of the cellular uptake of GP, cells were grown to subconfluence in Ø 10 cm culture dishes and treated with 5 µM GP for different time points. After two wash steps, cells were harvested in 2 ml PBS and centrifuged at 500 x g for 8 min at 4°C. After removal of the supernatant, cells were washed with PBS once and centrifuged again (5,000 x g for 6 min at 4°C). Subsequently, the cell pellets resuspended in 150 µl AcN were mixed and centrifuged at 20,000 x g for 5 min at 4°C. The HPLC conditions are mentioned above. For analysis, 50 µl of

the extract were injected. To quantify the protein amount of each sample, the solvent residue was evaporated and the cell pellet was solved in SDS lysis buffer. After sonication, protein concentrations were determined by the DC^{TM} Protein Assay Kit in accordance with the manufacturer's instructions. For quantification of the intracellular GP content, the measured concentration by HPLC was set in relation to the protein amount of each sample. The percentage of detectable GP was estimated by calculating the amount of GP measured at the first measurement point (t=15 min) in relation to the total amount of GP added extracellularly.

2.2.4 Mitochondrial membrane potential (ΔΨ$_m$)

Mitochondrial integrity plays an important role to maintain several processes within the cells. One key parameter is the mitochondrial membrane potential (ΔΨ$_m$) (Tilokani et al. 2018). To assess ΔΨ$_m$, cells were seeded on glass bottom dishes until achievement of 50% confluence. Subsequently, cells were mock-treated and treated with 2.5 µM GP for 2 and 4 h. Carbonyl cyanide m-chlorophenyl hydrazine (CCCP) at a concentration of 10 µM for 2 h served as positive control due to its functions as uncoupler of oxidative phosphorylation (Leblanc 1971). Hereinafter, cells were washed one time with PBS followed by the addition of 100 nM tetramythelrhodamine methyl ester (TMRM) and 100 nM MitoTRACKER™ for 30 min at 37°C. After a further washing step with PBS, 2 ml of fresh incubation medium was added and cells were analysed with a spinning disc confocal microscope. The weakening of fluorescence signal of TMRM induced by several stressor, such as apoptosis stimuli, compared to control cells indicate a loss of ΔΨ$_m$ (Scaduto and Grotyohann 1999, Creed and McKenzie 2019). The quantification of fluorescence intensity was performed using Image J. The ΔΨ$_m$ is defined as quotient of TMRM and MitoTRACKER™. The mock-treated control was set at 100%.

2.2.5 Mitochondrial fragmentation

To assess the mitochondrial morphology, cells were treated as described in 0. For evaluation, MitoTRACKER™ images were used. Quantification was performed using at least 30 cells per sample and according to Duvezin-Caubet et al. (Duvezin-Caubet et al. 2006): *tubular* (at least one mitochondrial tube ≥5 µm), *intermediate* (at least one tubule ≥0.5 µm and ≤5 µm) and *fragmented* (no tubules ≥0.5 µm).

2.2.6 Fluorescent measurement of H$_2$O$_2$ using HyPer and SypHer

For measuring intracellular H$_2$O$_2$ levels, the redox sensor HyPer was used which contains a H$_2$O$_2$ sensing domain (OxyR) and a circularly permuted Yellow Fluorescence Protein (cpYFP) resulting in a change of fluorescence spectrum in the presence of H$_2$O$_2$. SypHer serves as

negative control as a mutation in the OxyR domain leads to redox insensitivity (Bilan and Belousov 2016, Booth et al. 2016, Booth et al. 2016).

Cells were seeded onto glass bottom dishes and were transfected using GeneJuice with 1 µg of the following plasmids: mito HyPer (mitochondrial matrix targeted), mito SypHer (mitochondrial matrix targeted, HyPer (cytosolic) and SypHer (cytosolic). After 8 h, cells were treated with 2.5 µM GP or mock-treated for further 16 h until microscopy. Imaging and quantification were performed as described earlier (Haasler et al. 2021). Briefly, live-cell fluorescence analysis was performed by Dr. Arun Kondadi using Leica SP8 confocal microscope. Instrument's settings include 93x glycerol objective (N.A. =1.3) at 2x zoom at 37°C and 5% CO_2. Single optical plane images were obtained by excitation at 488 and 405 nm and emission channel between 495 and 545 nm. For validation of the experiment, 100 µM H_2O_2 was added as positive control to the cells and directly imaged. For quantification of the ratio at 488 and 405 nm, Fiji software was used (custom written macro). The analysis of the data was performed by Thanos Tsigaras. Cytosolic and matrix-targeted HyPer and SypHer plasmids were a kind gift from Prof. György Hajnóczky (Thomas Jefferson University, Philadelphia, USA). The fluorescence based H_2O_2 measurements were performed at the Centre for Advance Imaging (CAi), Heinrich Heine University Düsseldorf.

2.2.7 *Intracellular ROS measurement (DCF assay)*

The formation of intracellular reactive oxygen species (ROS) was measured by 2',7'-dichlorodihydrofluorescein diacetate (H_2DCF-DA). The principle is based on the entering of the cell permeable substance which is intracellularly cleaved by esterases. The formed H_2DCF can be further oxidized by ROS to the fluorescent DCF which can be measured by fluorescence (Chen et al. 2010). The assay was performed in 24-well plates and technical triplicates were used for each experiment. Cells were grown to subconfluence and treated with 100 µM H_2DCF-DA in Hanks' Balances Salt Solution (HBSS) for 30 min at 37°C in a humified atmosphere. After that, they were washed twice with HBSS and treated with different concentrations of GP or mock-treated. H_2O_2 at a concentration of 2 mM served as positive control. As components of DMEM were described to catalyse the production of H_2O_2, HBSS medium was chosen to avoid possible interferences (Brubacher and Bols 2001, Boulton et al. 2011, Tetz et al. 2013). The DCF fluorescence measurement was started directly after adding the substances with a plate reader in 5 min intervals (ex: 485 nm, em: 520 nm). For quantification, the basal ROS level was subtracted from the amount of ROS measured after 90 min. Mock-treated control was set at 1.

2.2.8 Caspase activity assay

Caspase activity is one of early key events occurring in the process of apoptosis within cells (Cohen 1997, Elmore 2007). To investigate whether the substances induce apoptosis, caspases activity assays were performed according to the manufacturer's specification. In principle, a selective substrate for the used caspase was added to the cells which can be cleaved by active caspases. The formation of the fluorogenic product was fluorometrically measured and an increase correlated with the activation of caspases upon apoptosis. To distinguish between intrinsic and fluorometrically extrinsic apoptosis, both initiator caspases 8 and 9 were analysed as well as the effector caspase 3/7 functioned as point of no return in the apoptotic pathway.

In this thesis, cells were grown to subconfluence in 96-well plates and incubated with different concentrations of GP or mock-treated for 6 and 24 h, respectively. Staurosporine (Sts) at a concentration of 20 µM served as positive control. Technical duplicates were used for each experiment. After that, the substrate caspase working solutions (3/7, 8 or 9) were prepared and added for further 1 h. As control for a caspase dependent mechanism, the inhibitor zVAD-(OMe)-FMK was added 10 min prior to the end of the incubation time to prevent the cleavage of the substrate. Cell-free wells served as background. Subsequently, the fluorescence was measured using a plate reader under different emission and excitations wavelengths dependent on the caspase (Tab. 2.3). For quantification, the background values were subtracted, the mock-treated control was set at 1 and the treatment in relation to control.

Tab. 2.3 Experimental settings to measure different caspase activities .

Component	Excitation	Emission	Cut off
Caspase 3/7	360 nm	470 nm	420 nm
Caspase 8	370 nm	450 nm	420 nm
Caspase 9	375 nm	435 nm	420 nm

2.2.9 Preparation of cell lysate

Cells were grown to subconfluence in cell culture dishes in different sizes dependent on the experiment (Ø 3, 6, 10 cm) and treated with different substances for various time points. Subsequently, the supernatant was collected in a 10 ml falcon, cells were detached by a cell scraper and transferred to the falcon. To detach all cells from the dish, it was washed with 5 ml PBS. After centrifugation at 500 x g for 5 min at 4°C, the pellet was washed with 500 µl PBS, transferred into a fresh 2 ml tube and centrifuged again at 14,000 x g for 10 min at 4°C. After that, the supernatant was discarded and the pellet was lysed in an appropriate volume of SDS

lysis buffer according to the size of the pellet. The samples were stored at -20°C until further use.

2.2.10 Determination of protein concentration according to Lowry

The protein quantification of the lysed cell samples was based on the principle of Lowry using the DC™ protein assay kit in accordance to the manufacturer's instructions with minor modifications. The principle of the protein measurement with the folin phenol reagent was described by Lowry in 1951 (Lowry et al. 1951). First, copper (II) ions are complexed by peptide bonds to form blue dye complexes in alkali named Biuret reaction. Secondly, copper (II) ions are reduced to copper (I) ions, which then convert the reduction of yellow phosphomolybdic-phosphotungstic reagent to molybdenum blue. The resulting blue coloration was measured at 750 nm using a photometer.

To measure the protein amount, 10 µl of each sample was incubated with 100 µl reagent A' consisting of reagents A and S (50:1, v/v) and 750 µl reagent B in a plastic cuvette for 15 min in the dark. Subsequently, the optical density (OD) was photometrically measured and the amount of protein was calculated using a protein standard curve of bovine serum albumin (BSA, Fig. 2.4).
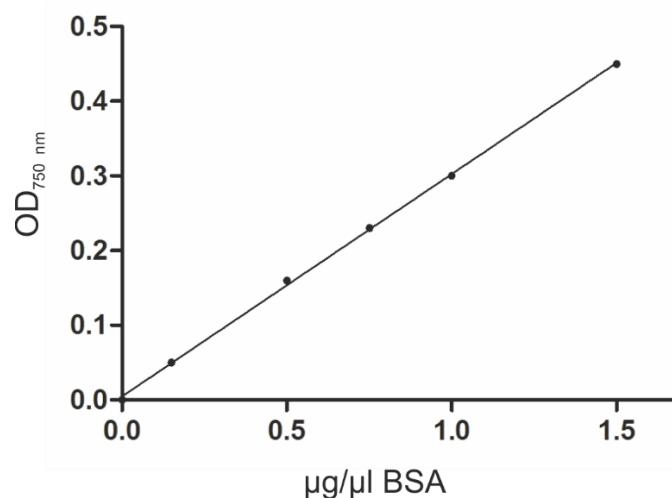
Fig. 2.4 BSA protein standard curve.

2.2.11 SDS PAGE and Western Blot

Sodium dodecyl sulfate polyacrylamide gel electrophoresis (SDS PAGE) is a variant of gel electrophoreses for the separation of a cell lysate in an electric field developed by Laemmli (Laemmli 1970). The charge of the proteins is masked by adding negatively charged SDS, which binds to these (Takagi et al. 1975). Moreover, the addition of 2-mercaptoethanol and heating of the samples lead to the linearisation of the proteins. Thereby, the separation of the

proteins is only according to molecular mass. The polymerization of the gel is initiated by free radicals and consists of acrylamide and bisacrylamide forming a defined pore size dependent on the applied concentration (Blatter et al. 1972). The SDS PAGE is a discontinuous gel electrophoresis based on a Tris-HCl/Tris-glycerol buffer system (Laemmli 1970). For that, two different density polyacrylamide gels were used. A wide pore stacking gel (5%) which enables the collection and concentration of all proteins at the interface to a narrow-pored running SDS gel (12 and 15%) in order to ensure a simultaneous entry of the proteins into it. In the running gel, the separation of the proteins takes place in accordance to their size. A constant current of 20 mA per gel was applied for the stacking gel and increased up to 40 mA for the running gel. To determine the size of the proteins, a prestained protein ladder consisting of proteins of defined size was used.

For immobilization of the proteins on a solid matrix, they were blotted onto a polyvinylidene difluoride (PVDF) membrane by electroblotting. The semi-dry transfer consisted of a horizontal transfer sandwich which is set between a cathode and anode (Fig. 2.5). The filter papers were equilibrated in anode and cathode buffer, respectively, as well as the PVDF membrane was activated in 100% MeOH. The transfer is performed at constant current (75 mA per gel) for 1.5 h.
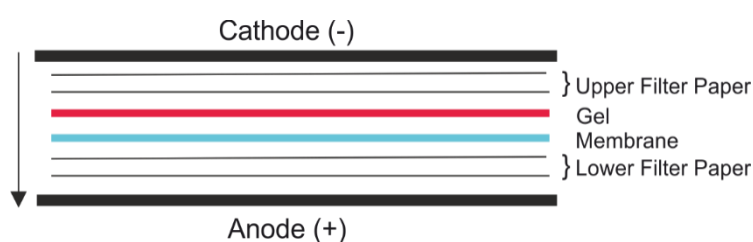
Fig. 2.5 Scheme of semi-dry transfer. The arrow shows the direction of transfer.

For visualization the proteins of interests, immunoblotting was performed. After electrophoretic transfer onto a PVDF membrane, this was blocked with blocking buffer (5% (w/v) BSA or 5% (w/v) milk powder in 1x TBS-T) to saturate unspecific binding sites. After that, the membrane was incubated with the first antibody (see 2.1.8) diluted in the blocking buffer (1:1,000) at 4°C while shaking overnight. All further steps were carried out with shaking at RT. After washing of the membrane thrice with 1x TBS-T for 15 min, the secondary antibody (see 2.1.8) was added in blocking buffer (1:15,000, 5% milk powder in 1x TBS-T) for 1 h. Subsequently, the membrane was washed three times with 1x TBS-T for 15 min. Since the secondary antibodies are coupled to Horseradish peroxidase (HRP), these could be detected by a chemiluminescence reaction (Zhang et al. 2018). For that, the membrane was treated with luminol/peroxidase solution (1:1). The principle is based on the oxidation of luminol to 3-aminophthalate by HRP resulting in a light signal monitored by the Fusion SL Advance gel documentation device. As the intensity of the signal is proportional to the amount of protein

bound, a semiquantitative determination of the protein was performed. Housekeeping genes (GAPDH, beta tubulin, beta actin) were used as internal loading controls and quantification of proteins was done using the FusionCapt Advance software.

2.2.12 Reuse of PVDF membranes

Dependent on the experiment, the expression level of more than one protein was addressed. For that purpose, the PVDF membrane was prepared for reuse. For removal of bound antibodies, stripping buffer was added to the membrane which was shaken for 25 min in a water bath at 37°C. Subsequently, the membrane was washed thrice with 1x TBS-T for 15 min at RT followed by blocking and antibody incubation as described in 2.2.11.

2.2.13 Coomassie blue staining

To examine the consistent transfer from a polyacrylamide gel onto a PVDF membrane, Coomassie blue staining can be performed, especially when internal loading did not work properly. As the staining is irreversible, it was done after measurement of all proteins of interest. The staining was performed according to a protocol published elsewhere with minor modifications (Goldman et al. 2016). The membrane was incubated with Coomassie staining solution (0.05% Coomassie, 20% MeOH, 7.5% acetic acid) for 5 min while shaking. After that, it was washed several times with Coomassie destaining solution (50% MeOH, 1% acetic acid) until the desired colouring was reached and dried at RT. The protein lanes were detected by the Fusion SL Advance gel documentation device.

2.2.14 Mitochondria isolation

For determination of intracellular localization of proteins, the whole cell lysate was separated into a mitochondrial and cytosolic fraction. The protocol was performed with minor modifications as described before (Wieckowski et al. 2009). Cells were grown to subconfluence in $\varnothing$ 10 cm dishes and treated with different substances for various time points. After treatment, cells were washed with 5 ml ice cold PBS and detached using a cell scraper. Cells of four dishes were pooled in a 15 ml tube and centrifuged at 500 x g for 5 min at 4°C. The supernatant was discarded and cells were lysed in 2 ml ice cold lysis buffer (210 mM mannitol, 70 mM sucrose,1 mM EDTA, 20 mM HEPES, 1x protease inhibitor) for 10 min on ice. Subsequently, cells were homogenised using Sterican® cannula ($\varnothing$ 0.90 x 40 mm, 20 G) and centrifuged at 600 x g for 10 min at 4°C. If the supernatant was turbid, cells were centrifuged again at 1,000 x g for 10 min at 4°C. The supernatant was transferred to a fresh 2 ml tube and centrifuged at 6,500 x g for 15 min at 4°C. After that, the supernatant containing the cytosol was collected in a fresh 2 ml tube. The pellet including the mitochondrial fraction

was washed with 500 µl lysis buffer, centrifuged at 6,500 x g for 10 min and resuspend in 50 µl of lysis buffer. The protein concentration of the fractions followed the method of Lowry described in 2.2.10.

2.2.15 Protein precipitation

A precipitation was performed to concentrate the protein lysate for subsequent use in Western Blot analysis. A defined amount of protein (20-30 µg) was incubated with one-quarter volume with TCA (1.42 g/ml dH$_2$O) for 10 min at 4°C. Then, the samples were centrifuged at 14,000 x g for 5 min at 4°C. After removal of the supernatant, 200 µl ice cold acetone was added and centrifuged again. This step was repeated once. Subsequently, the supernatant was removed, the pellet was dried at 95°C in a heating block and resuspended in SDS lysis buffer and Laemmli buffer. The samples were used for Western Blot.

2.2.16 RNA interference

To investigate the role of individual genes in particular biochemical pathways, RNA interference (RNAi) experiments were performed. The first discovery of this method was in the nematode C.*elegans* (Fire et al. 1998). The principle based on a loss-of-function mutation in individual genes through the gene specific degradation by double stranded RNA at the posttranscriptional level (Han 2018).

To establish the transient knockdown, cells were grown to subconfluence in 6-well plates and treated with the respective siRNA according to the manufacturer's specifications with minor modifications (Tab. 2.4). First, the transfection reagent Lipofectamine® RNA iMAX was diluted in serum free OptiMEM® Medium (1:16 ratio), vortexed for 20 sec and incubated for 5 min. Then, the siRNA was diluted in OptiMEM® to the desired concentration. The diluted siRNA was mixed with diluted Lipofectamine® RNAiMAX reagent (1:1 ratio) and incubated for further 5 min. Meanwhile, cells were washed once with PBS and fresh growth medium was added (2.25 ml/6-well). For transfection, the formed siRNA-lipid complex was added dropwise to the cells (250 µl/6-well) and incubated for different periods of time. After incubation, cells were lysed as described earlier (see 2.2.9) and prepared for Western Blot analysis to verify the efficiency of the knockdown at protein level (see 0). Negative siRNA and treatment with transfection reagent only served as negative control. The used siRNAs are listed in 2.1.7. The transfection efficiency was calculated using FusionCapt Advance Software to quantify the protein amount in relation to the respective control. The time point showing the best efficiency was used for the further experiments.

Tab. 2.4 Pipetting scheme of RNAiMAX transfection procedure according to the manufacturer's specification.

Component	24-well	6-well
Opti-MEM® Medium	50 µl	150 µl
Lipofectamin® RNAiMAX reagent	3 µl	9 µl
Opti-MEM® Medium	50 µl	150 µl
siRNA (10 µM Stock)	1 µl	3 µl
Diluted siRNA	50 µl	150 µl
Diluted Lipofectamine® RNAiMAX reagent	50 µl	150 µl
siRNA-lipid complex per well	50 µl	250 µl
Final siRNA used per well	5 pmol	25 pmol

To investigate whether the transient knockdown of Drp1 has an effect on mitochondrial morphology, cells were seeded on glass bottom dishes. The cells were treated as described before. After the optimal siRNA incubation time, cells were washed and incubated with different substances for defined time points. Subsequently, mitochondrial morphology was assessed as described in 2.2.5.

2.2.17 Extracellular LDH measurement

Loss of membrane integrity is one marker of an inflammatory cell death. The most prominent form is necrosis but there exists also a programmed form called necroptosis which leads to a rupture of the cell membrane (Zhang et al. 2018). To measure this, the extracellular amount of lactate dehydrogenase, an intracellular enzyme catalysing the conversion from pyruvate to lactate and vice versa, can be detected using a LDH ELISA.

Subconfluent cells were mock-treated or treated with GP for 6, 24 and 48 h. The detergent triton-X-100 (500 ppm) was used as positive control. After incubation, the supernatant was collected and centrifuged at 2,000 x g for 10 min at RT. The supernatant (50 µl/well) was used for the LDH Elisa. Duplicates were performed for each condition. The assay was performed in accordance to the manufacturer's specifications. For quantification, the cell number was determined using a Neubauer counting chamber. A standard curve was included in each experiment. One example is shown in Fig. 2.6. The absorbance was measured at 450 nm and the amount of extracellular LDH was derived from the standard curve. Triton-X-100 treated samples were set at 100% release and all other conditions were set in relation to it. Then, mock-treated control was set at 1.
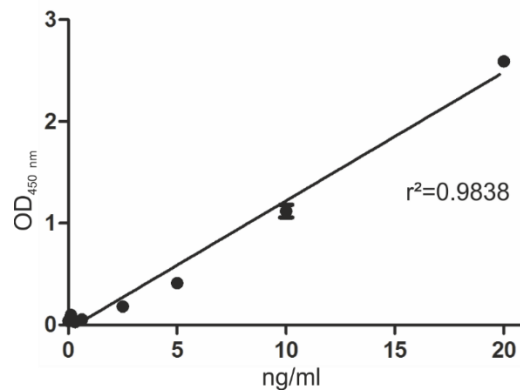
Fig. 2.6 Standard curve for determination of extracellular LDH content.

2.2.18 Trypan blue staining

For determination of the cell membrane integrity, trypan blue exclusion method was performed. Trypan blue is a diazo dye and is negatively charged which prevents its interaction with intact cells. The staining allows discriminating between viable cells and cells with damaged membranes since the dyes can enter the latter because of a cell lysis or membrane permeability (Tran et al. 2011).

In this study, cells were grown in 6-well plates to subconfluence. Then, cells were mock-treated or treated with different concentration of GP alone or in combination with Nec1, a necroptosis inhibitor, respectively. H_2O_2 at a concentration of 2 mM served as positive control. After incubation, the supernatants of the cells were collected in a fresh tube and cells were washed with 1 ml PBS once which was also collected in the tube. Subsequently, 200 µl of trypsin was added and incubated for 5 min in a humidified atmosphere (37°C, 5% CO_2) to detach the cells. The reaction was stopped by adding 800 µl growth medium and the suspension was added to the supernatant. After mixing, 10 µl of the cell suspension was mixed with 10 µl of a 0.4% trypan blue solution and 10 µl of this was used to determine the number of unstained and blue coloured cells using a Neubauer counting chamber. Duplicates were counted on each condition. For evaluation, the total cell number was calculated and the percentage of cells with an intact membrane and permeable cells was determined, respectively.

2.2.19 Seahorse Experiments (Cell characterisation and Mito Stress Test)

To assess mitochondrial function in cells, the Seahorse XF Cell Mito Stress Test was performed based on the measurement of the oxygen consumption rate (OCR). Reduction of molecular oxygen to water by electron transport through the electron transport chain (ETC) is coupled with protonmotive force (Δp) generated by proton pumps which allow the use of cellular respiration to determine energy metabolism. The oxygen consumption comprises of measuring flow of electrons through the respiratory chain and the consumption of Δp. The following

parameters can be measured during the Mito Stress Test: basal, ATP-linked and maximal respiration as well as spare respiratory capacity (SRC), proton leak and non-mitochondrial respiration (Divakaruni et al. 2014).

The basal respiration comprises of ATP synthesis and proton leak. The percentage of the ATP production can be determined after the addition of the ATP synthase inhibitor oligomycin, which decreases the oxygen consumption. The difference between the values represents the ATP production. Basal respiration usually does not show the full capacity of cellular respiration. The use of protonophores like FCCP allows to determine the maximal respiration. The principle is based on the dissipation of the Δp which leads to the maximum activation of the ETC to maintain it. Due to a small optimum of FCCP, it is important to test different concentrations of FCCP in each cell line to find the concentration resulting in maximal respiration. The spare respiratory capacity (SRC) represents the cell's ability to respond to increased energy demand. It can be calculated by the difference between the maximal and basal respiration. Lowered SRC can indicate mitochondrial dysfunction or enhanced ATP demand. Lastly, the complex I (rotenone) and complex III (antimycin A) inhibitors are applied to completely inhibit mitochondrial respiration. The remaining oxygen consumption is due to non-mitochondrial respiration. The proton leak can be calculated from the difference between basal respiration and ATP production (Divakaruni et al. 2014).
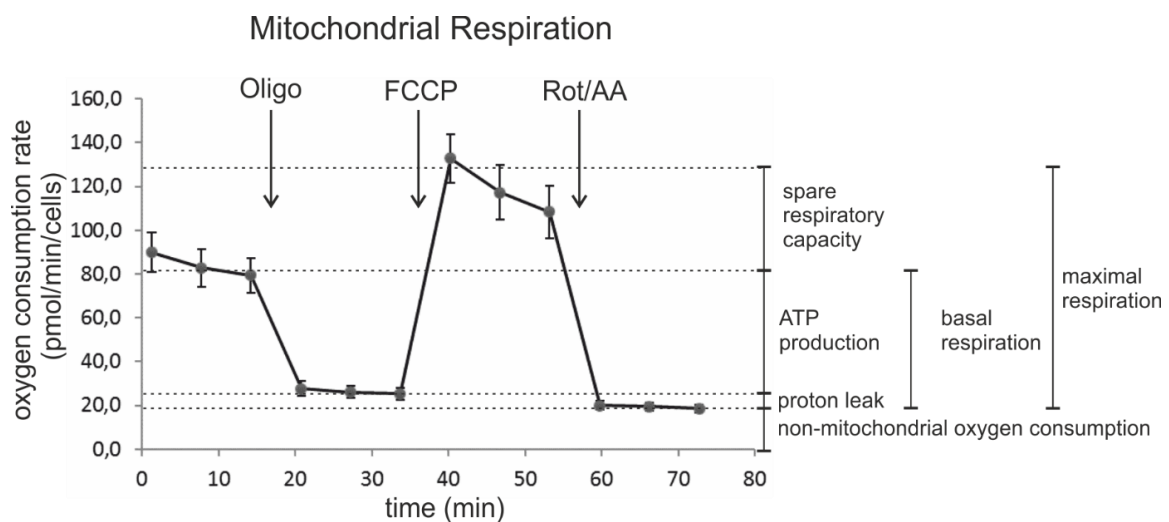
Fig. 2.7 Measurement example of oxygen consumption using the Mito Stress Test. Oxygen consumption of untreated A375 melanoma cells is shown in response to the stressors oligomycin (Oligo), FCCP and rotenone plus antimycin A (Rot/AA). Automatic calculation of the parameters spare respiratory capacity (SRC), ATP production, proton leak, non-mitochondrial oxygen consumption, basal and maximal respiration using the Agilent Seahorse Wave Desktop software.

To determine the most suitable conditions for Seahorse experiments, a cell line characterization of each cell line was performed. For that, a different number of cells were seeded overnight in a Seahorse 96-well plate (80 µl/well) as well as different concentrations of

FCCP were tested. The sensor was equilibrated in Seahorse equilibration buffer in a CO_2 free incubator overnight. As it was important to use cells growing in a monolayer, the appearance of the cells was controlled under a light microscope. The cells were washed with Seahorse medium once and 180 µl Seahorse medium was left on the cells which was incubated for 1 h in a CO_2 free incubator at 37°C. Meanwhile, the cartridge was loaded. Oligomycin at a concentration of 20 µM was added in port A and FCCP was filled with increasing concentrations in port B to D (Tab. 2.5). The sensor was put into Seahorse XFe96 analyser and was equilibrated with respect to pH and O_2 values. After that, the cell plate was loaded and the measurement started. One cycle of measurement consists of thrice mixing for 30 sec and measuring for 3 min. Then, the injection from the respective port took place and the measurement cycle was repeated. For normalisation, Hoechst staining was performed. A working concentration of Hoechst solution (160 µM) was prepared in PBS and 27 µl was added to each well. The plate was shaken for 3 sec followed by a five-minute incubation in the dark. Subsequently, the fluorescence was measured using a plate reader (ex: 361 nm, em: 486 nm). For evaluation, the mean of the background values was subtracted from the measuring data, which were then inserted into the Agilent Seahorse Wave Desktop software.

Tab. 2.5 Pipetting scheme of cell characterization for Seahorse experiments.

Row	Port	Injection volume	Compound	Final concentration
1: background, cell free 2-6: increasing number of cells	A	20	Oligo (20 µM)	2 µM
	B	22	FCCP (1.25 µM)	0.125 µM
	C	25	FCCP (1.25 µM)	0.25 µM
	D	27	FCCP (2.5 µM)	0.5 µM
7-11: increasing number of cells 12: background, cell free	A	20	Oligo (20 µM)	2 µM
	B	22	FCCP (5 µM)	0.5 µM
	C	25	FCCP (5 µM)	1 µM
	D	27	FCCP (10 µM	2 µM

For subsequent Mito Stress Test, optimal cell numbers and FCCP concentrations were figured out based on the cell characterisation assays. These differ between the used cell lines and are listed in Tab. 2.6. As described before, the appropriate cell numbers were seeded overnight in a Seahorse 96-well plate as well as the sensor was equilibrated in Seahorse equilibration buffer in a CO_2 free incubator overnight. All cells were washed and were untreated, mock-treated or treated with different concentrations of GP in Seahorse medium (eight replicates/conditions) and were incubated for 1 h in a CO_2 free incubator at 37°C. Meanwhile, the cartridge was loaded with appropriate concentrations of Oligo (Port A), FCCP (Port B) and

Rot/AA (Port C). After equilibrating of the sensor in the Seahorse devise relating to pH and O_2 values, the cell plate was loaded and the measurement started. As mentioned previously, one cycle of measurement consists of thrice mixing for 0.5 min and measuring for 3 min. Then, the injection took place and the measurement cycle was repeated. After measuring the OCR, Hoechst staining was performed for normalisation as described before.

Tab. 2.6 Overview of chosen parameters for Seahorse experiments.

Cell line	Seeded cell number	Final concentration (µM)		
		Oligo	FCCP	Rot/AA
A375	20,000	2	0.5	0.5
SCL-1	15,000	2	0.5	0.5
NHEM	20,000	2	1	0.5
NHEK	20,000	2	0.5	0.5
NHDF	17,000	2	2	0.5

For analysis of the data, the Agilent Seahorse Wave Desktop software was used. The raw data were normalised to the corresponding Hoechst staining. The program calculated the parameters based on the OCR, including basal, maximal and non-mitochondrial respiration, SRC, proton leak and ATP production. The percentage of each parameter was referred to untreated cells. At least three experiments of each cell line were performed. As it was important to exclude effects of the solvents, the statistical analysis was referred to mock-treated cells.

2.2.20 Immunostaining

Immunofluorescence experiments were performed to visualize the protein of interest in a cellular context using antibodies. Cells were grown until a confluence of 50-70% onto 6-well plates containing coverslips and, then, treated with the appropriate substance. After the incubation, cells were washed with warm (37°C) PBS twice. For fixation, preheated (37°C) 4% paraformaldehyde (PFA) was added for 20 min at RT. After that, cells were washed three times with PBS. All steps were performed without shaking at RT, unless otherwise stated. For permeabilization, 1 ml triton-X-100 (0.15% in PBS) was added for 15 min. Subsequently, the solution was removed and cells were blocked in 10% normal goat serum (NGS) in PBS for further 15 min. The concerned primary antibody was diluted 1:100 in 1% NGS in PBS and 100 µl was added to each coverslip. The cells were incubated at 4°C overnight. The primary antibody was kept and stored at -20°C for further use. To wash off the primary antibody, the cells were washed with PBS three times for 10 min. The secondary antibody (100 µl/coverslip) at a concentration of 0.1% in 1% NGS in PBS was added and incubated for 1 h in the dark. After discarding of the antibody solution and three washing steps with PBS for 10 min in the

dark, the coverslips were fixed on the microscopic slides using ProLong™ Gold Antifade Mountant with DAPI. The samples were stored at 4°C. Immunofluorescences of pRIP3 and RIP3 after GP treatment were recorded using a spinning disk microscope by Mathias Golombek. The intensity of the signals was calculated using Image J. At least 10 pictures of each condition were quantified. The ratio of pRIP3 to RIP3 was determined and mock-treated control was set at 1.

2.2.21 Transient transfection of pEGFP-LC3 II

Different methods can be used to monitor autophagic flux. One approach is based on the use of a fusion protein, which consists of a GFP and a LC3 II fragment. The fusion protein is cleaved within the autolysosomes during autophagy and the released, free GFP can be detected by Western Blot analysis. Thus, the measurement of free GFP indicates an autophagic flux (Mizushima et al. 2010). For that reason, a plasmid encoding enhanced GFP (EGFP)-LC3 II fusion protein was used. EGFP-LC3 II was a kind gift from Karla Kirkegaard (Addgene plasmid # 11546; http://n2t.net/addgene:11546; RRID: Addgene_11546) (Jackson et al. 2005).

The streaking and isolation of E. *coli* on LB agar plates were performed according to the manufacturer's instructions. Briefly, LB agar plates containing 50 µM kanamycin sulphate were used to streak the bacteria over the plate using an inoculation loop. After incubation overnight at 37°C, single colonies were visible. A single colony was picked and transferred in a 15 ml falcon containing 5 ml LB medium supplemented with 50 µM kanamycin sulphate. The bacteria were grown overnight at 37°C. For long term storage (-80°C), glycerol stocks were prepared containing 500 µl of the overnight culture and 500 µl of sterile glycerol. For plasmid isolation, an overnight culture was inoculated as described before and the isolation was performed using the QIAprep Spin Miniprep Kit according to the manufacturer's instructions. The DNA concentration of the plasmid was measured using a spectrometer. The plasmid was stored at -20°C until further use.

For transient transfection, cells were grown to subconfluence in 6-well plates and treated with the plasmid according to the manufacturer's specifications with minor modifications. For one approach, 3 µl of the transfection reagent GeneJuice® was mixed in 100 µl serum free OptiMEM® medium vortexed for 20 sec and incubated for 5 min at RT. After addition of 1 µg DNA, the mix was incubated for further 20 min and added dropwise to the cells. As negative control, cells were only treated with transfection reagent lacking the plasmid. After 48 h incubation with the plasmid, cells were washed once with PBS and mock-treated or treated with 2.5 µM GP for further 24 h. Subsequently, cell lysates were prepared as described in

2.2.9. For detection of the construct (EGFP-LC3 II), free EGPF and LC3 II, Western Blot analysis was performed.

2.2.22 Statistics

Means were calculated from at least three independent experiments, unless otherwise stated. Error bars represent the standard error of mean (SEM). Statistical analysis was performed by one-way ANOVA with post-hoc test (Dunnett or Bonferroni) or student's t-test using Graph Pad Prism 5; *$p \leq 0.05$; **$p \leq 0.01$ and ***$p \leq 0.001$ were chosen as levels of significance.

3 Results

The incidence of skin tumours is constantly increasing in the last decades (ZfKD 2019, ZfKD 2021). Growing resistance of tumour cells requires the on-going development of new therapeutic approaches (Flaherty et al. 2012, Gracia-Cazaña et al. 2016, Luke et al. 2017). This study focussed on substances which are able to induce cell death in tumours cells without affecting normal cells. The tumour cells used in this work include A375 melanoma cells, an aggressive and fast-growing tumour of the skin (Miller and Mihm 2006, Janostiak et al. 2019), and SCL-1 carcinoma cells, the second most common form of skin cancer (Que et al. 2018). As representatives of normal (healthy) cells, human normal epidermal melanocytes (NHEM) and normal human normal epidermal keratinocytes (NHEK) as well as normal human dermal fibroblasts (NHDF) were chosen.

3.1 Skin cancer cells exhibited high expression of anti-apoptotic Bcl-2 proteins

Tumour cells are characterised by different properties including the evasion of cell death in order to proliferate uncontrollably (Hanahan and Weinberg 2011). Therefore, high expression of anti-apoptotic proteins is often observed in several tumour cells (Yip and Reed 2008). The Bcl-2 protein family is a key regulator in the programmed form of cell death called apoptosis and a misbalance towards anti-apoptotic proteins results in survival of tumour cells (Korsmeyer et al. 1993, Mohammad et al. 2015). To examine whether A375 melanoma and SCL-1 carcinoma cells exhibit high expression of pro-survival Bcl-2 proteins in comparison to NHEM, NHEK and NHDF, the basal expression of members of the Bcl-2 protein family was determined by Western Blot (Fig. 3.1). The expression of the anti-apoptotic protein Bcl-2 was significantly increased in A375 melanoma cells and Bcl-xL in SCL-1 carcinoma cells. In contrast, no trend in the expression of pro-apoptotic Bax between tumour and normal cells was apparent.

One possibility to overcome the survival strategy of tumour cells by upregulating of anti-apoptotic Bcl-2 proteins, is the use of antagonists, so-called BH3 mimetic substances, which disturb the balance of the Bcl-2 protein family by binding the anti-apoptotic members and release of pro-apoptotic members of the Bcl-2 family. Thus, the pro-apoptotic protein can induce apoptosis (Zhang et al. 2007, Mohammad et al. 2015). In this study, two different BH3 mimetic substances were tested in the following.
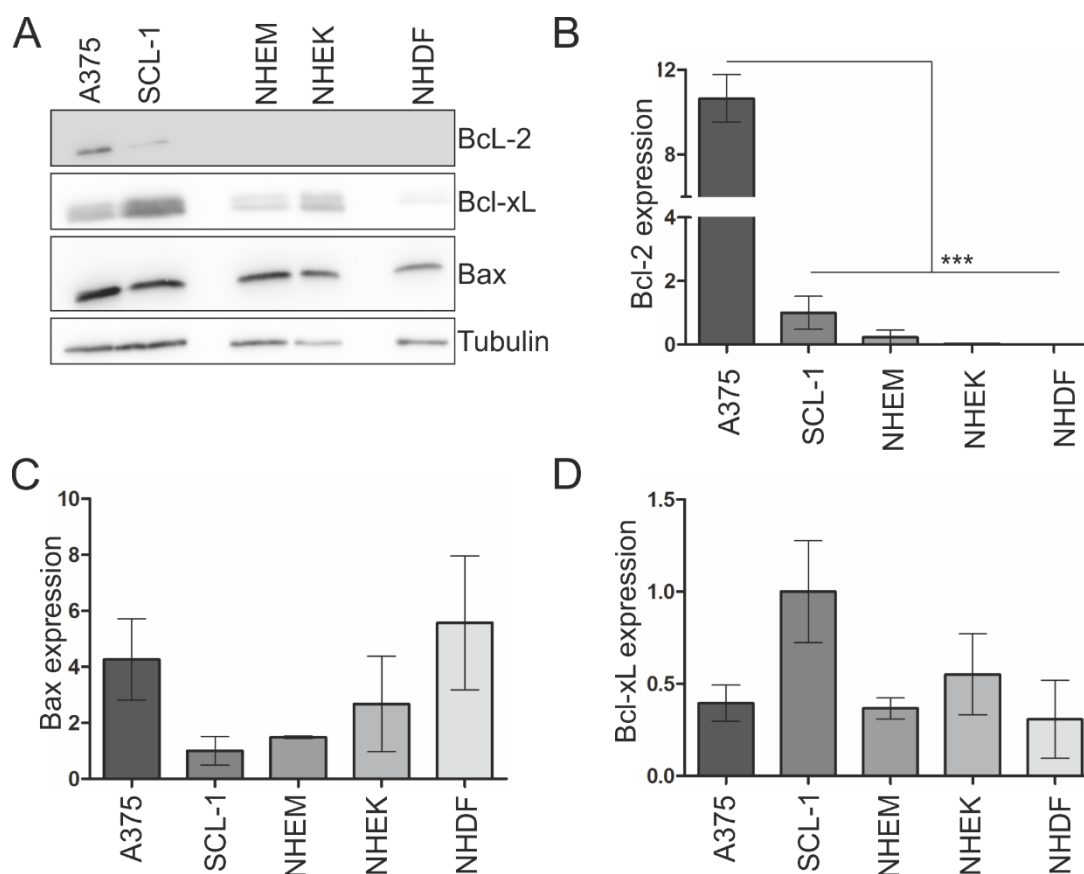
Fig. 3.1 Tumour cells exhibited higher expression of anti-apoptotic Bcl-2 proteins compared to normal cells. Basal protein expression of anti-apoptotic (Bcl-2, Bcl-xL) and pro-apoptotic proteins (Bax) in tumour cells (A375 melanoma cells, SCL-1 carcinoma cells) and normal cells (melanocytes (NHEM), keratinocytes (NHEK), fibroblasts (NHDF)) were determined by Western Blot. **a** A representative Blot is depicted. Tubulin served as loading control. **b-d** Densitometric analysis of the Western Blots was performed. The protein amount was set in relation to the respective loading control. Data represent means ± SEM of three independent experiment, n=3. One-way ANOVA with Bonferroni's Multiple Comparison Test was used for the determination of statistical significance. ***$p < 0.001$.

3.2 ABT-199 lowered cell viability in both tumour and normal (healthy) cells

ABT-199 is an inhibitor which is described to bind the anti-apoptotic Bcl-2 resulting in cell death of tumour cells (Adams and Cory 2018, Casara et al. 2018, Guo et al. 2020). It is the first BH3 mimetic compound approved by the U.S. Food and Drug Administration (FDA). Since 2016, Venclexta (venetoclax/ABT-199) are used as oral Bcl-2 inhibitor for the treatment of patients with chronic lymphocytic leukaemia (CLL) with a 17p deletion (FDA 2019). The effect of ABT-199 on cell viability was determined in both tumour and normal cells. For that, the cells were treated with different concentrations of the compound for 96 h and cell viability was measured using the MTT assay (Fig. 3.2). ABT-199 decreased cell viability dose dependently in A375 melanoma cells (Fig. 3.2a), SCL-1 carcinoma cells (Fig. 3.2b), NHEM (Fig. 3.2c), NHEK (Fig. 3.2d) and NHDF (Fig. 3.2e). ABT-199 showed a similar effect on normal cells compared to

both tumour cell lines which is reflected in the calculation of the IC_{50} values (Fig. 3.2f). These indicate the concentration at which half of the effect, here 50% of cell viability, is achieved. The smaller the value, the stronger the effect. The strongest effect was observed in NHEK ($IC_{50}=0.7$ μM), the weakest in NHDF ($IC_{50}=2.6$ μM).
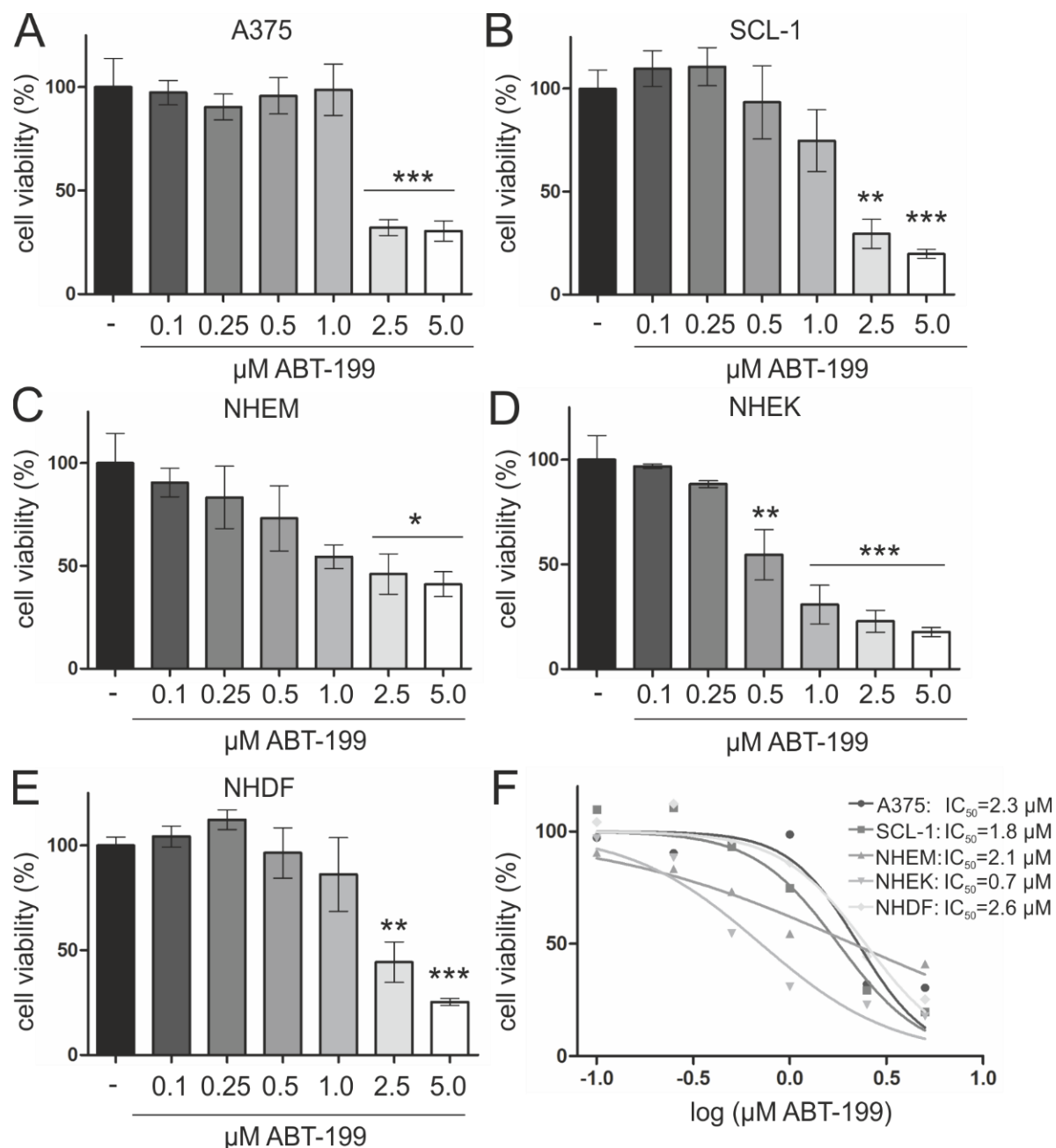
Fig. 3.2 Effect of ABT-199 on the cell viability of skin cancer and normal cells. **a-e** To determine the effect of ABT-199 on cell viability, A375 melanoma cells (**a**), SCL-1 carcinoma cells (**b**), melanocytes (NHEM) (**c**), keratinocytes (NHEK) (**d**) and fibroblasts (NHDF) (**e**) were treated with different concentrations of ABT-199 for 96 h. Cell viability was measured by MTT assay. Mock-treated control was set at 100%. Data represent means ± SEM of at least three independent experiments, n≥3. One-way ANOVA with Dunnett's Multiple Comparison Test was used for the determination of statistical significance. *$p<0.05$, **$p<0.01$, ***$p<0.001$. **f** Calculation of IC_{50} values after ABT-199 treatment in all cells after 96 h. IC_{50} value were calculated by non-linear curve fit analysis.

The occurrence of unwanted side effects often limits the application of anti-cancer drugs. In context of a minimisation of toxic effect on normal cells, ABT-199 was not used for further experiments as normal cells partially respond more sensitive to this compound.

3.3 GP exerted a selective effect on cell viability on tumour cells

Gossypol (GP), a natural compound derived from cotton seed plant (Adams et al. 1960), is described to act as a pan-Bcl-2 inhibitor by antagonising Bcl-2, Bcl-xL and MCL-1 (Kitada et al. 2003, Oliver et al. 2005, Lessene et al. 2008, Kang and Reynolds 2009). It consists of (+) and (-) enantiomers (Fig. 3.3), whereby the latter called AT101 and is orally bioavailable (Opydo-Chanek et al. 2017). The effect of (±) GP on cell viability of skin tumour and normal cells were tested. After 96 h treatment of GP on A375 melanoma cells (Fig. 3.4a), SCL-1 carcinoma cells (Fig. 3.4b), NHEM (Fig. 3.4c), NHEK (Fig. 3.4d) and NHDF (Fig. 3.4e), cell viability was determined by MTT assay. GP lowered cell viability in both tumour cell lines in a dose dependent manner. A complete loss of cell viability was determined in the higher concentration range between 2 and 5 µM GP. In contrast to that, only the highest concentration of 5 µM significantly lowered cell viability in melanocytes and fibroblasts.
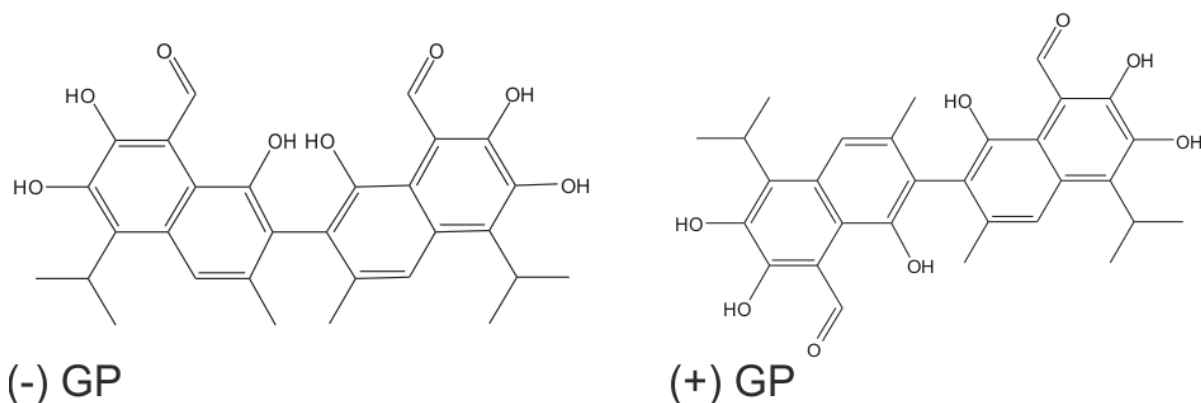

Fig. 3.3 Chemical structures of GP's enantiomers (-, +).

Fig. 3.4 Effect of GP on the cell viability of skin cancer and normal cells. **a-e** To examine the effect of GP on cell viability, A375 melanoma cells (**a**), SCL-1 carcinoma cells (**b**), melanocytes (NHEM) (**c**), keratinocytes (NHEK) (**d**) and fibroblasts (NHDF) (**e**) were treated with different concentrations of GP for 96 h. Cell viability was measured by MTT assay. Mock-treated control was set at 100%. Data represent means ± SEM of at least three independent experiments, n≥3. One-way ANOVA with Dunnett's Multiple Comparison Test was used for the determination of statistical significance. *p<0.05, **p<0.01, ***p<0.001. Data referred to A375 and NHEM were already published in (Haasler et al. 2021).

As MTT itself was described to be toxic and the measuring principle is based on the enzyme activity within the cells (Riss et al. 2004), a second cell viability assay was chosen to confirm the previous data (Fig. 3.5). For that, cells were treated for 96 h as described above and cell viability was measured using the SRB assay which is based on the staining of total protein amount (Maydt et al. 2013). GP significantly lowered the cell viability in a dose dependent

manner at concentrations ≥1.5 μM in SCL-1 carcinoma cells (Fig. 3.5b). The strongest effect of GP was observed in A375 melanoma cells (Fig. 3.5a) as already concentrations as low as 1.5 μM resulted in a complete loss of cell viability. The effect of GP was less on normal cells. Similar to the MTT data, the highest concentration of 5 μM significantly lowered cell viability significantly in NHEM (Fig. 3.5c), NHDF (Fig. 3.5e) and also NHEK (Fig. 3.5d).
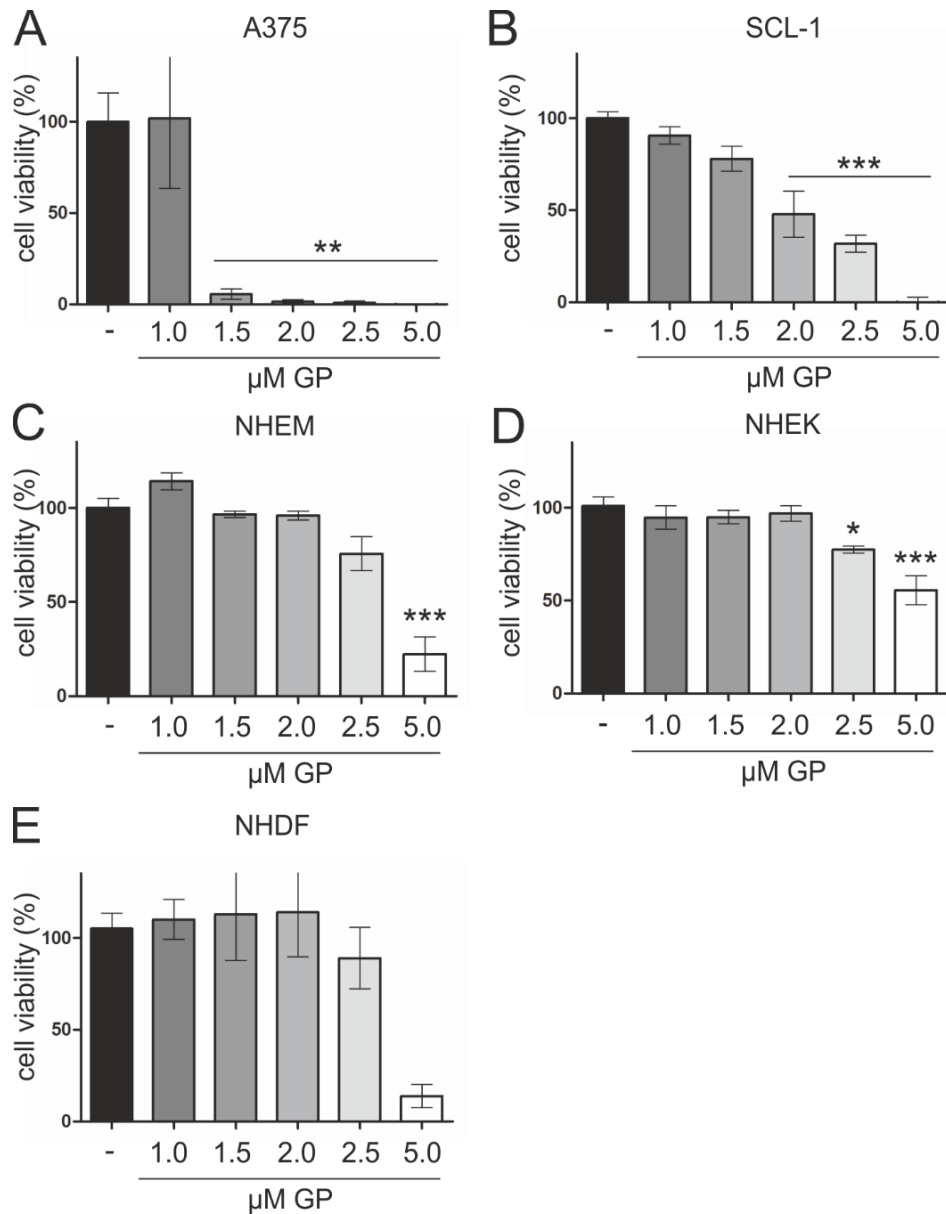
Fig. 3.5 Effect of GP on the cell viability of skin cancer cells and normal cells. **a-e** To examine the effect of GP on cell viability, A375 melanoma cells (**a**), SCL-1 carcinoma cells (**b**), melanocytes (NHEM) (**c**), keratinocytes (NHEK) (**d**) and fibroblasts (NHDF) (**e**) were treated with different concentrations of GP for 96 h. Cell viability was measured by SRB assay. Mock-treated control was set at 100%. Data represent means ± SEM of at least three independent experiments in A375, SCL-1, NHEM, NHEK, n≥3. Two experiments were performed in NHDF, n=2. One-way ANOVA with Dunnett's Multiple Comparison Test was used for the determination of statistical significance. *$p<0.05$, **$p<0.01$, ***$p<0.001$. Data referred to A375 and NHEM were already published in (Haasler et al. 2021).

Since low concentrations of GP had a strong effect on cell viability in tumour cells after 96 h, the different concentrations were tested in a time course in A375 melanoma and SCL-1 carcinoma cells. GP lowered the cell viability in A375 melanoma cells in a dose and time dependent manner. After 24 h, the concentration of 1.5 µM GP reduced the cell viability almost half (Fig. 3.6 a, c). A decrease of cell viability was also observed in SCL-1 carcinoma cells but the effect is less pronounced in these cells compared to A375 melanoma cells (Fig. 3.6b, d).
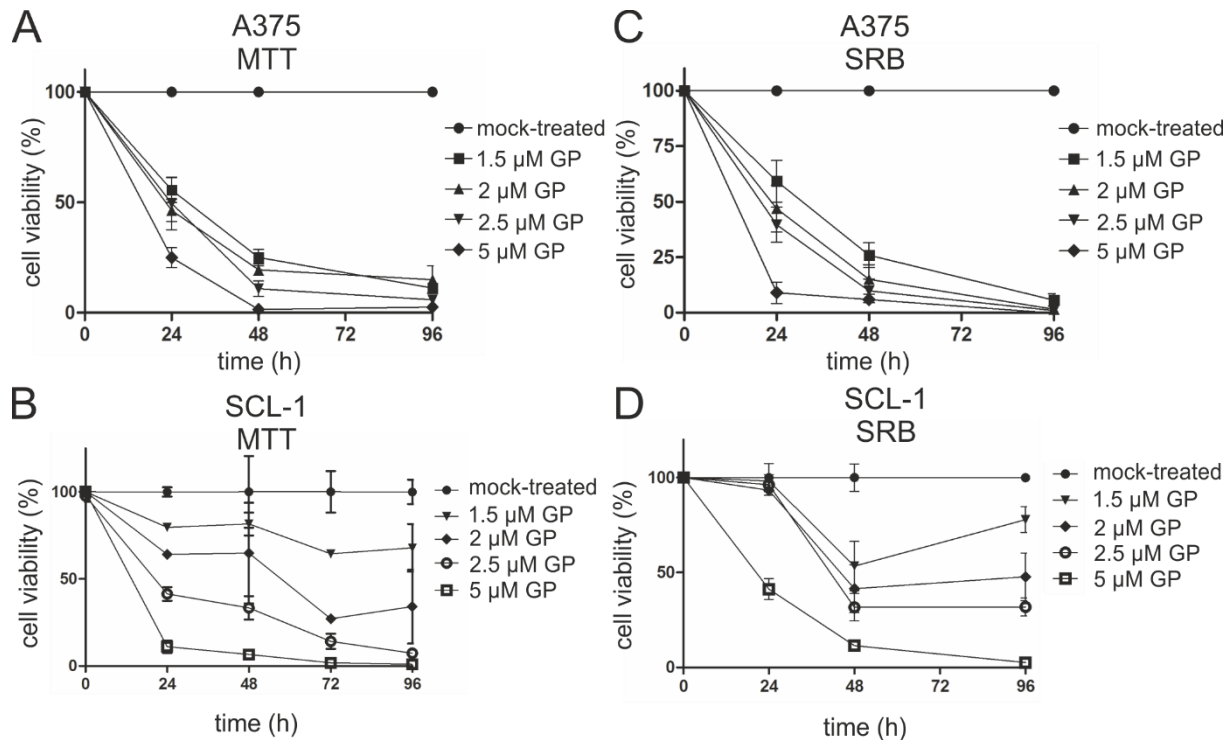
Fig. 3.6 Effect of GP on the cell viability of skin cancer cells. Subconfluent A375 melanoma (**a, c**) and SCL-1 carcinoma cells (**b, d**) were treated with different concentrations of GP for different time periods. Cell viability was determined by MTT (**a, b**) and SRB (**c, d**) assay. Mock-treated control was set at 100%. Data represent means ± SEM of at least three independent experiments, n≥3. Data (**a, c**) were already published in (Haasler et al. 2021).

To estimate the magnitude of the effect of GP on the cells, the IC_{50} values were calculated (Fig. 3.7, Fig. 3.8). The smaller the value, the stronger is the effect. After 24 h, depending on the performed cell viability assay (Fig. 3.7a), the IC_{50} value ranged from 1.86 (MTT) and 2.14 (SRB) in A375 melanoma cells which further decreased up to 96 h (Fig. 3.7b and c). The effect of GP on SCL-1 carcinoma cells is a little less compared to A375 melanoma cells. The IC_{50} values were 2.79 (MTT) and 3.05 (SRB) after 24 h treatment (Fig. 3.8a). However, a strong decrease in these values was shown after 96 h (Fig. 3.8b, c). For comparison of the effect between tumour and normal cells, the IC_{50} values for 96 h treatment were summarized in Tab. 3.1.The factor between the tumour and normal cells was at least 2-fold with the exemption of comparison between SCL-1 carcinoma cells and NHDF in regard to the IC_{50} values derived from the MTT assay. The greatest difference was between NHEK and both tumour cells. The

differences in IC_{50} values may indicate a therapeutic window where tumour cells could be killed successfully and normal cells remain predominantly intact at the same time. With regard to undesirable side effects after the administration of chemotherapeutic agents, it is desirable that these substances show such a therapeutic range.
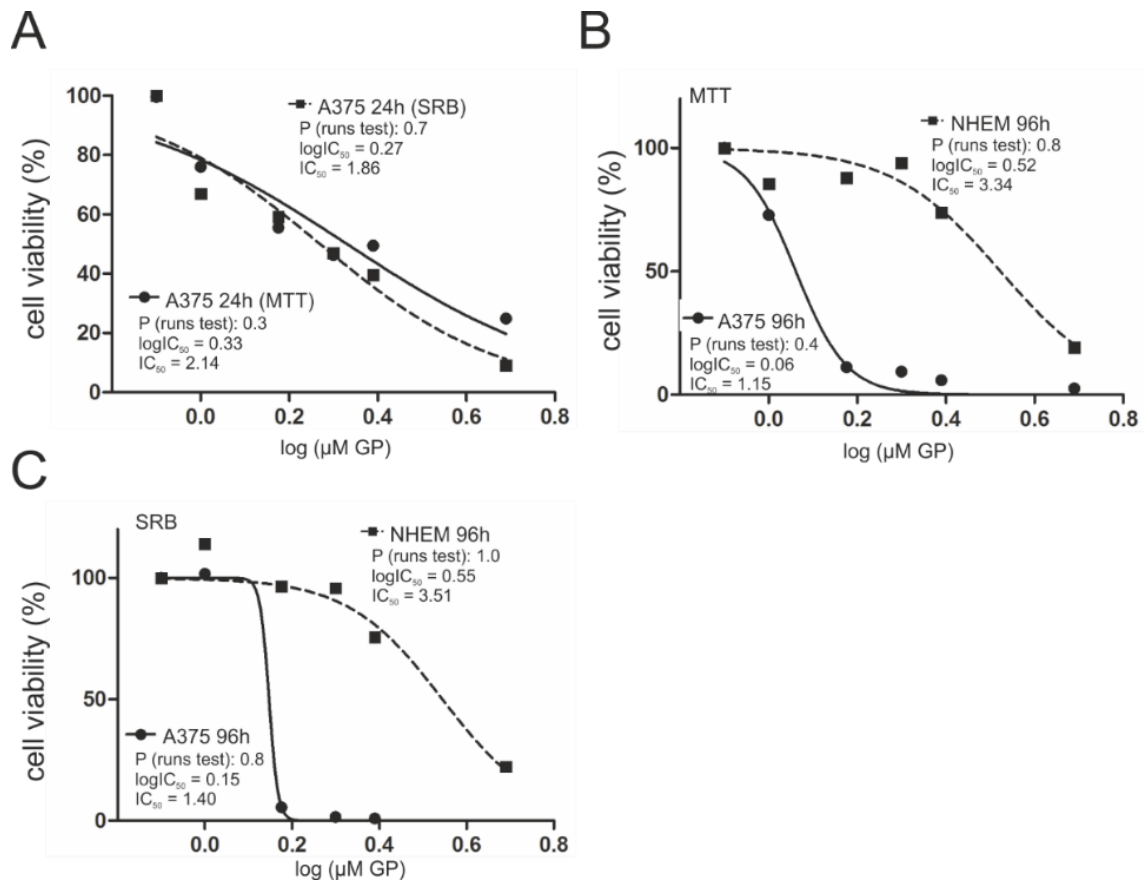
Fig. 3.7 Calculation of IC_{50} values after GP treatment in A375 melanoma cells and melanocytes (NHEM).**a** A375 melanoma cells were treated with different concentrations of GP for 24 h. Cell viability was measured by MTT (continuous line) and SRB (dotted line). **b-c** A375 melanoma cells (continuous lines) and NHEM (dotted lines) were incubated with different concentrations of GP for 96h. MTT (**b**) and SRB (**c**) assay were used to determine the effect on cell viability. The means of at least three independent experiments were shown, n≥3. IC_{50} values were calculated by non-linear curve fit analysis. Data were already published in (Haasler et al. 2021).
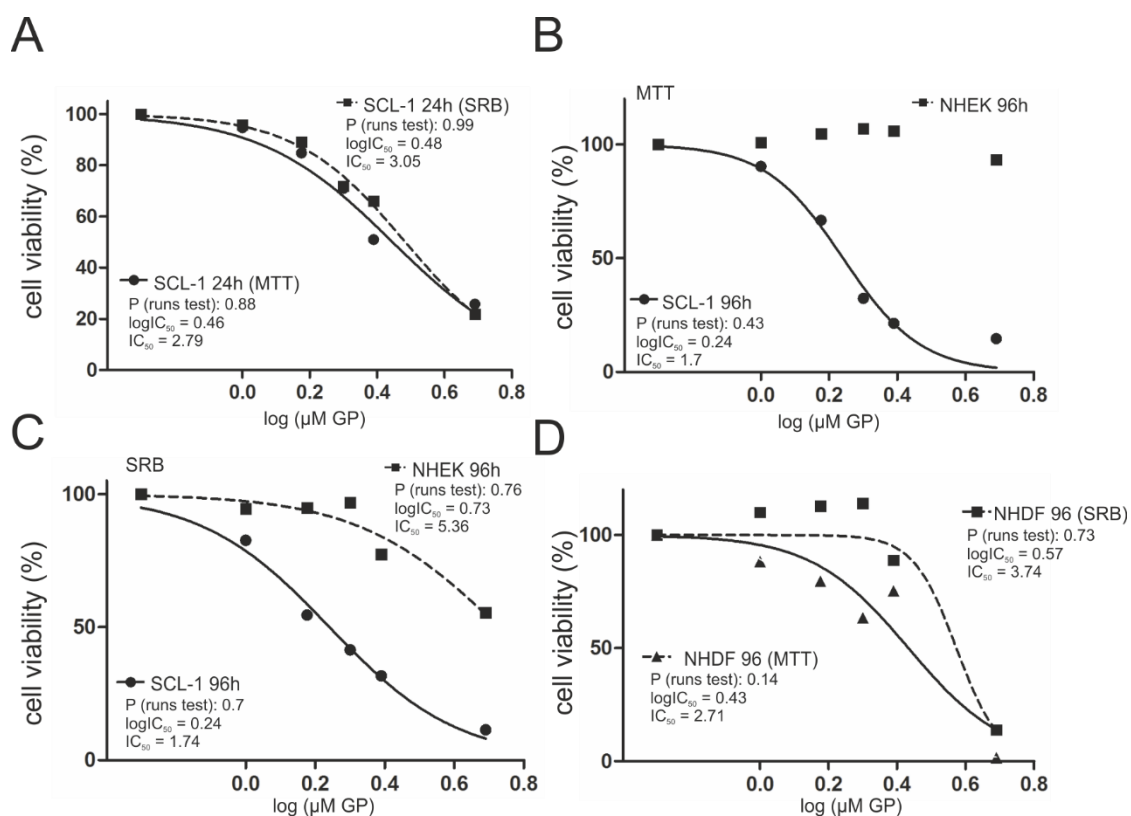
Fig. 3.8 Calculation of IC_{50} values after GP treatment in SCL-1 carcinoma cells, keratinocytes (NHEK) and fibroblasts (NHDF). **a** SCL-1 carcinoma cells were treated with different concentrations of GP for 24 h. Cell viability was measured using MTT (continuous line) and SRB (dotted line). **b-c** SCL-1 carcinoma cells (continuous lines) and NHEK (dotted lines) were incubated with different concentrations of GP for 96h. MTT (**b**) and SRB (**c**) assay were used to determine the effect on cell viability. **d** NHDF were treated with different concentrations of GP for 96 h. MTT (continuous line) and SRB (dotted line) were used for the determination of cell viability. The means of at least three independent experiments in SCL-1 and NHEK were shown, n≥3, and at least two independent experiments in NHDF, n≥2. IC_{50} values were calculated by non-linear curve fit analysis.

Tab. 3.1 Overview of IC_{50} values in tumour and normal cells after GP treatment for 96 h. Values were calculated from MTT and SRB assay (Fig. 3.7, Fig. 3.8). *n.d.* (not determined).

Cell line	IC_{50} (96h, MTT)	IC_{50} (96h, SRB)
A375	1.15	1.40
SCL-1	1.70	1.74
NHEM	3.34	3.51
NHEK	n.d.	5.36
NHDF	2.7	3.74

To understand the molecular mechanism of GP in tumour cells compared to normal cells, a concentration of 2.5 µM was chosen for the majority of upcoming experiments. This

concentration already showed subtoxic effects up to 24 h and toxic effects up to 48 h in tumour cells. At these time points, the NHEM, NHEK and NHDF not affected after treatment with 2.5 µM GP.

3.4 Cellular uptake of GP

The experiments regarding cytotoxicity of GP showed a selective effect of this compound. To examine whether the selective effect of GP is due to differences in uptake, the concentration of GP within the cells was determined by HPLC. Therefore, A375 melanoma cells, SCL-1 carcinoma cells, NHEM, NHEK and NHDF were incubated with 5 µM GP for 0.25, 1 and 2 h. The results are shown in Fig. 3.9. The average of intracellular concentrations of GP was about 10 µg per mg protein. The detectable amount of GP (t=0.25 h) within the cells related to the amount of GP applied was on the average of 15%. There was no difference in the absorbed GP amount between tumour and normal cells. In tendency, the amount of intracellular GP decreased over time in all cells.
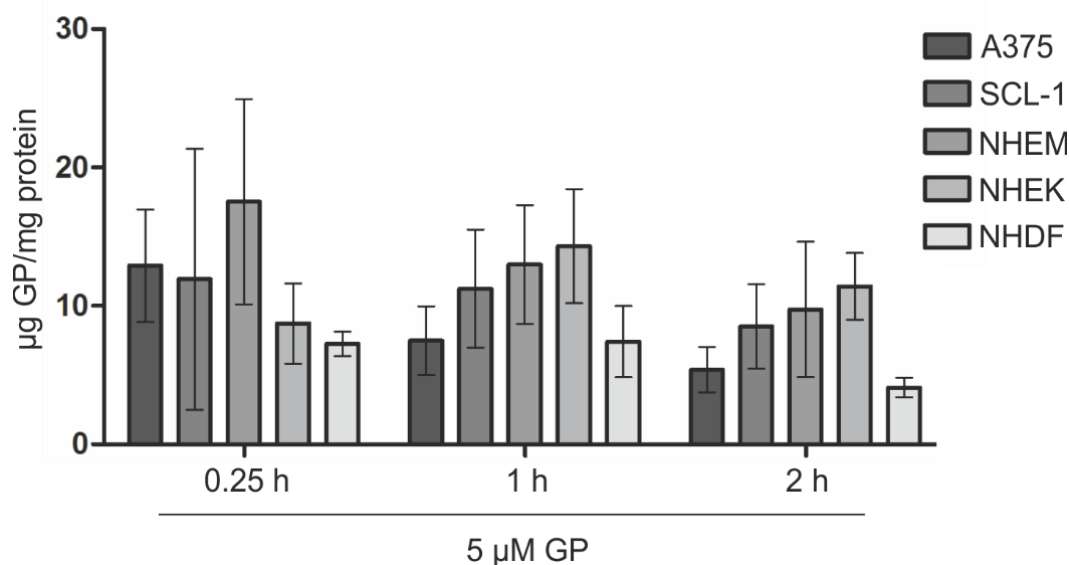
Fig. 3.9 Cellular uptake of GP. Detection of intracellular GP content in tumour cells (A375 melanoma cells and SCL-1 carcinoma cells) and normal cells (melanocytes (NHEM), keratinocytes (NHEK), fibroblasts (NHDF)). Cells were harvested after treatment with 5 µM GP for 0.25, 1 and 2 h and analysed by HPLC. The amount of intracellular GP was related to the respective protein level. Data represent means ± SEM of three independent experiments, n=3. Data referred to A375 and NHEM were already published in (Haasler et al. 2021).

3.5 Parental GP exerted the cytotoxic effect

Due to the reported low stability of GP in plasma (Jia et al. 2008) and the measured time-dependent decrease of the intracellular GP concentration in the cells (Fig. 3.9), the stability of GP was tested in different solutions including acetonitrile (AcN), H_2O and cell culture media

(DMEM, MBM). GP was stable in AcN but was degraded more than half in H_2O up to 5 h remaining thereafter at this level. In comparison, GP was completely lost after few hours in DMEM and MBM (Fig. 3.10, Fig. 3.11).
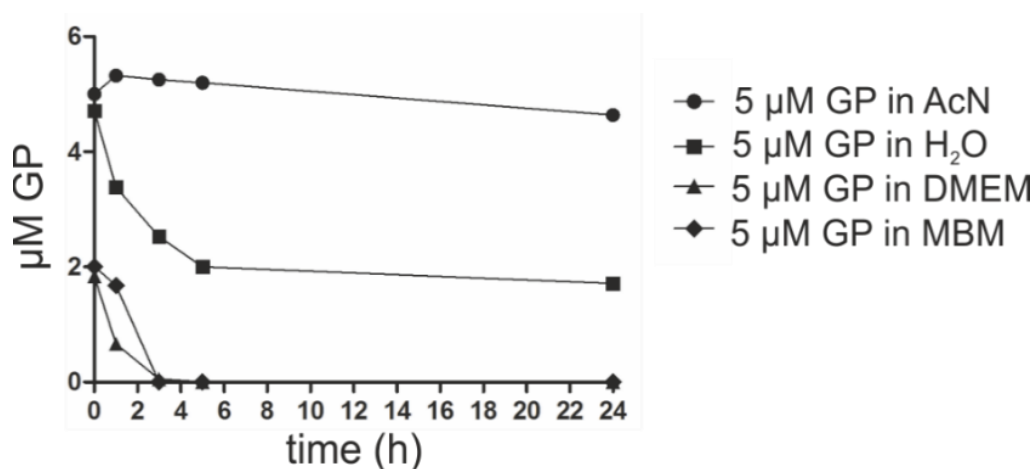
Fig. 3.10 Stability of GP in a cell-free system. GP at a concentration of 5 µM was added to acetonitrile (AcN), H_2O, DMEM as well as Melanocyte Basal Medium (MBM) and incubated for different time points in a humidified atmosphere. Following, the amount of GP was detected by HPLC. Data were already published in (Haasler et al. 2021).
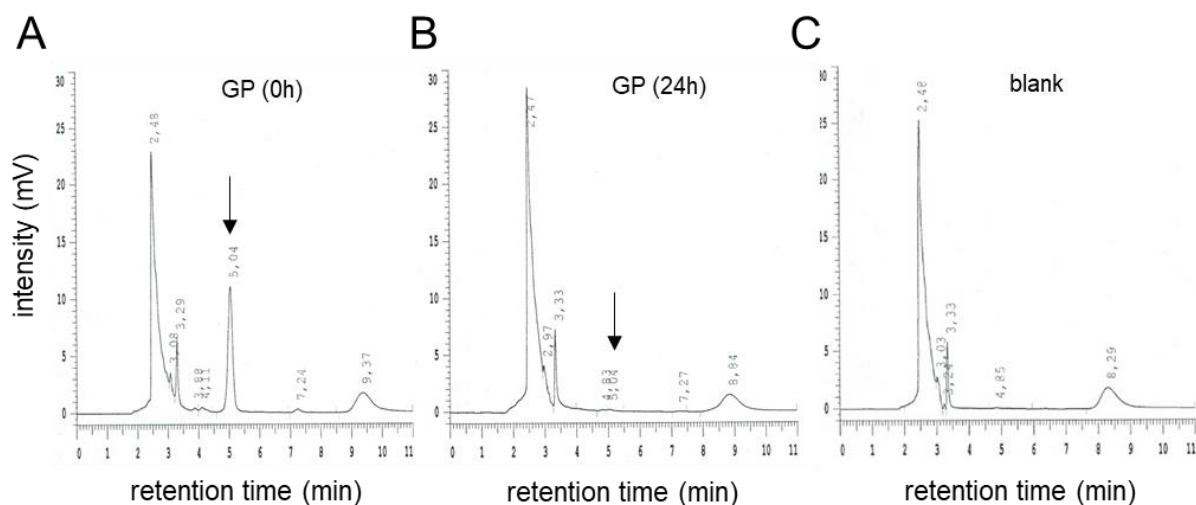
Fig. 3.11 Stability of GP in DMEM in a cell-free system. For determination of the stability of GP in cell culture medium, the compound was incubated for 24 h in DMEM in a humidified atmosphere. **a, b** GP was detected by HPLC directly after adding (**a**) and after 24 h incubation in DMEM (**b**). The arrows indicate the retention time point of GP. **c** As control, DMEM without GP was injected to HPLC referred to as "blank".

Due to the rapid degradation of GP in DMEM, the questions raised whether the non-decomposed ("parental") GP or a degradation product was responsible for the reduction of cell viability in skin tumour cells. For that, A375 melanoma and SCL-1 carcinoma cells were treated directly with GP or with decomposed GP which was preincubated in DMEM for 5 h in a humidified atmosphere. Decomposed GP was obtained after treatment of parental GP for 5 h

in DMEM. The cell viability was measured after 24 and 48 h treatment using the MTT assay (Fig. 3.12). The GP induced decrease in cell viability in A375 melanoma (Fig. 3.10a) and SCL-1 carcinoma cells (Fig. 3.10b) was significantly abolished after degradation of GP indicating that the parental compound exerted the cytotoxic effect.
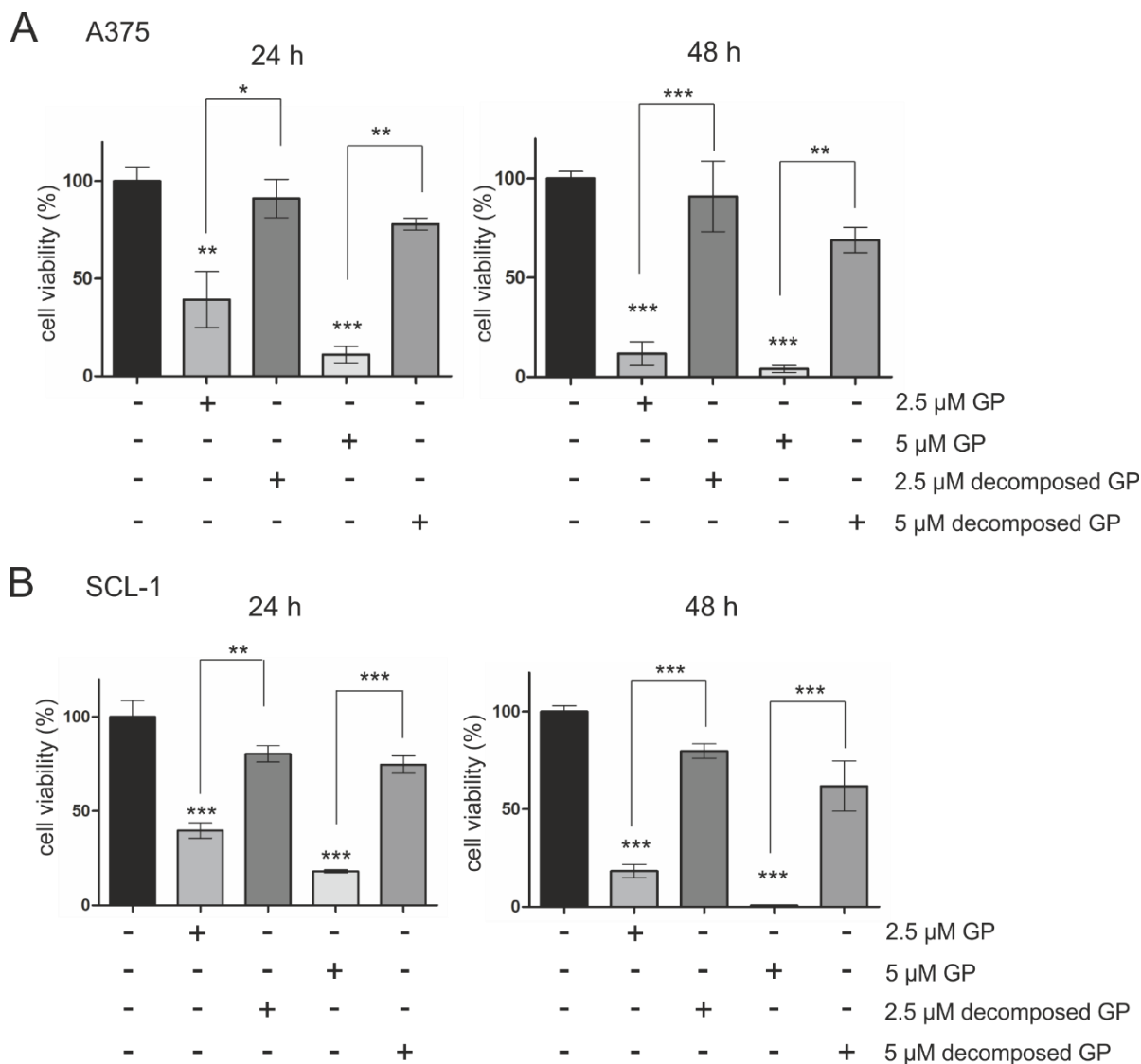
Fig. 3.12 Effect of parental GP on the cell viability of tumour cells. **a-b** Subconfluent A375 melanoma (**a**) and SCL-1 carcinoma cells (**b**) were treated with both decomposed GP or parental GP directly for 24 and 48 h. Cell viability was measured by MTT assay. The mock-treated control was set at 100%. Data represent means ± SEM of three independent experiments, n=3. One-way ANOVA with Bonferroni's Multiple Comparison Test was used for the determination of statistical significance. *p<0.05, **p<0.01, ***p<0.001. Data referred to A375 (**a**) were already published in (Haasler et al. 2021).

3.6 GP decreased mitochondrial membrane potential and induced mitochondrial fragmentation

BH3 mimetic substances are described to induce the mitochondrial dependent apoptotic pathway through binding to anti-apoptotic Bcl-2 proteins which correlates with a change in mitochondrial membrane potential ($\Delta\psi_m$) (Henz et al. 2019). To examine whether GP has an effect on mitochondria, the $\Delta\psi_m$ was investigated. Due to the selectivity of GP on the cell viability, the effect on mitochondrial dysfunction associated with changes of $\Delta\psi_m$ was studied not only on tumour cells, but also on normal cells to determine if the compound showed different effects there as well. GP significantly diminished $\Delta\psi_m$ after 4 h in A375 melanoma (Fig. 3.13a, b) and SCL-1 carcinoma cells (Fig. 3.14a, b). In contrast, no decrease of $\Delta\psi_m$ was observed in NHEM (Fig. 3.13d, e), NHEK (Fig. 3.14d, e) and NHDF (Fig. 3.15a, b). In tendency, $\Delta\psi_m$ increased slightly but not significantly in the normal cells. With regard to a reported correlation between a drop in $\Delta\psi_m$ and a change in mitochondrial fragmentation being a measure for mitochondrial dysfunction (Legros et al. 2002, Tang et al. 2018), the mitochondrial morphology was assessed after GP treatment in all cells. GP induced a fragmentation in about 80% of A375 melanoma cells (Fig. 3.13c) and SCL-1 carcinoma cells (Fig. 3.14c) after 2 h which was further increased over 95% after 4 h similar to CCCP treated cells, which served as a positive control. As opposed to the tumour cells, no change in mitochondrial morphology after GP treatment was determined in NHEK (Fig. 3.14f). The number of intermediate mitochondria was increased after GP treatment about 20% in NHEM (Fig. 3.13f) and about 50% in NHDF but the percentage of fragmented cells was below 15% (Fig. 3.15c).
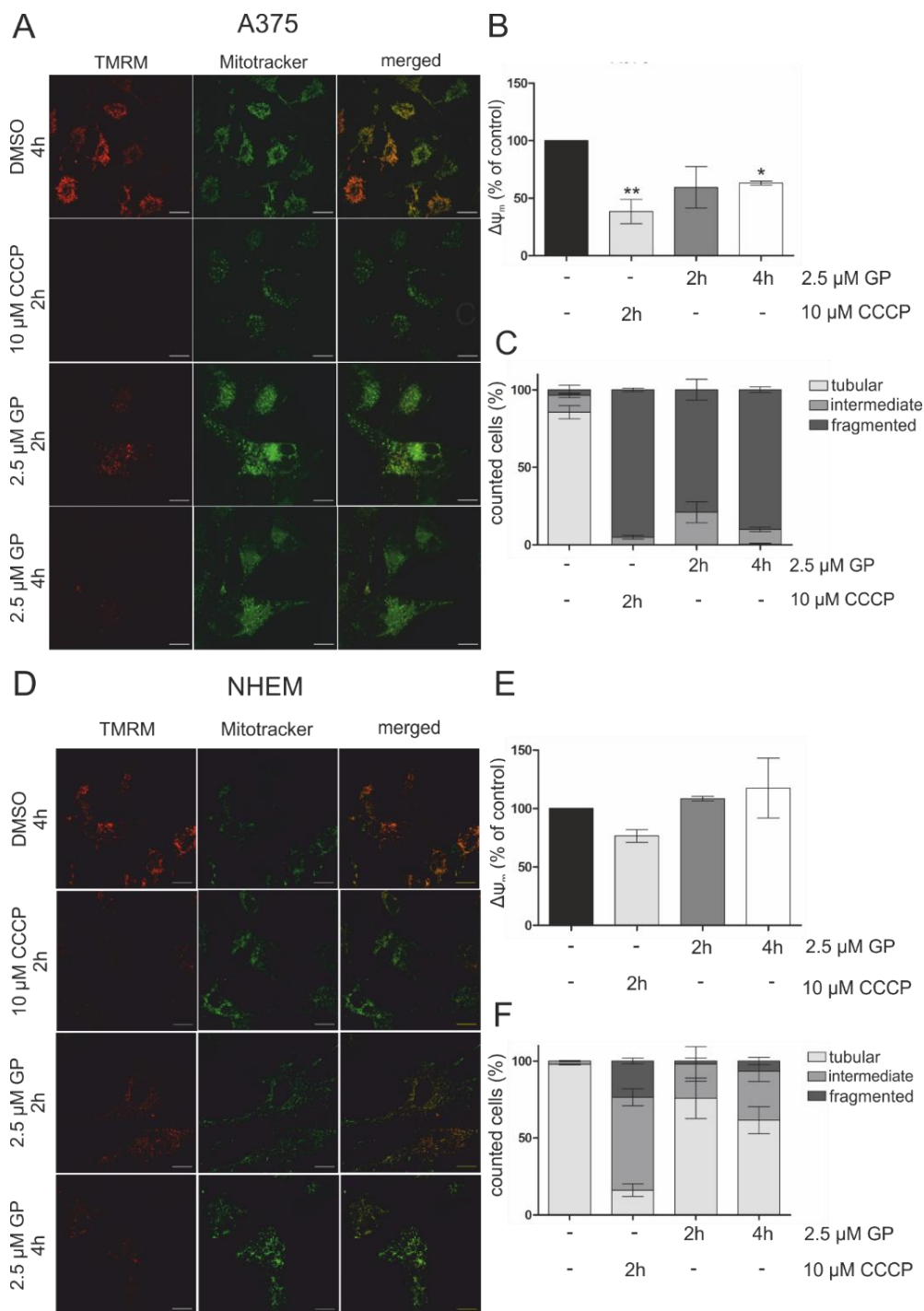
Fig. 3.13 Effect of GP on mitochondrial membrane potential ($\Delta\psi_m$) and mitochondrial fragmentation in A375 melanoma cells and melanocytes (NHEM). Subconfluent A375 melanoma cells (**a-c**) and NHEM (**d-f**) were mock-treated or treated with 2.5 µM GP for 2 and 4 h, respectively. CCCP at a concentration of 10 µM (2h) served as positive control. Subsequently, cells were incubated with 100 nM TMRM and 100 nM MitoTRACKER™ Green for 30 min and analysed by confocal microscopy. The scale bar is 20 µm. **a, d** Representative pictures are shown. **b, e** Calculation of the intensity of TMRM to MitoTRACKER™ Green was performed using Image J. The mock-treated control was set at 100%. One-way ANOVA with Dunnett's Multiple Comparison Test was used for the determination of statistical significance. *$p < 0.05$, **$p < 0.01$ **c, f** For quantification of the mitochondrial morphology, at least 30 cells of each condition were used. Data represent means ± SEM of three independent experiments, n=3. Data were already published in (Haasler et al. 2021).
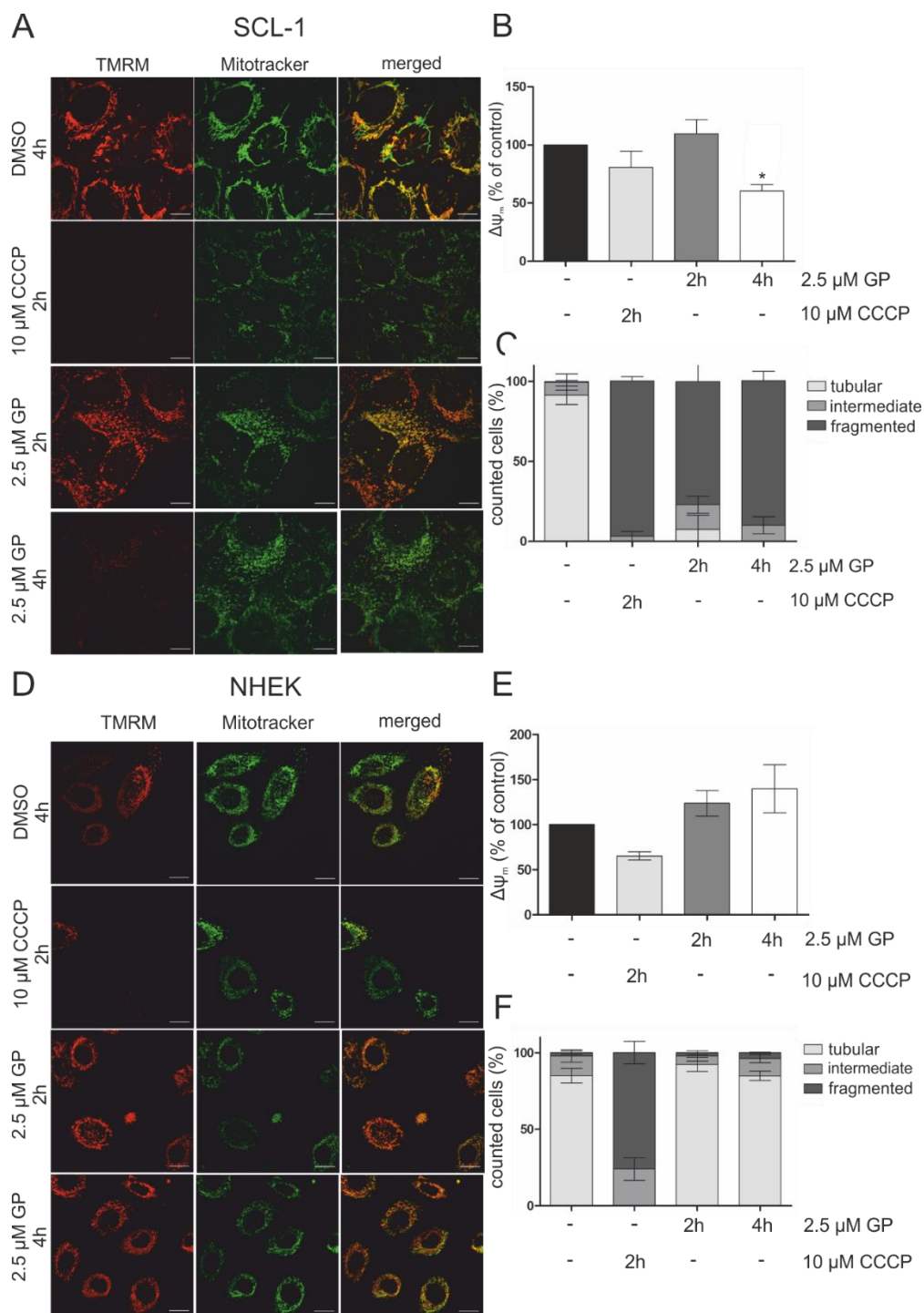
Fig. 3.14 Effect of GP on mitochondrial membrane potential mitochondrial ($\Delta\psi_m$) and fragmentation in SCL-1 carcinoma cells and keratinocytes (NHEK). Subconfluent SCL-1carcinoma cells (**a-c**) and NHEK (**d-f**) were mock-treated or treated with 2.5 μM GP for 2 and 4 h, respectively. CCCP at a concentration of 10 μM (2h) served as positive control. Subsequently, cells were incubated with 100 nM TMRM and 100 nM MitoTRACKER™ Green for 30 min and analysed by confocal microscopy. The scale bar is 20 μm. **a, d** Representative pictures are shown. **b, e** Calculation of the intensity of TMRM to MitoTRACKER™ Green was performed using Image J. The mock-treated control was set at 100%. One-way ANOVA with Dunnett's Multiple Comparison Test was used for the determination of statistical significance. *p<0.05. **c, f** For quantification of the mitochondrial morphology, at least 30 cells of each condition were used. Data represent means ± SEM, of three independent experiments, n=3.
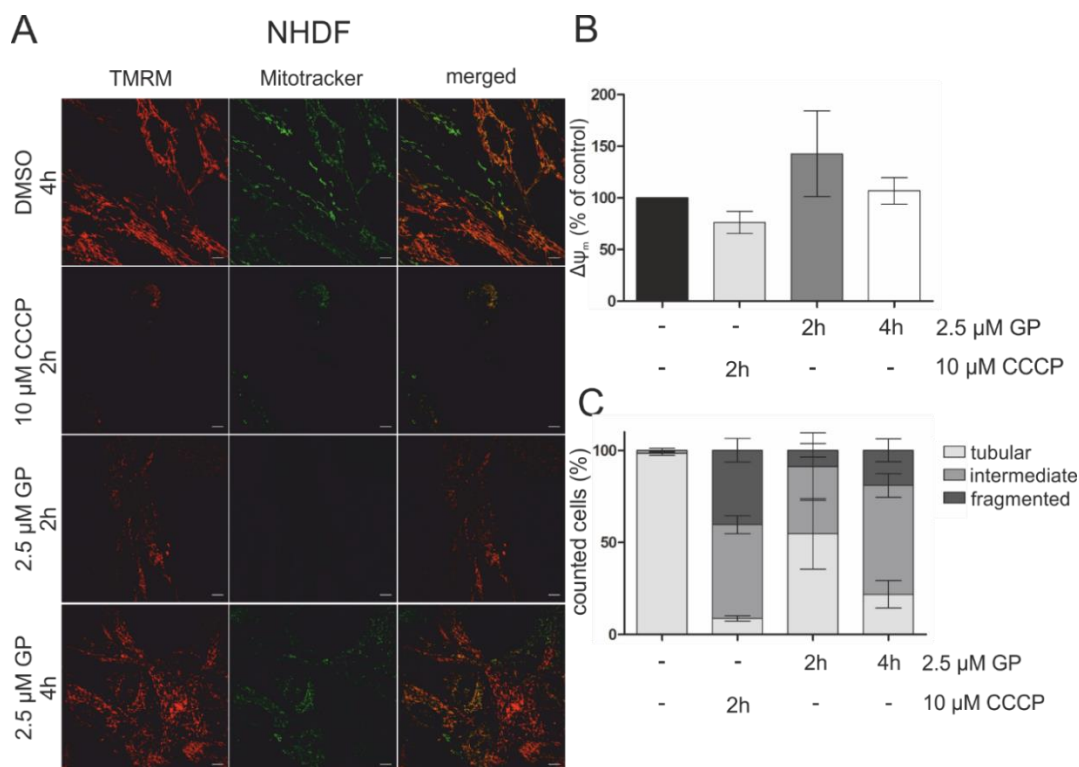
Fig. 3.15 Effect of GP on mitochondrial membrane potential ($\Delta\psi_m$) and mitochondrial fragmentation in fibroblasts (NHDF). Subconfluent NHDF (**a-c**) were mock-treated or treated with 2.5 µM GP for 2 and 4 h, respectively. CCCP at a concentration of 10 µM (2h) served as positive control. Subsequently, cells were incubated with 100 nM TMRM and 100 nM MitoTRACKER™ Green for 30 min and analysed by confocal microscopy. The scale bar is 10 µm. **a** Representative pictures are shown. **b** Calculation of the intensity of TMRM to MitoTRACKER™ Green was performed using Image J. The mock-treated control was set at 100%. One-way ANOVA with Dunnett's Multiple Comparison Test was used for the determination of statistical significance. **c** For quantification of the mitochondrial morphology, at least 30 cells of each condition were used. Data represent means ± SEM of three independent experiments, n=3.

3.7 GP affected oxidative phosphorylation

Mitochondria play an important role in bioenergetic processes and dysfunction can lead to minor or strong impacts on cells dependent on the magnitude of the impairment. Since energy production by oxidative phosphorylation requires an intact $\Delta\psi_m$ (Zorova et al. 2018), the effect of GP on mitochondrial respiration was determined using Seahorse XF Analyser. As the drop in $\Delta\psi_m$ occurred rapidly after GP was added to the cells, the cells were incubated for 1 h with different concentrations of GP until the Mito Stress Test was performed. The assay provides information about the oxygen consumption rate (OCR) after the addition of different mitochondrial stressors including oligomycin (Oligo), FCCP and rotenone/antimycin A (Rot/AA), from which the parameters "basal respiration", "ATP production", "spare respiratory capacity" and "proton leak" can be derived. The basal respiration was significantly increased about 2-fold in A375 melanoma cells after application of 2.5 µM GP (Fig. 3.16a, b). Additionally,

the ATP production was lowered at the same GP concentration to 50% compared to control level, the spare respiratory was completely lost and the proton leak was increased significantly (Fig. 3.16c-e). Similar effects were observed in SCL-1 carcinoma cells. After treatment with 0.5, 1 and 2.5 µM GP, the basal respiration rather tended to increase compared to untreated or mock-treated cells (Fig. 3.17a, b). Furthermore, at the lowest concentration of GP, an increase in ATP production was observed, but with increasing concentration the ATP production dropped to 50% of control level (Fig. 3.17c). The cells showed no spare respiratory capacity after treatment with 2.5 µM GP accompanied by a significant increase in the proton leak (Fig. 3.17d-e).
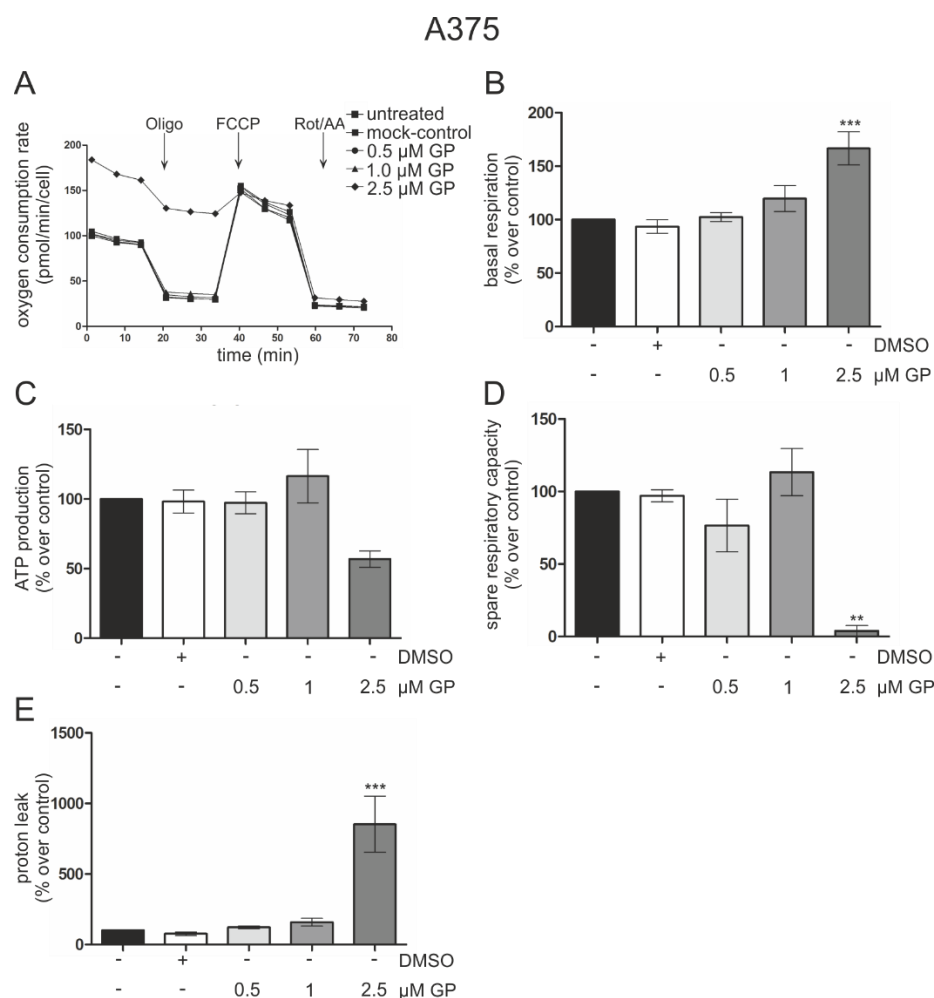
Fig. 3.16 Effect of GP on mitochondrial respiration in A375 melanoma cells. **a** After treatment with different concentrations of GP for 1 h, the oxygen consumption rate (OCR) was meascured after successive injection of oligomycin (Oligo), FCCP and rotenone/antiymcin A (Rot/AA) by Seahorse XF Analyser. A representative curve was depicted. **b-e** Based on the OCR in response to these mitochondrial stressors, the parameters "basal respiration" (**b**), "ATP production" (**c**), "spare respiratory capacity" (**d**) and "proton leak" (**e**) were calculated. The value of untreated cells were set at 100%. Data represent means ± SEM of three independent experiments, n=3. One-way ANOVA with Dunnett's Multiple Comparison Test was used for the determination of statistical significance between mock-treated (DMSO) and GP treated cells. **p<0.01 and ***p<0.001.

Fig. 3.17 Effect of GP on mitochondrial respiration in SCL-1 carcinoma cells. **a** After treatment with different concentrations of GP for 1 h, the oxygen consumption rate (OCR) was meascured after successive injection of oligomycin (Oligo), FCCP and rotenone/antiymcin A (Rot/AA) by Seahorse XF Analyser. A representative curve was depicted. **b-e** Based on the OCR in response to these mitochondrial stressors, the parameters "basal respiration" (**b**), "ATP production" (**c**), "spare respiratory capacity" (**d**) and "proton leak" (**e**) were calculated. The value of untreated cells were set at 100%. Data represent means ± SEM of three independent experiments, n=3. One-way ANOVA with Dunnett's Multiple Comparison Test was used for the determination of statistical significance between mock-treated (DMSO) and GP treated cells. *p<0.05, and **p<0.01.

Unlike the effect of GP on respiration in tumour cells, only minor effects were observed in normal (healthy) cells. The highest GP concentration of 2.5 µM increased the basal respiration significantly in NHEM without affecting the ATP production and spare respiratory capacity. The proton leak was raised after GP treatment but not significant in comparison to mock-treated cells (Fig. 3.18). Similar results were observed in NHEK. The basal respiration was enhanced slightly after GP treatment. In addition to that, the ATP production was unaffected after GP treatment and the spare respiratory capacity was lowered after treatment with 2.5 µM GP but this effect was not significant compared to mock-treated cells. The increase of the proton leak

after GP application was not significant (Fig. 3.19). The effects on mitochondrial respiration in NHDF were also less compared to both tumour cell lines. Significant changes were only observed at the highest GP treatment of 2.5 µM including an increase of basal respiration and proton leak as well as a 50% reduction of spare respiratory capacity. Interestingly, the ATP production was not affected after GP treatment (Fig. 3.20).
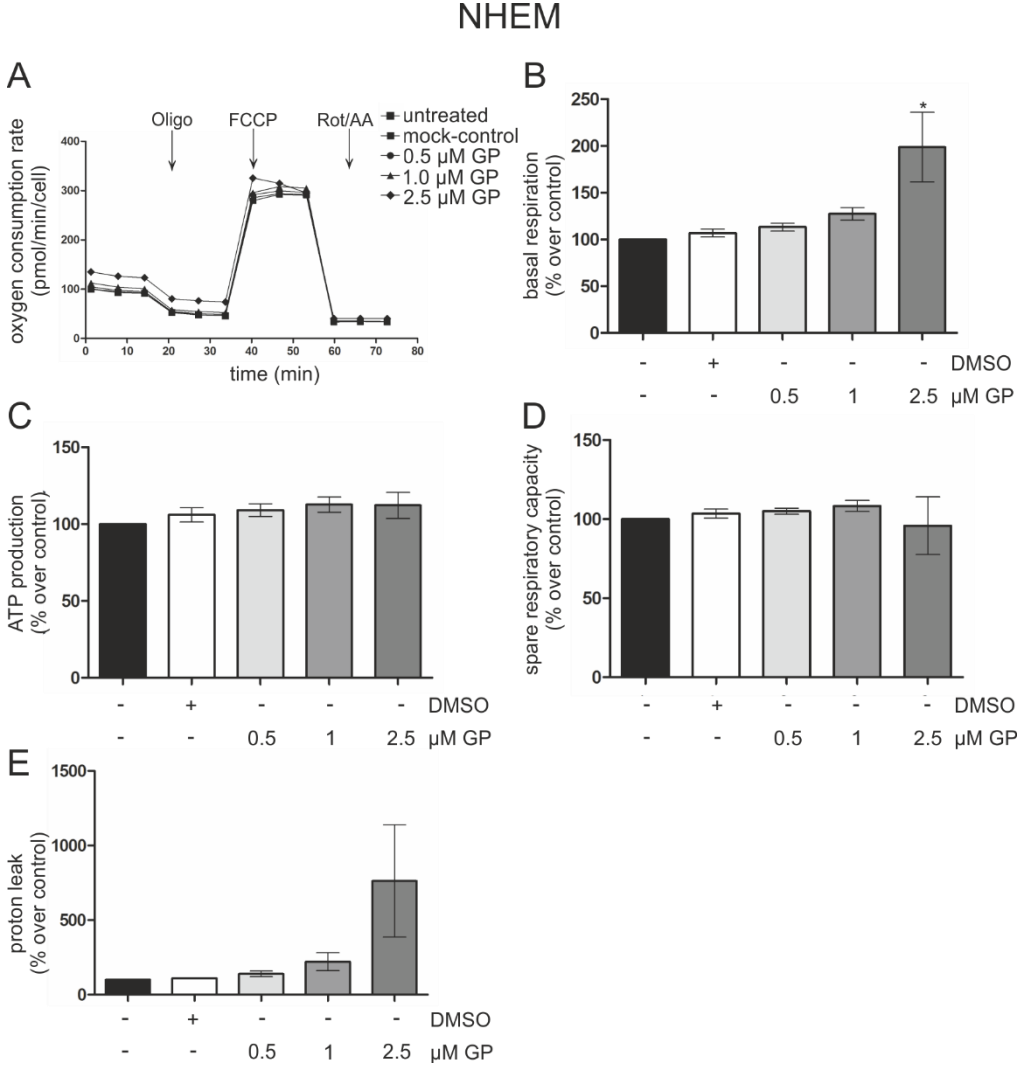
Fig. 3.18 Effect of GP on mitochondrial respiration in melanocytes (NHEM). **a** After treatment with different concentrations of GP for 1 h, the oxygen consumption rate (OCR) was meascured after successive injection of oligomycin (Oligo), FCCP and rotenone/antiymcin A (Rot/AA) by Seahorse XF Analyser. A representative curve was depicted. **b-e** Based on the OCR in response to these mitochondrial stressors, the parameters "basal respiration" (**b**), "ATP production" (**c**), "spare respiratory capacity" (**d**) and "proton leak" (**e**) were calculated. The value of untreated cells were set at 100%. Data represent means ± SEM of three independent experiments, n=3. One-way ANOVA with Dunnett's Multiple Comparison Test was used for the determination of statistical significance between mock-treated (DMSO) and GP treated cells. *p<0.05.

NHEK

Fig. 3.19 Effect of GP on mitochondrial respiration in keratinocytes (NHEK). **a** After treatment with different concentrations of GP for 1 h, the oxygen consumption rate (OCR) was meascured after successive injection of oligomycin (Oligo), FCCP and rotenone/antiymcin A (Rot/AA) by Seahorse XF Analyser. A representative curve was depicted. **b-e** Based on the OCR in response to these mitochondrial stressors, the parameters "basal respiration" (**b**), "ATP production" (**c**), "spare respiratory capacity" (**d**) and "proton leak" (**e**) were calculated. The value of untreated cells were set at 100%. Data represent means ± SEM of three independent experiments, n=3. One-way ANOVA with Dunnett's Multiple Comparison Test was used for the determination of statistical significance between mock-treated (DMSO) and GP treated cells. **p<0.01.

Fig. 3.20 Effect of GP on mitochondrial respiration in fibroblasts (NHDF). **a** After treatment with different concentrations of GP for 1 h, the oxygen consumption rate (OCR) was meascured after successive injection of oligomycin (Oligo), FCCP and rotenone/antiymcin A (Rot/AA) by Seahorse XF Analyser. A representative curve was depicted. **b-e** Based on the OCR in response to these mitochondrial stressors, the parameters "basal respiration" (**b**), "ATP production" (**c**), "spare respiratory capacity" (**d**) and "proton leak" (**e**) were calculated. The value of untreated cells were set at 100%. Data represent means ± SEM of three independent experiments, n=3. One-way ANOVA with Dunnett's Multiple Comparison Test was used for the determination of statistical significance between mock-treated (DMSO) and GP treated cells. **p<0.01 and ***p<0.001.

Consistent with GP induced impairment of mitochondrial membrane potential and mitochondrial respiration, proteomics analysis after 24 h GP treatment of A375 melanoma and SCL-1 carcinoma cells showed predominant effects on mitochondrial proteins (see appendix: Fig. 9.6). This mainly applied to the decrease of proteins of cellular compartments including respiratory chain complex, mitochondrial membranes, mitochondrial matrix and mitochondrion. Additionally, biological processes such as electron transport chain, mitochondrion organisation and aerobic respiration were downregulated. Western Blot performed for validation of the proteomics data showed that GP lowered the expression of NDUFB4, a subunit of the NADH

dehydrogenase (complex I), in A375 melanoma cells and SCL-1 carcinoma cells as well as in NHEM. Conversely, the expression was not changed in NHDF and upregulated in NHEK. Concomitantly, Mic60 belonging to the MICOS complex being part of the crista formation was almost completely lost in SCL-1 carcinoma cells and NHDF. The protein expression was almost lowered to 25% in A375 melanoma cells and half in NHEM compared to mock-treated cells. No effect was observed in NHEK (see appendix: Fig. 9.7). These data suggest that GP qualitatively affects mitochondrial respiration of all cells regarding basal respiration and proton leak. In contrast, the effect of GP on spare respiratory capacity and ATP production is due to the cell type specific demands. Tumour cells have higher energy demands than healthy cells. Thus, tumour cells exhibit higher respiration to meet this demand and therefore, they may be more susceptible to effects on respiration (Hanahan and Weinberg 2011, Barbi de Moura et al. 2012, Lee et al. 2020).

3.8   ROS independent mechanism of GP

Mitochondrial dysfunction including a drop in $\Delta\psi_m$, changes in mitochondrial morphology and respiration are reported to be linked with increased ROS formation (Korshunov et al. 1997, Yu et al. 2006, Serasinghe and Chipuk 2017). To assess whether the observed GP mediated effects were due to ROS formation, the DCF assay was performed. The assay measured the generation of intracellular ROS within cells (LeBel et al. 1992, Wang and Joseph 1999) is described to quickly provide data (Lebel and Bondy 1990). It was shown that tumour cells exhibited higher basal ROS levels compared to normal cells and, as a consequence, are more vulnerable against a further increase in the ROS amount, for example by exogeneous ROS sources (Alili et al. 2013, Aplak et al. 2020). For that reason, the basal ROS level was determined in both tumour and normal cells (Fig. 3.21a). A375 melanoma cells showed the highest basal ROS level, followed by SCL-1 carcinoma cells. The basal intracellular ROS contents in NHEM, NHEK and NHDF were at a similar range, but lower than the ROS amount of the tumour cells. The addition of different concentrations of GP did not enhance the intracellular ROS level after 90 min in both tumour and normal cells (Fig. 3.21b). On the contrary, the results showed a slight falling trend in the fluorescence intensity. For validation of the assay, 2 mM H_2O_2 was applied which induced an increase of the intracellular ROS level at least 4-fold over control.
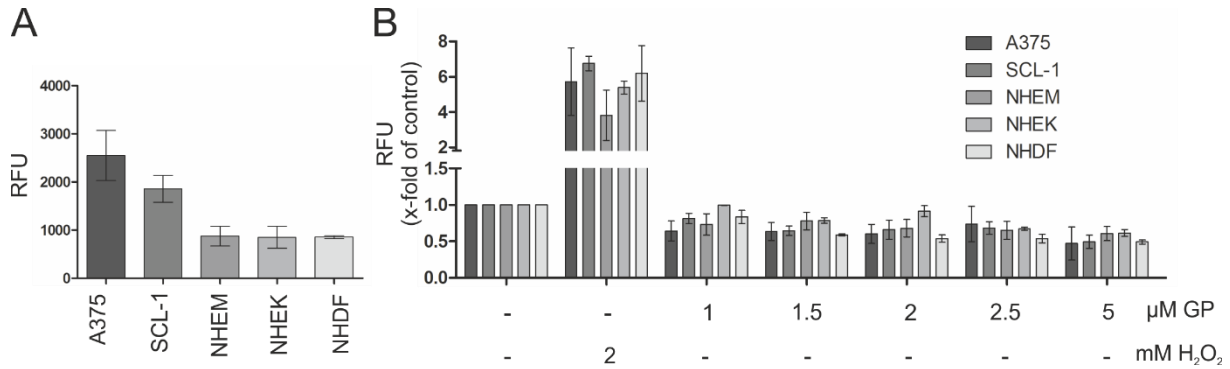
Fig. 3.21 Effect of GP on intracellular ROS formation. After addition of 100 µM H$_2$DCF-DA A375 melanoma cells, SCL-1 carcinoma cells, melanocytes (NHEM), keratinocytes (NHEK) and fibroblasts (NHDF) were mock-treated and treated with different concentration of GP, respectively, for 90 min. H$_2$O$_2$ (2 mM) served as positive control. The ROS generation was measured by DCF assay. *RFU* (relative fluorescence unit) **a** The starting measuring point of mock-treated cells was defined as basal ROS level. **b** To calculate the formation of ROS, the first measuring point (0 min) was subtracted from the last measuring point (90 min). The mock-treated control of each cell line was set at 1.0 and the treatment was set in relation to it. Data represent means ± SEM of at least three independent experiments in A375, SCL-1, NHEM and NHEK, n≥3, and two experiments in NHDF, n=2. Data referred to A375 and NHEM were already published in (Haasler et al. 2021).

To substantiate the DCF data, it was subsequently investigated whether the induced toxicity of GP in tumour cells can be affected in the presence of antioxidants. As the tumour cells showed the GP mediated toxicity, only A375 melanoma and SCL-1 carcinoma cells were pre-treated with different concentration of the antioxidant N-acetylcysteine (NAC) before 2.5 µM GP was added. The cell viability, measured by MTT assay, was decreased in GP treated cells independent of the presence of NAC (Fig. 3.22a, b). For validation of the assay, A375 melanoma cells were treated with 5 mM NAC in combination with and without 700 µM H$_2$O$_2$. The amount of NAC was sufficient to diminish the H$_2$O$_2$ induced toxicity significantly (Fig. 3.22c). Additionally, the antioxidant and vitamin E derivative trolox was tested in A375 melanoma cells to confirm the previous results. The presence of trolox did not abolish the GP induced reduction of cell viability (Fig. 3.22d), although the chosen concentrations of trolox were sufficient to significantly rescue H$_2$O$_2$ induced toxicity (Fig. 3.22e).
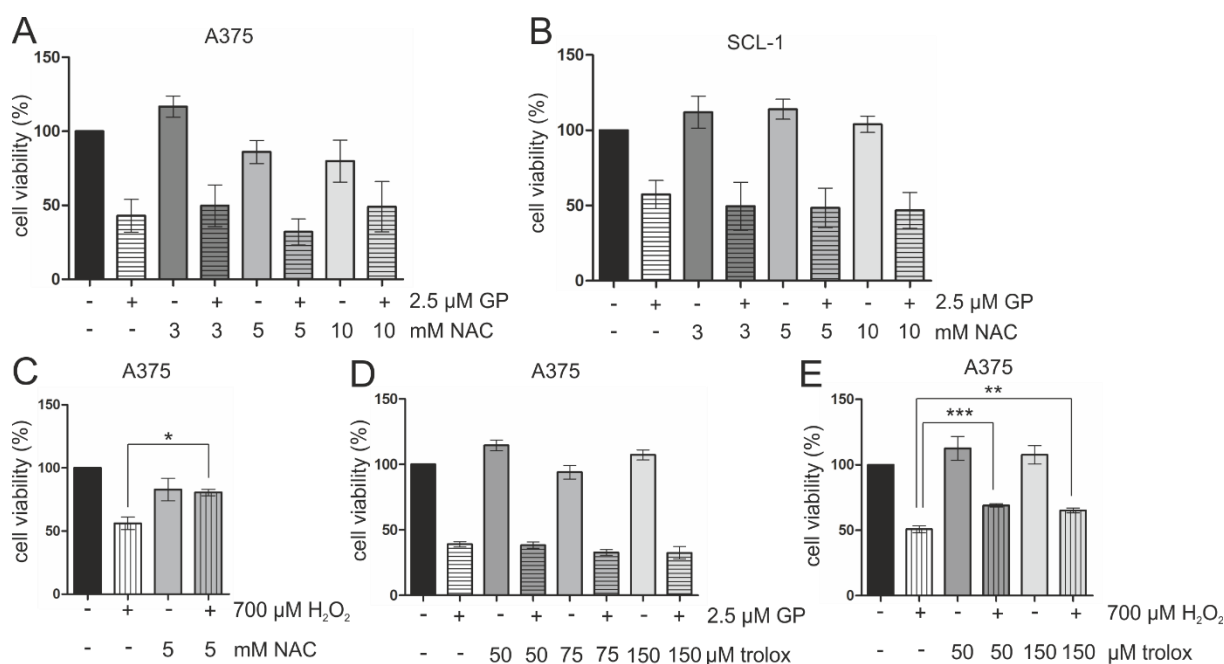
Fig. 3.22 Effect of combination treatment with GP and antioxidants on cell viability.**a, b** A375 melanoma (**a**) and SCL-1 carcinoma cells (**b**) were pre-treated with different concentration of the antioxidant N-acetylcysteine (NAC) for 4 h, followed by treatment with and without 2.5 µM GP for further 24 h. **c** A375 melanoma cells were pre-treated with 5 mM NAC and subsequent with and without 700 µM H_2O_2 for 24 h. **d, e** After pre-treatment with different concentration of the antioxidant trolox, A375 melanoma cells were mock treated or treated either with 2.5 µM GP (**d**) or with 700 µM H_2O_2 for 24 h. **a-e** Cell viability was measured by MTT assay. Data represent means ± SEM of at least three independent experiments, n≥3. Mock-treated control was set at 100%. For statistical significance, Student's *t*-test (**c**) and one-way ANOVA with Bonferroni's Multiple Comparison Test were performed (**a-b, d-e**). *$p<0.05$, **$p<0.01$ and ***$p<0.001$. Data referred to A375 (**a, c-e**) were already published in (Haasler et al. 2021).

After demonstrating that GP neither increased intracellular ROS level nor its cytotoxic effect could be rescued by antioxidants, another approach was performed to confirm that GP mediates ROS independent effects. In this regard, a redox sensor named HyPer was used which is a genetically encoded fluorescence-based ratiometric probe being a tool for the detection of intracellular H_2O_2 (Bilan and Belousov 2016, Booth et al. 2016). Due to the same effect of GP on both tumour cell lines and the complexity of this assay, only A375 melanoma cells were chosen for the experiment. HyPer contains a bacterial H_2O_2 sensing domain (OxyR) and a circularly permuted Yellow Fluorescence Protein (cpYFP). In the presence of H_2O_2, cysteine at the position 199 was oxidized leading to a conformational change of the OxyR domain and, consecutively, to an alteration in the fluorescence emission of cpYFP. As HyPer is also sensitive to changes in the pH value, SypHer was also applied. SypHer was reported as redox insensitive but pH sensitive sensor and was used in this study as control (Booth et al. 2016). The insensitivity to H_2O_2 is based on a single mutation in C199S in comparison to HyPer. Both HyPer and SypHer can be targeted to specific compartments intracellularly

allowing the detection of H_2O_2 in the mitochondria (mito) and the cytosol (Weller et al. 2014). After transient transfection with HyPer, SypHer, mitoHyPer and mitoSypHer, A375 melanoma cells were mock-treated or treated with 2.5 µM GP for 16 h (Fig. 3.23). The amount of H_2O_2 did not increase in the mitochondria and the cytosol after GP treatment compared to mock-treated cells. For validation of the assay, 100 µM H_2O_2 was used which significantly increased the fluorescence ratio signal. In summary, the GP mediated drop in cell viability of A375 melanoma and SCL-1 carcinoma cells accompanied by mitochondrial dysfunction is independent of the ROS level.
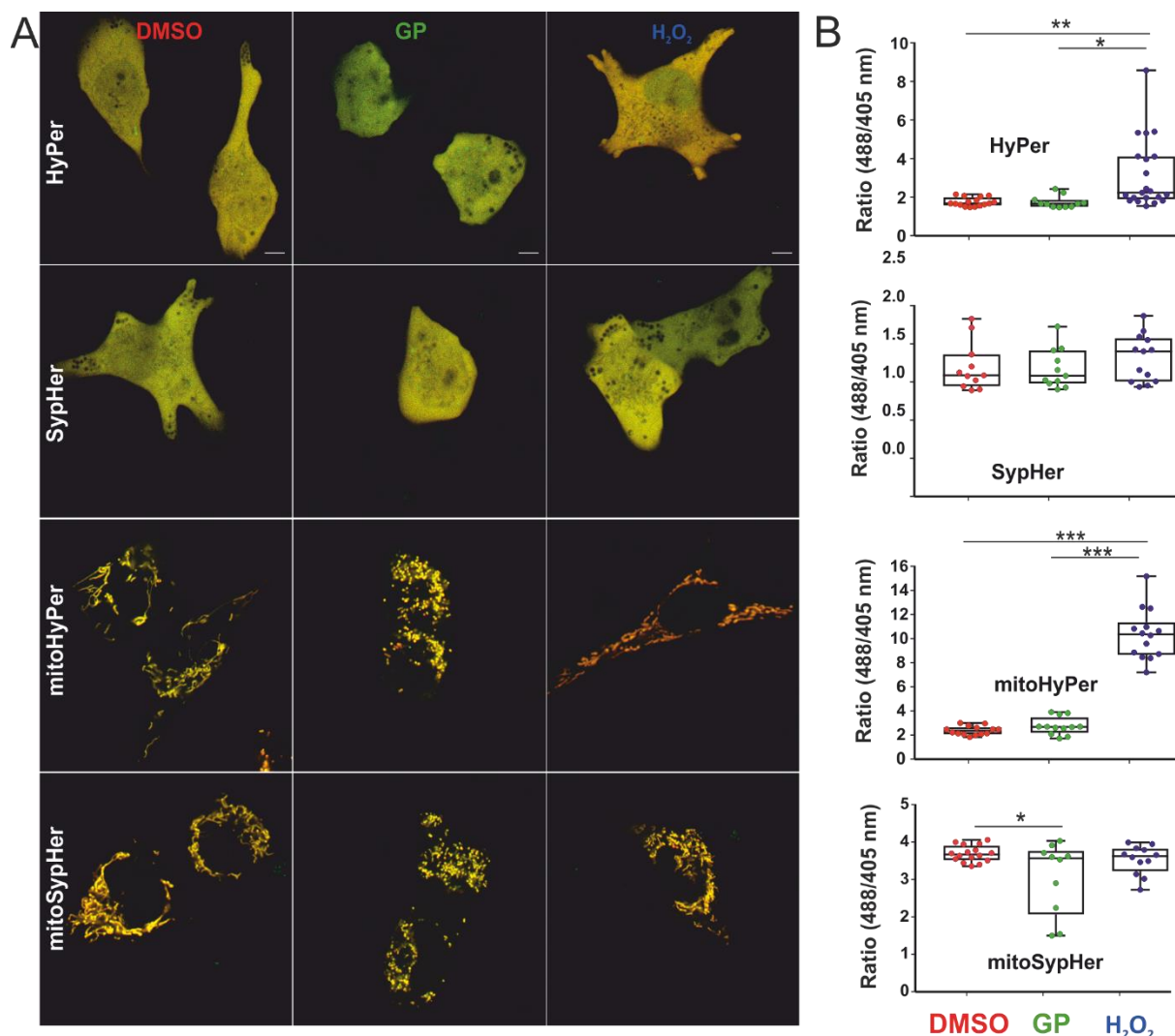
Fig. 3.23 Effect of GP on the generation of H_2O_2 in A375 melanoma cells. **a** After transient transfection of A375 melanoma cells with one of the four plasmids – HyPer (cytosolic), SypHer (cytosolic), mitoHyPer (mitochondrial matrix targeted) and mitoSypHer (mitochondrial matrix targeted) –, cells were mock-treated or treated with 2.5 µM GP for 16 h. H_2O_2 at a concentration of 100 µM served as positive control. Representative merged images of both channels are depicted. **b** Box plot analysis of H_2O_2 levels of each condition. The average intensity of ratiometric fluorescence of each cell is shown. For determination of statistical significance, Student's t-test was used. *$p < 0.05$, **$p < 0.01$ and ***$p < 0.001$. Data were already published in (Haasler et al. 2021).

3.9 GP induced apoptosis in A375 melanoma cells

BH3 mimetics were developed to bind anti-apoptotic proteins of the Bcl-2 family leading to oligomerisation of pro-apoptotic proteins which cause mitochondrial permeabilization and finally resulting in apoptosis (Henz et al. 2019). With respect to the calculated IC_{50} values after 24 h GP treatment ranging from 1.7 to 3.0 µM in tumour cells (Fig. 3.7a), a concentration of 2.5 µM was used for the majority of experiments relating to studies of cell death. Since GP, at a concentration of 2.5 µM, showed hardly any effect on cell viability in normal cells, only tumour cells were considered to study the death pathways. At first, the effect of GP on the release of inner mitochondrial proteins such as Smac/Diablo was determined in A375 melanoma cells. This protein exerts pro-apoptotic properties indirectly through the binding of inhibitors of apoptosis proteins (IAP) (Chai et al. 2000, Du et al. 2000, Verhagen et al. 2000). The treatment of GP increased the amount of Smac/Diablo in the cytosolic fraction over time indicating a preceding mitochondrial permeabilization. Staurosporine (Sts) served as positive control showing an increase of cytosolic Smac/Diablo (Fig. 3.24).
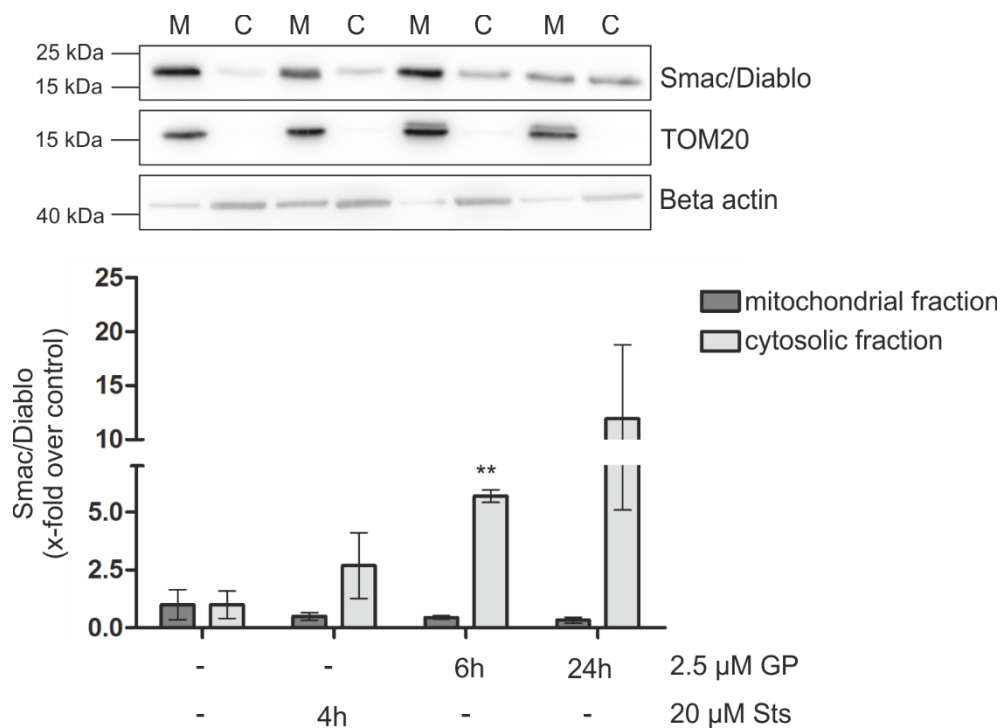
Fig. 3.24 Effect of GP on cytosolic release of Smac/Diablo in A375 melanoma cells. After incubation with 2.5 µM GP for 6 and 24 h, respectively, or 20 µM staurosporine (Sts) as positive control, cells were harvested and separated in mitochondrial and cytosolic fraction. Western Blot analysis of Smac/Diablo was performed. TOM20 was used as mitochondrial marker, beta actin as cytosolic marker. Quantification of the protein amount was calculated compared to the respective mock-treated control. Mock-treated control of both fractions was set at 1. Student's *t*-test was used for determination of statistical significance between mock-control and 2.5 µM GP treatment for 6 h. **p<0.01, n=3. Data were already published in (Haasler et al. 2021).

In addition to the release of Smac/Diablo, the activity of the initiator caspase 9 was increased 5 to 10-fold after GP treatment for 6 h in A375 melanoma cells (Fig. 3.25a). Furthermore, GP increased the activity of effector caspase 3/7 after 24 h and this was abolished by adding the pan-caspase inhibitor zVAD (Fig. 3.25b). Moreover, the expression levels of procaspase 3, the inactive caspase, and cleaved as well as full length PARP were determined in A375 melanoma cells. For that, the cells were treated with 2.5 and 5 µM GP up to 48 h. Both concentrations lowered the expression levels of procaspase 3 as well as induced PARP cleavage (Fig. 3.25c).
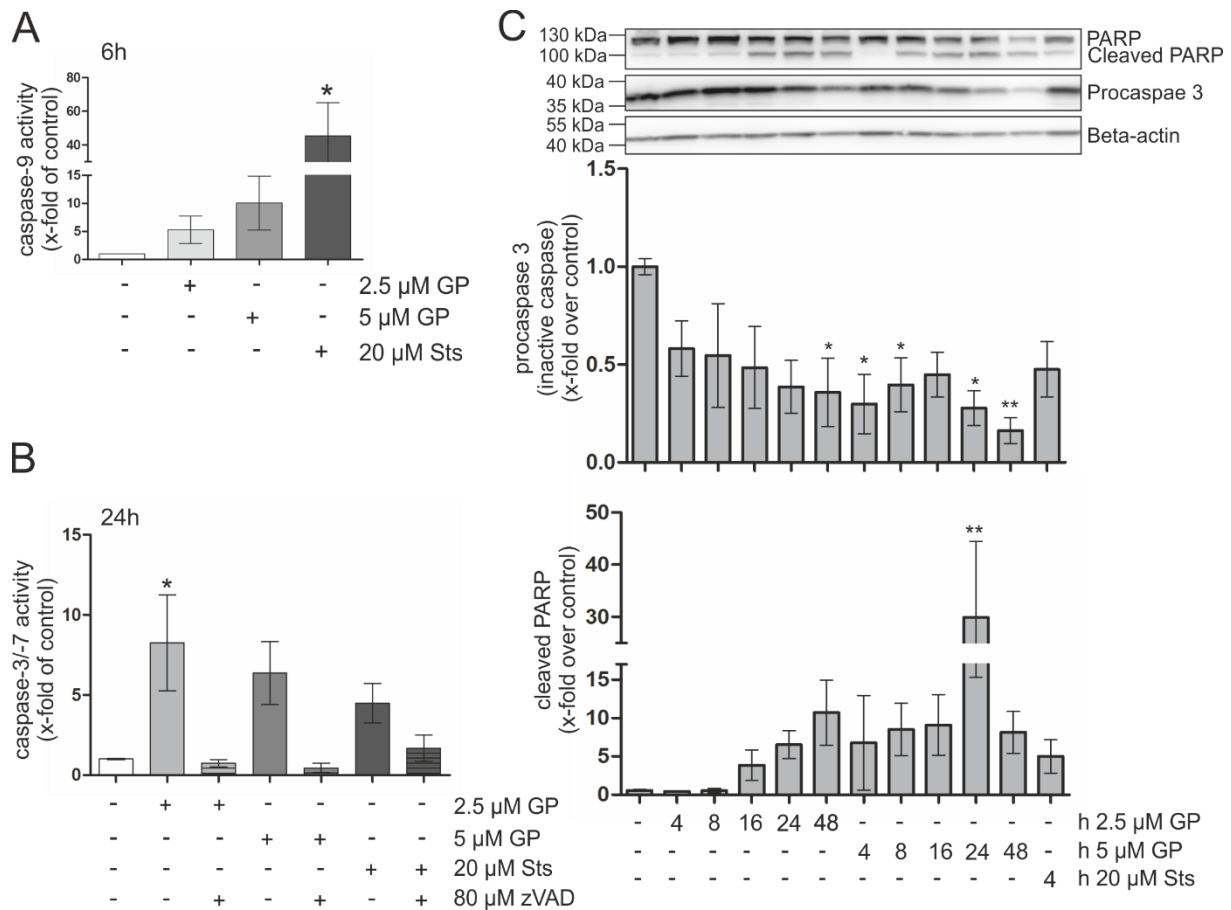
Fig. 3.25 Effect of GP on apoptotic markers in A375 melanoma cells. **a** Subconfluent A375 melanoma cells were treated with 2.5 and 5 µM GP for 6h. Staurosporine (Sts) at a concentration of 20 µM for 4 h served in all experiments as positive control for apoptosis induction. Caspase 9 activity was determined. Mock-treated control was set at 1. **b** A375 melanoma cells were treated with 2.5 and 5 µM GP for 24 h. zVAD (80 µM) was added 10 min before measuring of caspase 3/7 activity. Mock-treated control was set at 1. **c** Western Blot analysis of PARP cleavage and procaspase 3. For that, A375 melanoma cells were incubated with 2.5 and 5 µM GP for 4, 8, 16, 24 and 48 h. Beta-actin served as loading control. Quantification of procaspase 3 and cleaved PARP was determined. The x-fold increase of protein levels was compared to mock-treated control which was set at 1. A representative Blot was depicted. For determination of statistical significance, one-way ANOVA with Dunnett's Multiple Comparison Test was used. *p<0.05 and **p<0.01, n=3. Data were already published in (Haasler et al. 2021).

To confirm the GP induced caspase dependent apoptotic pathway in A375 melanoma cells, cell viability was assessed after GP treatment in combination with the caspase inhibitor zVAD (Fig. 3.26a). zVAD lowered the effect of GP significantly but not completely. At the same time, GP induced PARP cleavage was abolished in the presence of zVAD (Fig. 3.26b). Thus, these data substantiated that GP induced cell death through apoptosis in A375 melanoma cells.
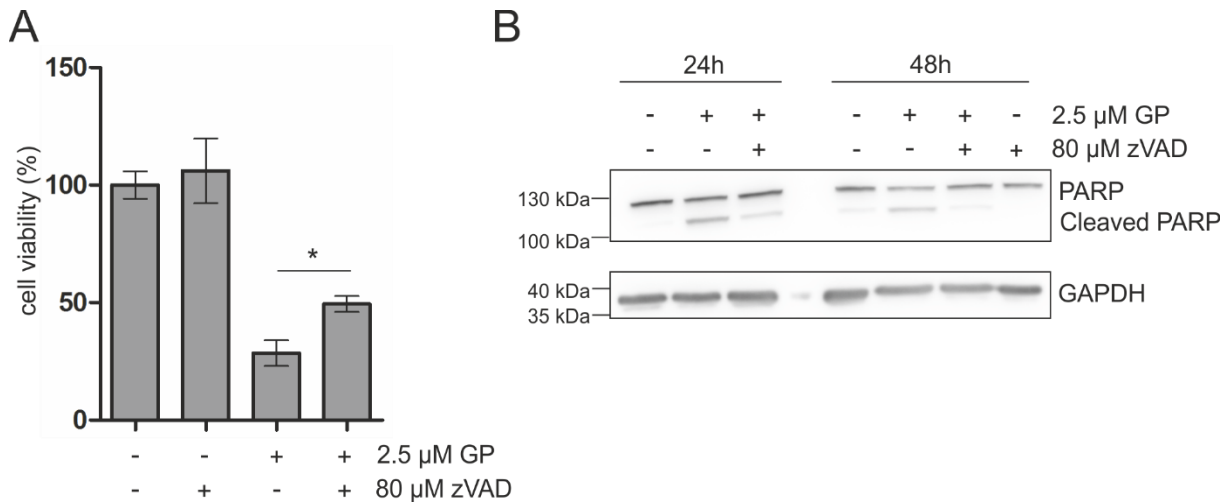
Fig. 3.26 Effect of the pan-caspase inhibitor zVAD on GP induced effects in A375 melanoma cells. **a** Cell viability was determined in A375 melanoma cells after treatment with 2.5 µM GP in the presence or absence of the caspase inhibitor zVAD (80 µM) for 24 h by MTT assay. Cell viability of mock-treated control was set at 100%. Data represent means ± SEM of three independent experiments, n=3. Student's *t*-test was used for determination of statistical significance between GP and combination treatment, *p<0.05, n=3. **b** After treatment with 2.5 µM GP, 80 µM zVAD or in combination for 24 and 48 h, expression of full length and cleaved PARP was determined by Western Blot. GAPDH was used as internal loading control. One representative Blot of three independent experiments is shown, n=3. Data were already published in (Haasler et al. 2021).

Since GP induced both apoptosis and mitochondrial fragmentation in A375 melanoma cells, the question was addressed whether Drp1, a GTPase being described to act as a major regulator in mitochondrial fission (Tilokani et al. 2018) and to be involved in apoptosis as well (Frank et al. 2001, Suen et al. 2008, Autret and Martin 2009), plays a role in those processes mediated by GP. Therefore, Drp1 was transiently downregulated in A375 melanoma cells (Fig. 3.27a) and mitochondrial morphology was studied after GP treatment for 2 and 4 h (Fig. 3.27b, c). No tubular structures were observed after GP treatment without Drp1 knockdown. GP induced intermediate and fragmented mitochondria were significantly decreased in Drp1 knockdown cells but did not reach control level. The results indicated that GP induced mitochondrial fragmentation is at least partly dependent on Drp1.
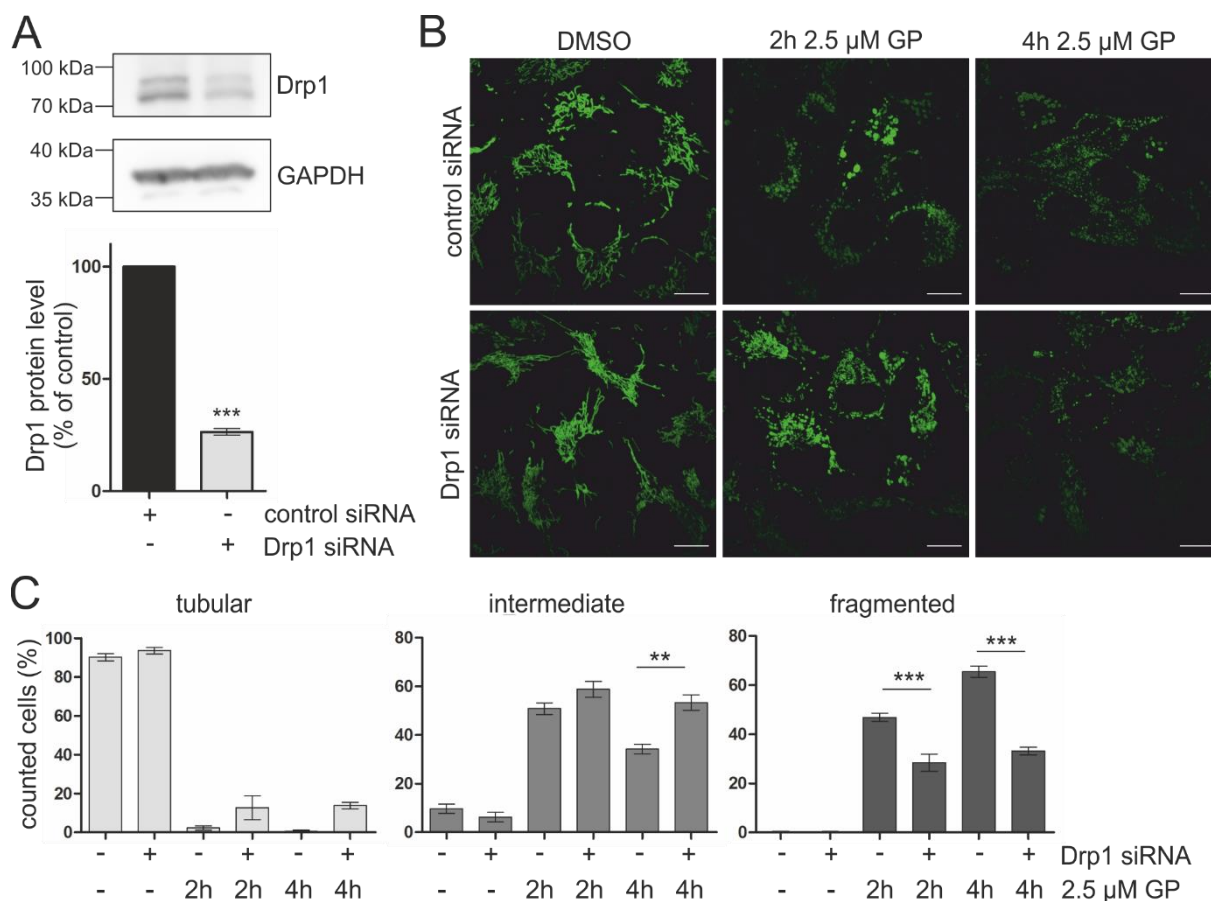
Fig. 3.27 Effect of Drp1 in GP induced fragmentation in A375 melanoma cells. **a** For transient Drp1 knockdown, A375 melanoma cells were incubated with DNM1L (Drp1) siRNA and control siRNA for 48 h, respectively. Western Blot analysis was performed to examine the knockdown efficiency. The quantification is shown below. Data represent means ± SEM of three independent experiments, n=3. One-way ANOVA with Dunnett's Multiple Comparison Test was used for determination of statistical significance. ***p<0.001. **b** To assess mitochondrial changes, Drp1 knockdown and control cells were mock-treated or treated with 2.5 µM GP for 2 and 4 h. Following, 100 nM MitoTRACKER™ was added to the cells and mitochondrial morphology was analysed by confocal microscopy. Representative pictures are shown. **c** Quantification of mitochondrial morphology. At least 30 cells of each conditions were counted and categorised in „tubular", „intermediate" and „fragmented". To determine statistical significance, one-way ANOVA with Bonferroni's Multiple Comparison Test was used. **p<0.01, ***p<0.001, n≥30, N=3. Data were already published in (Haasler et al. 2021).

3.10 GP did not induce apoptosis in SCL-1 carcinoma cells

Due to the potential of GP inducing a cytotoxic effect in both A375 melanoma cells and SCL-1 carcinoma cells, apoptosis markers were also analysed in carcinoma cells. In contrast to the previous results, GP did not activate the extrinsic initiator caspase 8 or the intrinsic initiator caspase 9. For validation of the assay, SCL-1 carcinoma cells were treated with 20 µM Sts resulting in a significant increase of both initiator caspases. Additionally, the effector caspases 3 and 7 were also not activated after GP treatment for 24 h (Fig. 3.28).
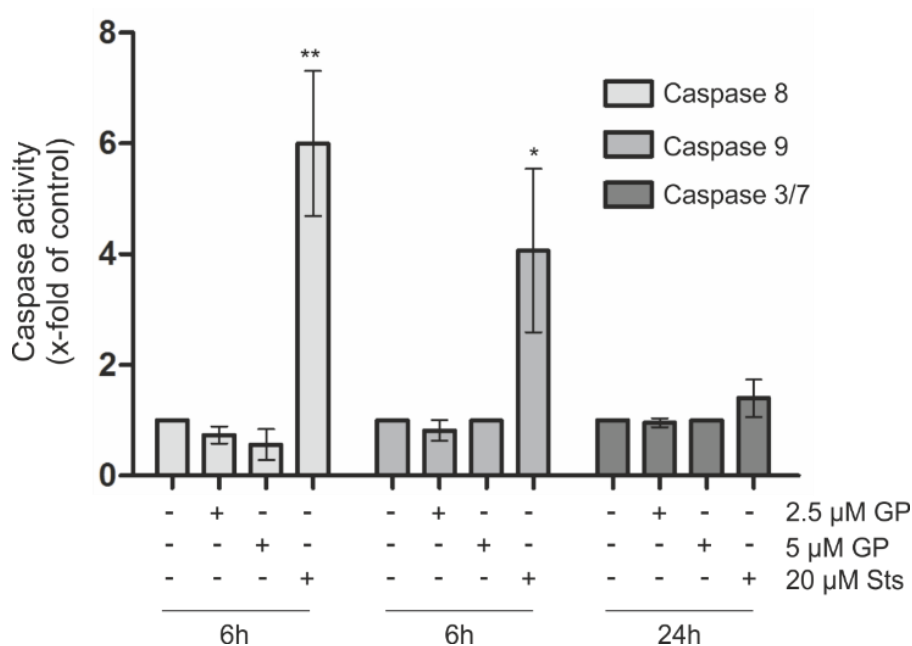
Fig. 3.28 Effect of GP on caspase activity in SCL-1 carcinoma cells.After treatment with 2.5 or 5 µM GP for 6 or 24 h, caspase activity was measured. Staurosporine (Sts, 20 µM) served as positive control. Mock-treated control was set at 1. Data represent means ± SEM of three independent experiments, n=3. One-way ANOVA with Dunnett's Multiple Comparison Test was used for the determination of statistical significance. *$p<0.05$, **$p<0.01$.

In order to verify these results, the expression levels of apoptosis relevant proteins were determined by Western Blot. For this purpose, SCL-1 carcinoma cells were treated with 2.5 and 5 µM GP up to 48 h to measure the protein expression of procaspase 3, the inactive form of caspase 3, as well as of full length and cleaved PARP (Fig. 3.29). GP treated cells showed no change in the amount of procaspase 3. Moreover, the cleaved PARP was increased over time after GP treatment but did not exceed control level. To demonstrate a caspase independent cell death of GP in SCL-1 carcinoma cells, cells were incubated with GP combined with the pan-caspase inhibitor zVAD (Fig. 3.30). The induced cytotoxic effect of GP did not change in the presence of zVAD indicating that the cell death occurred independent of apoptosis.
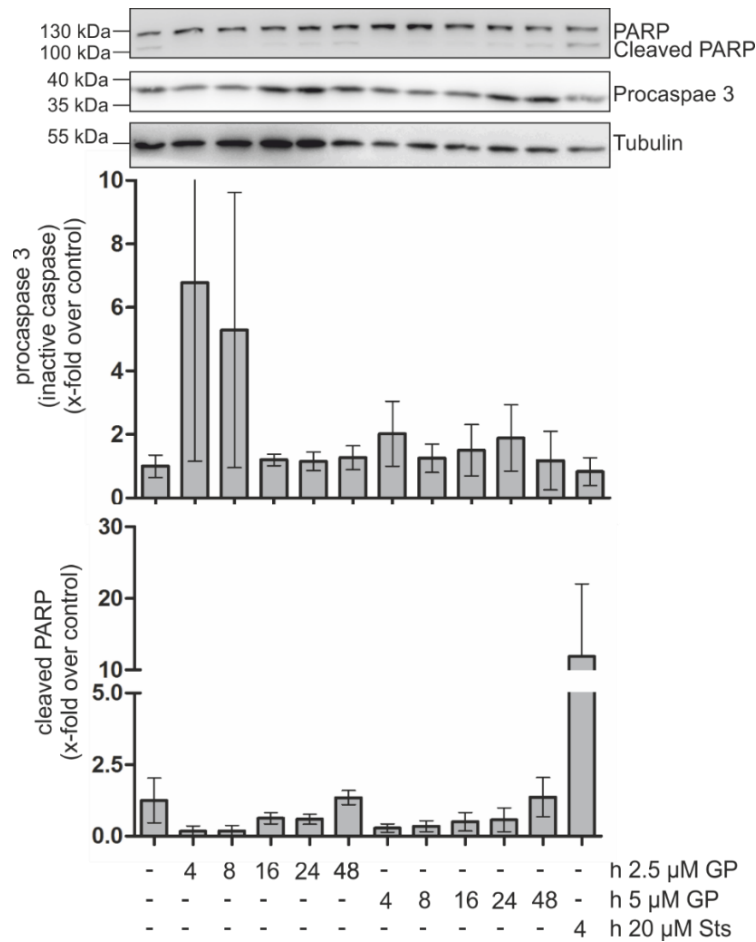
Fig. 3.29 Effect of GP on the expression levels of procaspase 3 and PARP in SCL-1 carcinoma cells. Subconfluent cells were treated with 2.5 or 5 μM GP for 4, 8, 16, 24 and 48 h. Mock-treated cells were used as negative control, 20 μM staurosporine (Sts) served as positive control. Protein expression of procaspase 3, full length and cleaved PARP was determined by Western Blot. Tubulin functioned as loading control. A representative blot of three independent experiments is depicted, n=3. Quantification of the protein amount was calculated compared to the respective control mock-treated control. Mock-treated control was set at 1.
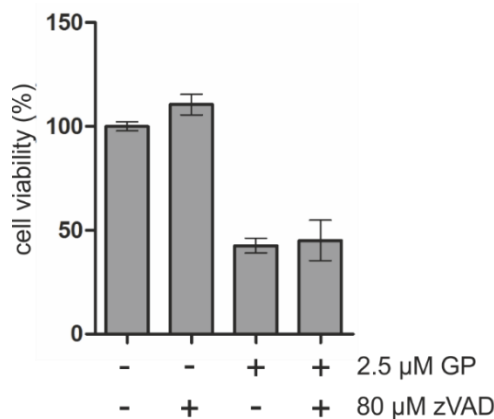
Fig. 3.30 Effect of GP in combination with a caspase inhibitor on cell viability of SCL-1 carcinoma cells. Subconfluent cells were pre-treated for 4 h with 80 μM of the pan-caspase inhibitor zVAD, followed by GP (2.5 μM) treatment for further 24 h. Cell viability was measured by MTT assay. Mock-treated control was set at 100%. Data represent means ± SEM of three independent experiments, n=3.

3.11 GP induced necroptosis in SCL-1 carcinoma cells

In contrast to A375 melanoma cells, no apoptotic markers could be detected in SCL-1 carcinoma cells. In the case of non-functional apoptosis, there is increasing evidence that necroptosis is a back-up cell death pathway to kill tumour cells effectively (Chen et al. 2016). Necroptosis is a programmed cell death sharing features with both apoptosis and necrosis. The molecular mechanisms are based on a signal cascade mediated by receptor-interacting serine/threonine protein kinase (RIP) 1 and RIP3 as well as mixed lineage kinase domain like pseudokinase (MLKL) (Gong et al. 2019). To figure out whether the necroptotic pathway was activated after GP treatment in SCL-1 carcinoma cells, a pharmacological inhibitor of the necroptotic pathway was tested. For this purpose, necrostatin-1 (Nec1) was chosen because this compound inhibits RIP1 and interrupts the signal cascade required for necroptotic cell death (Degterev et al. 2005). SCL-1 carcinoma cells were pre-treated with the RIP1 kinase inhibitor Nec1 prior to the GP treatment. The GP induced decrease in cell viability was significantly diminished in the presence of Nec1, indicating that necroptosis could be involved (Fig. 3.31b). As proof of principle, Nec1 was also tested in A375 melanoma cells. Whereas zVAD significantly rescued the cell viability in A375 melanoma cells (Fig. 3.26a), Nec1 had no impact on A375 melanoma cell viability (Fig. 3.31a).
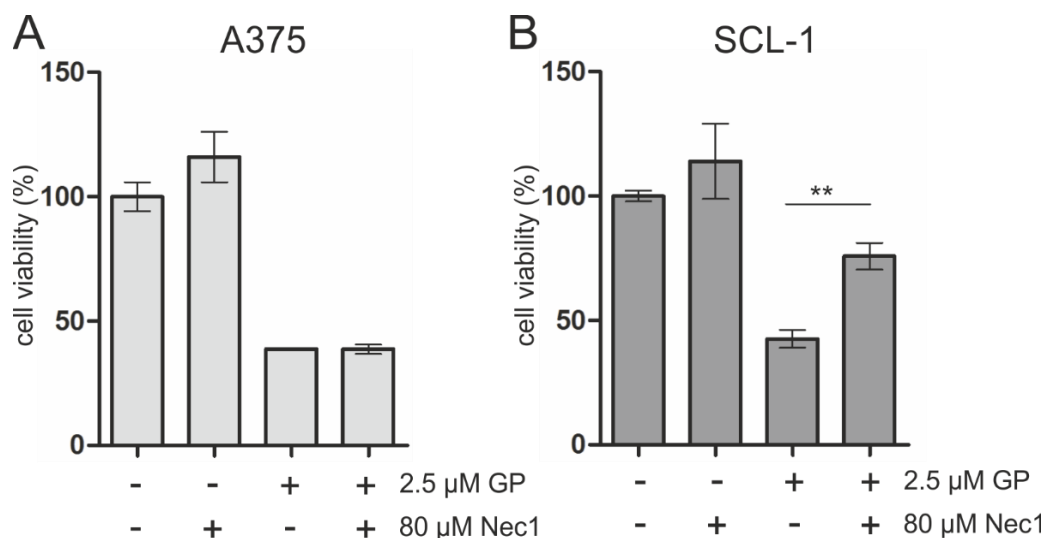
Fig. 3.31 Effect of GP in combination with a necroptosis inhibitor on cell viability of A375 melanoma and SCL-1 carcinoma cells. **a-b** After preincubation with 80 µM of the necroptosis inhibitor necrostatin-1 (Nec1) for 4 h, 2.5 µM GP was added to A375 melanoma (**a**) and SCL-1 carcinoma cells (**b**) for further 24 h. Cell viability was measured by MTT assay. Mock-treated cells were set at 100%. Data represent means ± SEM of three independent experiments, n=3. Student's *t*-test was used for determination of statistical significance. **p<0.01.

Although necroptosis is a regulated form of cell death, it has also similarities to necrosis including the loss of the integrity of the cellular membrane (Pasparakis and Vandenabeele

2015). To determine whether GP has an impact on the permeabilization of the cellular membrane, trypan blue staining was performed in SCL-1 carcinoma cells (Fig. 3.32). GP at a concentration of 2.5 µM initiated around 30% of the counted cells having permeabilized cell membranes after 24 h which further increased up to 50% after 48 h. The higher doses of GP (5 µM) enhanced this effect up to around 90% of cells with a loss in integrity of the cellular membrane. To demonstrate that this effect was due to necroptosis, a combination treatment with Nec1 was performed. Nec1 diminished the extent of damaged cells by GP indicating that necroptosis was involved in the cytotoxic effect of GP on SCL-1 carcinoma cells.
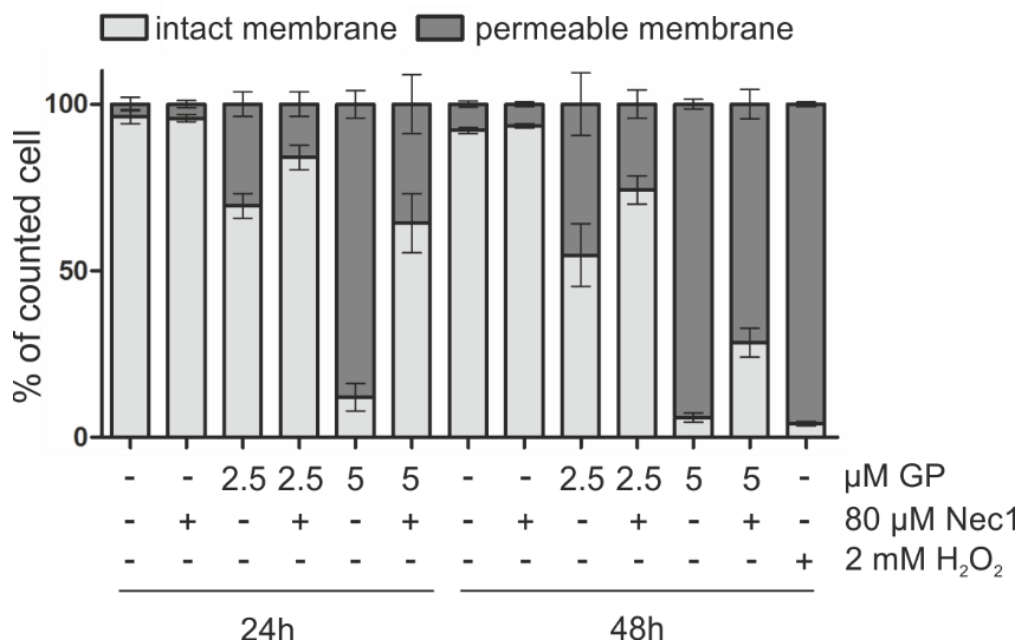
Fig. 3.32 Effect of GP in combination with Nec1 on cell membrane permeabilization in SCL-1 carcinoma cells. Subconfluent cells were pre-treated with 80 µM Nec1 for 4 h, followed by treatment with 2.5 and 5 µM GP for further 24 and 48 h. H_2O_2 (2 mM) was used as positive control. Subsequently, the number of cells was counted using trypan blue staining. Unstained cells were defined as containing an "intact membrane" and blue coloured cells as having a "permeable membrane". The total cell number of each condition was set at 100% and the percentage of cells with an intact versus a permeable membrane was shown of three independent experiments, n=3.

In order to confirm the necroptotic pathway in SCL-1 carcinoma cells, additional parameters have been tested. As a consequence of permeabilization of the membrane, cellular contents, such as lactate dehydrogenase (LDH), can be released. Therefore, the extracellular amount of LDH was measured after GP treatment for 6, 24 and 48 h in SCL-1 carcinoma cells (Fig. 3.33). The LDH release was slightly increased after the treatment of 2.5 µM GP for different time points, which was further enhanced using 5 µM GP.
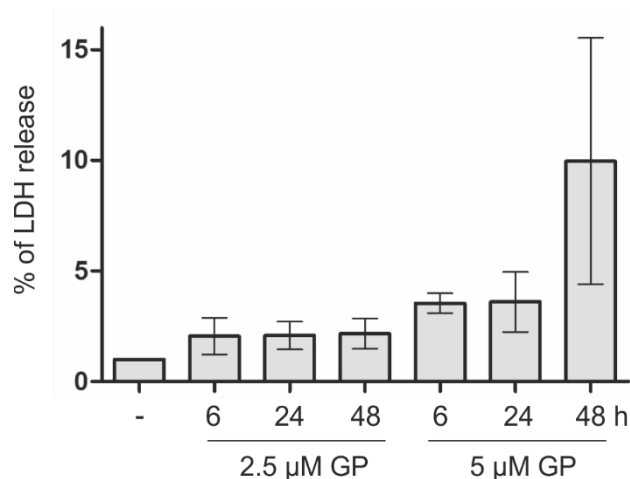
Fig. 3.33 Effect of GP on LDH release in SCL-1 carcinoma cells. After treatment of subconfluent cells with 2.5 and 5 µM GP for 6, 24 and 48 h, the LDH content was measured in the supernatant. Triton-X-100 (500 ppm) served as positive control and was set at 100% LDH release (not shown). Data represent x-fold increase of extracellular LDH compared to mock-treated control, which was set at 1. One-way ANOVA with Dunnett's Multiple Comparison Test was used for the determination of statistical significance, n=4.

As both permeabilization of the cellular membrane and LDH release cover late marker of the necroptotic pathway, early key events had to be examined as well. Necroptosis functions as a back-up mechanism when apoptosis is not working. In this context an involvement of caspase 8 activity was described. If caspase 8 is not functional, for example due to pharmacological inhibition, molecular cascades can be initiated leading to the induction of necroptosis (Fritsch et al. 2019, Uzunparmak et al. 2020). It was already shown that GP did not induce the activation of caspase 8 in SCL-1 carcinoma cells (Fig. 3.28). In that context, receptor-interacting protein (RIP) kinases play a crucial role. After dissociation of RIP1 from a complex including inactive caspase 8, the protein recruits RIP3 followed by an activation through reciprocal phosphorylation (Degterev et al. 2008, Gong et al. 2019). On this account, the phosphorylation of RIP3 was determined in GP treated SCL-1 carcinoma cells (Fig. 3.34). GP significantly elevated the phosphorylation of RIP3 in relation to unphosphorylated RIP3 after 24 h (Fig. 3.34b). Moreover, the pattern localisation of unphosphorylated RIP3 changed after treatment. Under basal conditions RIP3 was predominantly located around the nucleus, whereas it was uniformly distributed in the presence of GP (Fig. 3.34a). In summary, the data in context of necroptosis indicate that treatment of SCL-1 carcinoma cells with GP resulted in a necroptotic cell death.
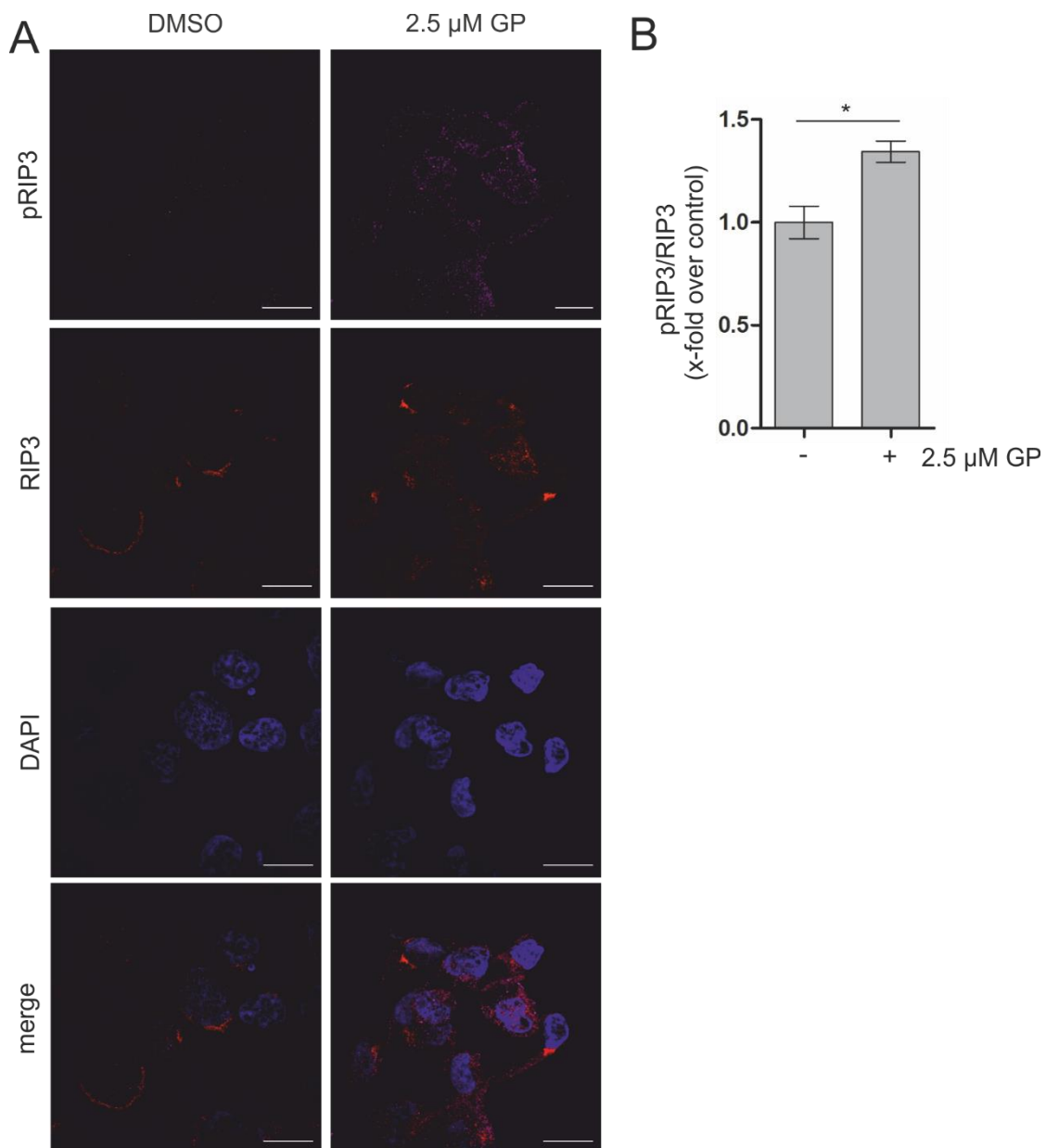
Fig. 3.34 Effect of GP on phosphorylation of RIP3 in SCL-1 carcinoma cells. **a** After incubation with and without 2.5 µM GP for 24 h, immunostaining against phosphorylated RIP3 (pRIP3) and unphosphorylated RIP3 (RIP3) was performed. DAPI was used for nucleus staining. Representative pictures are shown. Scale bars represent 20 µm. **b** For quantification, the fluorescence intensity of pRIP3 was set in relation to RIP3. Mock-treated control was set at 1. Data represent means ± SEM of three independent experiments, n=3. Student's *t*-test was used for the determination of statistical significance, *p<0.05

3.12 GP induced autophagic flux in both A375 melanoma and SCL-1 carcinoma cells

The effect of GP on the type of cell death was specific for the studied tumour cell lines. Regarding the only partial rescue of the cytotoxic effect due to the use of apoptosis and necroptosis inhibitors, respectively, additional pathways dealing with cell death have to be

involved in both tumour cell lines. In addition to the known interaction with members of the Bcl-2 protein family during apoptosis, BH3 mimetics are also described to disrupt the interaction between Bcl-2 and Beclin-1 leading to the induction of autophagy (Maiuri et al. 2007). In this context, the impact of GP on autophagy was examined in both A375 melanoma and SCL-1 carcinoma cells. One marker for the autophagosome that emerges during autophagy is the conversion of LC3 I to the lipid derivative phosphatidylethanolamine (PE) forming LC3 II. Due to the increased hydrophobicity of the latter, it has a faster electrophoretic mobility than LC3 I despite its higher molecular weight (Klionsky et al. 2016).
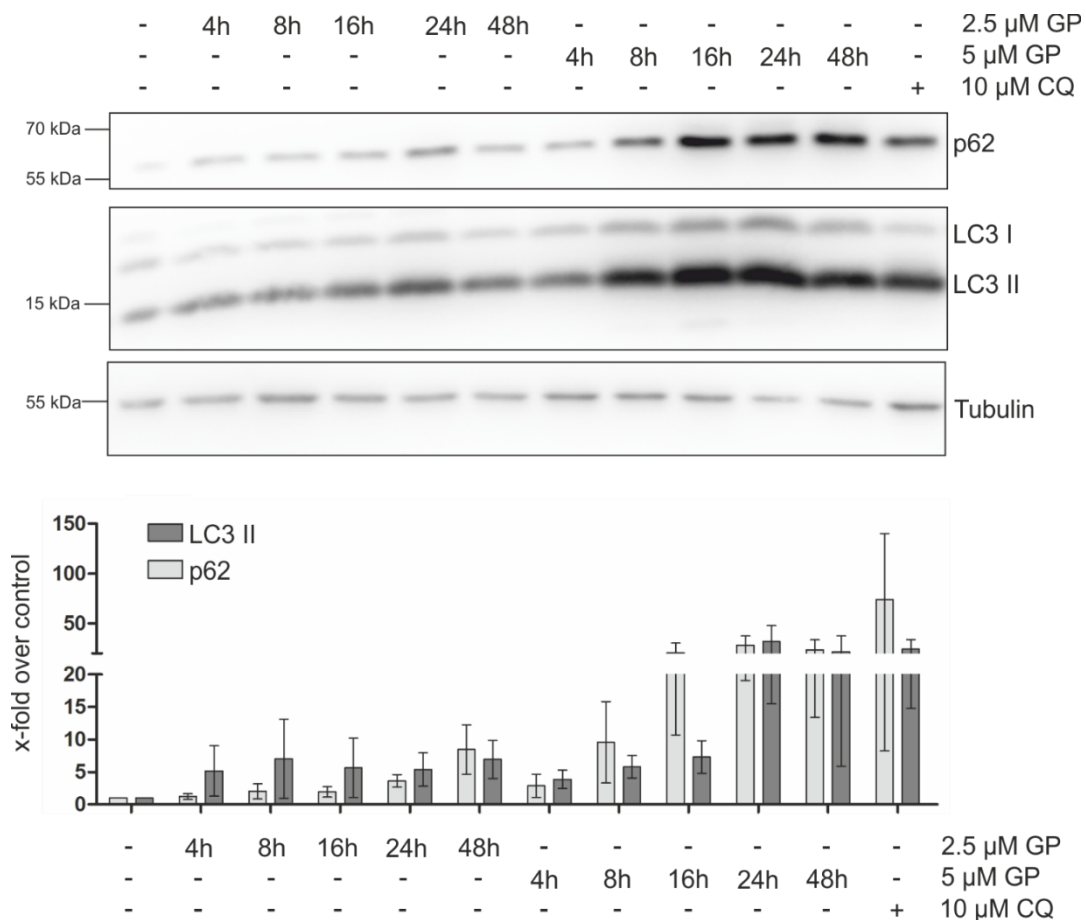
Fig. 3.35 Effect of GP on expression of autophagy related proteins in A375 melanoma cells. Subconfluent cells were treated with 2.5 or 5 µM GP for 4, 8, 16, 24 and 48 h. The autophagy inhibitor chloroquine (CQ, 10 µM, 48 h) was used as positive control. Protein expression of p62 and LC3 II was determined by Western Blot analysis. Tubulin was used as loading control. A representative blot is shown. The quantification of the protein expression was presented below. The amounts of p62 and LC3 II, respectively, were referred to tubulin. Mock-treated control was set at 1. Data represent means ± SEM of three independent experiments, n=3. One-way ANOVA with Dunnett's Multiple Comparison Test was used for the determination of statistical significance.

In A375 melanoma cells, 2.5 µM GP increased the expression level of LC3 II about 5-fold after 4 h which slightly increased further up to 48 h. At a concentration of 5 µM GP the level of LC3 II was elevated up to 40-fold, which was similar to chloroquine (CQ) treated cells (Fig. 3.35). CQ

originally discovered as antimalarial drug inhibits autophagic flux through impairment of the fusion of autophagosomes and primary lysosomes (Mauthe et al. 2018). Similarly, both GP concentrations time-dependently increased the expression of LC3 II from 2 to 8-fold in SCL-1 carcinoma cells (Fig. 3.36). Furthermore, p62 (sequestosome 1/SQSTM1) was used as an additional marker to monitor autophagy. This scaffold protein plays a pivotal role in the process of autophagy through the direct interaction with LC3 II leading to autophagosome formation (Johansen and Lamark 2011, Mizushima and Komatsu 2011, Weidberg et al. 2011). After GP treatment, the amount of p62 was increased time-and dose-dependently in A375 melanoma (Fig. 3.35) and SCL-1 carcinoma cells (Fig. 3.36). Although upregulation of p62 is usually associated with inhibition of autophagy, several studies showed that increased p62 at both mRNA and protein levels also correlate with an autophagic flux depending on the cell type (Colosetti et al. 2009, Zheng et al. 2011, Sahani et al. 2014).
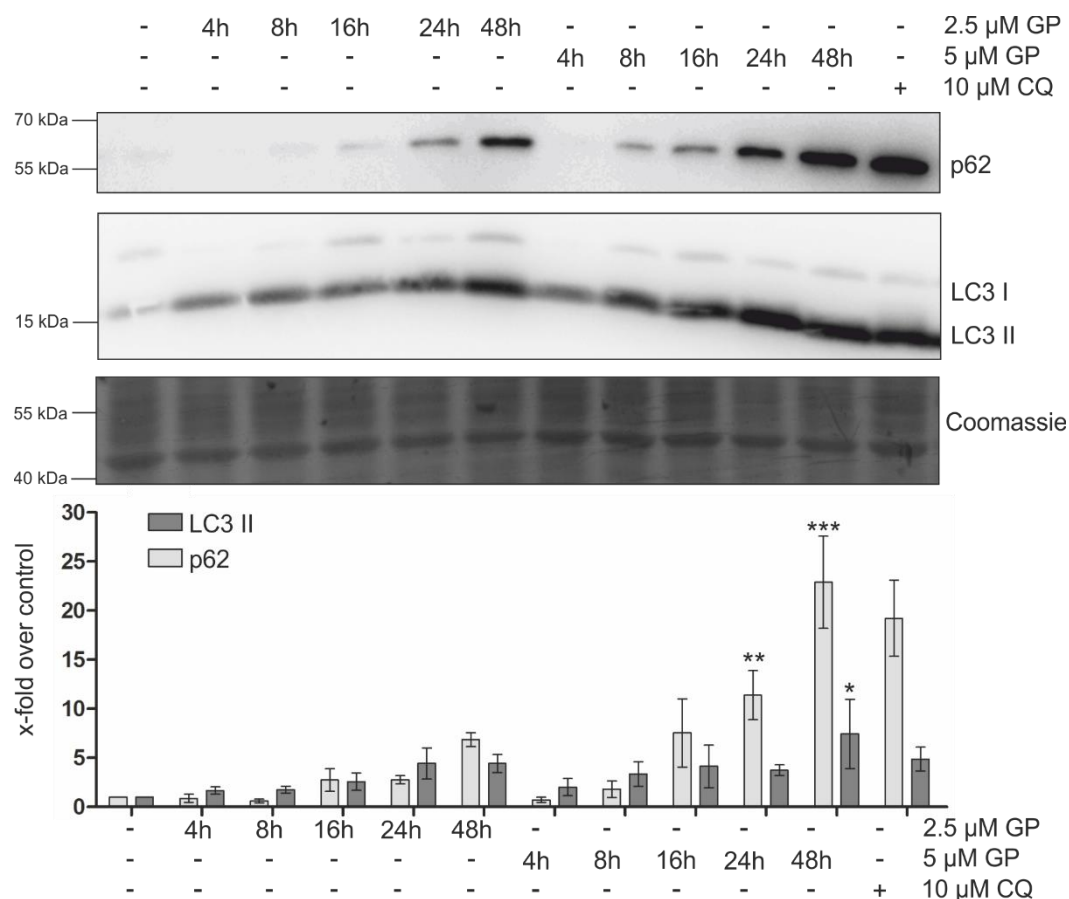
Fig. 3.36 Effect of GP on expression of autophagy related proteins in SCL-1 carcinoma cells. Subconfluent cells were treated with 2.5 or 5 µM GP for 4, 8, 16, 24 and 48 h. The autophagy inhibitor chloroquine (CQ, 10 µM, 48 h) was used as positive control. Protein expressions of p62 and LC3 II were determined by Western Blot analysis. Coomassie staining was used as internal loading control. A representative blot is shown. The quantification of the protein expression was presented below. The amounts of p62 and LC3 II, respectively, were referred to loading control. Mock-treated control was set at 1. Data represent means ± SEM of three independent experiments, n=3. One-way ANOVA with Dunnett's Multiple Comparison Test was used for the determination of statistical significance. *p<0.05, **p<0.01, ***p<0.001.

A correlation between LC3 II levels and the number of autophagosomes was described earlier (Kabeya et al. 2000). The accumulation of LC3 II could be due to an autophagic flux as well as block. In the first scenario, an enhanced autophagosome synthesis accompanied by enhanced delivery of autophagic substrates to the lysosomes causes a higher generation than degradation of these molecules. In case of a block of LC3 II degradation, any steps after the formation of autophagosomes could be affected. This includes the impairment of trafficking, fusion and lysosomal enzyme activity (Rubinsztein et al. 2009). To figure out whether GP induce an autophagic flux or block, autophagy markers were examined in the presence or absence of the autophagy inhibitors CQ and bafilomycin A_1 (Baf).
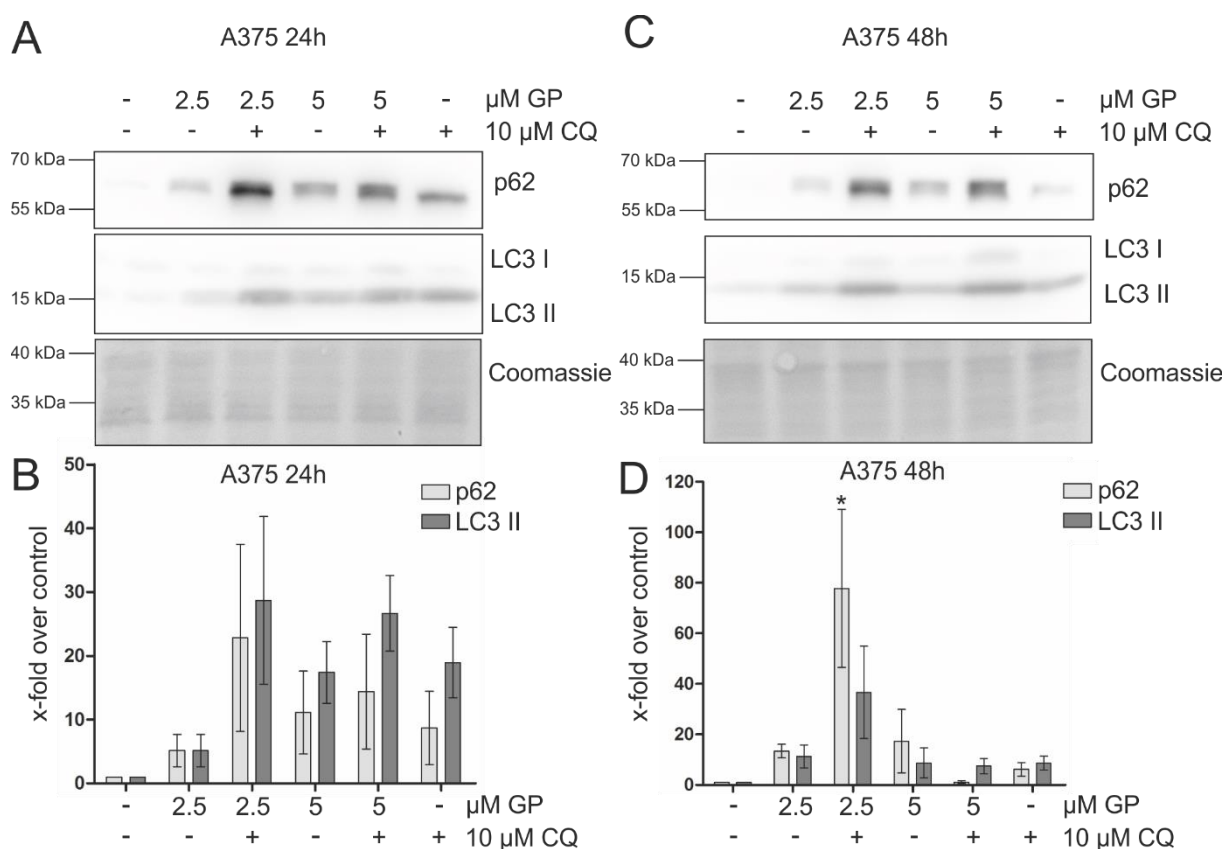
Fig. 3.37 Effect of combination treatment of GP and CQ in A375 melanoma cells. **a, c** Subconfluent cells were incubated with 2.5 and 5 μM GP alone or in combination with 10 μM CQ for 24 (**a**) and 48 h (**c**). Protein expression of p62 and LC3 II was determined by Western Blot analysis. Representative blots are shown. Coomassie staining was used as loading control. **b, d** Quantification of protein expression was referred to the loading control. Mock-treated control was set at 1. Data represent means ± SEM of three independent experiments, n=3. One-way ANOVA with Bonferroni's Multiple Comparison Test was used for the determination of statistical significance. *$p<0.05$.

GP increased the expression level of LC3 II after 24 and 48 dose-dependently in A375 melanoma cells (Fig. 3.37). After addition of 2.5 μM GP, the LC3 II levels were increased 5-to-10-fold in a time dependent manner compared to mock-treated cells, whereas the concentration of 5 μM GP nearly doubled these expression levels. Additionally, cells treated

with CQ alone showed a 20-fold upregulation of LC3 II after 24 h and a 10-fold increase after 48 h. In the presence of CQ a further increase in LC3 II was observed compared to GP and CQ alone treatment, respectively, with the exception of 5 µM GP after 48 h. Similar to these results, the same pattern of LC3 II expression was examined in SCL-1 carcinoma cells (Fig. 3.38). Thus, 2.5 µM GP induced a 2.5-fold increase of LC3 II after 24 h which was quadrupled after 48 h. A 5-fold upregulation of LC3 II was observed after addition of 5 µM GP for 24 h which further increased up to 30-fold after 48 h treatment. CQ alone enhanced the expression level of LC3 II approximately 5-fold after 24 h followed by an increase to 20-fold after 48 h. Furthermore, the enhanced expression level of LC3 II induced by GP or CQ alone was further increased in the presence of CQ at both time points. Following the guidelines how to monitor autophagy in mammalian cells (Mizushima et al. 2010), the data herein indicated an autophagic flux induced by GP in A375 melanoma and SCL-1carcinoma cells at least at 24 h.
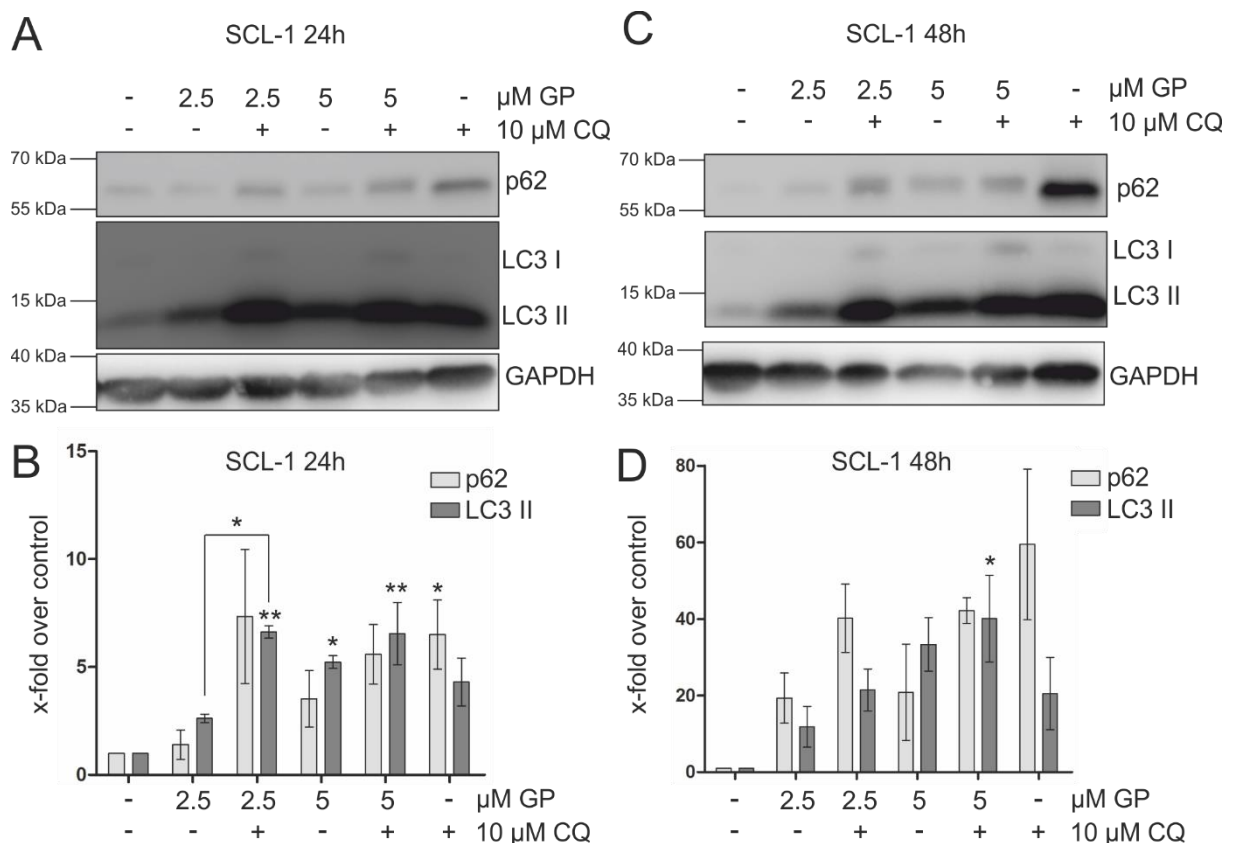
Fig. 3.38 Effect of combination treatment of GP and CQ in SCL-1 carcinoma cells. **a, c** Subconfluent cells were incubated with 2.5 and 5 µM GP alone or in combination with 10 µM CQ for 24 (**a**) and 48 h (**c**). Protein expression of p62 and LC3 II was determined by Western Blot analysis. Representative Blots were depicted. GAPDH was used as internal loading control. **b, d** Quantification of protein expression in relation to the loading control. Mock-treated control was set at 1. Data represent means ± SEM of three independent experiments, n=3. One-way ANOVA with Bonferroni's Multiple Comparison Test was used for the determination of statistical significance. *p<0.05, **p<0.01.

To demonstrate that GP induced an autophagic flux in both tumour cell lines, a further autophagy inhibitor was used for a combination treatment. Baf inhibits the last stage of autophagy through its V-ATPase inhibitor activity resulting in an increase of lysosomal pH (Yamamoto et al. 1998, Klionsky et al. 2016, Mauthe et al. 2018). For confirmation of the previous data, the lowest concentration of 2.5 µM GP was chosen as this concentration is already sufficient to increase LC3 II expression levels in both tumour cell lines. Furthermore, rapamycin (Rapa), an inducer of autophagy through the inhibition of the mechanistic target of rapamycin complex 1 (mTORC1) (Waldner et al. 2016), was used as experimental approach (Fig. 3.39, Fig. 3.40).
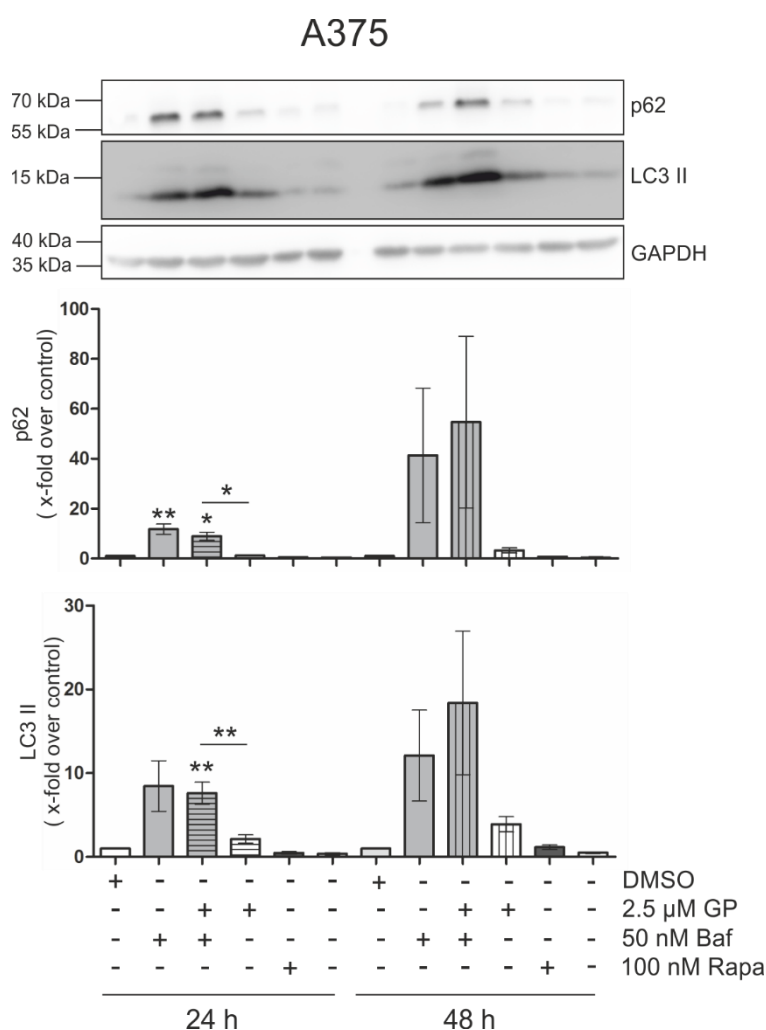
Fig. 3.39 Effect of combination treatment of GP and bafilomycin A_1 (Baf) in A375 melanoma cells. Subconfluent cells were incubated with 2.5 µM GP alone or in combination with 50 nM Baf for 24 and 48 h. As controls, cells were mock-treated, treated with the autophagy inhibitor Baf (50 nM) only or with the autophagy inducer Rapa (100 nM), respectively. Protein expression levels of p62 and LC3 II were determined by Western Blot analysis. A representative blot is shown. GAPDH was used as loading control. Quantification of protein expression was referred to the loading control. Mock-treated control was set at 1. Data represent means ± SEM of three independent experiments, n=3. One-way ANOVA with Bonferroni's Multiple Comparison Test was used for the determination of statistical significance. *$p<0.05$, **$p<0.01$.

GP enhanced LC3 II expression levels approximately 2.5-fold after 24 h which was doubled after 48 h in A375 melanoma cells (Fig. 3.39). In the presence of Baf the amount of LC3 II achieved a 4-fold increase at both time points. In comparison to the combination treatment, Baf only treated cells showed the same LC3 II level after 24 h but less after 48 h. Addition of Rapa resulted in a slight increase of LC3 II expression after 48 h indicating that the degradation of molecules exceeded the number of generated molecules. Levels of p62 were only marginally increased after Baf treatment in the presence or absence of GP. Likewise, the expression of p62 was upregulated 10-fold over control level after 24 h and 30-fold after 48 h in the presence of Baf in SCL-1 carcinoma cells (Fig. 3.40). In the presence of GP, the amount slightly increased after 24 h, whereas the levels decreased in tendency after 48 h. GP alone increased p62 expression levels approximately 5-fold at 24 h that further enhanced to around a 10-fold increase compared to the control level. No change in the expression level was observed in untreated or Rapa treated cells. Additionally, the LC3 II protein amount was examined. GP induced a 5-fold increase at both time points. In the presence of Baf, the expression levels were doubled. Compared to addition of Baf alone, the combination treatment showed in tendency an increase in the protein levels of LC3 II. Rapa showed minor effects towards an enhancement of LC3 II.To determine whether these protein patterns indicate an autophagic flux or block, the data were evaluated in context of the criteria described earlier (Rubinsztein et al. 2009). Higher LC3 II levels after a combination treatment compared to Baf alone indicates an increase of autophagosome formation. Furthermore, when the LC3 II protein level is enhanced by a compound and further rises in the presence of Baf, LC3 II degradation occur via autophagic flux. If the level is the same, it indicates a partial block of LC3 II degradation. Transferred to the Western Blot results, GP induced both the formation of autophagosomes and the LC3 II degradation in SCL-1 carcinoma cells after 24 and 48 h. Similarly, LC3 II degradation was induced in A375 melanoma cells at both timepoints, whereas the formation of autophagosomes occurred after 48 h.
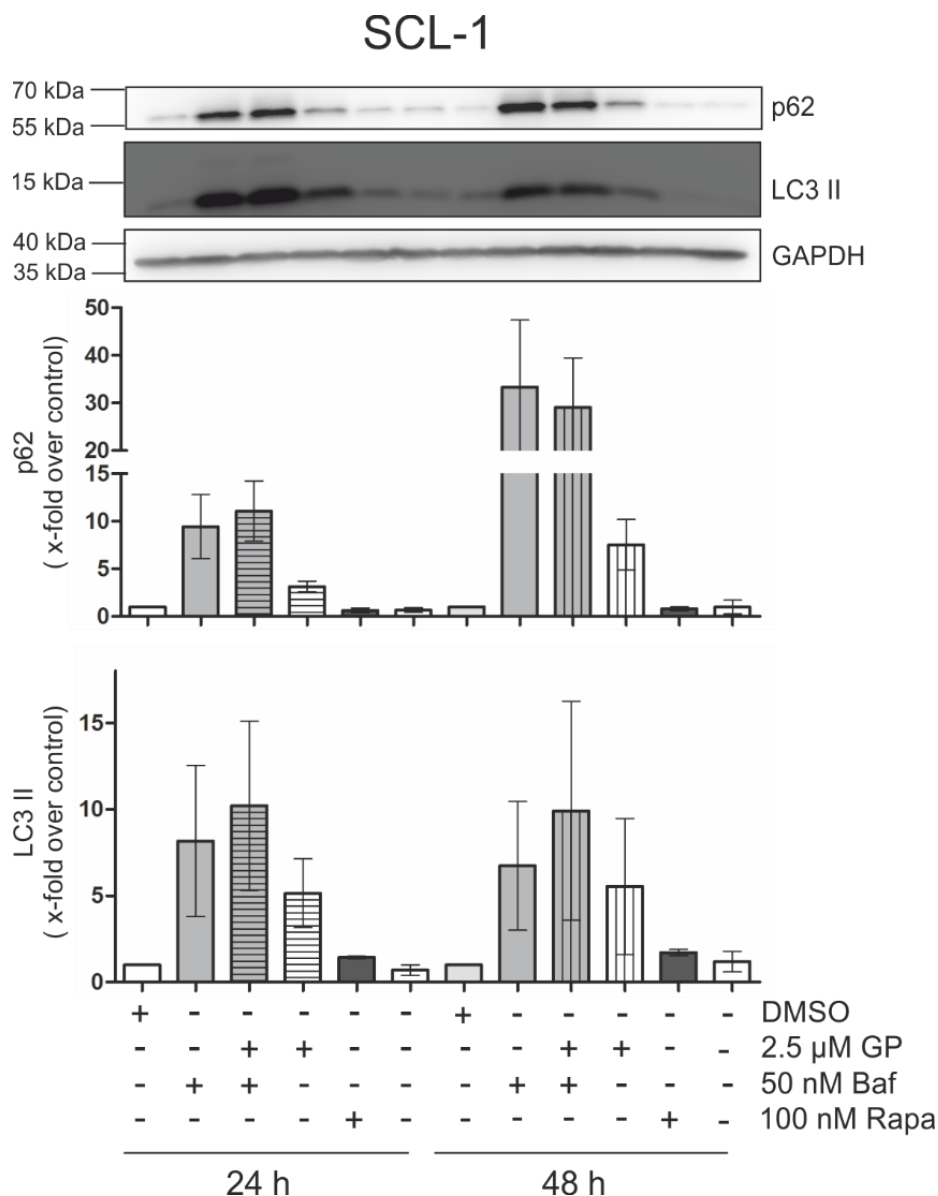
Fig. 3.40 Effect of combination treatment of GP and bafilomycin A₁ ((Baf) in SCL-1 carcinoma cells. Subconfluent cells were incubated with 2.5 µM GP alone or in combination with 50 nM Baf for 24 and 48 h. As controls, cells were mock-treated, treated with the autophagy inhibitor Baf (50 nM) only or with the autophagy inducer Rapa (100 nM), respectively. Protein expression levels of p62 and LC3 II were determined by Western Blot analysis. A representative blots was shown. GAPDH was used as loading control. Quantification of protein expression was referred to the loading control. Mock-treated control was set at 1. Data represent means ± SEM of three independent experiments, n=3. One-way ANOVA with Bonferroni's Multiple Comparison Test was used for the determination of statistical significance.

To confirm the previous results indicating an autophagic flux in A375 melanoma and SCL-1carcinoma cells, an EGFP-LC3 II plasmid was used for final representative transient transfection experiment (Jackson et al. 2005). Due to the same effect of GP in both tumour cells, only SCL-1 carcinoma cells were chosen to represent both cell lines. The principle of this approach is based on the cleavage of an EGFP-LC3 II construct during autophagy. During an autophagic flux the EGFP-LC3 II fusion protein is transported to autophagosomes and

90

autolysosomes, followed by the cleavage of the fusion protein to LC3 II and free GFP. After GP treatment, transiently transfected cells showed a signal in free GFP which was not present in mock-treated cells (Fig. 3.41). The EGFP-LC3 II fusion protein was detectable by both antibodies which recognize LC3 II and GFP.
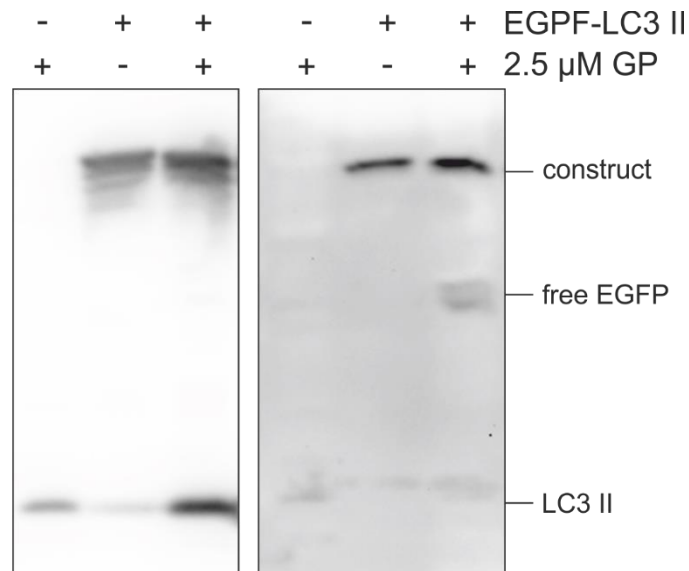
Fig. 3.41 Effect of GP on cleavage of EGFP-LC3 II construct in SCL-1 carcinoma cells. After transient transfection of SCL-1 carcinoma cells with an EGFP-LC3 II plasmid for 48 h, cells were mock-treated or treated with 2.5 µM GP for 24 h. Non-transfected (-) cells were used as negative control. Western Blot analysis of cell lysate was performed to examine EGFP-LC3 II, free EGPF and LC3 II levels. Left panel: detection of EGFP-LC3 II and LC3 II using a LC3 II antibody. Right panel: detection of EGFP-LC3 II and free EGFP using a GFP antibody, n=1.

In summary, all experiments with respect to autophagy indicated an induction of autophagic flux by GP treatment in A375 melanoma and SCL-1 carcinoma cells. The partial rescue of cell viability by apoptosis or necroptosis inhibitors suggested the participation of other pathways required for cell death in these tumour cell lines. However, it can be only speculated that the induction of autophagy might result in additional cell death in A375 melanoma and SCL-1 carcinoma cells.

3.13 Own participation in already published data

In this thesis, parts of the results have already been published (Haasler et al. 2021). These included Fig. 3.4a, c, Fig. 3.5a, c, Fig. 3.6a, c, Fig. 3.7, Fig. 3.9 (data referring to A375 melanoma cells and NHEM), Fig. 3.10, Fig. 3.12a, Fig. 3.13, Fig. 3.21 (data referring to A375 and NHEM), Fig. 3.22a, c-e, Fig. 3.23, Fig. 3.24, Fig. 3.25, Fig. 3.26 and Fig. 3.27.All necessary steps regarding the cultivation of the cells such as seeding of adequate cell numbers for the respective experiments were performed on my own.

Fig. 3.4a, c and Fig. 3.5a, c indicated the effect of GP on cell viability in A375 melanoma and NHEM after 96 h using the MTT and SRB assay, respectively. I performed all experiments and evaluated the data.

Fig. 3.6a, c showed the effect of GP on cell viability in A375 melanoma cells which was tested with different concentrations at various time points using the MTT and SRB assay. I performed the experiments and evaluated the data.

Fig. 3.7 indicated the IC_{50} values after GP treatment which were calculated in A375 melanoma cells and NHEM. The data used for the analysis were derived from MTT and SRB data. All related experiments were performed and analysed on my own.

Fig. 3.9 showed the cellular uptake of GP within the cells. The data referring to A375 melanoma cells and NHEM were published. I prepared the samples which were used for HPLC analysis. The HPLC experiments were performed and the detected peaks were quantified by Peter Graf. I measured the protein amount of the samples and calculated the absorbed amount of GP in the cells.

Fig. 3.10 presented the stability experiments of GP in cell-free systems. For that, the stability of GP was tested in acetonitrile (AcN), H_2O, DMEM and MBM. The amount of GP was measured by HPLC. This experiment was performed and evaluated by Peter Graf.

In Fig. 3.12a, the effect of parental and decomposed GP on cell viability was examined in A375 melanoma cells. I treated the cells, performed the MTT and evaluated the results. To determine that GP was completely lost after 5 h preincubation in DMEM, HPLC analysis was performed by Peter Graf.

Fig. 3.13 showed the effect of GP on mitochondrial membrane potential and mitochondrial fragmentation in A375 melanoma cells and NHEM. To examine these parameters, confocal microscopy analysis was performed. Treatment of the cells, microscopy and evaluation of the data were performed by me.

In Fig. 3.21, the DCF assay was performed to investigate the effect of GP on ROS formation. The data referring to A375 melanoma cells and NHEM were published. I performed all experiments and evaluated the results.

Fig. 3.22a, c-e presented the assessment of cell viability by GP in presence of antioxidant agents. Treatment of the cells, followed by MTT assay and evaluation of the data were performed on my own.

Fig. 3.23 depicted the effect of GP on generation of H_2O_2 in A375 melanoma cells. I transfected the cells. Treatment, microscopic analysis and evaluation of the data were done by Dr. Arun Kondadi and Thanos Tsigaras.

In Fig. 3.24, fractionation analysis was performed in order to examine whether GP induce cytosolic release of Smac/Diablo in A375 melanoma cells. The experiments as well as the evaluation were carried out on my own.

The effect of GP on apoptosis markers was shown in Fig. 3.25. The caspase activity assays, Western Blot experiments as well as the evaluation of the data were performed by me.

Fig. 3.26 presented rescue experiments of GP regarding cell viability and PARP cleavage in the presence of the pan-caspase inhibitor zVAD. Treatment of the cells, MTT assay, Western Blot analysis and the evaluation of the data were performed on my own.

In Fig. 3.27, the role of Drp1 in GP induced fragmentation in A375 melanoma cells was examined. For this purpose, knockdown experiments were performed followed by confocal microscope analysis to assess mitochondrial morphology. I did all related experiments and evaluated the data.

The manuscript was written on my own.

4 Discussion

Due to a modest response, increased resistance and recurrence, a big challenge in current cancer therapy is still the efficient killing of cancer cells including both non-melanoma and melanoma cells (Zbytek et al. 2008, Que et al. 2018, Krensel et al. 2019, Bertrand et al. 2020, Stratigos et al. 2020). In the here present thesis, SCL-1 carcinoma cells have been chosen as representative of cutaneous squamous cell carcinoma (CSCC, non-melanoma) and A375 melanoma cells as representative for malignant melanoma. One therapeutic strategy is addressing individual hallmarks of cancer, for example to prevent the evasion of apoptosis and thereby to overcome resistant tumour cells (Hanahan and Weinberg 2011). In this context, BH3 mimetics have been developed to antagonise anti-apoptotic Bcl-2 proteins in order to release pro-apoptotic proteins resulting in the induction of apoptosis (Zhang et al. 2007, Vogler 2014, Mohammad et al. 2015). Elevated expression levels of anti-apoptotic proteins are observed in various types of cancer, including skin cancer (Zhang et al. 2002, Yip and Reed 2008, Vogler 2014, Lee et al. 2019). The mere presence of anti-apoptotic proteins in tumour cells does not indicate that this amount is increased proportionally for the respective tissue. Therefore, the expression level should be compared with the respective normal cells. The basal expression of Bcl-2 is elevated in A375 melanoma cells in comparison to normal human epidermal melanocytes (NHEM) (Fig. 3.1). This finding is consistent with the literature, as high levels of anti-apoptotic proteins of the Bcl-2 protein family in melanoma cells are reported (Eberle and Hossini 2008, Lee et al. 2019). The high level of anti-apoptotic proteins has the objective of binding the pro-apoptotic proteins to stimulate apoptosis (Merino et al. 2018). In addition, Bcl-xL and Bcl-2 are particularly overexpressed in SCL-1 carcinoma cells under basal conditions as compared to normal human epidermal keratinocytes (NHEK), whereas Bcl-2 levels are notable less compared to A375 melanoma cells (Fig. 3.1). These data are in line with the literature, as elevated Bcl-xL levels were found in samples of patients with CSCC (Vasiljevic et al. 2009). Additionally, lacking of Bcl-2 staining was observed in CSCC compared to basal cell carcinoma (BCC) which could be a possible explanation for low Bcl-2 levels in SCL-1 carcinoma cells in comparison to other tumour cells (Cerroni and Kerl 1994). Since both tumour cells showed increased expression of at least one anti-apoptotic protein, treatment with BH3 mimetics could be a promising approach to trigger apoptosis. For that purpose, two different BH3 mimetic compounds were chosen: ABT-199 and (±) gossypol (GP). ABT-199 offers the advantage of having already received FDA approval for certain types of leukaemia (FDA 2019). In addition, GP, a natural BH3 mimetic derived from cotton seed plants (Adams et al. 1960), showed promising data in treatment of resistant A375 melanoma cells (Janostiak et al. 2019). However, the complete underlying mechanism remains still unknown.

4.1 Finding out the compound exerting toxic effects in tumour cells without affecting normal cells

First, it was studied whether the two compounds, ABT-199 and GP, affect cell viability of skin tumour cells. After 96 h, ABT-199 decrease cell viability of more than 50% in tumour cells at a concentration of 2.5 µM (Fig. 3.2a, b). GP showed a stronger effect at the same time point at concentration above 1.5 µM in A375 melanoma cells and 2 µM in SCL-1 carcinoma cells (Fig. 3.4a, b, Fig. 3.5a, b). With regard to use these compounds as a potential anti-cancer drug, it is not only important to have a cytotoxic effect on tumour cells, but also to minimise side effects on normal (healthy) cells, as these can limit the application due to poor tolerability (Oun et al. 2018, Songbo et al. 2019). Regrettably, ABT-199 drastically lowered cell viability of NHEM and NHEK. The response of normal human dermal fibroblasts (NHDF) to the compound was similar to the tumour cells (Fig. 3.2c-e). But in contrast, only the highest concentration of GP significantly decreased cell viability in normal cells indicating a desirable selective effect of GP on tumour cells (Fig. 3.4c-e, Fig. 3.5c-e). These data are consistent with other publications reporting that cell viability of oral keratinocytes and human fibroblasts were not affected after 5-day treatment with 5 µM (-) GP (AT-101). Furthermore, IC_{50} values of (±) GP treatment for 5-days was about 20 µM for breast epithelial cells (Jaroszewski et al. 1990, Oliver et al. 2004, Wolter et al. 2006). For that reason, GP was chosen for the following experiments to figure out the underlying mechanism using concentrations that are not toxic in normal cells.

4.2 Cellular uptake and stability of GP

GP induced a selective cytotoxic effect on A375 melanoma and SCL-1carcinoma cells. Uptake experiments showed that 10 µg GP per mg protein on average is taken up with no apparent difference between tumour and normal cells (Fig. 3.9). These data suggested that the reason for the selectivity of GP was not due to different (cell type specific) uptake rates. The decrease of detectable GP within cells over time indicated a low stability of the compound in aqueous solutions which was confirmed by HPLC analysis (Fig. 3.10). Most studies focussed only on stabilisation experiments in different solvents (Wang et al. 2019). However, especially in cell culture medium, GP was rapidly decomposed or metabolised raising the questions whether parental (not decomposed) GP or a decomposition/oxidation product caused cytotoxicity in tumour cells. Treatment with parental GP or decomposed GP (metabolites) demonstrated that the parental compound affected the cell viability of A375 melanoma and SCL-1carcinoma cells (Fig. 3.12). Consistent with this, Gilbert and co-worker showed that GP was more potent than gossypolone, the major metabolite of GP, in breast cancer cells (Gilbert et al. 1995, Dao et al. 2000). However, another study demonstrated that both GP and gossypolone exhibited similar cytotoxic effects in cancer cells (Shelley et al. 1999). Here, it was shown that the

undecomposed GP itself was necessary for its effectiveness in A375 melanoma and SCL-1carcinoma cells. Therefore, the occurrence of potential metabolites or oxidation products were not further investigated.

4.3 Mitochondrial impairment by GP treatment

Mitochondria are essential for the regulation of bioenergetic demands as well as other physiological processes including calcium homeostasis, redox signalling, apoptosis and autophagy (Tilokani et al. 2018). Mitochondrial membrane potential ($\Delta\psi_m$) derived from proton-pump dependent electron transport chain (ETC) plays a crucial role in cell fate (Löffler and Petrides 1997, Zorova et al. 2018). Opening of mitochondrial permeability transition pore (MPTP) in response to several stimuli lowers $\Delta\psi_m$ triggering cell fate towards death (Qiu et al. 2014, Basit et al. 2017). The postulated mode of action of BH3 mimetics is evident: the trapping of anti-apoptotic members of the Bcl-2 protein family (e.g., Bcl-2, Bcl-xL, MCL-1) resulting in release and oligomerisation of pro-apoptotic proteins (e.g., Bax and Bak) which cause mitochondrial outer membrane permeabilization (Zhang et al. 2007, Vogler 2014, Mohammad et al. 2015). In that context, ABT-199 (Bcl-2 inhibitor), S63845 (Mcl-1 inhibitor) and A-1331852 (Bcl-xL inhibitor) have been described to affect $\Delta\psi_m$ in haematological malignancies accompanied by swollen mitochondria, rupture of the mitochondrial outer membrane as well as loss of cristae structure. These findings indicate a role of anti-apoptotic proteins in the maintenance of mitochondrial integrity (Henz et al. 2019). Furthermore, GP reduced $\Delta\psi_m$ in non-small cell lung cancer cells after 24 h (Kang et al. 2016). In this thesis, 2.5 µM GP lowered $\Delta\psi_m$ by 50% in A375 melanoma and SCL-1 carcinoma cells. Interestingly, no changes in $\Delta\psi_m$ were observed for NHEM, NHEK and NHDF (Fig. 3.13b, e, Fig. 3.14b, e, Fig. 3.15b). Since a drop in $\Delta\psi_m$ is one of the first events that happened when cells undergo programmed cell death, whether as a prerequisite or as a consequence of the release of mitochondrial proteins (Heiskanen et al. 1999, Madesh et al. 2002, Ly et al. 2003, Deng et al. 2013), these results suggested that tumour cells are more likely to be triggered to induce cell death in response to GP treatment. Consistent with the drop of $\Delta\psi_m$ in both skin cancer cell lines, GP had a strong impact on mitochondrial morphology resulting in almost complete fragmentation in A375 melanoma and SCL-1 carcinoma cells. The same dose was not sufficient to induce the same drastic effect in normal cells (Fig. 3.13c, f, Fig. 3.14c, f, Fig. 3.15c). Mitochondrial morphology comprises rapid fusion and fission events, which are referred to as mitochondrial dynamics (Liesa et al. 2009, Tilokani et al. 2018). As a loss of $\Delta\psi_m$ and mitochondrial fission are related to each other (Legros et al. 2002, Tang et al. 2018), the data suggested that only tumour cells are affected within a defined concentration range of GP.

In addition to the impact of mitochondrial dysfunction on cell death, mitochondria also play a major role in cellular energy production. In mammalian cells, required energy is mainly produced by oxidative phosphorylation (OXPHOS). Cancer cells usually differ from normal cells in this aspect, as they obtain their required energy primarily from glycolysis, even in the presence of oxygen. This process is named aerobic glycolysis and is termed in tumour cells as Warburg effect (Warburg 1956, Vander Heiden et al. 2009). It has long been assumed that cancer cells exclusively perform glycolysis for energy production, but several studies suggest that OXPHOS also plays an important role in numerous tumour types especially during metastasis (Ho et al. 2012, Yu et al. 2017). In this context, cancer cells show higher OXPHOS rates as compared to normal counterparts (Lee et al. 2020). For example, Barbi de Moura and co-workers showed that metastatic melanoma exhibit higher OXPHOS than NHEM (Barbi de Moura et al. 2012). Moreover, melanoma xenografts exert one of the highest oxygen consumptions rates (OCR) compared to other xenograft models (Kallinowski et al. 1989, Ho et al. 2012). Three energetic states are described in cancer cells including Warburg state, oxidative state and a hybrid state consisting of the two former mentioned. In contrast, normal cells usually use either OXPHOS or glycolysis depending on substrate availability (Yu et al. 2017). Here, a concentration of 2.5 µM GP increased basal respiration and proton leak in tendency in tumour and normal cells. However, ATP production was significantly decreased in A375 melanoma and SCL-1 carcinoma cells compared to normal cells. Additionally, tumour cells showed no spare respiratory capacity (SRC) after GP treatment, while NHEK and NHDF still showed at least half of the SRC compared to control (Fig. 3.16-Fig. 3.20). The SRC, also named mitochondrial reserve capacity (Marchetti et al. 2020), indicates the ability to deal with altered energy demand in response to certain stimuli or stressors. It correlates with plasticity and is thus a measure of adaptability of the cell. A loss of SRC can be a sign for mitochondrial dysfunction including impaired ATP production resulting in cell death (Marchetti et al. 2020). GP seems to qualitatively affect mitochondrial respiration in both tumour and normal cells, however, the effect is stronger in tumour cells. One possible explanation could be the altered metabolism of these cells. Thus, cancer cells exhibited higher respiration to meet their energy demand (Hanahan and Weinberg 2011, Barbi de Moura et al. 2012, Lee et al. 2020).

Moderate increase in proton permeability accompanied by lowered ROS production and SCR as well as enhanced basal respiration, are described as "mild uncoupling" effect (Johnson-Cadwell et al. 2007, Marchetti et al. 2020). Early studies demonstrated that GP functions as an uncoupler of respiratory chain and OXPHOS in rat liver mitochondria (Abou-Donia and Dieckert 1974) and spermatids (Nakamura et al. 1988). Furthermore, Benz and co-workers showed supportive evidence that GP's anti-mitochondrial effects may correlate with its ability to inhibit relevant enzymes (Benz et al. 1990). In accordance with these findings, some studies showed that GP also working as pan-inhibitor of aldehyde dehydrogenases (ALDH) caused

ATP depletion in combination with phenformin, an inhibitor of mitochondrial respiratory chain complex I, resulting in death of non-small cell lung cancer cells (Kang et al. 2016, Lee et al. 2018) as well as in glioblastoma tumour spheres (Park et al. 2018). One explanation for the selectivity of GP with respect to ATP depletion could be the used electron source for ATP production. NADH production by ALDH is a major source of NADH in tumour cells, whereas normal cells obtain the required NADH from the tricarboxylic acid (TCA) cycle. Thereby, normal cells are not affected by inhibition of ALDH (Lee et al. 2018, Lee et al. 2020). Consistent with this, many cancer cells show elevated ALDH levels compared to normal cells (Park et al. 2018).

In addition to the reported ALDH inhibiting effect of GP, the proteomics data herein showed that GP decreased the expression level of several mitochondrial proteins in A375 melanoma and SCL-1 carcinoma cells, especially with regard to mitochondrial respiratory chain (Fig. 9.5). This result is in line with a study that examined the effect of (-) GP (AT 101) on glioblastoma cells and found a downregulation of mitochondrial proteins (Meyer et al. 2018). In this thesis, the protein levels of several subunits of the NADH: Ubiquinone Oxidoreductase (complex I) of the tumour cells were especially be lowered after 2.5 µM GP treatment. Furthermore, components of cytochrome b-c1 complex (complex III) and ATP synthase (complex V) were negatively affected by GP in both tumour cell lines as well as the succinate dehydrogenase (complex II) in SCL-1 carcinoma cells (Tab. 9.3, Tab. 9.5). As complex I oxidising NADH is the rate limiting step in ETC (Matsuzaki and Humphries 2015, Kang et al. 2016), its downregulation might have the strongest effect on respiration in skin cancer cells. Interestingly, GP decreased expression of NDUFB4, which was chosen as representative of complex I, in both tumour cells and NHEM, whereas no effect was observed in NHDF and an elevated expression level in NHEK. Furthermore, proteins of the mitochondrial contact site and cristae organizing system (MICOS) like Mic60 and Mic19 are downregulated in A375 melanoma and SCL-1 carcinoma cells, respectively. Western Blot analysis showed that 2.5 µM GP decreased Mic60 expression in tumour cells as well as in NHEM and NHDF. However, when the expression level of A375 melanoma and SCL-1 carcinoma cells were compared with their normal counterpart, the effect of GP was more significant on tumour cells (Fig. 9.7). Some studies demonstrated a correlation between Mic60 knockdown and impairment of OXPHOS activity (Yang et al. 2015, Van Laar et al. 2016) indicating that the loss of this protein was also involved in GP mediated negative impact of mitochondrial respiration, especially in tumour cells. In contrast, hexokinase II (HK2) catalysing the first step in glycolysis was elevated after GP treatment in A375 melanoma cells, SCL-1 carcinoma cells, NHEM and NHDF. In many cancer cells high HK2 levels were observed in comparison to the normal counterparts (Lis et al. 2016, Li et al. 2020) correlating with elevated glycolysis in tumour cells (Garcia et al. 2019, Shi et al. 2019, Du et al. 2020). These data indicated that GP might drive skin cancer cells towards glycolysis.

Taken together, GP affected mitochondria in a number of ways including loss of $\Delta\psi_m$, change in mitochondrial dynamics and respiration, especially in skin cancer cells. The effect of GP on mitochondrial respiration and glycolysis could be an explanation for its effectiveness as well as selectivity. As mentioned above, cancer cells can exhibit three different energy states: Warburg, oxidative and hybrid state. The latter state facilitates adaption of tumour cells to different tumour environmental settings through metabolic plasticity. One strategy to make cancer cells more vulnerable is to force these cells away from the hybrid state (Yu et al. 2017). Thus, GP might show promising results due to the impairment of the oxidative state within subsequent shift towards the Warburg state (glycolysis).

4.4 Cell death pathways initiated by GP

The development of so-called BH3 mimetics was mainly aimed to trigger apoptosis in target cells, especially in tumour cells which normally would evade from cell death by different mechanisms (Hanahan and Weinberg 2011). Antagonising of anti-apoptotic Bcl-2 family activate the release of pro-apoptotic proteins and thus stimulate apoptotic processes (Zhang et al. 2007, Vogler 2014, Mohammad et al. 2015). For that reason, the effect of GP on cell death was studied in tumour cells using again a concentration of 2.5 µM which was not toxic in normal cells as well as a high dose (5 µM) to substantiate the effect. In A375 melanoma cells, GP induced a drop of $\Delta\psi_m$ and an increase of mitochondrial fission which was followed by the release of Smac/Diablo at early timepoints (Fig. 3.24). The pro-apoptotic function of this protein is due to the inhibition of inhibitors of apoptosis proteins (IAP) resulting in caspase activity (Chai et al. 2000, Du et al. 2000, Verhagen et al. 2000). Subsequent to the activation of the initiator caspase 9 of the intrinsic apoptotic pathway after 6 h GP treatment in A375 melanoma cells, the effector caspases 3 and 7 were activated upon 24 h. Furthermore, the expression levels of procaspase 3, the inactive form, were decreased in a time and dose-dependent manner, accompanied by increased PARP cleavage (Fig. 3.25). These findings were consistent with the literature reporting that 10 µM of (-) GP induced Smac/Diablo dependent apoptosis in cisplatin-resistant ovarian cancer cells (Hu et al. 2012). Moreover, treatment with 12.5 µM of (-) GP for 48 h resulted in cleavage of caspases and PARP in malignant mesothelioma (Benvenuto et al. 2018). Additionally, Kim and co-workers showed that GP induced caspase dependent apoptosis in temozolomide-resistant glioblastoma cells (Kim et al. 2019). The requirement of caspases in GP induced cell death in A375 melanoma cells was demonstrated by preincubation of the cells with the pan-caspase inhibitor zVAD. In the presence of zVAD, the cell viability was partly rescued as well as PARP cleavage was abolished, indicating the involvement of caspases in this pathway (Fig. 3.26). Although many studies showed that BH3 mimetics not only induce apoptosis but also affect mitochondria resulting in enhanced fission, there are only some studies that addressed which proteins are

involved in this process. In mammalian cells, three GTPases of mitochondrial dynamin family members are described to control mitochondrial dynamics. These include mitofusin (Mfn) regulating fusion of the outer membrane, optic atrophy protein (Opa1) controlling inner membrane fusion and dynamin-1 like protein (Drp1), which is required for mitochondrial fission (Wang et al. 2018). The BH3 mimetic compounds ABT-199, A1331852 and A1210477 induced fragmentation and apoptosis in a Drp1 dependent manner in multiple myeloma, non-small cell lung carcinoma, cervical and breast cancer cells (Milani et al. 2017). In addition, the MCL-1 inhibitor S63845 caused Drp1 dependent mitochondrial fission in human cardiomyocytes (Rasmussen et al. 2020). In contrast, pharmacological inhibition of Drp1 using the chemical mitochondrial division inhibitor 1 (M-Divi-1) enhanced the cytotoxic effect of ABT-263 and A1210477 in melanoma cells (Mukherjee et al. 2018). Furthermore, the use of Drp1 siRNA and the negative mutant Drp1 K38A showed no effect on fragmentation induced by the GP derivatives BI97CI and BI1121 in non-small cell lung cancer cells (Varadarajan et al. 2013). In this thesis, the involvement of Drp1 in mitochondrial fission induced by GP in A375 was demonstrated by knockdown experiments. In the absence of Drp1, the percentage of fragmented cells was diminished indicating that Drp1 was at least partly required (Fig. 3.27). Interestingly, the effect of GP on mitochondrial morphology occurred in a ROS independent manner which was pointed out by the use of A375 melanoma cells expressing the redox sensor HyPer (Fig. 3.23) providing novel insight into the mode of action of GP in these cells (Haasler et al. 2021).

Conversely to the finding in A375 melanoma cells, SCL-1 carcinoma cells showed another behaviour with regard to cell death upon GP treatment. Although drastic effects on mitochondria were observed in SCL-1 cells, including a loss of $\Delta\psi_m$ and elevated mitochondrial fission, no apoptotic markers were found (Fig. 3.28, Fig. 3.29). The lack of caspase activities of caspases 8, 9, 3 and 7, accompanied by no change in procaspase 3 expression levels or PARP cleavage indicated that another death pathway was induced in these skin cancer cells. Preincubation with cell death inhibitors such as zVAD (apoptosis) and necrostatin-1 (Nec1, necroptosis) resulted in a partial rescue of GP induced cytotoxicity in the presence of Nec1, whereas zVAD had no effect (Fig. 3.30, Fig. 3.31b). This result suggested that necroptosis might be involved in SCL-1 carcinoma cells. Consistently, another BH3 mimetic, Obatoclax, induced necroptosis in human oral squamous cell carcinoma in a Nec1 dependent manner (Sulkshane and Teni 2017). Necroptosis is a programmed form of cell death that undergoes a successive phosphorylation cascade of receptor-interacting serine/threonine-protein kinases (RIP) and their substrates resulting in the rupture of the plasma membrane, the release of cytosolic components, and finally in an inflammatory response (Degterev et al. 2008, Wang et al. 2014, Martin 2016, Kearney and Martin 2017). The necroptotic pathway shares morphological features of necrosis, including plasma membrane permeabilization and release

of intracellular content (He et al. 2009, Christofferson and Yuan 2010, Gong et al. 2019). Here, GP induced LDH release as well as increased permeabilization of the membrane, which was abolished in the presence of Nec1 (Fig. 3.32, Fig. 3.33). With regard to the underlying mechanism, phosphorylation of RIP3 was induced by GP (Fig. 3.34) playing an important role in the recruitment and activation of the mixed lineage kinase domain like pseudokinase (MLKL). MLKL activation causes the execution phase of necroptosis (Sun et al. 2012, Wang et al. 2014, Samson et al. 2020). The switch from apoptosis to necroptosis usually depends on the activation status of caspase 8. Functional caspase 8 induces the extrinsic pathway of apoptotic cell death, whereas the inhibition of caspase 8 triggers the formation of necrosome formation and thus promotes necroptotic cell death (Lin et al. 1999, Degterev et al. 2008, Fritsch et al. 2019). In line with this, no caspase 8 activity was observed in SCL-1 carcinoma cells suggesting that non-functional caspase 8 might be responsible for the switch of cell death pathways (Fig. 3.28). The interplay between mitochondrial effects and necroptosis was not fully understood. However, Maeda and co-workers showed that TNFα induced both necroptosis and mitochondrial fission in Jurkat cells. In their study, plasma membrane rupture occurs after fission events suggesting that a role for the mitochondrial changes could not be excluded (Maeda and Fadeel 2014). Others found out that mitochondrial fission was rather a bystander phenomenon than the causal originator of necroptosis (Remijsen et al. 2014). Conversely, Obatoclax, an inhibitor of anti-apoptotic proteins of the Bcl-2 family, induced mitochondrial fragmentation which can be rescued by Nec1. That indicates an involvement of fission in necroptosis (Sulkshane and Teni 2017). Here, phosphorylation of RIP3, LDH release and plasma membrane permeabilization were preceded by loss of $\Delta\psi_m$ and mitochondrial fission indicating that mitochondrial effects might play a role in GP induced necroptosis in SCL-1 carcinoma cells.

GP exerts pro-oxidative effects in several cancer cells (Xu et al. 2014, Zubair et al. 2016). Therefore, intracellular ROS formation was determined. In SCL-1 carcinoma cells, no ROS formation occurred after GP treatment at early timepoints (<2 h) (Fig. 3.21b). Additionally, the antioxidant N-acetylcysteine (NAC) did not rescue the cytotoxic effect of GP in concentration ranges which are sufficient to diminish H_2O_2 induced cytotoxicity. Consistently, A375 melanoma cells showed the same effect after GP treatment according to intracellular ROS formation and NAC treatment. Furthermore, the antioxidant and vitamin E derivate trolox had no effect on the cytotoxic effect in A375 melanoma cells (Fig. 3.22). Thus, the data herein indicated a ROS independent mechanism of GP. A ROS independent mechanism of GP was also confirmed in human leukaemia cells and malignant mesothelioma (Hou et al. 2004, Benvenuto et al. 2018). On the other side, necroptosis was also described to be triggered or accompanied by ROS formation (Tait et al. 2013, Basit et al. 2017, Sulkshane and Teni 2017). However, Zec and co-workers published that metal complexes induced caspase independent

necroptotic cell death without affecting ROS levels (Zec et al. 2014) indicating that necroptosis needs not necessarily ROS formation.

In summary, GP induced different cell type dependent cell death pathways in skin cancer cells, possibly because of the activation status of caspase 8 functioning as molecular switch between apoptotic (A375 melanoma cells) and necroptotic cell death (SCL-1 carcinoma cells). Mitochondrial effects ($\Delta\psi_m$ and fission) preceded cell death. The fragmentation in A375 melanoma cells is Drp1 dependent and a relationship of fission and apoptosis is well described (Frank et al. 2001, Suen et al. 2008, Autret and Martin 2009), whereas in SCL-1 carcinoma it remains unclear whether fragmentation causes or only runs in parallel to necroptosis. Moreover, the underlying pathways in both skin cancer cells acted in a ROS independent manner, thus providing novel insights into GP's mode of actions.

4.5 Role of autophagy in GP treated skin cancer cells

Even if the development of new substances is aimed to initiate very specific effects, so-called off-target effects are often observed. In context of the synthesis of BH3 mimetic compounds, which are designed to occupy the binding pocket of anti-apoptotic Bcl-2 family members to cause mitochondrial apoptosis, the induction of autophagy is of particular relevance (Opydo-Chanek et al. 2017). The protein Beclin-1 containing a BH3 domain and being involved in initial processes of autophagy binds to anti-apoptotic Bcl2 proteins. The Bcl-2-Beclin-1 complex prevents the induction of autophagy. Binding of BH3 mimetics, such as GP or ABT-737, to Bcl-2 or Bcl-xl disrupts their interaction with Beclin-1 resulting in the release and induction of autophagy through the formation of the PI3K complex (Maiuri et al. 2007, Zhang et al. 2007, Gao et al. 2010, Radogna et al. 2015). Additionally, activated Bax or Bak upon treatment with BH3 mimetics can phosphorylate AMPK and its substrate ULK1 causing an autophagic flux (Lindqvist et al. 2018). Autophagy exerts a dual role either as survival or death mechanism depending on the cellular state and the exposure to different stimuli (Fulda 2013, Doherty and Baehrecke 2018). For that reason, the effect of GP on autophagy was examined in A375 melanoma and SCL-1 carcinoma cells. Lipidated LC3 II increased already after 4 h GP treatment in both cancer cell lines indicating an increasing autophagosome formation. The expression of the scaffold protein p62 interacting with LC3 II was also time and dose dependently elevated in these cells (Fig. 3.35, Fig. 3.36). Since several studies demonstrated contradictory effects of expression levels of p62 including down- and upregulation during autophagic flux (Colosetti et al. 2009, Zheng et al. 2011, Sahani et al. 2014), the results could not be interpreted unequivocally. In the presence of the autophagy inhibitors chloroquine (CQ), which prevents fusion of autophagosome and lysosome (Mauthe et al. 2018), and bafilomycin A1 (Baf), which impairs the pH of the lysosomes thus preventing degradation processes

(Yamamoto et al. 1998, Klionsky et al. 2016), the LC3 II levels increased by GP were further enhanced, indicating degradation of LC3 II during an autophagic flux. Additionally, the combination treatment exceeded the LC3 II expression levels compared to the treatment with the inhibitor alone suggesting that autophagosome formation was increased in SCL-1 carcinoma cells after 24 and 48 h and in A375 melanoma cells after 48 h (Fig. 3.37-Fig. 3.40) (Rubinsztein et al. 2009, Mizushima et al. 2010). Therefore, GP induced LC3 II turn over as well as the formation of autophagosomes in both skin cancer cells. These results were in line with the literature reporting that GP induced autophagy in prostate, glioma, breast, lymphoma, cervical and melanoma cell lines (Yu and Liu 2013, Radogna et al. 2015). However, induction of autophagy can result in both pro-survival and pro-death signalling (Yu and Liu 2013).

Autophagy is a conserved pathway for providing or generating energy in response to various stresses such as nutrient deprivation and hypoxia (Li et al. 2020). In mammalian cells, the term "autophagic cell death" (ACD) was established exhibiting characteristics like cytoplasmic vacuolisation, autophagosome formation and lysosomal clearance (Doherty and Baehrecke 2018). However, the interplay between ACD and other cell death pathways makes it difficult to distinguish ACD from the latter (Doherty and Baehrecke 2018, Denton and Kumar 2019). In addition, three forms of autophagy with regard to cell death are described: associated, mediated and dependent cell death. During the autophagy-associated cell death, induction of both autophagy and another cell death pathway (e.g., apoptosis) occurs. Thereby, autophagy does not play an active role, but is only accompanying the cell death. The autophagy-mediated form of cell death is characterised by cell death being induced by autophagy. Only the autophagy-dependent cell death takes place in the absence of apoptosis or other types of cell death (Klionsky et al. 2016, Galluzzi et al. 2017, Denton and Kumar 2019).

For this reason, an interplay of different signalling pathways must be critically questioned as to whether autophagy truly triggers cell death or only facilitates other cell death pathways. In this thesis, autophagy markers were already observed at early time points (4 h). Prior to this, mitochondrial morphology towards fragmentation is already affected by GP, which is referred to apoptosis induction and possibly associated with necroptosis. Simultaneously with the LC3 II increase, procaspase 3 expression was decreased accompanied by enhanced PARP cleavage in A375 melanoma cells. From these data, it can be deduced that both autophagy and apoptosis were induced in A375 melanoma cells at approximately the same time indicating a parallel mode of action. With regard to necroptosis, LDH release was already observed within 6 h treatment of GP in SCL-1 carcinoma suggesting the same conclusion as before. Necroptotic and autophagic flux are running parallel in SCL-1 carcinoma. Parallel signalling pathways are supported by the mode of action of BH3 mimetics, which can trigger both the

mitochondrial pathway via released pro-apoptotic proteins and autophagy through unbound Beclin-1 via binding to Bcl-2 (Gao et al. 2010).

The question whether autophagic flux induced by GP caused cell death in the studied skin cancer cells is difficult to answer. It was supported by the fact that both apoptosis (zVAD) and necroptosis (Nec1) inhibitors were only able to partly rescue the cytotoxic effect of GP in A375 melanoma and SCL-1 carcinoma cells, respectively, implying that the cytotoxicity has to be triggered by an additional form of cell death. Furthermore, the magnitude of intracellular damage, like the impairment of mitochondrial dysfunction, may decide whether permanent autophagy results in cell death (Yu and Liu 2013) as well as whether fission events are necessary for mitochondrial autophagy (Twig et al. 2008, Guan et al. 2018). Here, GP was shown to fragment over 80% of mitochondria in A375 melanoma and SCL-1 carcinoma cells, being a drastic damage. It can be speculated that this damage primarily triggers autophagy for clearance, which can lead to cell death after exceeding a certain threshold. One possibility to assess an involvement of autophagy in cell death is the use of autophagy inhibitors or knockdown of autophagy-relevant genes. However, one has to consider that several inhibitors, like CQ, not only prevent autophagic processes but also exhibit other functions having an impact on the experimental outcome. Moreover, knockdown of several genes including ATG genes should rescue cell viability induced by the compound, but some proteins are described to induce cell death in an autophagy independent manner (Mizushima et al. 2010, Doherty and Baehrecke 2018, Plantone and Koudriavtseva 2018). In addition, it was reported that GP induced cytoprotective autophagy in ATG5 knockout A375 melanoma which is independent of the canonical autophagy pathway (Kim et al. 2016). In contrast, another group showed autophagic cell death in melanoma cells (Jang and Lee 2014). These opposing results show the complexity of the various signalling pathways and the challenge to placing them correctly in the cellular context.

In conclusion, an autophagic flux was induced in A375 melanoma and SCL-1 carcinoma cells after GP treatment. The partial rescue of cell viability by apoptosis or necroptosis inhibitors indicated the involvement of other pathways required for cell death in these cancer cells. However, it can be only speculated whether the severe mitochondrial impairment is responsible for excessive autophagy resulting in cell death in A375 melanoma and SCL-1 carcinoma cells. But at this stage of the studies, it cannot be determined whether GP initiates associated, mediated or dependent autophagy in context of the observed cell death.

4.6 Putative mechanism of GP

The natural compound GP, originally tested as male contraceptive (Adams et al. 1960), exerts anti-tumour activities. The main focus lies on its role in apoptosis, as GP binds to several anti-

apoptotic proteins of the Bcl-2 protein family leading to mitochondrial cell death pathway as mentioned above (Zeng et al. 2019). Recent studies also address the function of GP in autophagy and necrosis (Xu et al. 2014, Opydo-Chanek et al. 2017, Meyer et al. 2018, Masuelli et al. 2020). Interestingly, the compound shows a broad spectrum of different activities dependent on the characteristics of the cell. This can explain opposing effects such as ROS dependent and independent mechanisms (Hou et al. 2004, Xu et al. 2014, Zubair et al. 2016, Benvenuto et al. 2018). Different types of skin cancer, including melanocytic and non-melanoma types, are still the focus of current research, as there is a need for new drugs due to high incidences, developing resistance and poor response rates (Zbytek et al. 2008, Burton et al. 2016, Ribero et al. 2017). (±) GP, (-) GP (AT 101) and its derivates are being investigated in some studies for a cytotoxic effect on tumour cells demonstrating promising results. Janostiak and co-workers showed that AT 101 can induce toxicity in chemotherapy resistant A375 melanoma cells (Janostiak et al. 2019). However, the underlying mechanism is not explored, instead it is assumed that the postulated mode of action is based on apoptosis induction via Bcl-2 proteins. Additionally, the role of GP in combination with valproic acid or hyperthermia are investigated in A375 melanoma cells with regard to the apoptotic pathway (Zhao et al. 2015, Shi et al. 2018). In addition to that, the effect of (-) GP was tested in squamous cell carcinoma, particularly in head and neck cancer (Oliver et al. 2004, Wolter et al. 2006). Most of these studies addressed the apoptotic pathway as death executioner but no data referred to the necroptotic pathway in squamous cell carcinoma.

In this study the effect of GP was examined in A375 melanoma (melanocytic skin cancer) and SCL-1 carcinoma cells (non-melanoma skin cancer) using concentrations that are not toxic in their normal counterparts. The putative mechanism of GP on these tumour cells are shown in Fig. 4.1. GP acting through binding to Bcl-2, Bcl-xL or MCL-1 (Kitada et al. 2003, Oliver et al. 2005, Lessene et al. 2008, Kang and Reynolds 2009) cause mitochondrial outer membrane permeabilization (MOMP). In A375 melanoma cells, GP induced the release of mitochondrial proteins like Smac/Diablo into the cytosol, followed by apoptosis induction which could be abolished in the presence of the pan-caspase inhibitor zVAD. Conversely, the detection of necroptotic markers, including phosphorylation of RIP3, Nec1 dependent membrane permeabilization and LDH release demonstrated the involvement of necroptosis in occurring cell death in SCL-1 carcinoma cells. Impairment of mitochondria with regard to OXPHOS, $\Delta\psi_m$ and mitochondrial fission was observed in both cell types. This could be a possible explanation for the selectivity of GP on tumour cells. Moreover, mitochondrial fission was regulated by Drp1 in A375 melanoma cells. In addition to apoptosis and necroptosis, autophagy was also involved in GP's mode of action in both cancer cell lines. Autophagic flux was activated at the same time as apoptotic and necroptotic markers, respectively, suggesting that they occurred in parallel.
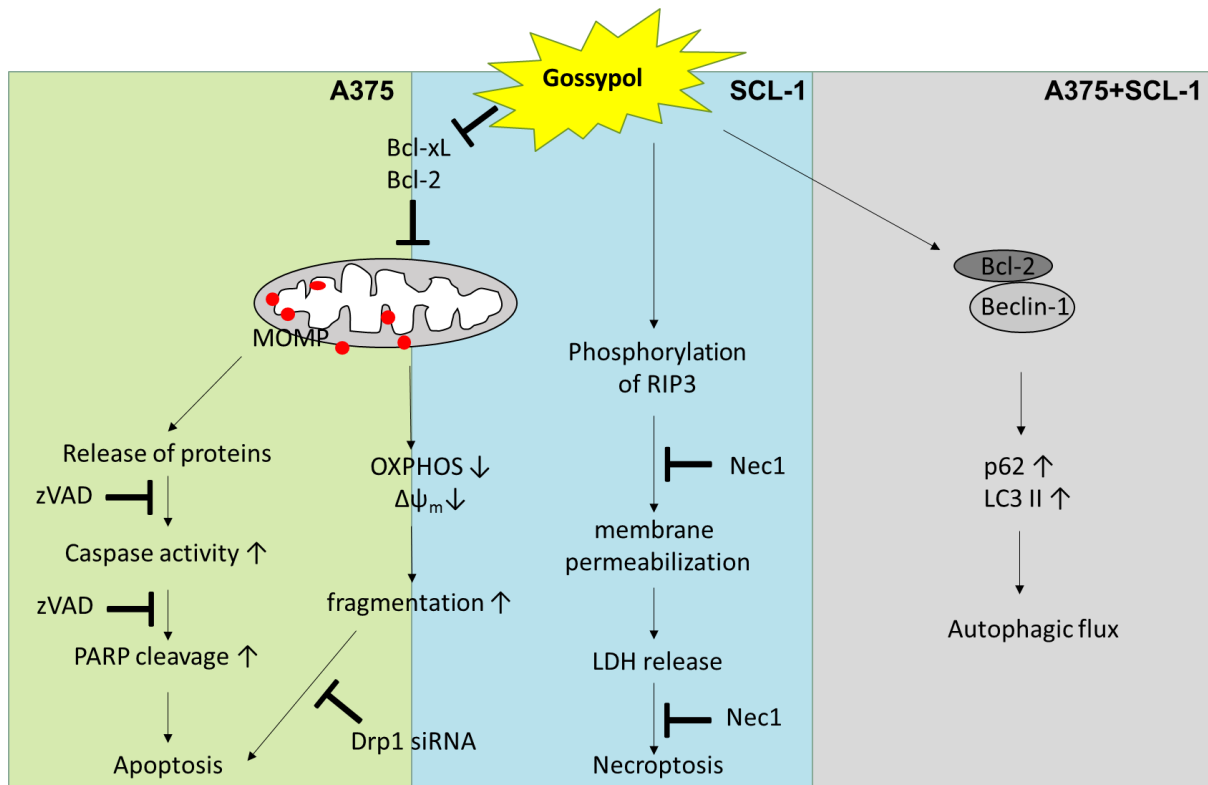
Fig. 4.1 Putative mode of action of GP in A375 melanoma and SCL-1carcinoma cells.

In summary, this thesis showed a selective concentration dependent toxicity of GP on A375 melanoma and SCL-1 carcinoma cells compared to normal (healthy) cells suggesting a potential therapeutic window to effectively treat these tumour cells. Interestingly, parental GP and not its metabolites are essential for the cytotoxic effect in the tumour cell lines. Moreover, GP induced different cell death pathways in these skin cancer cells, and both pathways were independent of ROS formation. Additionally, both death pathways were accompanied by an induction of autophagic flux. In A375 melanoma cells, GP activated the caspase dependent apoptotic cell death, accompanied by a drop of $\Delta\psi_m$ and Drp1 dependent mitochondrial fission. Conversely, GP induced a necroptotic pathway in SCL-1 carcinoma cells which is possibly linked with mitochondrial dysfunction including loss of $\Delta\psi_m$ and mitochondrial fragmentation. The simultaneous detection of cell death (apoptosis or necroptosis) and autophagy markers suggested that these pathways are running in parallel (which could be termed as associated autophagy, see above). However, to verify whether the autophagic flux really deals with that associated autophagy or it finally results in cell death, too, further studies are needed. Currently, one could only speculate that severe (mitochondrial) damage by GP might stimulate autophagy for clearance which resulted in excessive autophagic flux and finally in cell death. Taken together, the different susceptibility of cells to GP demonstrated promising results in the effective treatment of these skin cancer cells without affecting normal cells.

5 Future perspectives

Increased incidences of cancer require the on-going development of new drugs which specifically combat cancer cells. It is important not only to find substances which kill the tumour cells, but also to understand how exactly these compounds can act on these cells and on the normal (healthy) counterparts. Many Bcl-2 inhibitors have already been tested in preclinical and clinical studies. Numerous studies show that especially a combination treatment is the method of choice resulting in promising data (Han et al. 2019). For that reason, it is necessary to know the underlying mechanism of each compound. In this thesis, it was shown that GP has a therapeutic concentration range in which tumour cells are selectively killed without the involvement of ROS. With regard to a possible combination treatment of skin cancer, substances which induce ROS in combination with GP could be suitable. Since tumour cells exhibit higher basal ROS levels and their antioxidant systems are already fully activated, a further increase of ROS in combination with GP mediated damaging effect on mitochondrial dynamics could be a promising treatment approach. In contrast, normal (healthy) cells, which exert low basal ROS level and still have residual antioxidant capacities, do not show that toxic behaviours as tumour cells do (Alili et al. 2013, Aplak et al. 2020). However, considering that GP shows even small effects on mitochondria in normal cells and, a careful handling of such a combination treatment is mandatory. Aside from the evasion from apoptotic processes often resulting in the development of resistance against chemotherapeutic drugs (Hanahan and Weinberg 2011), the evasion from necroptosis is recently discussed in context of cancer resistance (Gong et al. 2019). Therefore, targeting necroptosis could also be a possible approach to combat skin cancer. It has been described that Smac mimetics induce necroptosis in caspase 8-deficient colorectal cancer cells to overcome both necroptosis and apoptosis resistance (He et al. 2017, Zhu et al. 2019). The role of necroptotic cell death was not fully understand yet and further studies are required. Substances which target different signalling pathways depending on the cell type offer an advantage to overcome existing resistance through affecting back-up mechanisms in cancer cells. In summary, BH3 mimetics represent a promising tool for the treatment of cancer. However, due to several off-targets effects the underlying mechanism cannot be generalised and, consequently, should be studied in the respective cell lines.

6 Summary

Cancer is one of the most common cause of cell death worldwide. An increased incidence of skin cancer being accompanied by resistance formation requires the development of new anti-cancer drugs. As the evasion of cell death presents one hallmark of cancer, small molecules, so-called BH3 mimetics, have been developed to bind to anti-apoptotic Bcl-2 protein family members resulting in release of pro-apoptotic proteins and the induction of apoptosis. Gossypol (GP) is a natural polyphenolic compound from cotton seed exhibiting anti-tumour properties. The effect of GP on two types of skin cancer was studied *in vitro*. To examine the underlying mechanism of GP in these tumour cells, concentrations were used which show a selective toxicity on the tumour cells but no damaging effect on normal (healthy) cells as normal human epidermal melanocytes (NHEM), normal human epidermal keratinocytes (NHEK) and normal human dermal fibroblasts (NHDF).

GP was rapidly uptaken by both tumour and normal cells, followed by impairment of mitochondrial respiration, $\Delta\psi_m$ as well as mitochondrial dynamic primarily in the tumour cells. Even though GP is not stable in aqueous solutions, it was demonstrated that the original (parental) compound and not its metabolites exhibited the cytotoxic effect on both studied skin cancer cell lines. Interestingly, GP initiated different cell death pathways in tumour cells. In A375 melanoma cells, GP activated the mitochondrial apoptotic pathway including release of the inner mitochondrial protein Smac/Diablo, activated initiator and effector caspases and PARP cleavage. In the presence of the pan-caspase inhibitor zVAD, caspase activity and PARP cleavage were abolished as well as the cytotoxic effect of GP was significantly lowered in A375 melanoma cells. In contrast, treatment of GP resulted in the necroptotic pathway in SCL-1 carcinoma cells. This pathway is characterized by successive phosphorylation cascades of RIP and their substrate MLKL causing plasma membrane rupture, accompanied by release of intracellular contents. In SCL-1 carcinoma cells, GP induced phosphorylation of RIP3, an increase in membrane permeabilization as well as LDH release. Furthermore, a combination treatment with the necroptosis inhibitor Nec1 demonstrated a partial rescue from the cytotoxic effect of GP in these cells. An only partial rescue of cell viability in the presence of zVAD and Nec1 indicated the involvement of an additional pathway leading to cell death. Anti-apoptotic Bcl-2 proteins bind not only to pro-apoptotic proteins, but also to Beclin-1 playing an important role in the initiation of autophagy. An activation of an autophagic flux by GP, which ran in parallel to apoptosis or necroptosis, was determined in both tumour cell types.

In conclusion, the different susceptibility of cells to GP showed promising results in the effective treatment of these skin cancer cells without affecting their normal counterparts *in vitro*.

7 Zusammenfassung

Krebs ist nach Herz-Kreislauf-Erkrankungen die häufigste Todesursache weltweit. Die steigenden Inzidenzen von Hautkrebs sowie die zunehmende Bildung von Resistenzen erfordern die kontinuierliche Entwicklung neuer Krebsmedikamente. Die Vermeidung des regulatorischen (apoptotischen) Zelltodes ist nur eine Strategie der Tumorzelle zu überleben. Aus diesem Grund wurden Moleküle, sogenannte BH3 mimetische Substanzen, entwickelt, die in diesen Mechanismus eingreifen. BH3 Mimetika verdrängen pro-apoptotische Proteine aus ihrer Bindung an anti-apoptotische Bcl-2 Proteine, wodurch pro-apoptotische Proteine freigesetzt werden, die zu den Mitochondrien translozieren und dort Apoptose auslösen. Gossypol (GP) ist eine natürlich vorkommende BH3 mimetische Substanz, die eine anti-tumorale Wirkung zeigt. Der Effekt von GP wurde auf zwei unterschiedliche Typen von Hauttumoren in dieser Arbeit untersucht. Um den zugrunde liegenden Mechanismus von GP auf diese Tumorzellen herauszuarbeiten, wurden Konzentrationen untersucht, die selektiv toxisch in den Hautkrebszellen sind, aber dabei keine schädigende Wirkung auf die normalen (gesunden) Zellen wie Melanozyten, Keratinozyten und Fibroblasten zeigen.

Auch wenn die Aufnahme von GP bereits nach kurzen Zeitpunkten in normalen und Tumorzellen nachgewiesen werden konnte, traten die durch GP ausgelösten mitochondrialen Veränderungen hauptsächlich bei den Tumorzellen auf. Obwohl GP nicht stabil in wässriger Lösung ist, konnte gezeigt werden, dass die parentale Substanz die Zytotoxizität in beiden Hauttumorzellen auslöst. Interessanterweise aktivierte GP unterschiedliche Signalwege, die zum Tod der Hauttumorzellen führten. Der Nachweis apoptotischer Marker, wie die Freisetzung mitochondrialer Proteine und die Aktivierung von Caspasen, zeigten einen apoptotischen Zelltod in den Melanomzellen. Dagegen induzierte GP Nekroptose, eine regulierte Form der Nekrose, in den Plattenepithelkarzinomzellen. Dieser zeichnet sich durch eine Phosphorylierung und damit Aktivierung bestimmter Kinasen wie RIP3 und MLKL aus, was zu einer Ruptur der Zellmembran, zu der Freisetzung intrazellulärer Bestandteile und final zum Zelltod führt.

Die nur teilweise Aufhebung des toxischen Effekts von GP in Anwesenheit von zVAD und Nec1 auf beiden Hauttumorzellen deutet auf die Beteiligung eines zusätzlichen Signalweges hin. Anti-apoptotische Bcl-2 Protein binden nicht nur an pro-apoptotischen Proteinen, sondern auch an Beclin-1, welches eine Rolle in der Initiation der Autophagie spielt. Die Zugabe von GP bewirkte eine Aktivierung des autophagischen Flux', der vermutlich parallel zur Apoptose beziehungsweise Nekroptose abläuft.

Zusammengefasst zeigt die unterschiedliche Empfindlichkeit der Zellen gegenüber GP vielversprechende Ergebnisse hinsichtlich einer effektiven Behandlung der getesteten Hauttumorzellen ohne Beeinträchtigung der normalen Zellen *in vitro*.

8 References

Abbasi, N. R., H. M. Shaw, D. S. Rigel, R. J. Friedman, W. H. McCarthy, I. Osman, A. W. Kopf and D. Polsky (2004). "Early diagnosis of cutaneous melanoma: revisiting the ABCD criteria." JAMA **292**(22): 2771-2776.

Abou-Donia, M. B. and J. W. Dieckert (1974). "Gossypol: uncoupling of respiratory chain and oxidative phosphorylation." Life Sci **14**(10): 1955-1963.

Adams, J. M. and S. Cory (2018). "The BCL-2 arbiters of apoptosis and their growing role as cancer targets." Cell Death Differ **25**(1): 27-36.

Adams, R., T. A. Geissman and J. D. Edwards (1960). "Gossypol, a pigment of cottonseed." Chem Rev **60**: 555-574.

Adrain, C., B. M. Murphy and S. J. Martin (2005). "Molecular ordering of the caspase activation cascade initiated by the cytotoxic T lymphocyte/natural killer (CTL/NK) protease granzyme B." J Biol Chem **280**(6): 4663-4673.

Akgul, B., J. C. Cooke and A. Storey (2006). "HPV-associated skin disease." J Pathol **208**(2): 165-175.

Alili, L., M. Sack, C. von Montfort, S. Giri, S. Das, K. S. Carroll, K. Zanger, S. Seal and P. Brenneisen (2013). "Downregulation of tumor growth and invasion by redox-active nanoparticles." Antioxid Redox Signal **19**(8): 765-778.

Aplak, E., C. von Montfort, L. Haasler, D. Stucki, B. Steckel, A. S. Reichert, W. Stahl and P. Brenneisen (2020). "CNP mediated selective toxicity on melanoma cells is accompanied by mitochondrial dysfunction." PLoS One **15**(1): e0227926.

Armstrong, B. K. and A. Kricker (2001). "The epidemiology of UV induced skin cancer." J Photochem Photobiol B **63**(1-3): 8-18.

Autret, A. and S. J. Martin (2009). "Emerging role for members of the Bcl-2 family in mitochondrial morphogenesis." Mol Cell **36**(3): 355-363.

Axe, E. L., S. A. Walker, M. Manifava, P. Chandra, H. L. Roderick, A. Habermann, G. Griffiths and N. T. Ktistakis (2008). "Autophagosome formation from membrane compartments enriched in phosphatidylinositol 3-phosphate and dynamically connected to the endoplasmic reticulum." Journal of Cell Biology **182**(4): 685-701.

Balch, C. M., A. C. Buzaid, S. J. Soong, M. B. Atkins, N. Cascinelli, D. G. Coit, I. D. Fleming, J. E. Gershenwald, A. Houghton, Jr., J. M. Kirkwood, et al. (2001). "Final version of the American Joint Committee on Cancer staging system for cutaneous melanoma." J Clin Oncol **19**(16): 3635-3648.

Barbi de Moura, M., G. Vincent, S. L. Fayewicz, N. W. Bateman, B. L. Hood, M. Sun, J. Suhan, S. Duensing, Y. Yin, C. Sander, et al. (2012). "Mitochondrial respiration--an important therapeutic target in melanoma." PLoS One **7**(8): e40690.

Basit, F., L. M. van Oppen, L. Schockel, H. M. Bossenbroek, S. E. van Emst-de Vries, J. C. Hermeling, S. Grefte, C. Kopitz, M. Heroult, P. Hgm Willems, et al. (2017). "Mitochondrial complex I inhibition triggers a mitophagy-dependent ROS increase leading to necroptosis and ferroptosis in melanoma cells." Cell Death Dis **8**(3): e2716.

Bedoui, S., M. J. Herold and A. Strasser (2020). "Emerging connectivity of programmed cell death pathways and its physiological implications." Nature Reviews Molecular Cell Biology **21**(11): 678-695.

Benvenuto, M., R. Mattera, J. I. Sticca, P. Rossi, C. Cipriani, M. G. Giganti, A. Volpi, A. Modesti, L. Masuelli and R. Bei (2018). "Effect of the BH3 Mimetic Polyphenol (-)-Gossypol (AT-101) on the in vitro and in vivo Growth of Malignant Mesothelioma." Front Pharmacol **9**: 1269.

Benz, C. C., M. A. Keniry, J. M. Ford, A. J. Townsend, F. W. Cox, S. Palayoor, S. A. Matlin, W. N. Hait and K. H. Cowan (1990). "Biochemical correlates of the antitumor and antimitochondrial properties of gossypol enantiomers." Mol Pharmacol **37**(6): 840-847.

Bertrand, J., E. Steingrimsson, F. Jouenne, B. Paillerets and L. Larue (2020). "Melanoma Risk and Melanocyte Biology." Acta Dermato Venereologica **100**(11).

Bertrand, M. J., S. Milutinovic, K. M. Dickson, W. C. Ho, A. Boudreault, J. Durkin, J. W. Gillard, J. B. Jaquith, S. J. Morris and P. A. Barker (2008). "cIAP1 and cIAP2 facilitate cancer cell survival by functioning as E3 ligases that promote RIP1 ubiquitination." Mol Cell **30**(6): 689-700.

Bichakjian, C. K., T. Olencki, S. Z. Aasi, M. Alam, J. S. Andersen and R. Blitzblau. (2018). "NCCN Clinical Practice Guidelines in Oncology: Squasmous cell skin cancer." from https://oncolife.com.ua/doc/nccn/Squamous_Cell_Skin_Cancer.pdf.

Bilan, D. S. and V. V. Belousov (2016). "HyPer Family Probes: State of the Art." Antioxidants & Redox Signaling **24**(13): 731-751.

Blatter, D. P., F. Garner, K. Van Slyke and A. Bradley (1972). "Quantitative Electrophoresis in Polyacrylamide Gels of 2-40%." Journal of Chromatography(64): 147-155.

Booth, D. M., B. Enyedi, M. Geiszt, P. Varnai and G. Hajnoczky (2016). "Redox Nanodomains Are Induced by and Control Calcium Signaling at the ER-Mitochondrial Interface." Mol Cell **63**(2): 240-248.

Booth, D. M., S. K. Joseph and G. Hajnoczky (2016). "Subcellular ROS imaging methods: Relevance for the study of calcium signaling." Cell Calcium **60**(2): 65-73.

Boukamp, P., W. Tilgen, R. T. Dzarlieva, D. Breitkreutz, D. Haag, R. K. Riehl, A. Bohnert and N. E. Fusenig (1982). "Phenotypic and genotypic characteristics of a cell line from a squamous cell carcinoma of human skin." J Natl Cancer Inst **68**(3): 415-427.

Boulton, S., A. Anderson, H. Swalwell, J. R. Henderson, P. Manning and M. A. Birch-Machin (2011). "Implications of using the fluorescent probes, dihydrorhodamine 123 and 2',7'-dichlorodihydrofluorescein diacetate, for the detection of UVA-induced reactive oxygen species." Free Radic Res **45**(2): 139-146.

Brash, D. E., J. A. Rudolph, J. A. Simon, A. Lin, G. J. McKenna, H. P. Baden, A. J. Halperin and J. Ponten (1991). "A role for sunlight in skin cancer: UV-induced p53 mutations in squamous cell carcinoma." Proc Natl Acad Sci U S A **88**(22): 10124-10128.

Breslow, A. (1970). "Thickness, cross-sectional areas and depth of invasion in the prognosis of cutaneous melanoma." Ann Surg **172**(5): 902-908.

Breuninger, H., K. Brantsch, T. Eigentler and H. M. Hafner (2012). "Comparison and evaluation of the current staging of cutaneous carcinomas." J Dtsch Dermatol Ges **10**(8): 579-586.

Brubacher, J. L. and N. C. Bols (2001). "Chemically de-acetylated 2',7'-dichlorodihydrofluorescein diacetate as a probe of respiratory burst activity in mononuclear phagocytes." J Immunol Methods **251**(1-2): 81-91.

Burton, K. A., K. A. Ashack and A. Khachemoune (2016). "Cutaneous Squamous Cell Carcinoma: A Review of High-Risk and Metastatic Disease." Am J Clin Dermatol **17**(5): 491-508.

Casara, P., J. Davidson, A. Claperon, G. Le Toumelin-Braizat, M. Vogler, A. Bruno, M. Chanrion, G. Lysiak-Auvity, T. Le Diguarher, J. B. Starck, et al. (2018). "S55746 is a novel orally active BCL-2 selective and potent inhibitor that impairs hematological tumor growth." Oncotarget **9**(28): 20075-20088.

Cerroni, L. and H. Kerl (1994). "Aberrant bcl-2 protein expression provides a possible mechanism of neoplastic cell growth in cutaneous basal-cell carcinoma." J Cutan Pathol **21**(5): 398-403.

Chai, J., C. Du, J. W. Wu, S. Kyin, X. Wang and Y. Shi (2000). "Structural and biochemical basis of apoptotic activation by Smac/DIABLO." Nature **406**(6798): 855-862.

Champa, D., M. A. Russo, X. H. Liao, S. Refetoff, R. A. Ghossein and A. Di Cristofano (2014). "Obatoclax overcomes resistance to cell death in aggressive thyroid carcinomas by countering Bcl2a1 and Mcl1 overexpression." Endocr Relat Cancer **21**(5): 755-767.

Chandrashekar, P., N. Ahmadinejad, J. Wang, A. Sekulic, J. B. Egan, Y. W. Asmann, S. Kumar, C. Maley and L. Liu (2020). "Somatic selection distinguishes oncogenes and tumor suppressor genes." Bioinformatics **36**(6): 1712-1717.

Chang, H. Y. and X. Yang (2000). "Proteases for cell suicide: functions and regulation of caspases." Microbiol Mol Biol Rev **64**(4): 821-846.

Chang, N. C. (2020). "Autophagy and Stem Cells: Self-Eating for Self-Renewal." Front Cell Dev Biol **8**: 138.

Chang, Y. S., K. T. Yeh, N. C. Hsu, S. H. Lin, T. J. Chang and J. G. Chang (2010). "Detection of N-, H-, and KRAS codons 12, 13, and 61 mutations with universal RAS primer multiplex PCR and N-, H-, and KRAS-specific primer extension." Clin Biochem **43**(3): 296-301.

Chapman, P. B., A. Hauschild, C. Robert, J. B. Haanen, P. Ascierto, J. Larkin, R. Dummer, C. Garbe, A. Testori, M. Maio, et al. (2011). "Improved survival with vemurafenib in melanoma with BRAF V600E mutation." N Engl J Med **364**(26): 2507-2516.

Chen, D., J. Yu and L. Zhang (2016). "Necroptosis: an alternative cell death program defending against cancer." Biochim Biophys Acta **1865**(2): 228-236.

Chen, X., Z. Zhong, Z. Xu, L. Chen and Y. Wang (2010). "2',7'-Dichlorodihydrofluorescein as a fluorescent probe for reactive oxygen species measurement: Forty years of application and controversy." Free Radic Res **44**(6): 587-604.

Cho, Y. S., S. Challa, D. Moquin, R. Genga, T. D. Ray, M. Guildford and F. K. Chan (2009). "Phosphorylation-driven assembly of the RIP1-RIP3 complex regulates programmed necrosis and virus-induced inflammation." Cell **137**(6): 1112-1123.

Christofferson, D. E. and J. Yuan (2010). "Necroptosis as an alternative form of programmed cell death." Curr Opin Cell Biol **22**(2): 263-268.

Cichorek, M., M. Wachulska, A. Stasiewicz and A. Tyminska (2013). "Skin melanocytes: biology and development." Postepy Dermatol Alergol **30**(1): 30-41.

Clark, W. H., Jr., L. From, E. A. Bernardino and M. C. Mihm (1969). "The histogenesis and biologic behavior of primary human malignant melanomas of the skin." Cancer Res **29**(3): 705-727.

Cohen, G. M. (1997). "Caspases: the executioners of apoptosis." Biochem J **326 (Pt 1)**: 1-16.

Coleman, A. W. and J. R. Coleman (1980). "Characterization of the methylxanthine-induced propagated wave phenomenon in striated muscle." J Exp Zool **212**(3): 403-413.

Colosetti, P., A. Puissant, G. Robert, F. Luciano, A. Jacquel, P. Gounon, J. P. Cassuto and P. Auberger (2009). "Autophagy is an important event for megakaryocytic differentiation of the chronic myelogenous leukemia K562 cell line." Autophagy **5**(8): 1092-1098.

Corchado-Cobos, R., N. Garcia-Sancha, R. Gonzalez-Sarmiento, J. Perez-Losada and J. Canueto (2020). "Cutaneous Squamous Cell Carcinoma: From Biology to Therapy." Int J Mol Sci **21**(8).

Cory, S. and J. M. Adams (2002). "The Bcl2 family: regulators of the cellular life-or-death switch." Nat Rev Cancer **2**(9): 647-656.

Cox, J., M. Y. Hein, C. A. Luber, I. Paron, N. Nagaraj and M. Mann (2014). "Accurate proteome-wide label-free quantification by delayed normalization and maximal peptide ratio extraction, termed MaxLFQ." Mol Cell Proteomics **13**(9): 2513-2526.

Creed, S. and M. McKenzie (2019). "Measurement of Mitochondrial Membrane Potential with the Fluorescent Dye Tetramethylrhodamine Methyl Ester (TMRM)." Methods Mol Biol **1928**: 69-76.

Czabotar, P. E., G. Lessene, A. Strasser and J. M. Adams (2014). "Control of apoptosis by the BCL-2 protein family: implications for physiology and therapy." Nat Rev Mol Cell Biol **15**(1): 49-63.

D'Arcy, M. S. (2019). "Cell death: a review of the major forms of apoptosis, necrosis and autophagy." Cell Biol Int **43**(6): 582-592.

D'Orazio, J., S. Jarrett, A. Amaro-Ortiz and T. Scott (2013). "UV radiation and the skin." Int J Mol Sci **14**(6): 12222-12248.

Dao, V. T., C. Gaspard, M. Mayer, G. H. Werner, S. N. Nguyen and R. J. Michelot (2000). "Synthesis and cytotoxicity of gossypol related compounds." Eur J Med Chem **35**(9): 805-813.

Davies, H., G. R. Bignell, C. Cox, P. Stephens, S. Edkins, S. Clegg, J. Teague, H. Woffendin, M. J. Garnett, W. Bottomley, et al. (2002). "Mutations of the BRAF gene in human cancer." Nature **417**(6892): 949-954.

Degterev, A., J. Hitomi, M. Germscheid, I. L. Ch'en, O. Korkina, X. Teng, D. Abbott, G. D. Cuny, C. Yuan, G. Wagner, et al. (2008). "Identification of RIP1 kinase as a specific cellular target of necrostatins." Nat Chem Biol **4**(5): 313-321.

Degterev, A., Z. Huang, M. Boyce, Y. Li, P. Jagtap, N. Mizushima, G. D. Cuny, T. J. Mitchison, M. A. Moskowitz and J. Yuan (2005). "Chemical inhibitor of nonapoptotic cell death with therapeutic potential for ischemic brain injury." Nat Chem Biol **1**(2): 112-119.

Deng, S., H. Yuan, J. Yi, Y. Lu, Q. Wei, C. Guo, J. Wu, L. Yuan and Z. He (2013). "Gossypol acetic acid induces apoptosis in RAW264.7 cellsviaa caspase-dependent mitochondrial signaling pathway." Journal of Veterinary Science **14**(3): 281.

Denton, D. and S. Kumar (2019). "Autophagy-dependent cell death." Cell Death Differ **26**(4): 605-616.

Divakaruni, A. S., A. Paradyse, D. A. Ferrick, A. N. Murphy and M. Jastroch (2014). "Analysis and interpretation of microplate-based oxygen consumption and pH data." Methods Enzymol **547**: 309-354.

Doherty, J. and E. H. Baehrecke (2018). "Life, death and autophagy." Nat Cell Biol **20**(10): 1110-1117.

Du, C., M. Fang, Y. Li, L. Li and X. Wang (2000). "Smac, a mitochondrial protein that promotes cytochrome c-dependent caspase activation by eliminating IAP inhibition." Cell **102**(1): 33-42.

Du, W., N. Liu, Y. Zhang, X. Liu, Y. Yang, W. Chen and Y. He (2020). "PLOD2 promotes aerobic glycolysis and cell progression in colorectal cancer by upregulating HK2." Biochem Cell Biol **98**(3): 386-395.

Duvezin-Caubet, S., R. Jagasia, J. Wagener, S. Hofmann, A. Trifunovic, A. Hansson, A. Chomyn, M. F. Bauer, G. Attardi, N. G. Larsson, et al. (2006). "Proteolytic processing of OPA1 links mitochondrial dysfunction to alterations in mitochondrial morphology." J Biol Chem **281**(49): 37972-37979.

Ea, C. K., L. Deng, Z. P. Xia, G. Pineda and Z. J. Chen (2006). "Activation of IKK by TNFalpha requires site-specific ubiquitination of RIP1 and polyubiquitin binding by NEMO." Mol Cell **22**(2): 245-257.

Eberle, J. and A. M. Hossini (2008). "Expression and function of bcl-2 proteins in melanoma." Curr Genomics **9**(6): 409-419.

Elmore, S. (2007). "Apoptosis: a review of programmed cell death." Toxicol Pathol **35**(4): 495-516.

Euvrard, S., J. Kanitakis and A. Claudy (2003). "Skin cancers after organ transplantation." N Engl J Med **348**(17): 1681-1691.

Fadok, V. A., D. R. Voelker, P. A. Campbell, J. J. Cohen, D. L. Bratton and P. M. Henson (1992). "Exposure of phosphatidylserine on the surface of apoptotic lymphocytes triggers specific recognition and removal by macrophages." J Immunol **148**(7): 2207-2216.

FDA, Food and Drug Administration. (2016). "FDA approves new drug for chronic lymphocytic leukemia in patients with a specific chromosomal abnormality." from https://www.fda.gov/news-events/press-announcements/fda-approves-new-drug-chronic-lymphocytic-leukemia-patients-specific-chromosomal-abnormality.

FDA, Food and Drug Administration. (2019). "FDA approves venetoclax for CLL and SLL." from https://www.fda.gov/drugs/resources-information-approved-drugs/fda-approves-venetoclax-cll-and-sll.

Fire, A., S. Xu, M. K. Montgomery, S. A. Kostas, S. E. Driver and C. C. Mello (1998). "Potent and specific genetic interference by double-stranded RNA in Caenorhabditis elegans." Nature **391**(6669): 806-811.

Fitzpatrick, T. B. (1988). "The validity and practicality of sun-reactive skin types I through VI." Arch Dermatol **124**(6): 869-871.

Flaherty, K. T., J. R. Infante, A. Daud, R. Gonzalez, R. F. Kefford, J. Sosman, O. Hamid, L. Schuchter, J. Cebon, N. Ibrahim, et al. (2012). "Combined BRAF and MEK inhibition in melanoma with BRAF V600 mutations." N Engl J Med **367**(18): 1694-1703.

Frank, S., B. Gaume, E. S. Bergmann-Leitner, W. W. Leitner, E. G. Robert, F. Catez, C. L. Smith and R. J. Youle (2001). "The role of dynamin-related protein 1, a mediator of mitochondrial fission, in apoptosis." Dev Cell **1**(4): 515-525.

Friedman, R. J., D. S. Rigel and A. W. Kopf (1985). "Early detection of malignant melanoma: the role of physician examination and self-examination of the skin." CA Cancer J Clin **35**(3): 130-151.

Fritsch, M., S. D. Gunther, R. Schwarzer, M. C. Albert, F. Schorn, J. P. Werthenbach, L. M. Schiffmann, N. Stair, H. Stocks, J. M. Seeger, et al. (2019). "Caspase-8 is the molecular switch for apoptosis, necroptosis and pyroptosis." Nature **575**(7784): 683-687.

Fritsch, P. (2009). Dermatologie und Venerologie für das Studium. Heidelberg, Springer Medizin Verlag.

Fu, T. M., Y. Li, A. Lu, Z. Li, P. R. Vajjhala, A. C. Cruz, D. B. Srivastava, F. DiMaio, P. A. Penczek, R. M. Siegel, et al. (2016). "Cryo-EM Structure of Caspase-8 Tandem DED Filament Reveals Assembly and Regulation Mechanisms of the Death-Inducing Signaling Complex." Mol Cell **64**(2): 236-250.

Fulda, S. (2013). "The mechanism of necroptosis in normal and cancer cells." Cancer Biol Ther **14**(11): 999-1004.

Galluzzi, L., E. H. Baehrecke, A. Ballabio, P. Boya, J. M. Bravo-San Pedro, F. Cecconi, A. M. Choi, C. T. Chu, P. Codogno, M. I. Colombo, et al. (2017). "Molecular definitions of autophagy and related processes." EMBO J **36**(13): 1811-1836.

Gandini, S., F. Sera, M. S. Cattaruzza, P. Pasquini, D. Abeni, P. Boyle and C. F. Melchi (2005). "Meta-analysis of risk factors for cutaneous melanoma: I. Common and atypical naevi." Eur J Cancer **41**(1): 28-44.

Gao, P., C. Bauvy, S. Souquere, G. Tonelli, L. Liu, Y. Zhu, Z. Qiao, D. Bakula, T. Proikas-Cezanne, G. Pierron, et al. (2010). "The Bcl-2 homology domain 3 mimetic gossypol induces both Beclin 1-dependent and Beclin 1-independent cytoprotective autophagy in cancer cells." J Biol Chem **285**(33): 25570-25581.

Garbe, C., P. Terheyden, U. Keilholz, O. Kolbl and A. Hauschild (2008). "Treatment of melanoma." Dtsch Arztebl Int **105**(49): 845-851.

Garcia, S. N., R. C. Guedes and M. M. Marques (2019). "Unlocking the Potential of HK2 in Cancer Metabolism and Therapeutics." Curr Med Chem **26**(41): 7285-7322.

Gilbert, N. E., J. E. O'Reilly, C. J. Chang, Y. C. Lin and R. W. Brueggemeier (1995). "Antiproliferative activity of gossypol and gossypolone on human breast cancer cells." Life Sci **57**(1): 61-67.

Goebeler, M. and H. Hamm (2017). Basiswissen Dermatologie. Würzburg, Springer-Verlag GmbH Deutschland.

Gogvadze, V., S. Orrenius and B. Zhivotovsky (2006). "Multiple pathways of cytochrome c release from mitochondria in apoptosis." Biochim Biophys Acta **1757**(5-6): 639-647.

Goldman, A., S. Harper and D. W. Speicher (2016). "Detection of Proteins on Blot Membranes." Curr Protoc Protein Sci **86**: 10 18 11-10 18 11.

Gong, Y., Z. Fan, G. Luo, C. Yang, Q. Huang, K. Fan, H. Cheng, K. Jin, Q. Ni, X. Yu, et al. (2019). "The role of necroptosis in cancer biology and therapy." Mol Cancer **18**(1): 100.

Gracia-Cazaña, T., S. González and Y. Gilaberte (2016). "Resistance of Nonmelanoma Skin Cancer to Nonsurgical Treatments. Part I: Topical Treatments." Actas Dermo-Sifiliográficas (English Edition) **107**(9): 730-739.

Guan, R., W. Zou, X. Dai, X. Yu, H. Liu, Q. Chen and W. Teng (2018). "Mitophagy, a potential therapeutic target for stroke." J Biomed Sci **25**(1): 87.

Guo, Z., T. Song, Z. Xue, P. Liu, M. Zhang, X. Zhang and Z. Zhang (2020). "Using CETSA assay and a mathematical model to reveal dual Bcl-2/Mcl-1 inhibition and on-target mechanism for ABT-199 and S1." Eur J Pharm Sci **142**: 105105.

Haasler, L., A. K. Kondadi, T. Tsigaras, C. von Montfort, P. Graf, W. Stahl and P. Brenneisen (2021). "The BH3 mimetic (+/-) gossypol induces ROS-independent apoptosis and mitochondrial dysfunction in human A375 melanoma cells in vitro." Arch Toxicol **95**(4): 1349-1365.

Hailey, D. W., A. S. Rambold, P. Satpute-Krishnan, K. Mitra, R. Sougrat, P. K. Kim and J. Lippincott-Schwartz (2010). "Mitochondria supply membranes for autophagosome biogenesis during starvation." Cell **141**(4): 656-667.

Han, C. W., M. S. Jeong and S. B. Jang (2017). "Structure, signaling and the drug discovery of the Ras oncogene protein." BMB Rep **50**(7): 355-360.

Han, H. (2018). RNA Interference to Knock Down Gene Expression. Disease Gene Identification**:** 293-302.

Han, Z., J. Liang, Y. Li and J. He (2019). "Drugs and Clinical Approaches Targeting the Antiapoptotic Protein: A Review." Biomed Res Int **2019**: 1212369.

Hanahan, D. and R. A. Weinberg (2011). "Hallmarks of cancer: the next generation." Cell **144**(5): 646-674.

Hayashi-Nishino, M., N. Fujita, T. Noda, A. Yamaguchi, T. Yoshimori and A. Yamamoto (2009). "A subdomain of the endoplasmic reticulum forms a cradle for autophagosome formation." Nat Cell Biol **11**(12): 1433-1437.

He, G. W., C. Gunther, V. Thonn, Y. Q. Yu, E. Martini, B. Buchen, M. F. Neurath, M. Sturzl and C. Becker (2017). "Regression of apoptosis-resistant colorectal tumors by induction of necroptosis in mice." J Exp Med **214**(6): 1655-1662.

He, S., L. Wang, L. Miao, T. Wang, F. Du, L. Zhao and X. Wang (2009). "Receptor interacting protein kinase-3 determines cellular necrotic response to TNF-alpha." Cell **137**(6): 1100-1111.

Heiskanen, K. M., M. B. Bhat, H. W. Wang, J. Ma and A. L. Nieminen (1999). "Mitochondrial depolarization accompanies cytochrome c release during apoptosis in PC6 cells." J Biol Chem **274**(9): 5654-5658.

Henz, K., A. Al-Zebeeby, M. Basoglu, S. Fulda, G. M. Cohen, S. Varadarajan and M. Vogler (2019). "Selective BH3-mimetics targeting BCL-2, BCL-XL or MCL-1 induce severe mitochondrial perturbations." Biol Chem **400**(2): 181-185.

Hiddemann, W. and C. Bartram (2010). Die Onkologie. Heidelberg, Springer Medizin Verlag.

High, L. M., B. Szymanska, U. Wilczynska-Kalak, N. Barber, R. O'Brien, S. L. Khaw, I. B. Vikstrom, A. W. Roberts and R. B. Lock (2010). "The Bcl-2 homology domain 3 mimetic ABT-737 targets the apoptotic machinery in acute lymphoblastic leukemia resulting in synergistic in vitro and in vivo interactions with established drugs." Mol Pharmacol **77**(3): 483-494.

Ho, J., M. B. de Moura, Y. Lin, G. Vincent, S. Thorne, L. M. Duncan, L. Hui-Min, J. M. Kirkwood, D. Becker, B. Van Houten, et al. (2012). "Importance of glycolysis and oxidative phosphorylation in advanced melanoma." Mol Cancer **11**: 76.

Hou, D. X., T. Uto, X. Tong, T. Takeshita, S. Tanigawa, I. Imamura, T. Ose and M. Fujii (2004). "Involvement of reactive oxygen species-independent mitochondrial pathway in gossypol-induced apoptosis." Arch Biochem Biophys **428**(2): 179-187.

Hu, W., F. Wang, J. Tang, X. Liu, Z. Yuan, C. Nie and Y. Wei (2012). "Proapoptotic protein Smac mediates apoptosis in cisplatin-resistant ovarian cancer cells when treated with the anti-tumor agent AT101." J Biol Chem **287**(1): 68-80.

Jackson, W. T., T. H. Giddings, Jr., M. P. Taylor, S. Mulinyawe, M. Rabinovitch, R. R. Kopito and K. Kirkegaard (2005). "Subversion of cellular autophagosomal machinery by RNA viruses." PLoS Biol **3**(5): e156.

Jang, G. H. and M. Lee (2014). "BH3-mimetic gossypol-induced autophagic cell death in mutant BRAF melanoma cells with high expression of p21Cip(1).)." Life Sci **102**(1): 41-48.

Janostiak, R., P. Malvi and N. Wajapeyee (2019). "Anaplastic Lymphoma Kinase Confers Resistance to BRAF Kinase Inhibitors in Melanoma." iScience **16**: 453-467.

Jaroszewski, J. W., O. Kaplan and J. S. Cohen (1990). "Action of gossypol and rhodamine 123 on wild type and multidrug-resistant MCF-7 human breast cancer cells: 31P nuclear magnetic resonance and toxicity studies." Cancer Res **50**(21): 6936-6943.

Jia, L., L. C. Coward, C. D. Kerstner-Wood, R. L. Cork, G. S. Gorman, P. E. Noker, S. Kitada, M. Pellecchia and J. C. Reed (2008). "Comparison of pharmacokinetic and metabolic profiling among gossypol, apogossypol and apogossypol hexaacetate." Cancer Chemother Pharmacol **61**(1): 63-73.

Johansen, T. and T. Lamark (2011). "Selective autophagy mediated by autophagic adapter proteins." Autophagy **7**(3): 279-296.

Johnson-Cadwell, L. I., M. B. Jekabsons, A. Wang, B. M. Polster and D. G. Nicholls (2007). "'Mild Uncoupling' does not decrease mitochondrial superoxide levels in cultured cerebellar granule neurons but decreases spare respiratory capacity and increases toxicity to glutamate and oxidative stress." J Neurochem **101**(6): 1619-1631.

Kabeya, Y., N. Mizushima, T. Ueno, A. Yamamoto, T. Kirisako, T. Noda, E. Kominami, Y. Ohsumi and T. Yoshimori (2000). "LC3, a mammalian homologue of yeast Apg8p, is localized in autophagosome membranes after processing." EMBO J **19**(21): 5720-5728.

Kallinowski, F., K. H. Schlenger, S. Runkel, M. Kloes, M. Stohrer, P. Okunieff and P. Vaupel (1989). "Blood flow, metabolism, cellular microenvironment, and growth rate of human tumor xenografts." Cancer Res **49**(14): 3759-3764.

Kandoth, C., M. D. McLellan, F. Vandin, K. Ye, B. Niu, C. Lu, M. Xie, Q. Zhang, J. F. McMichael, M. A. Wyczalkowski, et al. (2013). "Mutational landscape and significance across 12 major cancer types." Nature **502**(7471): 333-339.

Kang, J. H., S. H. Lee, J. S. Lee, B. Nam, T. W. Seong, J. Son, H. Jang, K. M. Hong, C. Lee and S. Y. Kim (2016). "Aldehyde dehydrogenase inhibition combined with phenformin treatment reversed NSCLC through ATP depletion." Oncotarget **7**(31): 49397-49410.

Kang, M. H. and C. P. Reynolds (2009). "Bcl-2 inhibitors: targeting mitochondrial apoptotic pathways in cancer therapy." Clin Cancer Res **15**(4): 1126-1132.

Kearney, C. J. and S. J. Martin (2017). "An Inflammatory Perspective on Necroptosis." Mol Cell **65**(6): 965-973.

Kerr, J. F., A. H. Wyllie and A. R. Currie (1972). "Apoptosis: a basic biological phenomenon with wide-ranging implications in tissue kinetics." Br J Cancer **26**(4): 239-257.

Kim, H. Y., B. I. Lee, J. H. Jeon, D. K. Kim, S. G. Kang, J. K. Shim, S. Y. Kim, S. W. Kang and H. Jang (2019). "Gossypol Suppresses Growth of Temozolomide-Resistant Glioblastoma Tumor Spheres." Biomolecules **9**(10).

Kim, N. Y., B. I. Han and M. Lee (2016). "Cytoprotective role of autophagy against BH3 mimetic gossypol in ATG5 knockout cells generated by CRISPR-Cas9 endonuclease." Cancer Lett **370**(1): 19-26.

Kimura, S., T. Noda and T. Yoshimori (2008). "Dynein-dependent movement of autophagosomes mediates efficient encounters with lysosomes." Cell Struct Funct **33**(1): 109-122.

King, K. L. and J. A. Cidlowski (1998). "Cell cycle regulation and apoptosis." Annu Rev Physiol **60**: 601-617.

Kinzler, K. W. and B. Vogelstein (1997). "Cancer-susceptibility genes. Gatekeepers and caretakers." Nature **386**(6627): 761, 763.

Kischkel, F. C., S. Hellbardt, I. Behrmann, M. Germer, M. Pawlita, P. H. Krammer and M. E. Peter (1995). "Cytotoxicity-dependent APO-1 (Fas/CD95)-associated proteins form a death-inducing signaling complex (DISC) with the receptor." EMBO J **14**(22): 5579-5588.

Kitada, S., M. Leone, S. Sareth, D. Zhai, J. C. Reed and M. Pellecchia (2003). "Discovery, characterization, and structure-activity relationships studies of proapoptotic polyphenols targeting B-cell lymphocyte/leukemia-2 proteins." J Med Chem **46**(20): 4259-4264.

Klionsky, D. J. (2008). "Autophagy revisited: a conversation with Christian de Duve." Autophagy **4**(6): 740-743.

Klionsky, D. J., K. Abdelmohsen, A. Abe, M. J. Abedin, H. Abeliovich, A. Acevedo Arozena, H. Adachi, C. M. Adams, P. D. Adams, K. Adeli, et al. (2016). "Guidelines for the use and interpretation of assays for monitoring autophagy (3rd edition)." Autophagy **12**(1): 1-222.

Klionsky, D. J., J. M. Cregg, W. A. Dunn, Jr., S. D. Emr, Y. Sakai, I. V. Sandoval, A. Sibirny, S. Subramani, M. Thumm, M. Veenhuis, et al. (2003). "A unified nomenclature for yeast autophagy-related genes." Dev Cell **5**(4): 539-545.

Koehler, B. C., A. L. Scherr, S. Lorenz, C. Elssner, N. Kautz, S. Welte, D. Jaeger, T. Urbanik and H. Schulze-Bergkamen (2014). "Pan-Bcl-2 inhibitor obatoclax delays cell cycle progression and blocks migration of colorectal cancer cells." PLoS One **9**(9): e106571.

Konopleva, M., R. Contractor, T. Tsao, I. Samudio, P. P. Ruvolo, S. Kitada, X. Deng, D. Zhai, Y. X. Shi, T. Sneed, et al. (2006). "Mechanisms of apoptosis sensitivity and resistance to the BH3 mimetic ABT-737 in acute myeloid leukemia." Cancer Cell **10**(5): 375-388.

Kornek, T. and M. Augustin (2013). "Skin cancer prevention." J Dtsch Dermatol Ges **11**(4): 283-296; quiz 297-288.

Korshunov, S. S., V. P. Skulachev and A. A. Starkov (1997). "High protonic potential actuates a mechanism of production of reactive oxygen species in mitochondria." FEBS Letters **416**(1): 15-18.

Korsmeyer, S. J., J. R. Shutter, D. J. Veis, D. E. Merry and Z. N. Oltvai (1993). "Bcl-2/Bax: a rheostat that regulates an anti-oxidant pathway and cell death." Semin Cancer Biol **4**(6): 327-332.

Korsmeyer, S. J., M. C. Wei, M. Saito, S. Weiler, K. J. Oh and P. H. Schlesinger (2000). "Pro-apoptotic cascade activates BID, which oligomerizes BAK or BAX into pores that result in the release of cytochrome c." Cell Death Differ **7**(12): 1166-1173.

Krensel, M., J. Petersen, P. Mohr, C. Weishaupt, J. Augustin and I. Schafer (2019). "Estimating prevalence and incidence of skin cancer in Germany." J Dtsch Dermatol Ges **17**(12): 1239-1249.

Kruiswijk, F., C. F. Labuschagne and K. H. Vousden (2015). "p53 in survival, death and metabolic health: a lifeguard with a licence to kill." Nat Rev Mol Cell Biol **16**(7): 393-405.

Kwa, R. E., K. Campana and R. L. Moy (1992). "Biology of cutaneous squamous cell carcinoma." J Am Acad Dermatol **26**(1): 1-26.

Laemmli, U. K. (1970). "Cleavage of structural proteins during the assembly of the head of bacteriophage T4." Nature **227**(5259): 680-685.

Lane, D. P. (1992). "Cancer. p53, guardian of the genome." Nature **358**(6381): 15-16.

Larkin, J., V. Chiarion-Sileni, R. Gonzalez, J. J. Grob, C. L. Cowey, C. D. Lao, D. Schadendorf, R. Dummer, M. Smylie, P. Rutkowski, et al. (2015). "Combined Nivolumab and Ipilimumab or Monotherapy in Untreated Melanoma." N Engl J Med **373**(1): 23-34.

Lebel, C. P. and S. C. Bondy (1990). "Sensitive and rapid quantitation of oxygen reactive species formation in rat synaptosomes." Neurochem Int **17**(3): 435-440.

LeBel, C. P., H. Ischiropoulos and S. C. Bondy (1992). "Evaluation of the probe 2',7'-dichlorofluorescin as an indicator of reactive oxygen species formation and oxidative stress." Chem Res Toxicol **5**(2): 227-231.

Leblanc, O. H., Jr. (1971). "The effect of uncouplers of oxidative phosphorylation on lipid bilayer membranes: Carbonylcyanidem-chlorophenylhydrazone." J Membr Biol **4**(1): 227-251.

Lee, E. F., T. J. Harris, S. Tran, M. Evangelista, S. Arulananda, T. John, C. Ramnac, C. Hobbs, H. Zhu, G. Gunasingh, et al. (2019). "BCL-XL and MCL-1 are the key BCL-2 family proteins in melanoma cell survival." Cell Death Dis **10**(5): 342.

Lee, J.-S., H. Lee, H. Jang, S. M. Woo, J. B. Park, S.-H. Lee, J. H. Kang, H. Y. Kim, J. Song and S.-Y. Kim (2020). "Targeting Oxidative Phosphorylation Reverses Drug Resistance in Cancer Cells by Blocking Autophagy Recycling." Cells **9**(9).

Lee, S., J. S. Lee, J. Seo, S. H. Lee, J. H. Kang, J. Song and S. Y. Kim (2018). "Targeting Mitochondrial Oxidative Phosphorylation Abrogated Irinotecan Resistance in NSCLC." Sci Rep **8**(1): 15707.

Legros, F., A. Lombes, P. Frachon and M. Rojo (2002). "Mitochondrial fusion in human cells is efficient, requires the inner membrane potential, and is mediated by mitofusins." Mol Biol Cell **13**(12): 4343-4354.

Lessene, G., P. E. Czabotar and P. M. Colman (2008). "BCL-2 family antagonists for cancer therapy." Nat Rev Drug Discov **7**(12): 989-1000.

Letai, A., M. C. Bassik, L. D. Walensky, M. D. Sorcinelli, S. Weiler and S. J. Korsmeyer (2002). "Distinct BH3 domains either sensitize or activate mitochondrial apoptosis, serving as prototype cancer therapeutics." Cancer Cell **2**(3): 183-192.

Levine, B. (2007). "Cell biology: autophagy and cancer." Nature **446**(7137): 745-747.

Li, J., T. McQuade, A. B. Siemer, J. Napetschnig, K. Moriwaki, Y. S. Hsiao, E. Damko, D. Moquin, T. Walz, A. McDermott, et al. (2012). "The RIP1/RIP3 necrosome forms a functional amyloid signaling complex required for programmed necrosis." Cell **150**(2): 339-350.

Li, J., J. Viallet and E. B. Haura (2008). "A small molecule pan-Bcl-2 family inhibitor, GX15-070, induces apoptosis and enhances cisplatin-induced apoptosis in non-small cell lung cancer cells." Cancer Chemother Pharmacol **61**(3): 525-534.

Li, W. C., C. H. Huang, Y. T. Hsieh, T. Y. Chen, L. H. Cheng, C. Y. Chen, C. J. Liu, H. M. Chen, C. L. Huang, J. F. Lo, et al. (2020). "Regulatory Role of Hexokinase 2 in Modulating Head and Neck Tumorigenesis." Front Oncol **10**: 176.

Li, X., S. He and B. Ma (2020). "Autophagy and autophagy-related proteins in cancer." Mol Cancer **19**(1): 12.

Liang, X. H., L. K. Kleeman, H. H. Jiang, G. Gordon, J. E. Goldman, G. Berry, B. Herman and B. Levine (1998). "Protection against fatal Sindbis virus encephalitis by beclin, a novel Bcl-2-interacting protein." J Virol **72**(11): 8586-8596.

Liesa, M., M. Palacin and A. Zorzano (2009). "Mitochondrial dynamics in mammalian health and disease." Physiol Rev **89**(3): 799-845.

Lin, Q. H., F. C. Que, C. P. Gu, D. S. Zhong, D. Zhou, Y. Kong, L. Yu and S. W. Liu (2017). "ABT-263 induces G1/G0-phase arrest, apoptosis and autophagy in human esophageal cancer cells in vitro." Acta Pharmacol Sin **38**(12): 1632-1641.

Lin, Y., A. Devin, Y. Rodriguez and Z. G. Liu (1999). "Cleavage of the death domain kinase RIP by caspase-8 prompts TNF-induced apoptosis." Genes Dev **13**(19): 2514-2526.

Lindqvist, L. M., D. Frank, K. McArthur, T. A. Dite, M. Lazarou, J. S. Oakhill, B. T. Kile and D. L. Vaux (2018). "Autophagy induced during apoptosis degrades mitochondria and inhibits type I interferon secretion." Cell Death Differ **25**(4): 784-796.

Lis, P., M. Dylag, K. Niedzwiecka, Y. H. Ko, P. L. Pedersen, A. Goffeau and S. Ulaszewski (2016). "The HK2 Dependent "Warburg Effect" and Mitochondrial Oxidative Phosphorylation in Cancer: Targets for Effective Therapy with 3-Bromopyruvate." Molecules **21**(12).

Liu, Y., T. Liu, T. Lei, D. Zhang, S. Du, L. Girani, D. Qi, C. Lin, R. Tong and Y. Wang (2019). "RIP1/RIP3-regulated necroptosis as a target for multifaceted disease therapy (Review)." Int J Mol Med **44**(3): 771-786.

Liu, Z. G. and D. Jiao (2019). "Necroptosis, tumor necrosis and tumorigenesis." Cell Stress **4**(1): 1-8.

Löffler, G. and P. E. Petrides (1997). Biochemie und Pathobiochemie, Springer-Verlag.

Lowry, O., N. Rosebrough, A. L. Farr and R. Randall (1951). "Protein Measurement with the Folin Phenol Reagent." Journal of Biological Chemistry **193**(1): 265-275.

Luke, J. J., K. T. Flaherty, A. Ribas and G. V. Long (2017). "Targeted agents and immunotherapies: optimizing outcomes in melanoma." Nat Rev Clin Oncol **14**(8): 463-482.

Ly, J. D., D. R. Grubb and A. Lawen (2003). "The mitochondrial membrane potential (deltapsi(m)) in apoptosis; an update." Apoptosis **8**(2): 115-128.

Madesh, M., B. Antonsson, S. M. Srinivasula, E. S. Alnemri and G. Hajnoczky (2002). "Rapid kinetics of tBid-induced cytochrome c and Smac/DIABLO release and mitochondrial depolarization." J Biol Chem **277**(7): 5651-5659.

Maeda, A. and B. Fadeel (2014). "Mitochondria released by cells undergoing TNF-alpha-induced necroptosis act as danger signals." Cell Death Dis **5**: e1312.

Maere, S., K. Heymans and M. Kuiper (2005). "BiNGO: a Cytoscape plugin to assess overrepresentation of gene ontology categories in biological networks." Bioinformatics **21**(16): 3448-3449.

Maiuri, M. C., G. Le Toumelin, A. Criollo, J. C. Rain, F. Gautier, P. Juin, E. Tasdemir, G. Pierron, K. Troulinaki, N. Tavernarakis, et al. (2007). "Functional and physical interaction between Bcl-X(L) and a BH3-like domain in Beclin-1." EMBO J **26**(10): 2527-2539.

Manna, P. R. and D. M. Stocco (2011). "The role of specific mitogen-activated protein kinase signaling cascades in the regulation of steroidogenesis." J Signal Transduct **2011**: 821615.

Mantovani, F., L. Collavin and G. Del Sal (2019). "Mutant p53 as a guardian of the cancer cell." Cell Death Differ **26**(2): 199-212.

Marchetti, P., Q. Fovez, N. Germain, R. Khamari and J. Kluza (2020). "Mitochondrial spare respiratory capacity: Mechanisms, regulation, and significance in non-transformed and cancer cells." FASEB J **34**(10): 13106-13124.

Marghoob, N. G., K. Liopyris and N. Jaimes (2019). "Dermoscopy: A Review of the Structures That Facilitate Melanoma Detection." J Am Osteopath Assoc **119**(6): 380-390.

Martin, S. J. (2016). "Cell death and inflammation: the case for IL-1 family cytokines as the canonical DAMPs of the immune system." FEBS J **283**(14): 2599-2615.

Masuelli, L., M. Benvenuto, V. Izzi, E. Zago, R. Mattera, B. Cerbelli, V. Potenza, S. Fazi, S. Ciuffa, I. Tresoldi, et al. (2020). "In vivo and in vitro inhibition of osteosarcoma growth by the pan Bcl-2 inhibitor AT-101." Invest New Drugs **38**(3): 675-689.

Matsuzaki, S. and K. M. Humphries (2015). "Selective inhibition of deactivated mitochondrial complex I by biguanides." Biochemistry **54**(11): 2011-2021.

Mauthe, M., I. Orhon, C. Rocchi, X. Zhou, M. Luhr, K. J. Hijlkema, R. P. Coppes, N. Engedal, M. Mari and F. Reggiori (2018). "Chloroquine inhibits autophagic flux by decreasing autophagosome-lysosome fusion." Autophagy **14**(8): 1435-1455.

Maydt, D., S. De Spirt, C. Muschelknautz, W. Stahl and T. J. Muller (2013). "Chemical reactivity and biological activity of chalcones and other alpha,beta-unsaturated carbonyl compounds." Xenobiotica **43**(8): 711-718.

McDonnell, T. J., P. Troncoso, S. M. Brisbay, C. Logothetis, L. W. Chung, J. T. Hsieh, S. M. Tu and M. L. Campbell (1992). "Expression of the protooncogene bcl-2 in the prostate and its association with emergence of androgen-independent prostate cancer." Cancer Res **52**(24): 6940-6944.

Merino, D., G. L. Kelly, G. Lessene, A. H. Wei, A. W. Roberts and A. Strasser (2018). "BH3-Mimetic Drugs: Blazing the Trail for New Cancer Medicines." Cancer Cell **34**(6): 879-891.

Meyer, N., S. Zielke, J. B. Michaelis, B. Linder, V. Warnsmann, S. Rakel, H. D. Osiewacz, S. Fulda, M. Mittelbronn, C. Munch, et al. (2018). "AT 101 induces early mitochondrial dysfunction and HMOX1 (heme oxygenase 1) to trigger mitophagic cell death in glioma cells." Autophagy **14**(10): 1693-1709.

Micheau, O. and J. Tschopp (2003). "Induction of TNF Receptor I-Mediated Apoptosis via Two Sequential Signaling Complexes." Cell **114**(2): 181-190.

Migden, M. R., D. Rischin, C. D. Schmults, A. Guminski, A. Hauschild, K. D. Lewis, C. H. Chung, L. Hernandez-Aya, A. M. Lim, A. L. S. Chang, et al. (2018). "PD-1 Blockade with Cemiplimab in Advanced Cutaneous Squamous-Cell Carcinoma." N Engl J Med 379(4): 341-351.

Milani, M., D. P. Byrne, G. Greaves, M. Butterworth, G. M. Cohen, P. A. Eyers and S. Varadarajan (2017). "DRP-1 is required for BH3 mimetic-mediated mitochondrial fragmentation and apoptosis." Cell Death Dis 8(1): e2552.

Miller, A. J. and M. C. Mihm, Jr. (2006). "Melanoma." N Engl J Med 355(1): 51-65.

Mizushima, N. (2007). "Autophagy: process and function." Genes Dev 21(22): 2861-2873.

Mizushima, N. and M. Komatsu (2011). "Autophagy: renovation of cells and tissues." Cell 147(4): 728-741.

Mizushima, N. and T. Yoshimori (2007). "How to interpret LC3 immunoblotting." Autophagy 3(6): 542-545.

Mizushima, N., T. Yoshimori and B. Levine (2010). "Methods in mammalian autophagy research." Cell 140(3): 313-326.

Mohammad, R. M., I. Muqbil, L. Lowe, C. Yedjou, H. Y. Hsu, L. T. Lin, M. D. Siegelin, C. Fimognari, N. B. Kumar, Q. P. Dou, et al. (2015). "Broad targeting of resistance to apoptosis in cancer." Semin Cancer Biol 35 Suppl: S78-S103.

Montero, J. and A. Letai (2018). "Why do BCL-2 inhibitors work and where should we use them in the clinic?" Cell Death Differ 25(1): 56-64.

Moquin, D. M., T. McQuade and F. K. Chan (2013). "CYLD deubiquitinates RIP1 in the TNFalpha-induced necrosome to facilitate kinase activation and programmed necrosis." PLoS One 8(10): e76841.

Morita, A. (2007). "Tobacco smoke causes premature skin aging." J Dermatol Sci 48(3): 169-175.

Morris, L. G. and T. A. Chan (2015). "Therapeutic targeting of tumor suppressor genes." Cancer 121(9): 1357-1368.

Mosmann, T. (1983). "Rapid colorimetric assay for cellular growth and survival: application to proliferation and cytotoxicity assays." J Immunol Methods 65(1-2): 55-63.

Mukherjee, N., A. Strosnider, B. Vagher, K. A. Lambert, S. Slaven, W. A. Robinson, C. M. Amato, K. L. Couts, J. G. T. Bemis, J. A. Turner, et al. (2018). "BH3 mimetics induce apoptosis independent of DRP-1 in melanoma." Cell Death Dis 9(9): 907.

Müller-Esterl, W. (2018). Biochemie, Springer Verlag GmbH Deutschland.

Muroyama, A. and T. Lechler (2012). "Polarity and stratification of the epidermis." Semin Cell Dev Biol 23(8): 890-896.

Nagarajan, P., M. M. Asgari, A. C. Green, S. M. Guhan, S. T. Arron, C. M. Proby, D. E. Rollison, C. A. Harwood and A. E. Toland (2019). "Keratinocyte Carcinomas: Current Concepts and Future Research Priorities." Clin Cancer Res 25(8): 2379-2391.

Nagata, S. (2018). "Apoptosis and Clearance of Apoptotic Cells." Annu Rev Immunol 36: 489-517.

Najafov, A., H. Chen and J. Yuan (2017). "Necroptosis and Cancer." Trends Cancer 3(4): 294-301.

Nakamura, M., M. Ikeda, A. Suzuki, S. Okinaga and K. Arai (1988). "Metabolism of round spermatids: gossypol induces uncoupling of respiratory chain and oxidative phosphorylation." Biol Reprod 39(4): 771-778.

Nazarian, R., H. Shi, Q. Wang, X. Kong, R. C. Koya, H. Lee, Z. Chen, M. K. Lee, N. Attar, H. Sazegar, et al. (2010). "Melanomas acquire resistance to B-RAF(V600E) inhibition by RTK or N-RAS upregulation." Nature 468(7326): 973-977.

Oakes, S. R., F. Vaillant, E. Lim, L. Lee, K. Breslin, F. Feleppa, S. Deb, M. E. Ritchie, E. Takano, T. Ward, et al. (2012). "Sensitization of BCL-2-expressing breast tumors to chemotherapy by the BH3 mimetic ABT-737." Proc Natl Acad Sci U S A 109(8): 2766-2771.

Oberstein, A., P. D. Jeffrey and Y. Shi (2007). "Crystal structure of the Bcl-XL-Beclin 1 peptide complex: Beclin 1 is a novel BH3-only protein." J Biol Chem 282(17): 13123-13132.

Oliver, C. L., J. A. Bauer, K. G. Wolter, M. L. Ubell, A. Narayan, K. M. O'Connell, S. G. Fisher, S. Wang, X. Wu, M. Ji, et al. (2004). "In vitro effects of the BH3 mimetic, (-)-gossypol, on head and neck squamous cell carcinoma cells." Clin Cancer Res 10(22): 7757-7763.

Oliver, C. L., M. B. Miranda, S. Shangary, S. Land, S. Wang and D. E. Johnson (2005). "(-)-Gossypol acts directly on the mitochondria to overcome Bcl-2- and Bcl-X(L)-mediated apoptosis resistance." Mol Cancer Ther 4(1): 23-31.

Oltersdorf, T., S. W. Elmore, A. R. Shoemaker, R. C. Armstrong, D. J. Augeri, B. A. Belli, M. Bruncko, T. L. Deckwerth, J. Dinges, P. J. Hajduk, et al. (2005). "An inhibitor of Bcl-2 family proteins induces regression of solid tumours." Nature 435(7042): 677-681.

Opydo-Chanek, M., O. Gonzalo and I. Marzo (2017). "Multifaceted anticancer activity of BH3 mimetics: Current evidence and future prospects." Biochem Pharmacol 136: 12-23.

Orenstein, S. J. and A. M. Cuervo (2010). "Chaperone-mediated autophagy: molecular mechanisms and physiological relevance." Semin Cell Dev Biol 21(7): 719-726.

Oun, R., Y. E. Moussa and N. J. Wheate (2018). "The side effects of platinum-based chemotherapy drugs: a review for chemists." Dalton Trans 47(19): 6645-6653.

Park, C. M., M. Bruncko, J. Adickes, J. Bauch, H. Ding, A. Kunzer, K. C. Marsh, P. Nimmer, A. R. Shoemaker, X. Song, et al. (2008). "Discovery of an orally bioavailable small molecule inhibitor of prosurvival B-cell lymphoma 2 proteins." J Med Chem 51(21): 6902-6915.

Park, J., J. K. Shim, J. H. Kang, J. Choi, J. H. Chang, S. Y. Kim and S. G. Kang (2018). "Regulation of bioenergetics through dual inhibition of aldehyde dehydrogenase and mitochondrial complex I suppresses glioblastoma tumorspheres." Neuro Oncol 20(7): 954-965.

Pasparakis, M. and P. Vandenabeele (2015). "Necroptosis and its role in inflammation." Nature 517(7534): 311-320.

Patel, A. (2020). "Benign vs Malignant Tumors." JAMA Oncology 6(9).

Pattingre, S., A. Tassa, X. Qu, R. Garuti, X. H. Liang, N. Mizushima, M. Packer, M. D. Schneider and B. Levine (2005). "Bcl-2 antiapoptotic proteins inhibit Beclin 1-dependent autophagy." Cell 122(6): 927-939.

Pearson, J. S. and J. M. Murphy (2017). "Down the rabbit hole: Is necroptosis truly an innate response to infection?" Cell Microbiol 19(8).

Peng, L., Y. Wang, Y. Hong, X. Ye, P. Shi, J. Zhang and Q. Zhao (2017). "Incidence and relative risk of cutaneous squamous cell carcinoma with single-agent BRAF inhibitor and dual BRAF/MEK inhibitors in cancer patients: a meta-analysis." Oncotarget 8(47): 83280-83291.

Pickering, C. R., J. H. Zhou, J. J. Lee, J. A. Drummond, S. A. Peng, R. E. Saade, K. Y. Tsai, J. L. Curry, M. T. Tetzlaff, S. Y. Lai, et al. (2014). "Mutational Landscape of Aggressive Cutaneous Squamous Cell Carcinoma." Clinical Cancer Research 20(24): 6582-6592.

Pisal, R. V., H. Hrebikova, J. Chvatalova, D. Kunke, S. Filip and J. Mokry (2016). "Detection of Mycoplasma Contamination Directly from Culture Supernatant Using Polymerase Chain Reaction." Folia Biol (Praha) **62**(5): 203-206.

Plantone, D. and T. Koudriavtseva (2018). "Current and Future Use of Chloroquine and Hydroxychloroquine in Infectious, Immune, Neoplastic, and Neurological Diseases: A Mini-Review." Clin Drug Investig **38**(8): 653-671.

Qiu, Y., T. Yu, W. Wang, K. Pan, D. Shi and H. Sun (2014). "Curcumin-induced melanoma cell death is associated with mitochondrial permeability transition pore (mPTP) opening." Biochem Biophys Res Commun **448**(1): 15-21.

Que, S. K. T., F. O. Zwald and C. D. Schmults (2018). "Cutaneous squamous cell carcinoma: Incidence, risk factors, diagnosis, and staging." J Am Acad Dermatol **78**(2): 237-247.

R Core Team. (2019). "A language and environment for statistical computing. ." from http://www.R-project.org/.

Radogna, F., M. Dicato and M. Diederich (2015). "Cancer-type-specific crosstalk between autophagy, necroptosis and apoptosis as a pharmacological target." Biochem Pharmacol **94**(1): 1-11.

Rai, N. K., K. Tripathi, D. Sharma and V. K. Shukla (2005). "Apoptosis: a basic physiologic process in wound healing." Int J Low Extrem Wounds **4**(3): 138-144.

Rasmussen, M. L., N. Taneja, A. C. Neininger, L. Wang, G. L. Robertson, S. N. Riffle, L. Shi, B. C. Knollmann, D. T. Burnette and V. Gama (2020). "MCL-1 Inhibition by Selective BH3 Mimetics Disrupts Mitochondrial Dynamics Causing Loss of Viability and Functionality of Human Cardiomyocytes." iScience **23**(4): 101015.

Ravikumar, B., K. Moreau, L. Jahreiss, C. Puri and D. C. Rubinsztein (2010). "Plasma membrane contributes to the formation of pre-autophagosomal structures." Nat Cell Biol **12**(8): 747-757.

Remijsen, Q., V. Goossens, S. Grootjans, C. Van den Haute, N. Vanlangenakker, Y. Dondelinger, R. Roelandt, I. Bruggeman, A. Goncalves, M. J. Bertrand, et al. (2014). "Depletion of RIPK3 or MLKL blocks TNF-driven necroptosis and switches towards a delayed RIPK1 kinase-dependent apoptosis." Cell Death Dis **5**: e1004.

Ren, T., J. Shan, M. Li, Y. Qing, C. Qian, G. Wang, Q. Li, G. Lu, C. Li, Y. Peng, et al. (2015). "Small-molecule BH3 mimetic and pan-Bcl-2 inhibitor AT-101 enhances the antitumor efficacy of cisplatin through inhibition of APE1 repair and redox activity in non-small-cell lung cancer." Drug Des Devel Ther **9**: 2887-2910.

Renehan, A. G., C. Booth and C. S. Potten (2001). "What is apoptosis, and why is it important?" BMJ **322**(7301): 1536-1538.

Ribero, S., L. S. Stucci, G. A. Daniels and L. Borradori (2017). "Drug therapy of advanced cutaneous squamous cell carcinoma: is there any evidence?" Curr Opin Oncol **29**(2): 129-135.

Riss, T. L., R. A. Moravec, A. L. Niles, S. Duellman, H. A. Benink, T. J. Worzella and L. Minor (2004). Cell Viability Assays. Assay Guidance Manual. G. S. Sittampalam, A. Grossman, K. Brimacombe et al. Bethesda (MD).

Rubinsztein, D. C., A. M. Cuervo, B. Ravikumar, S. Sarkar, V. Korolchuk, S. Kaushik and D. J. Klionsky (2009). "In search of an "autophagomometer"." Autophagy **5**(5): 585-589.

Sahani, M. H., E. Itakura and N. Mizushima (2014). "Expression of the autophagy substrate SQSTM1/p62 is restored during prolonged starvation depending on transcriptional upregulation and autophagy-derived amino acids." Autophagy **10**(3): 431-441.

Sahu, R., S. Kaushik, C. C. Clement, E. S. Cannizzo, B. Scharf, A. Follenzi, I. Potolicchio, E. Nieves, A. M. Cuervo and L. Santambrogio (2011). "Microautophagy of cytosolic proteins by late endosomes." Dev Cell **20**(1): 131-139.

Sakahira, H., M. Enari and S. Nagata (1998). "Cleavage of CAD inhibitor in CAD activation and DNA degradation during apoptosis." Nature **391**(6662): 96-99.

Samson, A. L., Y. Zhang, N. D. Geoghegan, X. J. Gavin, K. A. Davies, M. J. Mlodzianoski, L. W. Whitehead, D. Frank, S. E. Garnish, C. Fitzgibbon, et al. (2020). "MLKL trafficking and accumulation at the plasma membrane control the kinetics and threshold for necroptosis." Nat Commun **11**(1): 3151.

Sattler, M., H. Liang, D. Nettesheim, R. P. Meadows, J. E. Harlan, M. Eberstadt, H. S. Yoon, S. B. Shuker, B. S. Chang, A. J. Minn, et al. (1997). "Structure of Bcl-xL-Bak peptide complex: recognition between regulators of apoptosis." Science **275**(5302): 983-986.

Scaduto, R. C., Jr. and L. W. Grotyohann (1999). "Measurement of mitochondrial membrane potential using fluorescent rhodamine derivatives." Biophys J **76**(1 Pt 1): 469-477.

Schaefer, M. H. and L. Serrano (2016). "Cell type-specific properties and environment shape tissue specificity of cancer genes." Sci Rep **6**: 20707.

Schneider, G., M. Schmidt-Supprian, R. Rad and D. Saur (2017). "Tissue-specific tumorigenesis: context matters." Nat Rev Cancer **17**(4): 239-253.

Schwammle, V., I. R. Leon and O. N. Jensen (2013). "Assessment and improvement of statistical tools for comparative proteomics analysis of sparse data sets with few experimental replicates." J Proteome Res **12**(9): 3874-3883.

Serasinghe, M. N. and J. E. Chipuk (2017). "Mitochondrial Fission in Human Diseases." Handb Exp Pharmacol **240**: 159-188.

Shannon, P., A. Markiel, O. Ozier, N. S. Baliga, J. T. Wang, D. Ramage, N. Amin, B. Schwikowski and T. Ideker (2003). "Cytoscape: a software environment for integrated models of biomolecular interaction networks." Genome Res **13**(11): 2498-2504.

Shelley, M. D., L. Hartley, R. G. Fish, P. Groundwater, J. J. Morgan, D. Mort, M. Mason and A. Evans (1999). "Stereo-specific cytotoxic effects of gossypol enantiomers and gossypolone in tumour cell lines." Cancer Lett **135**(2): 171-180.

Shi, T., Y. Ma, L. Cao, S. Zhan, Y. Xu, F. Fu, C. Liu, G. Zhang, Z. Wang, R. Wang, et al. (2019). "B7-H3 promotes aerobic glycolysis and chemoresistance in colorectal cancer cells by regulating HK2." Cell Death Dis **10**(4): 308.

Shi, Z., B. Lan, B. Peng, X. Wang, G. Zhang, X. Li and F. Guo (2018). "Combination therapy with BH3 mimetic and hyperthermia tends to be more effective on anti-melanoma treatment." Biochem Biophys Res Commun **503**(1): 249-256.

Singh, R., A. Letai and K. Sarosiek (2019). "Regulation of apoptosis in health and disease: the balancing act of BCL-2 family proteins." Nat Rev Mol Cell Biol **20**(3): 175-193.

Skehan, P., R. Storeng, D. Scudiero, A. Monks, J. McMahon, D. Vistica, J. T. Warren, H. Bokesch, S. Kenney and M. R. Boyd (1990). "New colorimetric cytotoxicity assay for anticancer-drug screening." J Natl Cancer Inst **82**(13): 1107-1112.

Songbo, M., H. Lang, C. Xinyong, X. Bin, Z. Ping and S. Liang (2019). "Oxidative stress injury in doxorubicin-induced cardiotoxicity." Toxicol Lett **307**: 41-48.

Stanbridge, E. (1971). "Mycoplasmas and cell cultures." Bacteriol Rev **35**(2): 206-227.

Stang, A., L. Khil, H. Kajuter, N. Pandeya, C. D. Schmults, E. S. Ruiz, P. S. Karia and A. C. Green (2019). "Incidence and mortality for cutaneous squamous cell carcinoma: comparison across three continents." J Eur Acad Dermatol Venereol **33 Suppl 8**: 6-10.

Stratigos, A. J., C. Garbe, C. Dessinioti, C. Lebbe, V. Bataille, L. Bastholt, B. Dreno, M. C. Fargnoli, A. M. Forsea, C. Frenard, et al. (2020). "European interdisciplinary guideline on invasive squamous cell carcinoma of the skin: Part 1. epidemiology, diagnostics and prevention." Eur J Cancer **128**: 60-82.

Su, Z., Z. Yang, L. Xie, J. P. DeWitt and Y. Chen (2016). "Cancer therapy in the necroptosis era." Cell Death Differ **23**(5): 748-756.

Suen, D. F., K. L. Norris and R. J. Youle (2008). "Mitochondrial dynamics and apoptosis." Genes Dev **22**(12): 1577-1590.

Sulkshane, P. and T. Teni (2017). "BH3 mimetic Obatoclax (GX15-070) mediates mitochondrial stress predominantly via MCL-1 inhibition and induces autophagy-dependent necroptosis in human oral cancer cells." Oncotarget **8**(36): 60060-60079.

Sun, L., H. Wang, Z. Wang, S. He, S. Chen, D. Liao, L. Wang, J. Yan, W. Liu, X. Lei, et al. (2012). "Mixed lineage kinase domain-like protein mediates necrosis signaling downstream of RIP3 kinase." Cell **148**(1-2): 213-227.

Sun, X., J. Yin, M. A. Starovasnik, W. J. Fairbrother and V. M. Dixit (2002). "Identification of a novel homotypic interaction motif required for the phosphorylation of receptor-interacting protein (RIP) by RIP3." J Biol Chem **277**(11): 9505-9511.

Tait, S. W., A. Oberst, G. Quarato, S. Milasta, M. Haller, R. Wang, M. Karvela, G. Ichim, N. Yatim, M. L. Albert, et al. (2013). "Widespread mitochondrial depletion via mitophagy does not compromise necroptosis." Cell Rep **5**(4): 878-885.

Takagi, T., K. Tsujii and K. Shirahama (1975). "Binding isotherms of sodium dodecyl sulfate to protein polypeptides with special reference to SDS-polyacylamide gel electrophoresis." J Biochem **77**(5): 939-947.

Tang, D., R. Kang, T. V. Berghe, P. Vandenabeele and G. Kroemer (2019). "The molecular machinery of regulated cell death." Cell Res **29**(5): 347-364.

Tang, Q., W. Liu, Q. Zhang, J. Huang, C. Hu, Y. Liu, Q. Wang, M. Zhou, W. Lai, F. Sheng, et al. (2018). "Dynamin-related protein 1-mediated mitochondrial fission contributes to IR-783-induced apoptosis in human breast cancer cells." J Cell Mol Med **22**(9): 4474-4485.

Tetz, L. M., P. W. Kamau, A. A. Cheng, J. D. Meeker and R. Loch-Caruso (2013). "Troubleshooting the dichlorofluorescein assay to avoid artifacts in measurement of toxicant-stimulated cellular production of reactive oxidant species." J Pharmacol Toxicol Methods **67**(2): 56-60.

The Global Cancer Observatory (2020). "Melanoma of the skin." Retrieved May 21, 2021, from https://gco.iarc.fr/today/data/factsheets/cancers/16-Melanoma-of-skin-fact-sheet.pdf.

Tilokani, L., S. Nagashima, V. Paupe and J. Prudent (2018). "Mitochondrial dynamics: overview of molecular mechanisms." Essays Biochem **62**(3): 341-360.

Tooze, S. A. and T. Yoshimori (2010). "The origin of the autophagosomal membrane." Nat Cell Biol **12**(9): 831-835.

Tran, M. and P. H. Reddy (2020). "Defective Autophagy and Mitophagy in Aging and Alzheimer's Disease." Front Neurosci **14**: 612757.

Tran, S. L., A. Puhar, M. Ngo-Camus and N. Ramarao (2011). "Trypan blue dye enters viable cells incubated with the pore-forming toxin HlyII of Bacillus cereus." PLoS One **6**(9): e22876.

Tse, C., A. R. Shoemaker, J. Adickes, M. G. Anderson, J. Chen, S. Jin, E. F. Johnson, K. C. Marsh, M. J. Mitten, P. Nimmer, et al. (2008). "ABT-263: a potent and orally bioavailable Bcl-2 family inhibitor." Cancer Res **68**(9): 3421-3428.

Twig, G., A. Elorza, A. J. Molina, H. Mohamed, J. D. Wikstrom, G. Walzer, L. Stiles, S. E. Haigh, S. Katz, G. Las, et al. (2008). "Fission and selective fusion govern mitochondrial segregation and elimination by autophagy." EMBO J **27**(2): 433-446.

Uzunparmak, B., M. Gao, A. Lindemann, K. Erikson, L. Wang, E. Lin, S. J. Frank, F. O. Gleber-Netto, M. Zhao, H. D. Skinner, et al. (2020). "Caspase-8 loss radiosensitizes head and neck squamous cell carcinoma to SMAC mimetic-induced necroptosis." JCI Insight **5**(23).

Van Laar, V. S., S. B. Berman and T. G. Hastings (2016). "Mic60/mitofilin overexpression alters mitochondrial dynamics and attenuates vulnerability of dopaminergic cells to dopamine and rotenone." Neurobiol Dis **91**: 247-261.

Vandenabeele, P., L. Galluzzi, T. Vanden Berghe and G. Kroemer (2010). "Molecular mechanisms of necroptosis: an ordered cellular explosion." Nat Rev Mol Cell Biol **11**(10): 700-714.

Vander Heiden, M. G., L. C. Cantley and C. B. Thompson (2009). "Understanding the Warburg effect: the metabolic requirements of cell proliferation." Science **324**(5930): 1029-1033.

Varadarajan, S., M. Butterworth, J. Wei, M. Pellecchia, D. Dinsdale and G. M. Cohen (2013). "Sabutoclax (BI97C1) and BI112D1, putative inhibitors of MCL-1, induce mitochondrial fragmentation either upstream of or independent of apoptosis." Neoplasia **15**(5): 568-578.

Varra, V., N. M. Woody, C. Reddy, N. P. Joshi, J. Geiger, D. J. Adelstein, B. B. Burkey, J. Scharpf, B. Prendes, E. D. Lamarre, et al. (2018). "Suboptimal Outcomes in Cutaneous Squamous Cell Cancer of the Head and Neck with Nodal Metastases." Anticancer Res **38**(10): 5825-5830.

Vasiljevic, N., K. Andersson, K. Bjelkenkrantz, C. Kjellstrom, H. Mansson, E. Nilsson, G. Landberg, J. Dillner and O. Forslund (2009). "The Bcl-xL inhibitor of apoptosis is preferentially expressed in cutaneous squamous cell carcinoma compared with that in keratoacanthoma." Int J Cancer **124**(10): 2361-2366.

Verhagen, A. M., P. G. Ekert, M. Pakusch, J. Silke, L. M. Connolly, G. E. Reid, R. L. Moritz, R. J. Simpson and D. L. Vaux (2000). "Identification of DIABLO, a mammalian protein that promotes apoptosis by binding to and antagonizing IAP proteins." Cell **102**(1): 43-53.

Visvader, J. E. (2011). "Cells of origin in cancer." Nature **469**(7330): 314-322.

Vogler, M. (2014). "Targeting BCL2-Proteins for the Treatment of Solid Tumours." Adv Med **2014**: 943648.

Voskoboinik, I., J. C. Whisstock and J. A. Trapani (2015). "Perforin and granzymes: function, dysfunction and human pathology." Nat Rev Immunol **15**(6): 388-400.

Waldner, M., D. Fantus, M. Solari and A. W. Thomson (2016). "New perspectives on mTOR inhibitors (rapamycin, rapalogs and TORKinibs) in transplantation." Br J Clin Pharmacol **82**(5): 1158-1170.

Wang, H. and J. A. Joseph (1999). "Quantifying cellular oxidative stress by dichlorofluorescein assay using microplate reader." Free Radic Biol Med **27**(5-6): 612-616.

Wang, H., L. Sun, L. Su, J. Rizo, L. Liu, L. F. Wang, F. S. Wang and X. Wang (2014). "Mixed lineage kinase domain-like protein MLKL causes necrotic membrane disruption upon phosphorylation by RIP3." Mol Cell **54**(1): 133-146.

Wang, L., Y. Liu, Y. Zhang, A. Yasin and L. Zhang (2019). "Investigating Stability and Tautomerization of Gossypol-A Spectroscopy Study." Molecules **24**(7).

Wang, S., X. Shi, S. Wei, D. Ma, O. Oyinlade, S. Q. Lv, M. Ying, Y. A. Zhang, S. M. Claypool, P. Watkins, et al. (2018). "Kruppel-like factor 4 (KLF4) induces mitochondrial fusion and increases spare respiratory capacity of human glioblastoma cells." J Biol Chem **293**(17): 6544-6555.

Warburg, O. (1956). "On the origin of cancer cells." Science **123**(3191): 309-314.

Webb, M. C., F. Compton, P. A. Andrews and C. G. Koffman (1997). "Skin tumours posttransplantation: a retrospective analysis of 28 years' experience at a single centre." Transplant Proc **29**(1-2): 828-830.

Wei, M. C., W. X. Zong, E. H. Cheng, T. Lindsten, V. Panoutsakopoulou, A. J. Ross, K. A. Roth, G. R. MacGregor, C. B. Thompson and S. J. Korsmeyer (2001). "Proapoptotic BAX and BAK: a requisite gateway to mitochondrial dysfunction and death." Science **292**(5517): 727-730.

Wei, X., W. Duan, Y. Li, S. Zhang, X. Xin, L. Sun, M. Gao, Q. Li and D. Wang (2016). "AT101 exerts a synergetic efficacy in gastric cancer patients with 5-FU based treatment through promoting apoptosis and autophagy." Oncotarget **7**(23): 34430-34441.

Weidberg, H., E. Shvets and Z. Elazar (2011). "Biogenesis and cargo selectivity of autophagosomes." Annu Rev Biochem **80**: 125-156.

Weinberg, R. A. (1994). "Oncogenes and tumor suppressor genes." CA Cancer J Clin **44**(3): 160-170.

Wellbrock, C., M. Karasarides and R. Marais (2004). "The RAF proteins take centre stage." Nat Rev Mol Cell Biol **5**(11): 875-885.

Weller, J., K. M. Kizina, K. Can, G. Bao and M. Muller (2014). "Response properties of the genetically encoded optical H2O2 sensor HyPer." Free Radic Biol Med **76**: 227-241.

Wheeler, D. L., S. Huang, T. J. Kruser, M. M. Nechrebecki, E. A. Armstrong, S. Benavente, V. Gondi, K. T. Hsu and P. M. Harari (2008). "Mechanisms of acquired resistance to cetuximab: role of HER (ErbB) family members." Oncogene **27**(28): 3944-3956.

White, E. (2012). "Deconvoluting the context-dependent role for autophagy in cancer." Nat Rev Cancer **12**(6): 401-410.

Wieckowski, M. R., C. Giorgi, M. Lebiedzinska, J. Duszynski and P. Pinton (2009). "Isolation of mitochondria-associated membranes and mitochondria from animal tissues and cells." Nat Protoc **4**(11): 1582-1590.

Wijdeven, R. H., H. Janssen, L. Nahidiazar, L. Janssen, K. Jalink, I. Berlin and J. Neefjes (2016). "Cholesterol and ORP1L-mediated ER contact sites control autophagosome transport and fusion with the endocytic pathway." Nat Commun **7**: 11808.

Wolter, K. G., S. J. Wang, B. S. Henson, S. Wang, K. A. Griffith, B. Kumar, J. Chen, T. E. Carey, C. R. Bradford and N. J. D'Silva (2006). "(-)-gossypol inhibits growth and promotes apoptosis of human head and neck squamous cell carcinoma in vivo." Neoplasia **8**(3): 163-172.

Wu, D. (1989). "An overview of the clinical pharmacology and therapeutic potential of gossypol as a male contraceptive agent and in gynaecological disease." Drugs **38**(3): 333-341.

Wu, X. and J. A. Hammer (2014). "Melanosome transfer: it is best to give and receive." Curr Opin Cell Biol **29**: 1-7.

Wu, Y., G. Dong and C. Sheng (2020). "Targeting necroptosis in anticancer therapy: mechanisms and modulators." Acta Pharm Sin B **10**(9): 1601-1618.

Xu, R., E. Tian, H. Tang, C. Liu and Q. Wang (2014). "Proteomic analysis of gossypol induces necrosis in multiple myeloma cells." Biomed Res Int **2014**: 839232.

Xu, X., Y. Lai and Z. C. Hua (2019). "Apoptosis and apoptotic body: disease message and therapeutic target potentials." <u>Biosci Rep</u> **39**(1).

Yamamoto, A., Y. Tagawa, T. Yoshimori, Y. Moriyama, R. Masaki and Y. Tashiro (1998). "Bafilomycin A1 prevents maturation of autophagic vacuoles by inhibiting fusion between autophagosomes and lysosomes in rat hepatoma cell line, H-4-II-E cells." <u>Cell Struct Funct</u> **23**(1): 33-42.

Yan, W., Wistuba, II, M. R. Emmert-Buck and H. S. Erickson (2011). "Squamous Cell Carcinoma - Similarities and Differences among Anatomical Sites." <u>Am J Cancer Res</u> **1**(3): 275-300.

Yang, R. F., L. H. Sun, R. Zhang, Y. Zhang, Y. X. Luo, W. Zheng, Z. Q. Zhang, H. Z. Chen and D. P. Liu (2015). "Suppression of Mic60 compromises mitochondrial transcription and oxidative phosphorylation." <u>Sci Rep</u> **5**: 7990.

Yip, K. W. and J. C. Reed (2008). "Bcl-2 family proteins and cancer." <u>Oncogene</u> **27**(50): 6398-6406.

Yu, L. and S. Liu (2013). "Autophagy contributes to modulating the cytotoxicities of Bcl-2 homology domain-3 mimetics." <u>Semin Cancer Biol</u> **23**(6 Pt B): 553-560.

Yu, L., M. Lu, D. Jia, J. Ma, E. Ben-Jacob, H. Levine, B. A. Kaipparettu and J. N. Onuchic (2017). "Modeling the Genetic Regulation of Cancer Metabolism: Interplay between Glycolysis and Oxidative Phosphorylation." <u>Cancer Res</u> **77**(7): 1564-1574.

Yu, T., J. L. Robotham and Y. Yoon (2006). "Increased production of reactive oxygen species in hyperglycemic conditions requires dynamic change of mitochondrial morphology." <u>Proc Natl Acad Sci U S A</u> **103**(8): 2653-2658.

Yue, Z., S. Jin, C. Yang, A. J. Levine and N. Heintz (2003). "Beclin 1, an autophagy gene essential for early embryonic development, is a haploinsufficient tumor suppressor." <u>Proc Natl Acad Sci U S A</u> **100**(25): 15077-15082.

Zbytek, B., J. A. Carlson, J. Granese, J. Ross, M. C. Mihm, Jr. and A. Slominski (2008). "Current concepts of metastasis in melanoma." <u>Expert Rev Dermatol</u> **3**(5): 569-585.

Zec, M., T. Srdic-Rajic, A. Krivokuca, R. Jankovic, T. Todorovic, K. Andelkovic and S. Radulovic (2014). "Novel selenosemicarbazone metal complexes exert anti-tumor effect via alternative, caspase-independent necroptotic cell death." <u>Med Chem</u> **10**(8): 759-771.

Zeng, Y., J. Ma, L. Xu and D. Wu (2019). "Natural Product Gossypol and its Derivatives in Precision Cancer Medicine." <u>Curr Med Chem</u> **26**(10): 1849-1873.

ZfKD, Zentrum für Krebsregisterdaten (2019). "Nicht-melanotischer Hautkrebs (heller Hautkrebs)." from <u>https://www.krebsdaten.de/Krebs/DE/Content/Krebsarten/Nicht-melanotischer-Hautkrebs/nicht-melanotischer-hautkrebs_node.html;jsessionid=88303C7C707511332FC90BC10CBCDDF0.2_cid290</u>.

ZfKD, Zentrum für Krebsregisterdaten (2021). "Malignes Melanom der Haut." from <u>https://www.krebsdaten.de/Krebs/DE/Content/Krebsarten/Melanom/melanom_node.html</u>.

Zhang, B., I. Gojo and R. G. Fenton (2002). "Myeloid cell factor-1 is a critical survival factor for multiple myeloma." <u>Blood</u> **99**(6): 1885-1893.

Zhang, L., L. Ming and J. Yu (2007). "BH3 mimetics to improve cancer therapy; mechanisms and examples." <u>Drug Resist Updat</u> **10**(6): 207-217.

Zhang, W. and H. T. Liu (2002). "MAPK signal pathways in the regulation of cell proliferation in mammalian cells." <u>Cell Res</u> **12**(1): 9-18.

Zhang, Y., X. Chen, C. Gueydan and J. Han (2018). "Plasma membrane changes during programmed cell deaths." <u>Cell Res</u> **28**(1): 9-21.

Zhang, Z., J. Lai, K. Wu, X. Huang, S. Guo, L. Zhang and J. Liu (2018). "Peroxidase-catalyzed chemiluminescence system and its application in immunoassay." Talanta **180**: 260-270.

Zhao, G. X., L. H. Xu, H. Pan, Q. R. Lin, M. Y. Huang, J. Y. Cai, D. Y. Ouyang and X. H. He (2015). "The BH3-mimetic gossypol and noncytotoxic doses of valproic acid induce apoptosis by suppressing cyclin-A2/Akt/FOXO3a signaling." Oncotarget **6**(36): 38952-38966.

Zhao, Y., R. Li, W. Xia, J. Neuzil, Y. Lu, H. Zhang, X. Zhao, X. Zhang, C. Sun and K. Wu (2010). "Bid integrates intrinsic and extrinsic signaling in apoptosis induced by alpha-tocopheryl succinate in human gastric carcinoma cells." Cancer Lett **288**(1): 42-49.

Zheng, Q., H. Su, M. J. Ranek and X. Wang (2011). "Autophagy and p62 in cardiac proteinopathy." Circ Res **109**(3): 296-308.

Zhong, J. T., Y. Xu, H. W. Yi, J. Su, H. M. Yu, X. Y. Xiang, X. N. Li, Z. C. Zhang and L. K. Sun (2012). "The BH3 mimetic S1 induces autophagy through ER stress and disruption of Bcl-2/Beclin 1 interaction in human glioma U251 cells." Cancer Lett **323**(2): 180-187.

Zhu, F., W. Zhang, T. Yang and S.-d. He (2019). "Complex roles of necroptosis in cancer." Journal of Zhejiang University-SCIENCE B **20**(5): 399-413.

Zorova, L. D., V. A. Popkov, E. Y. Plotnikov, D. N. Silachev, I. B. Pevzner, S. S. Jankauskas, V. A. Babenko, S. D. Zorov, A. V. Balakireva, M. Juhaszova, et al. (2018). "Mitochondrial membrane potential." Anal Biochem **552**: 50-59.

Zou, H., Y. Li, X. Liu and X. Wang (1999). "An APAF-1.cytochrome c multimeric complex is a functional apoptosome that activates procaspase-9." J Biol Chem **274**(17): 11549-11556.

Zubair, H., S. Azim, H. Y. Khan, M. F. Ullah, D. Wu, A. P. Singh, S. M. Hadi and A. Ahmad (2016). "Mobilization of Intracellular Copper by Gossypol and Apogossypolone Leads to Reactive Oxygen Species-Mediated Cell Death: Putative Anticancer Mechanism." Int J Mol Sci **17**(5).

9 Appendix

The performed proteomics analysis after GP treatment in tumour cells, including the evaluation of data and the validation by Western Blot, is shown in the following.

9.1 Proteomics

To analyse whether GP induces changes at the level of proteins, the proteome of A375 melanoma and SCL-1carcinoma cells was investigated. For the proteomics approach, A375 melanoma and SCL-1carcinoma cells were grown to subconfluence in Ø 10 cm dishes and mock-treated and treated with 2.5 µM GP, respectively, for 4 and 24 h. Technical quadruples were used for the experiment. After treatment, cells were washed with PBS, detached by a cell scraper and transferred to a 2 ml tube which was weighted before. After centrifugation at 1,000 x g for 15 min at 4°C, the weight of the pellet was determined which was stored in liquid nitrogen until further use. The proteomics analysis including normalisation (Cox et al. 2014) was performed by the group "Functional Proteomics and Protein Analysis" at the Molecular Proteomics Laboratory (MPL) at Heinrich-Heine-University in Düsseldorf. The evaluation was carried out by Dr. Nahal Brocke-Ahmadinejad. For analysis, differentially expressed proteins were independently identified in the two datasets SCL-1 carcinoma ("SCL-1") and A375 melanoma ("A375") cells. In each sample differentially expressed candidates were defined for the two treatment timepoints (4 and 24 h), for treatment with 2.5 µM GP compared to mock-treated control. Correlation of intensities in replicates within each dataset showed high Pearson correlation. Only the distribution of intensities and Pearson correlation of one replicate sample in dataset A375 (R4_4h) showed very biased behaviour, so that it was excluded from further analysis (Fig. 9.1). Initially, differential expression analysis included 2162 identified protein groups in SCL-1 and 2297 in A375. Normalised intensities were filtered for proteins which showed values in at least three (SCL-1) or two (A375) replicates to provide most comprehensive replicate support for the statistical test. This step reduced the number of protein groups to 1688 (SCL-1) and 2018 (A375). Two different statistical tests were applied (limma and rank product) (Schwammle et al. 2013). The resulting p-values were corrected for multiple testing using the method according to (Schwammle et al. 2013). Significant candidates are those, which show in either of the two tests a corrected p-value ≤0.05 (Tab. 9.1, Tab. 9.2). The Volcano plots show the distribution of corrected p-values ($-\log_2$) in relation to the fold change (=ratio, $\log_2$). Data preparation, correlation analysis, volcano plots were performed in R (R Core Team 2019) (Fig. 9.3, Fig. 9.4). Comparisons of differentially expressed protein groups in the venn diagrams are based on gene names (Fig. 9.5).
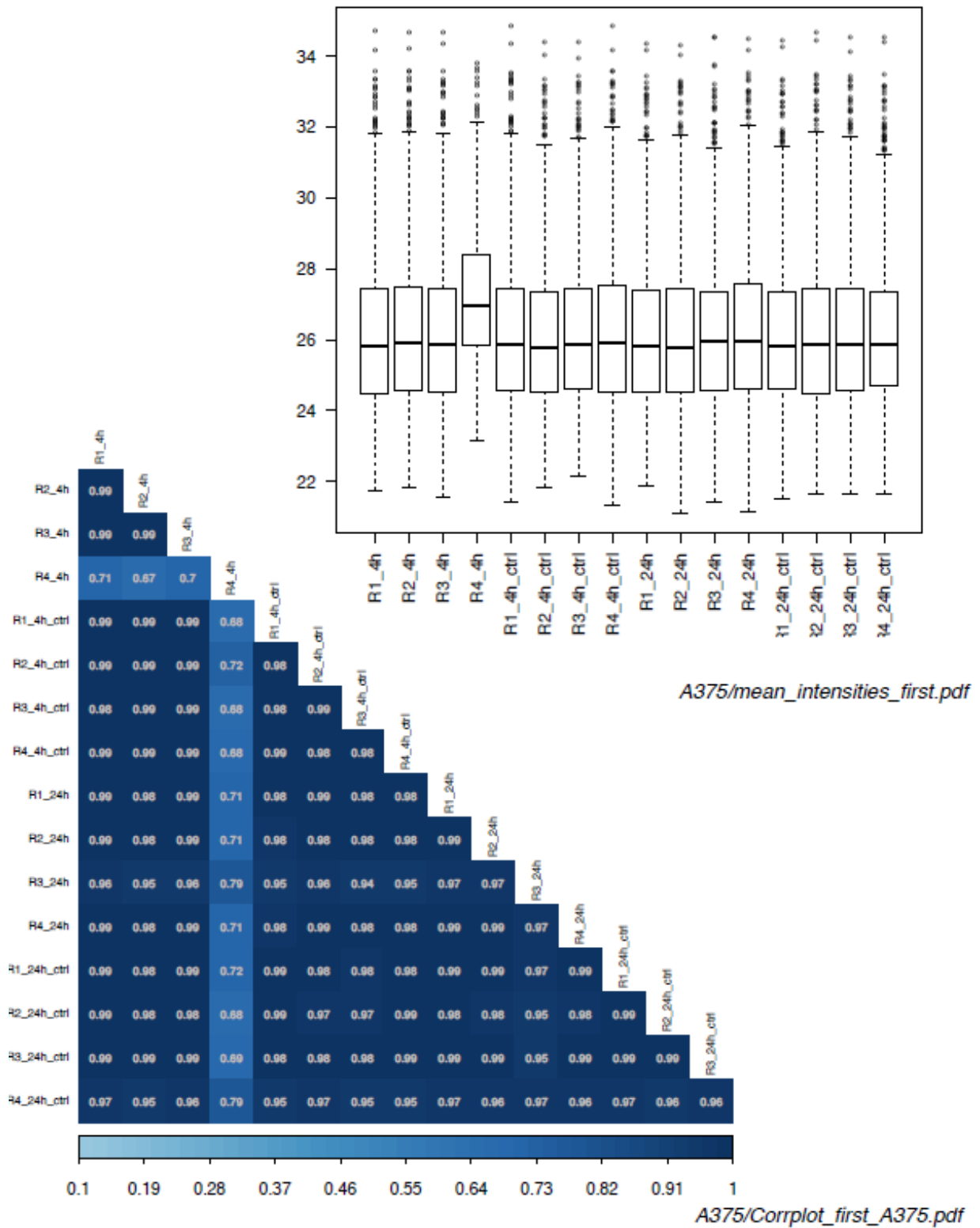
Fig. 9.1 Distribution of intensities and Pearson correlation in A375 melanoma cells.Due to differences in both, sample R4_4h was excluded from further analysis.
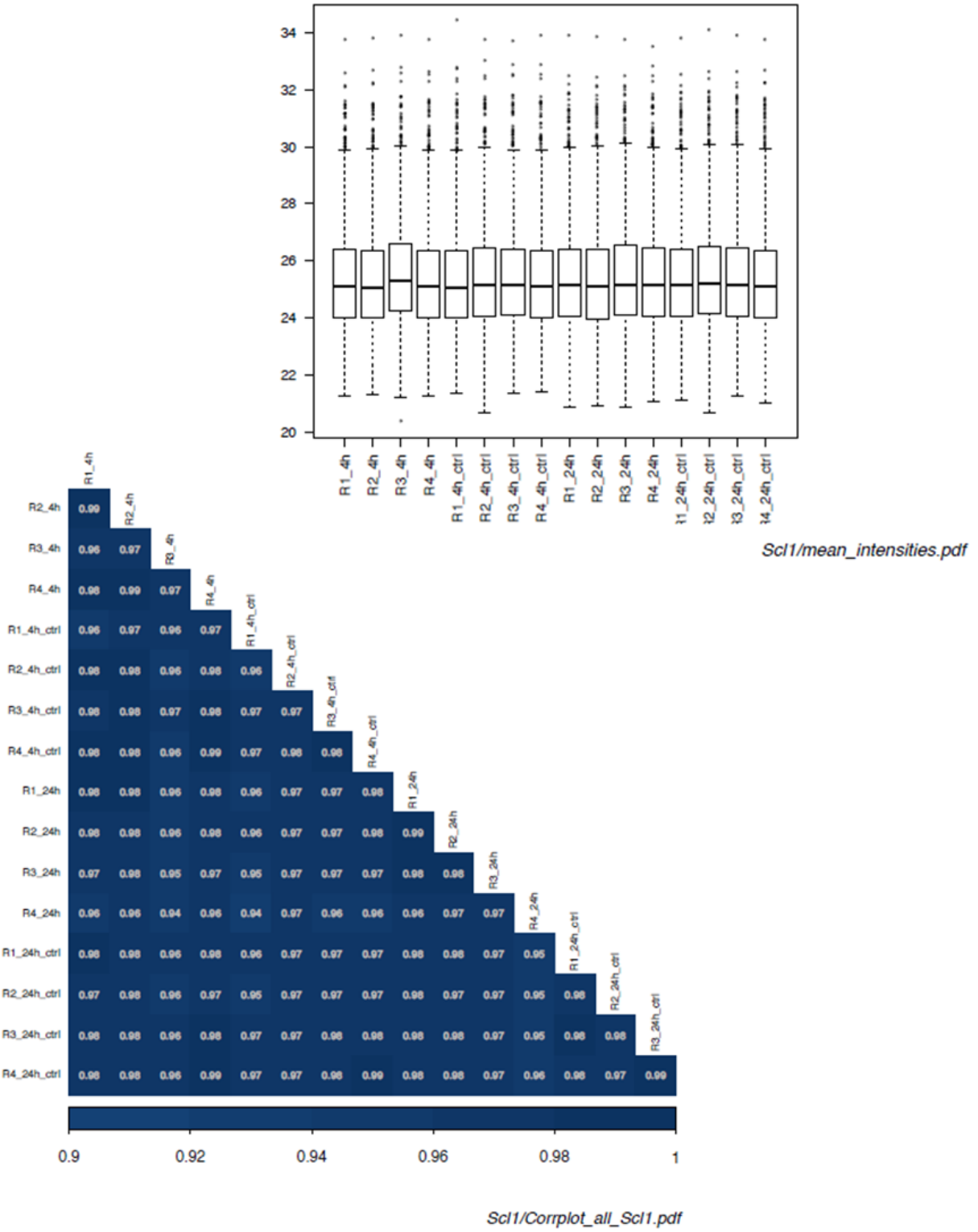
Fig. 9.2 Distribution of intensities and Pearson correlation in SCL-1 carcinoma cells.

Tab. 9.1 Number of significantly up- or downregulated proteins in SCL-1 carcinoma cellsSignificant means, if in either of the two test the corrected p-value is ≤0.05.

Gossypol vs Control	up-regulated	down-regulated
4h	0	0
24h	21	61

Scl1/Scl1_diffreg.xlsx

Tab. 9.2 Number of significantly up- or downregulated proteins in A375 melanoma cells. Significant means, if in either of the two test the corrected p-value is ≤0.05.

Gossypol vs Control	up-regulated	down-regulated
4h	0	0
24h	354	357

A375/A375_diffreg.xlsx

Scl1/Volcano_plots_GP_24h_Scl1.pdf
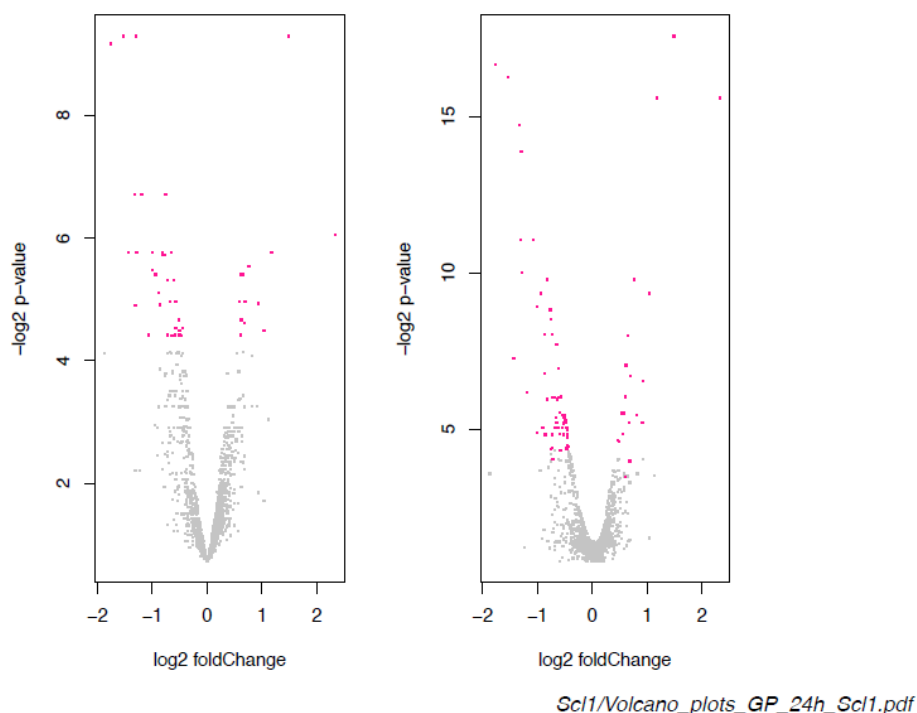
Fig. 9.3 Differentially expressed proteins after treatment with 2.5 µM GP compared to mock-treated cells are depicted in Volcano plots in SCL-1 carcinoma cells. The Volcano plots using limma (left panel) or rank product test (right panel) show the distribution of corrected p-values (-$\log_2$) in relation to the fold change (=ratio, $\log_2$). One should rank candidates of interest according to a high fold change and a low p-value (significance level of p≤0.05 is 4.32 (-$\log_2$)).
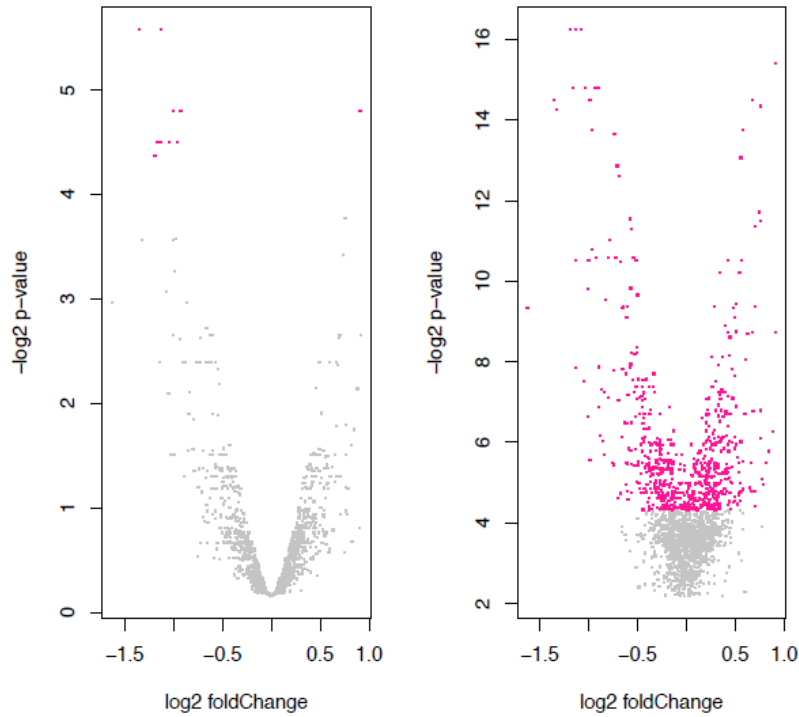
A375/Volcano_plots_GP_24h_A375.pdf

Fig. 9.4 Differentially expressed proteins after treatment with 2.5 µM GP compared to mock-treated cells are depicted in Volcano plots in A375 melanoma cells. The Volcano plots using limma (left panel) or rank product test (right panel) show the distribution of corrected p-values ($-\log_2$) in relation to the fold change (=ratio, $\log_2$). One should rank candidates of interest according to a high fold change and a low p-value (significance level of p≤0.05 is 4.32 ($-\log_2$)).
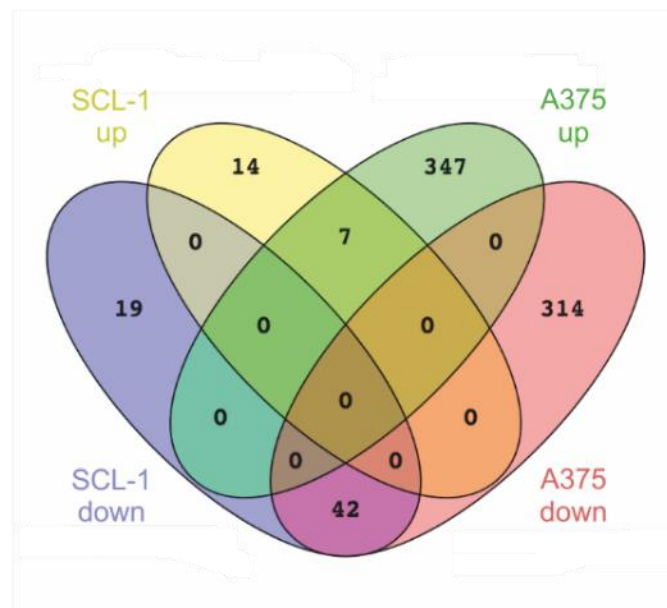
Fig. 9.5 Comparison of gene names found in both SCL-1 carcinoma and A375 melanoma cells included up- and downregulated proteins shown in a venn diagram.

Tab. 9.3 Overview of a range of significant downregulated proteins after GP treatment in A375 melanoma cells. In addition to the protein and gene names, the log of fold-change (logFC) as well as p-value of both limma (pvalue limma) and rank product (pvalue RP) are shown.

Protein names	Gene names	logFC	pvalue limma	pvalue RP
NADH dehydrogenase [ubiquinone] flavoprotein 2, mitochondrial	NDUFV2	-1,32526532	0,08459625	5,14E-05
NADH dehydrogenase [ubiquinone] 1 alpha subcomplex subunit 9, mitochondrial	NDUFA9	-1,19023688	0,048456356	1,29E-05
NADH dehydrogenase [ubiquinone] iron-sulfur protein 3, mitochondrial	NDUFS3	-1,13562179	0,044096094	1,29E-05
NADH-ubiquinone oxidoreductase 75 kDa subunit, mitochondrial	NDUFS1	-0,98746928	0,103760559	4,34E-05
NADH dehydrogenase [ubiquinone] flavoprotein 1, mitochondrial	NDUFV1	-0,93442669	0,163625844	3,51E-05
NADH dehydrogenase [ubiquinone] iron-sulfur protein 2, mitochondrial	NDUFS2	-0,92513734	0,035955526	0,000646547
NADH dehydrogenase [ubiquinone] 1 alpha subcomplex subunit 13	NDUFA13	-0,90103638	0,189909673	0,008484822
NADH dehydrogenase [ubiquinone] 1 alpha subcomplex subunit 10, mitochondrial	NDUFA10	-0,45978105	0,632033403	0,037367165
NADH dehydrogenase [ubiquinone] 1 beta subcomplex subunit 10	NDUFB10	-0,4497217	0,632033403	0,007584465
Cytochrome b-c1 complex subunit Rieske, mitochondrial;Cytochrome b-c1 complex subunit 11;Putative cytochrome	UQCRFS1;UQCRFS1P1	-1,0504062	0,234994377	0,005505415

b-c1 complex subunit Rieske-like protein 1				
Cytochrome b-c1 complex subunit 1, mitochondrial	UQCRC1	-0,61234813	0,189909673	0,001807377
ATP synthase subunit g, mitochondrial	ATP5L	-0,4615445	0,431764383	0,016230567
ATP synthase subunit gamma, mitochondrial	ATP5C1	-0,44958306	0,624770271	0,006009238
ATP synthase subunit O, mitochondrial	ATP5O	-0,44212326	0,405966057	0,015473539
ATP synthase subunit f, mitochondrial	ATP5J2;ATP5J2-PTCD1	-0,30110233	0,553072075	0,037321784
Pyruvate dehydrogenase E1 component subunit alpha, somatic form, mitochondrial	PDHA1	-0,41320497	0,386609729	0,036229122
Pyruvate dehydrogenase phosphatase regulatory subunit, mitochondrial	PDPR	-0,21196118	0,632033403	0,02984184
MICOS complex subunit MIC19	CHCHD3	-0,36745837	0,610104301	0,025103076
Mitochondrial import inner membrane translocase subunit TIM44	TIMM44	-0,31554533	0,441621514	0,034314119
Serine/threonine-protein phosphatase PGAM5, mitochondrial	PGAM5	-0,1487141	0,73668319	0,039454576

Tab. 9.4 Overview of a range of significant upregulated proteins after GP treatment in A375 melanoma cells. In addition to the protein and gene names, the log of fold-change (logFC) as well as p-value of both limma (pvalue limma) and rank product (pvalue RP) are shown.

Protein names	Gene names	logFC	pvalue limma	pvalue RP
Hexokinase; Hexokinase-2	HK2	0,90746975	0,03595553	2,30E-05
BH3-interacting domain death agonist; BH3-interacting domain death agonist p15; BH3-interacting domain death agonist p13; BH3-interacting domain death agonist p11	BID	0,81506345	0,3310134	0,02238335
Sequestosome-1	SQSTM1	0,75589803	0,07301314	0,0003479

Tab. 9.5 Overview of a range of significant downregulated proteins after GP treatment in SCL-1 carcinoma cells. In addition to the protein and gene names, the log of fold-change (logFC) as well as p-value of both limma (pvalue limma) and rank product (pvalue RP) are shown.

Protein names	Gene names	logFC	pvalue limma	pvalue RP
NADH dehydrogenase [ubiquinone] 1 alpha subcomplex subunit 9, mitochondrial	NDUFA9	-0,51566738	0,13314048	0,0352537
NADH dehydrogenase [ubiquinone] 1 beta subcomplex subunit 9	NDUFB9	-0,68206729	0,05654826	0,01547141
NADH-ubiquinone oxidoreductase 75 kDa subunit, mitochondrial	NDUFS1	-1,5282144	0,00159354	1,29E-05
NADH dehydrogenase [ubiquinone] iron-sulfur protein 3, mitochondrial	NDUFS3	-1,32831269	0,00950582	3,70E-05
NADH dehydrogenase [ubiquinone] flavoprotein 1, mitochondrial	NDUFV1	-1,29435138	0,00159354	6,70E-05
NADH dehydrogenase [ubiquinone] flavoprotein 2, mitochondrial	NDUFV2	-1,75836247	0,00173617	9,68E-06
Cytochrome b-c1 complex subunit 1, mitochondrial	UQCRC1	-0,44593912	0,04309061	0,0352537
Cytochrome b-c1 complex subunit Rieske, mitochondrial;Cytochrome b-c1 complex subunit 11;Putative cytochrome b-c1 complex subunit Rieske-like protein 1	UQCRFS1;UQCRFS1P1	-1,42943171	0,01837936	0,00656768
ATP synthase subunit alpha, mitochondrial	ATP5A1	-0,45437413	0,05750995	0,04424696

ATP synthase subunit O, mitochondrial	ATP5O	-0,51313457	0,0393500 3	0,0242851 6
Pyruvate dehydrogenase E1 component subunit alpha, somatic form, mitochondrial	PDHA1	-0,75754476	0,0725995 3	0,0483635 7
Succinate dehydrogenase [ubiquinone] flavoprotein subunit, mitochondrial	SDHA	-0,42259292	0,0745748 6	0,0456709 5
Succinate dehydrogenase [ubiquinone] iron-sulfur subunit, mitochondrial	SDHB	-0,45954946	0,1195868 5	0,0319939 1
MICOS complex subunit MIC60	IMMT	-0,55231224	0,0577818 3	0,0229572 2
Mitochondrial import inner membrane translocase subunit TIM50	TIMM50	-0,72330604	0,0252777 7	0,0154714 1

Tab. 9.6 Overview of a range of significant upregulated proteins after GP treatment in SCL-1 carcinoma cells. In addition to the protein and gene names, the log of fold-change (logFC) as well as p-value of both limma (pvalue limma) and rank product (pvalue RP) are shown.

Protein names	Gene names	logFC	pvalue limma	pvalue RP
Hexokinase; Hexokinase-2	HK2	1,17502915	0,01837936	2,03E-05
Sequestosome-1	SQSTM1	0,76010561	0,02161588	0,00113526

Gene ontology overrepresentation in up- and downregulated set of proteins were performed in cytoscape (Shannon et al. 2003) using the BiNGO application (Maere et al. 2005). GO resource files that were used in the cytoscape bingo app were downloaded on the 19th of November 2019 (go-basic.obo - data-version: releases/2019-10-07; http://geneontology.org/docs/download-ontology/). The distribution of up- and downregulated proteins in SCL-1 carcinoma and A375 melanoma cells related to cellular components (CC) were presented in Fig. 9.6.
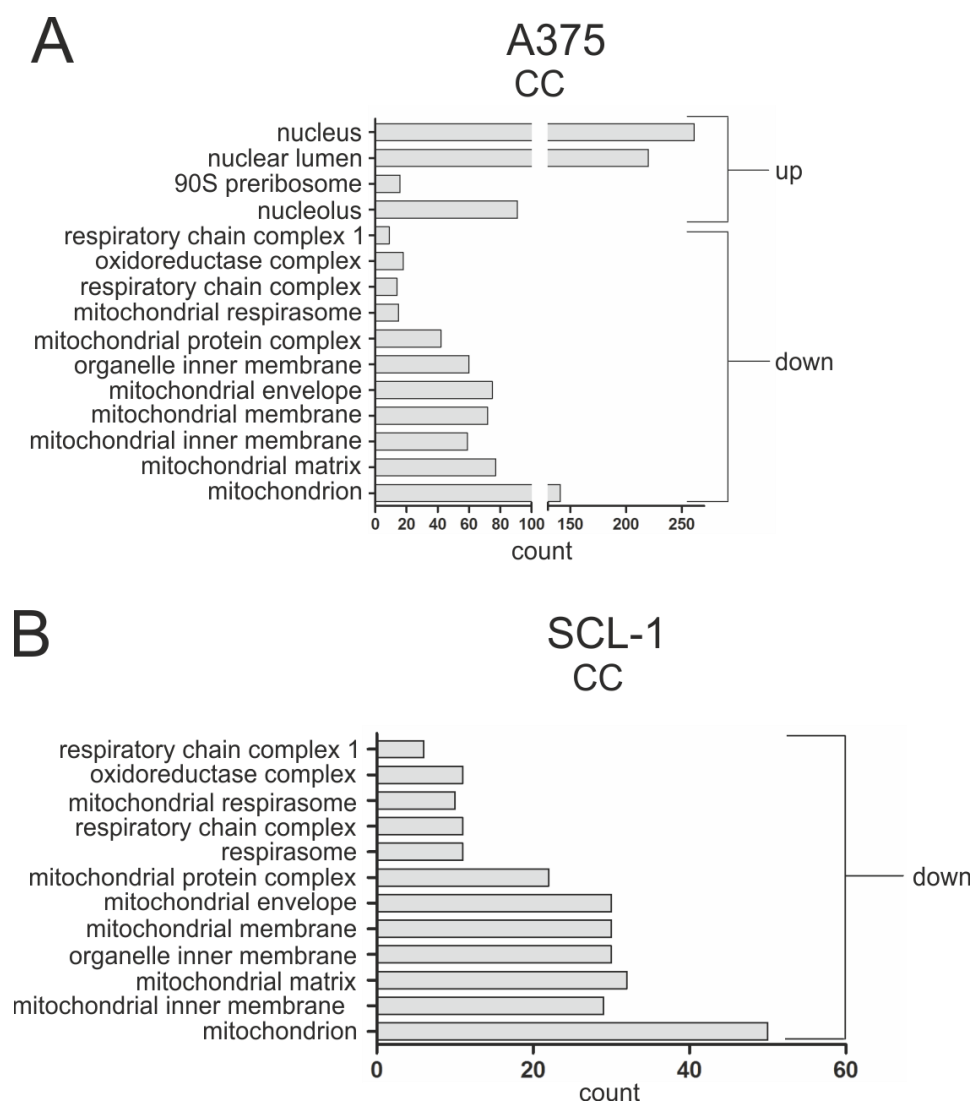
Fig. 9.6 Distribution of up-and downregulated proteins after GP treatment referring to cellular components (CC) in A375 melanoma (**a**) and SCL-1 carcinoma cells (**b**).

For validation of the proteomics data, the expression levels of NADH: Ubiquinone Oxidoreductase Subunit B4 (NDUFB4), as representative for mitochondrial complex I subunit, and Micos complex subunit Mic60, as representative for mitochondrial proteins, were determined after treatment with GP for 24 h by Western Blot. Furthermore, the expression level of hexokinase2 (HK2) was measured. In addition to both tumour cell lines, the protein expressions were also examined in normal human epidermal melanocytes (NHEM), normal human epidermal keratinocytes (NHEK) and normal human dermal fibroblasts (NHDF) (Fig. 9.7). Consistent with the proteomics data, HK2 was upregulated after GP treatment, whereas levels of NDUFB4 and Mic60 were decreased. In contrast, GP induced no change in HK2 and Mic60 level in NHEK as well as increased the expression of NDUFB4. NHEM showed an increase of HK2 similar to SCL-1 carcinoma cells and the same decrease in NDUFB4 expression levels compared to both tumour cells. However, the Mic60 levels were less downregulated in comparison to those. Furthermore, GP treatment resulted in a strong

decrease of Mic60 in NHDF, accompanied by an increase of NDUFB4 and HK2.
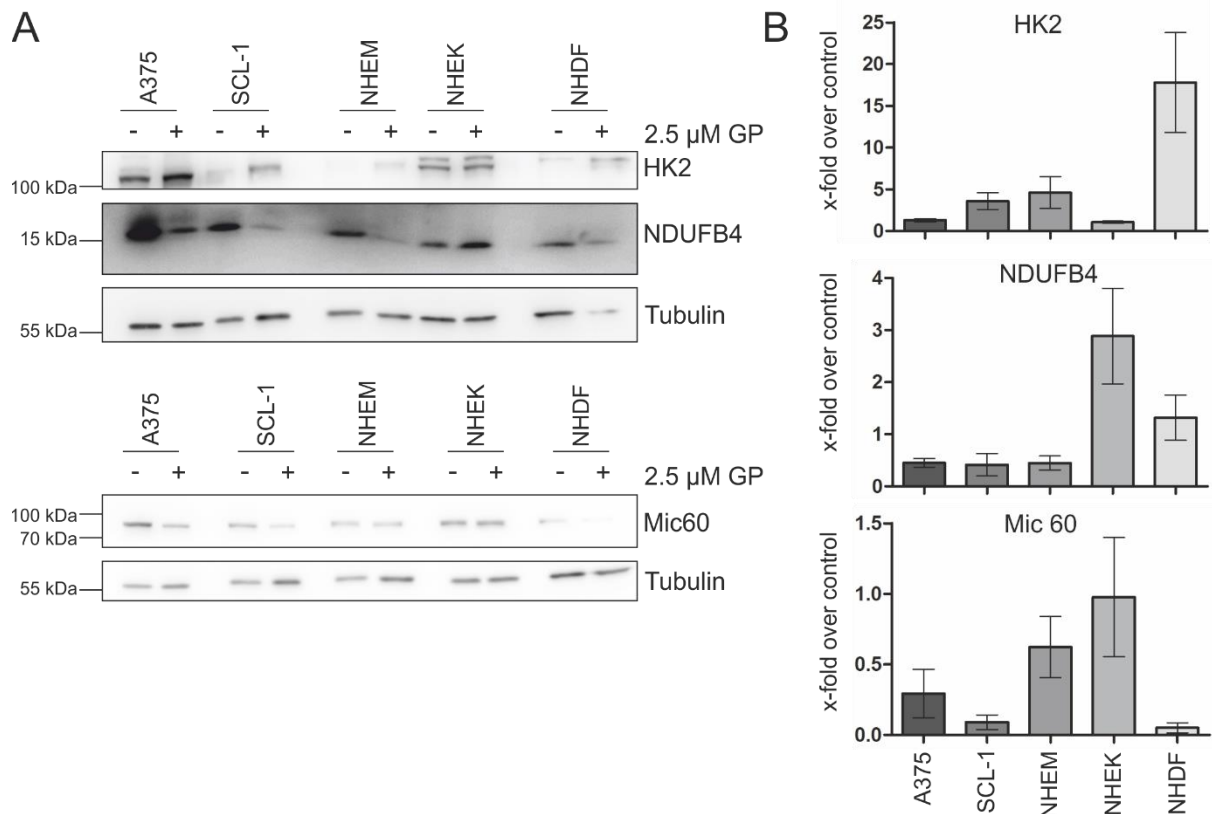
Fig. 9.7 Validation of proteomics data by Western Blot. **a** A375 melanoma cells, SCL-1 carcinoma cells, melanocytes (NHEM), keratinocytes (NHEK) and fibroblasts (NHDF) were treated with 2.5 µM GP or mock-treated for 24 h. Total cell lysate was used for the determination of expression levels of various proteins including hexokinase 2 (HK2), MICOS complex subunit MIC60 and NADH: Ubiquinone Oxidoreductase Subunit B4 (NDUFB4). Tubulin served as loading control. Representative blots of three independent experiments were depicted, n=3. **b** For densitometric analysis and subsequent quantification, the mock-treated control level was set at 1. The protein levels after GP treatment are only shown.

In summary, upregulation of HK2 as well as downregulation of NDUFB4 (complex I) and Mic60 expression levels were consistent with the proteomics approach (Tab. 9.3-Tab. 9.6).

10 Danksagung

An erster Stelle möchte ich mich besonders bei meinem Doktorvater Herrn Prof. Dr. Peter Brenneisen bedanken. Vielen, lieben Dank für die Bereitstellung des interessanten Promotionsthemas, die hervorragende Betreuung sowie die Möglichkeit an Weiterbildungen und an internationalen Konferenzen teilnehmen zu können. Es war eine lehrreiche Zeit und ich habe die vielen Diskussionen zu meiner Arbeit sehr geschätzt.

Ich möchte mich bei Herrn Prof. Dr. Matthias Kassack für die Übernahme der Ko-Betreuung meiner Dissertation bedanken. Vielen Dank für die freundliche Mitbetreuung.

Ich danke Herrn Prof. Dr. Andreas Reichert für die Möglichkeit, meine Dissertation an seinem Institut durchführen zu können.

Ein großer Dank gilt auch Herrn Prof. Dr. Wilhelm Stahl für die vielen Diskussionen und Ratschläge zu meiner Dissertation.

Einen besonderen Dank möchte ich Frau Dr. Claudia von Montfort aussprechen. Du standest mir immer mit Rat und Tat zur Seite und hast mich jederzeit unterstützt. Unsere Gespräche, auch gerne mit selbstgemachtem Cappuccino, sowie die gemeinsame Zeit in unserem Büro habe ich sehr genossen!

Ein herzliches Dankeschön geht an Lara Ebbert und Sarah Zerres. Mit eurer humorvollen, hilfsbereiten und sympathischen Art seid ihr mir ans Herz gewachsen! Lieben Dank für die gemeinsame, lustige Zeit, auch fernab von der Arbeit. Und danke, liebe Lara, für deine Unterstützung im Labor.

Ich bedanke mich auch herzlich bei Claudia Wyrich für die Hilfsbereitschaft bei sämtlichen, auftretenden Problemen im Labor und für eine schöne, gemeinsame Zeit.

Ich möchte mich bei Peter Graf für seinen unermüdlichen Einsatz in der Analytik bedanken. „Mal eben schnell die Aufnahme messen" kam nicht ganz hin, aber dank dir hat es überhaupt erst funktioniert.

Für das tolle Arbeitsklima und eine sehr schöne Zeit in der AG Brenneisen bedanke ich mich stellvertretend bei Nadja Schwarz, Chantal Wenzel und Shayan Motiei sowie bei Heide Krahl und David Stucki.

Ein großes Dankeschön gilt Frau Dr. Nahal Brocke-Ahmadinejad für die Problemlösungen zu sämtlichen IT-Fragen und für die Auswertung meiner Proteomics Daten.

Bei Laura Bierwald bedanke ich mich für ihre Hilfe bei sämtlichen organisatorischen Angelegenheiten und das ein oder andere nette Gespräch.